A guardian of balance: the role of BAF chromatin remodeling complex in astrogliogenesis during mouse forebrain development

Dissertation

for the award of the degree

“Doctor rerum naturalium.”

Faculty of Biology

of the Georg-August-Universität Göttingen

within the doctoral program Molecular Physiology of the Brain

of the Georg-August University School of Science (GAUSS)

submitted by

Kamila Anna Kiszka

Born in Myślenice, Poland

Göttingen, 2019

Thesis Committee

Prof. Dr. Jochen F. Staiger (first reviewer)
Institute for Neuroanatomy, University Medical Center, Göttingen

Prof. Dr. Thomas Dresbach (second reviewer)
Department of Anatomy and Embryology, University Medical Center, Göttingen

Prof. Dr. André Fischer
German Center for Neurodegenerative Diseases, University Medical Center, Göttingen

Members of the Examination Board

First Referee:

Prof. Dr. Jochen F. Staiger (first reviewer)
Institute for Neuroanatomy, University Medical Center, Göttingen

Second Referee:

Prof. Dr. Thomas Dresbach (second reviewer)
Department of Anatomy and Embryology, University Medical Center, Göttingen

Further members of the Examination Board

Prof. Dr. André Fischer
German Center for Neurodegenerative Diseases, University Medical Center, Göttingen

Prof. Dr. Ahmed Mansouri
Department of Molecular Cell Biology, MPI for Biophysical Chemistry, Göttingen
Department of Clinical Neurophysiology, University of Göttingen

Dr. Camin Dean
Trans-synaptic Signaling group, European Neuroscience Institute, Göttingen

Prof. Dr. Gregor Eichele
Department of Genes and Behaviour, MPI for Biophysical Chemistry, Göttingen

Date of the oral examination: 15 May 2019

I, Kamila Anna Kiszka, hereby certify that the present thesis has been written independently and with no other sources and aids than quoted. All results presented here were the fruit of my own labour unless stated otherwise.

……..

Göttingen, 31.03.2019

Table of Contents

Figures

Tables

List of Abbreviations

AGPs	Astroglial progenitors
ACSBG1	Acyl-CoA synthetase bubblegum family member 1
AS	Apical surface
BAF	BRG1/BRM associated factor
BLBP	Brain lipid-binding protein
BPs	Basal progenitors
BrdU	Bromodeoxyuridine
BRG1	Brahma related gene 1
CANu	Central amygdala nucleus
CASP3	Caspase 3
CCND1	Cyclin D1
CNS	Central nervous system
CP	Cortical plate
CPu	Caudate putamen
CTNNB1	β-catenin
dcKO	Double conditional knockout
DAPI	4’ 6-diaminodino-2-phenylindole
DIG	Digoxigenin
DG	Dentate gyrus
DMSO	Dimethyl sulfoxide
DP	Dorsal pallium
DPI	Days post injury
DW	Deep cerebral white
EdU	Ethynyl deoxyuridine
EGFP	Enhanced green fluorescent protein
ESCs	Embryonic stem cells
FG	Fast green
FI	Fluorescence intensity
GANT61	GLI anatgonist 61

GFAP	Glial fibrillary acidic protein
GLAST	Glutamate aspartate transporter
GLI1	Glioma associated oncogene 1
GO	Gene ontology
GS	Glutamine synthetase
hGFAP	Human glial fibrillary acidic protein
Het	Heterozygous
IP	Intraperitoneal
IZ	Intermediate zone
KO	Knockout
LCx	Lateral cortex
LGE	Lateral ganglionic eminence
LP	Lateral pallium
M1	Primary motor cortex
MCx	Medial cortex
MGE	Medial ganglionic eminence
M-L	Medio-lateral
NECs	Neuroepithelial cells
NFiA	Nuclear factor I A
NSCs	Neural stem cells
Olig2	Oligodendrocyte transcription factor 2
oRGPs	Outer radial glial progenitors
PBS	Phosphate buffered saline
PFA	Paraformaldehyde
PS	Pial surface
R-C	Rostro-caudal
SATB2	Special AT-rich sequence-binding protein 2
SSC	Standard saline citrate
RGCs	Radial glial cells
S1	Primary somatosensory cortex
S1BF	Primary somatosensory ´barrel´ cortex
SHH	Sonic hedgehog
SOX9	SRY-box 9 protein

SVZ	Subventricular zone
TBS	Tris buffer saline
TBST	Tris buffer 0.5% Triton-X 100 BSA
tdTOM	TdTomato
TF	Transcription factor
VP	Ventral pallium
VZ	Ventricular zone
WB	Western blot
WT	Wild type
σ	Standard deviation of the mean

Chapter 1

Introduction

The degree to which animals recognize and react to external stimuli thoroughly depends on the availability and complexity of their neural systems. While the rudimentary nervous tissue of *Caenorhabditis elegans* (*C. elegans*) enables some perception of environmental stimuli and subsequent adaptation, only the formation of a complex central nervous system (CNS) unlocks the superior cognitive power enjoyed, among others, by mammals (Arendt et al., 2016; Galizia and Lledo, 2013; Hobert, 2010; Metaxakis et al., 2018). Along its evolutionary refinement, the nervous system increased the number and diversity of its constituent cells, developed functionally specialized anatomical structures such as the hippocampus, and equipped itself with dazzling sensory arrays such as the retina. Among the many distinct cell types present in the brain, glia have evolved as morphologically and functionally distinct from neurons, and a tremendous increase of their abundance as well as a diversification of their physiological functions can be observed along the evolution of neural systems (Bullock and Horridge, 1965; Hartline, 2011; Verkhratsky et al., 2017; Zhang, 2001).

Astroglial cells in particular exhibit a dynamic phylogenetic expansion of their numbers as well as their cellular complexity (Andriezen, 1893; Leuba and Garey, 1989; Nedergaard et al., 2003; Oberheim et al., 2009; Oberheim et al., 2006; Vasile et al., 2017). For instance the nervous system of *C. elegans* maintains a 1:6 ratio of glia to neuron (50 glial cells for 302 neurons), whereas in adult human brains, astrocytes outnumber neurons and constitute the majority of neural cells (1.4 astrocyte per neuron) (Chaboub and Deneen, 2012; Freeman, 2010; Nedergaard et al., 2003; Sofroniew and Vinters, 2010; Vasile et al., 2017; von Bartheld et al., 2016). Moreover, species specific quantitative relations between neurons and astrocytes in adult individuals remain relatively constant, fluctuating only within minimal ranges (Bandeira et al., 2009; Brizzee and Jacobs, 1959; von Bartheld et al., 2016). This implies that astrocyte to neuron ratios correlate with varying levels of cognitive ability along the phylogenetic tree, but remain stable within a species, indicating that the

relative amount of neurons and astroglia may partly define brain performance (von Bartheld et al., 2016). Thus the increased functional competence of the mammalian brain is not to be attributed exclusively to neurons (Nedergaard et al., 2003; Robertson, 2014). In fact, advanced cognitive abilities are likely the result of precise cooperation between neurons and numerically superior astrocytes, which appears to execute important role in various facets of brain physiology (Clarke and Barres, 2013; Nedergaard et al., 2003; Oberheim et al., 2009; Oberheim et al., 2006; Robertson, 2013, 2014).

1.1 Physiological functions of astrocytes

Although glial cells were first described in the 19th century by Rudolf Virchow, they were once thought to provide little more than structural support for neurons (the term glia derives from the ancient Greek word for glue) (Distler et al., 1991; Meyer and Kaspar, 2017; Oberheim et al., 2012). Along the 20th century however, it became increasingly clear that astrocytes are involved in a wide range of critical physiological functions in the brain, of which we would like to draw a short and non-exhaustive list here.

One of the roles of astrocytes is to provide metabolic support for surrounding neurons, chiefly through glycolysis. This is possible because unlike most neurons, astrocytes extend processes that form endfeet in apposition to local blood vessels, enabling direct transport of glucose from the bloodstream through glucose transporter 1 (GLUT 1) and through the blood-brain barrier (Maher et al., 1994). In addition, astrocytes are the only type of brain cell known to store glucose in the form of glycogen in significant amounts (Brown and Ransom, 2007), and therefore are uniquely positioned to store as well as supply energy to the brain. The mechanisms by which astrocytes provide energy to neurons are summarized in what is known as the astrocyte-neuron lactate shuttle hypothesis (Pellerin and Magistretti, 1994). According to this hypothesis, glucose and glycogen are metabolized into lactate by astrocytes and shuttled to neurons in an activity-dependent manner. Indeed, astrocytes express glutamate receptors and transporters, enabling them to adjust the rate of lactate secretion to match the global level of neurotransmitter release in nearby neurons. Although various aspects of this elegant hypothesis are still a matter of debate, its central tenet has received a considerable degree of experimental support since its inception (Pellerin and Magistretti, 2012).

Another function of astrocytes is to maintain synaptic and extracellular homeostasis, according to the tripartite synapse hypothesis (Perea et al., 2009). While a typical synapse of the CNS is composed of a presynaptic and postsynaptic neuronal element, this hypothesis posits that each synapse is also enwrapped by the processes of a single astrocyte. These astrocytic endfeet are equipped with glutamate receptors and transporters, enabling astrocytes to sense glutamate release and

participate in the reuptake of neurotransmitter (Rose et al., 2017). These cells are therefore well positioned to contribute to the regulation of synaptic transmission. In addition, astrocytes express membrane-bound, inward rectifying K+ channels and adenosine triphosphate (ATP) dependent Na+/K+ pumps, allowing them to rapidly buffer the increase in extracellular potassium consecutive to neuronal firing (Simard and Nedergaard, 2004). Furthermore, astrocytes play a central role in regulating the water content of the CNS through aquaporin 4 (AQP4) channels located on astrocytic processes contacting local blood vessels (Simard and Nedergaard, 2004).

Finally, together with microglia and fibroblasts, astrocytes play an important protective role after brain damage through a process known as reactive astrogliosis (Sofroniew, 2009). Following neuronal death consecutive to inflammation, focal ischemia or brain injury, astrocytes become proliferative, adopt a hypertrophic morphology and increase glial fibrillary acidic protein (GFAP) expression. Reactive astrocytes migrate towards the site of damage and begin a process of encapsulation, culminating in the formation of a glial scar that insulates the site of injury from surrounding, healthy tissue (Sofroniew, 2009).

Additional roles of astrocytes that will not be discussed here include trafficking of molecules through the blood-brain barrier (Abbott et al., 2006), regulation of extracellular pH (Obara et al., 2008) and modulation of blood flow in relation to general levels of neuronal activity (Iadecola and Nedergaard, 2007). These multifaceted roles of astrocytes clearly speak for their importance to CNS function, well beyond that of mere “glue” (for more exhaustive reviews, see (Sofroniew and Vinters, 2010; Verkhratsky et al., 2017)). The functions of astrocytes described here are further enhanced by the fact that these cells form a functional syncytium (Scemes and Spray, 2004). In the cerebral cortex, the processes of astrocytes do not overlap extensively, instead the cortical parenchyma is tiled with a juxtaposition of individual astrocytes, each covering their individual domain. However, the extremities of neighbouring astrocytes are coupled by gap junctions enabling the passage of small signaling molecules, ions and travelling Ca^{2}+ waves (C. Charles et al., 1991), and which among other things expands the K+ buffering capacity of the astrocytic network (Scemes and Spray, 2004). This anatomical organization increases the potency of an already versatile cell type, and is obviously underpinned by the establishment of an appropriate ratio of astrocytes to neurons during brain development.

1.2 Development of neurons

The development of astrocytes has altogether received less attention than the development of neurons, however both processes share at least some common mechanisms (Chaboub and Deneen, 2013; Molofsky and Deneen, 2015). It is therefore useful to appreciate astroglial development with

respect to neuronal development, which we will shortly introduce here, focusing on cortical neurogenesis (Figure 1).

Neurons are born from radial glial cells (RGCs) which themselves descend from neuroepithelial cells (NECs) (Hartfuss et al., 2001; Rakic, 1982; Sahara and O'Leary, 2009). NECs are neural stem cells (NSCs) that proliferate between E8.5 and E12.5, expanding their pool by symmetric division (Martynoga et al., 2012; Nguyen et al., 2018). At the onset of neurogenesis (E10.5-E11.5), NECs begin expressing astroglial markers (e.g. glutamate aspartate transporter (GLAST) or brain lipid-binding protein (BLBP)) as well as adherens junctions, turning into RGCs (Dehay and Kennedy, 2007; Gotz and Huttner, 2005; Kriegstein and Alvarez-Buylla, 2009; Martynoga et al., 2012; Sahara and O'Leary, 2009). RGCs reside in the ventricular zone (VZ) and possess a short apical process contacting the ventricular surface (or apical surface, AS) as well as a long process contacting the pial surface (PS) (Arai and Taverna, 2017; Gotz and Huttner, 2005; Kriegstein and Alvarez-Buylla, 2009). These RGCs divide asymmetrically, producing deep layer neurons and other RGCs during early neurogenesis (E10-E14) (Kriegstein et al., 2006; Tuoc et al., 2013b). Preferentially during late neurogenesis, RGCs use asymmetric division to self-renew and produce basal (intermediate) progenitors (BPs) (Kriegstein et al., 2006; Pontious et al., 2008). BPs temporarily proliferate in subventricular zone (SVZ) before differentiating into superficial layer neurons (Kriegstein et al., 2006; Pontious et al., 2008).

Regardless of the modalities of their birth, successive generations of neurons migrate into the developing cortical plate (CP), either radially following the scaffold of radial glial fibers or by soma translocation (Marin-Padilla, 1978; Miyata et al., 2001). This mode of migration results in a peculiar pattern in the fully developed cortex: indeed, successive cohorts of migrating neurons form the familiar pattern of cortical layers, whereby each generation of excitatory neurons occupies a distinct layer in the cortex (Angevine and Sidman, 1961; Guy and Staiger, 2017; Rakic, 1974). Early born neurons occupy the deeper layers of the cortex, while late born neurons migrate past their predecessors to form the supragranular layers, shaping an inside-out pattern of cortical lamination (Angevine and Sidman, 1961; Rakic, 1974). A key feature of cortical layers that has greatly facilitated the study of neuronal development is the fact that individual layers can be identified by layer-specific markers (Guy and Staiger, 2017; Molyneaux et al., 2007; Popovitchenko and Rasin, 2017). For example, layer II/III neurons can be readily identified by expression of regulator of G protein signaling 8 (RGS8) (Gold et al., 1997; Wagener et al., 2010). Layer IV neurons, on the other hand, express high levels of RAR-related orphan receptor β (RORβ), and layer V is characterized by expression of coup-TFI interacting protein 2 (CTIP2) (Leid et al., 2004; Schaeren-Wiemers et al., 1997). In addition, BPs that give birth to neurons can be identified by their high expression of T-box brain protein 2 (TBR2) (Pinto et al., 2008; Tuoc et al., 2013b). The availability of such specific markers

of given developmental stages in the neuronal lineage has considerably helped our understanding of neuronal development. Alas, the same cannot be said of the development of the astroglial lineage.

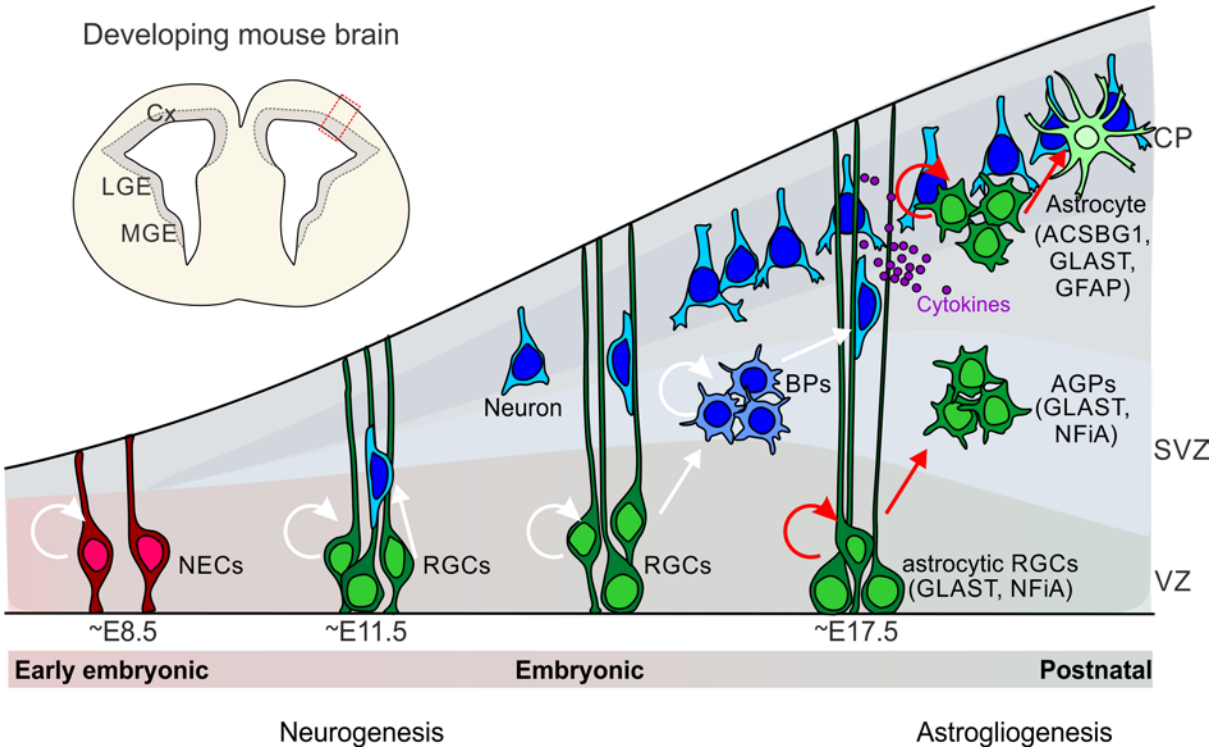

Figure 1 | Development of neurons and astrocytes in mouse cortex. Top left: schematic illustration of a coronal section through a developing mouse brain illustrating the three known germinal zones for astrocytes and neurons. Bottom: schematic depiction of cortical neurogenesis and astrogliogenesis in chronological order. The area illustrated corresponds to the inset at the top left. Briefly, cortical development begins with the self-renewal of embryonic NECs, which then differentiate into RGCs overexpressing astroglial markers (e.g. GLAST). RGCs begin producing neurons around E11.5 by direct neurogenesis. In later stages, RGCs produce neurons through indirect neurogenesis, by generating BPs that reside and proliferate in SVZ. Proliferating BPs eventually differentiate into neurons that migrate into the CP. Astrogliogenesis begins after neurogenesis, around E17.5 when RGCs (refered to as astrocytic RGCs) overexpress astroglial TFs (e.g. NFiA),detach form the surface of VZ in the form of AGPs, and then migrate, proliferate transiently, and finally differentiate into the mature astrocytes. The expression of mature astrocyte markers (e.g. GFAP) is believed to be triggered by neuron-derived cytokines. AGPs, astroglial progenitors; BPs, basal progenitors; CP, cortical plate; NECs, neuroepithelial cells; SVZ, subventricular zone; RGCs, radial glial cells; VZ, ventricular zone.

1.3 Development of astrocytes

As described above, our understanding of astrocyte physiology has dramatically improved over the last few decades (Khakh and Sofroniew, 2015). Similarly, our contemporary view of neuronal

development appears rather exhaustive (Chaboub and Deneen, 2012; Gallo and Deneen, 2014; Kwan et al., 2012; Martynoga et al., 2012). However, our knowledge of astrocyte development and its molecular control has evidently lagged behind (Chaboub and Deneen, 2013; Sloan and Barres, 2014; Yang et al., 2013). Accordingly, we have very little knowledge of the transcription factors (TFs), or epigenetic regulation involved in even the simplest steps of astrogliogenesis (Freeman, 2010; Molofsky et al., 2012). This is partly due to the fact that unlike neurons, no single known molecular marker permits unambiguous identification of the distinct stages of astroglial development (Chaboub and Deneen, 2013; Molofsky et al., 2012). This regrettable situation arises from the fact that astroglial development has not enjoyed the same degree of attention as neuronal development, as these cells were long believed to provide little more than passive and structural support to neurons (Molofsky et al., 2012). In fact, the very idea that distinct stages of development should be characterized by the expression of a unique combination of markers derives from studies on developing neurons and oligodendrocytes, but it is not clear whether the same logic must apply to astroglial development (Chaboub and Deneen, 2013; Molofsky and Deneen, 2015). For instance, similarly to neurons, astrocytes are known to derive from RGCs of VZ that differentiate towards astrocytes through the process of migrating and transiently amplifying astroglial progenitor or premature astrocyte (which we will henceforth refer to as AGPs) (Kriegstein and Alvarez-Buylla, 2009; Schitine et al., 2015; Schiweck et al., 2018). RGCs express a set of markers that are persistently found at all above listed stages of astroglial development, (such as BLBP or GLAST), making it difficult to rely on these markers to identify distinct developmental steps (Gotz and Barde, 2005; Molofsky and Deneen, 2015; Molofsky et al., 2012).

In spite of these difficulties, investigations of astroglial development have met with some success, and depict an overall diverse and complex process whereby astroglial cells originate from several areas and periods in time (Bayraktar et al., 2014; Minocha et al., 2017; Schiweck et al., 2018). Accordingly, lineage tracing experiments indicate that during embryonic development, forebrain astrocytes arise from three main germinal regions, namely VZ of cortex as well as medial and lateral ganglionic eminences (MGE and LGE respectively; Figure 1) (Bayraktar et al., 2014; Minocha et al., 2017; Tsai et al., 2012). Generally, astrogliogenesis is considered to begin once neurogenesis is complete, which is estimated to occur between E16.5 and E18.5 in mouse cortex (Ge et al., 2012; Miller and Gauthier, 2007; Minocha et al., 2017; Molofsky and Deneen, 2015). The source of astroglial cells lies with RGCs of VZ, which begin producing neurons around E11.5, then switch to production of astroglia instead (Costa et al., 2009; Schiweck et al., 2018). In the spinal cord, this switch in cellular fate is accompanied by the upregulated expression of TFs: nuclear factor I A (NFiA) and SRY-box 9 protein (SOX9) in RGCs, and this has traditionally been generalized to cortex (Chaboub and Deneen, 2013; Deneen et al., 2006; Kang et al., 2012; Nagao et al., 2016). Both of these TFs were

shown to be indispensable and sufficient for the initiation of astrogliogenesis (Molofsky et al., 2012). There are several processes through which RGCs generate astroglia (Ge and Jia, 2016; Kriegstein and Alvarez-Buylla, 2009). The best known of these processes begins when RGCs delaminate and migrate out of germinal zones by soma translocation after retracting their apical and subsequently basal processes (Kriegstein and Alvarez-Buylla, 2009; Noctor et al., 2008; Voigt, 1989). This corresponds to a change in the morphology of the differentiating cell, which turns from a bipolar, RGC-like towards a multipolar, astroglial-like morphology (Kriegstein and Alvarez-Buylla, 2009). Once outside of germinal zones, at least a fraction of these cells proliferate and become what can be considered transiently amplifying AGPs, which ultimately differentiate into astrocytes (Gallo and Deneen, 2014; Ge and Jia, 2016; Kriegstein and Alvarez-Buylla, 2009; Namihira and Nakashima, 2013). Another process begins when RGCs divide asymmetrically to generate AGPs which then migrate radially outside of VZ (Molofsky and Deneen, 2015; Schitine et al., 2015). In both these cases the identification of AGPs is possible solely because of their localization, as these cells express the same set of astroglial markers as their progenitors, RGCs (Guillemot, 2007; Minocha et al., 2015). Another known source of cortical mature astrocytes lies in the postnatal SVZ, which also spawns AGPs that migrate out of their germinal zone into the cortex before proliferating and differentiating locally (Ge and Jia, 2016; Molofsky and Deneen, 2015; Schitine et al., 2015; Schiweck et al., 2018; Tien et al., 2012). Importantly, some locally multiplying AGPs also express markers typical for mature astrocytes despite their proliferative capacities (Ge et al., 2012; Tabata, 2015). Collectively, these processes begin between E16.5 and E18.5 and continue well into early postnatal life (for the sake of simplicity, we will henceforth consider that they start at E17.5) (Schiweck et al., 2018). It is generally considered that RGCs constitute the main source of cortical AGPs in embryonic and early postnatal life, while SVZ-descending AGPs become increasingly important at later times (Ge and Jia, 2016; Kriegstein and Alvarez-Buylla, 2009). But regardless of their place and time of origin, AGPs proliferating and differentiating locally constitute the main source of mature astrocytes and enable the expansion of astroglial population in postnatal forebrain (Bandeira et al., 2009; Gallo and Deneen, 2014; Ge and Jia, 2016; Ge et al., 2012; Schiweck et al., 2018).

The molecular events governing transient proliferation of astroglia are not well known, despite their impressive 6 to 8 fold increase observed during postnatal development and achieved through symmetric divisions (Bandeira et al., 2009; Ge and Jia, 2016). Most studies on the topic addressed aberrant astroglial overproliferation in a pathological context, such as formation of gliomas or reactive astrogliosis (Gallo and Deneen, 2014). However, what knowledge exists highlights the role of the mitogen activated protein/ extracellular signal-regulated kinase (MAP/ERK) signaling pathway, potentially dependent on epidermal growth factor receptor (EGFR) activation (Li et al., 2012; Molofsky and Deneen, 2015; Tien et al., 2012). For instance, it was shown in spinal cord that AGPs

proliferate upon upregulation of ERK1/2 and its upstream B-Raf Serine/Threonine-protein (BRAF) (Tien et al., 2012). Similarly, constitutively active MEK1 was shown to stimulate proliferation of GFAP -positive premature cortical astrocytes (Li et al., 2012). In addition some reports have implicated the sonic hedgehog (SHH) signaling pathway in the initiation of AGPs proliferation (Gallo and Deneen, 2014; Wallace and Raff, 1999). Overall, much remains to be elucidated about the molecular signaling pathways orchestrating astroglia proliferation in the context of normal brain development (Molofsky and Deneen, 2015; Tien et al., 2012).

The process of terminal differentiation implies that cells exit the proliferation cycle and turn into functional, quiescent astrocytes (Ge and Jia, 2016; Kriegstein and Alvarez-Buylla, 2009; Molofsky and Deneen, 2015). Although the molecular mechanisms underlying this phenomenon are not fully clear, neuron-derived cytokines are known to promote the expression of markers typical for adult astroglia (Barnabe-Heider et al., 2005; Kanski et al., 2014). Markers commonly used to identify this developmental stage include GFAP, acyl-CoA synthetase bubblegum family member 1 (ACSBG1) or glutamine synthetase (GS), however their reliability is somewhat questionable as they have also been found in proliferative astroglia (Chaboub and Deneen, 2013; Gallo and Deneen, 2014; Tabata, 2015).

Finally, the germinal zone in which astroglia are born determines their ultimate allocation: cells derived from cortical VZ populate the cortex and corpus callosum, those born in LGE migrate to the striatum and piriform cortex, and astrocytes descending from MGE-born progenitors are allocated to ventral pallidum and striatum (Bayraktar et al., 2014; Tsai et al., 2012).

The diverse origins of mature astrocytes briefly described here raises difficult questions. On the one hand, it is remarkable that cells born from various mechanisms differentiate into a cell type, the astrocyte, which integrates into a unified network that performs coherent physiological functions (Molofsky and Deneen, 2015; Sofroniew and Vinters, 2010). On the other hand, because astrogliogenesis begins after neurogenesis is complete, it is impressive that the various processes that give birth to mature astrocytes can coordinate to maintain a proper numerical ratio of astrocyte to neurons (Miller and Gauthier, 2007). This raises the question of the molecular events deciding upon cell fate and numbers. Is there a universal molecular factor that drives progenitors born at various places and time towards a common fate, and does this factor control the proliferation of progenitors and ultimately the number of mature astrocytes born from them?

1.4 Chromatin remodeling BAF complex

The process of cellular differentiation, from progenitor to fully mature and differentiated cell can be understood as a sequence of activation of one or several gene expression programs (Sokpor et al.,

2017). A key aspect in the activation or repression of genetic programs is the process of chromatin remodeling, by which chromatin can be opened into the accessible euchromatin or closed in the form of heterochromatin, respectively enabling or preventing the binding of TFs necessary for the initiation of transcription (Coskun et al., 2012; Hirabayashi and Gotoh, 2010; Juliandi et al., 2010; Narayanan and Tuoc, 2014a; Ronan et al., 2013; Sokpor et al., 2017; Watson and Tsai, 2017). A crucial chromatin regulator is the ATP-dependent SWItch/Sucrose Non-Fermentable (mSWI/SNF), better known as BRG1/BRM-associated factor (BAF), a multi-subunit chromatin remodeling complex, henceforth referred to as BAF complex (Ho and Crabtree, 2010; Wang et al., 1996).

BAF complex from the biochemical side

Biochemically, the BAF complex is a conglomerate of 15 or more different protein subunits, comprising core and peripheral elements (Ho and Crabtree, 2010; Kadoch and Crabtree, 2015; Lessard et al., 2007; Wu et al., 2007). The core subunits of the BAF complex include the ubiquitous BAF47 as well as two scaffolding subunits, BAF170 and/or BAF155, providing structural support for the assembly of the entire BAF complex (Mashtalir et al., 2018; Narayanan et al., 2015; Phelan et al., 1999; Sokpor et al., 2017). In addition, the BAF complex core also comprises one of two ATPase subunits, brahma related gene 1 (BRG1) or brahma (BRM) (Ho and Crabtree, 2010; Lessard et al., 2007; Wang et al., 1996). Peripheral subunits (also referred to as variant subunits) bind to the core subunits, and exhibit far greater diversity (Ho and Crabtree, 2010; Mashtalir et al., 2018). As a result of this diversity, it is believed that hundreds of possible permutations exist in assembling discrete BAF complexes (Narayanan and Tuoc, 2014a; Ronan et al., 2013; Sokpor et al., 2017). Because distinct subunits possess various protein domains (including but not limited to, DNA binding domains as well as bromo- and chromodomains, etc.), the properties of the BAF complex as a whole is a reflection of its particular subunit composition (Ho and Crabtree, 2010; Sokpor et al., 2017; Yoo and Crabtree, 2009). Accordingly, BAF complex interacts with TFs, coactivators, corepressors and histone modifiers in a manner that depends on its assembly (Ho and Crabtree, 2010; Narayanan et al., 2015; Narayanan and Tuoc, 2014a; Wu, 2012). This structural and functional diversity is presumed to endow the BAF complex with the ability to regulate gene expression profiles in a cell lineage-specific manner (Ho and Crabtree, 2010; Sokpor et al., 2017). For example, in embryonic stems cells (ESCs), proliferation and pluripotency are associated with the presence of a BAF complex comprising BRG1, BAF60a/b, BAF155 and BAF250a but not BRM, BAF60c, BAF170 and BAF250b (Ho et al., 2009; Kaeser et al., 2008; Kidder et al., 2009; Sokpor et al., 2017). In another example, neuronal progenitors express BAF45A and BAF53A, which is replaced by BAF45B and BAF53B as progenitors leave mitosis and differentiate into neurons (Ho and Crabtree, 2010; Olave et al., 2002; Yoo et al., 2009). Interestingly, the BAF53B subunit is a key regulator of activity-dependent dendritic morphogenesis

in neurons (Wu et al., 2007). From a mechanistic point of view, it is plausible that all possible combinations of the BAF complex share a similar mode of action, namely the utilization of energy derived from the hydrolysis of ATP by its core subunits BRG1 or BRM to orchestrate structural changes within the chromatin by direct alteration of histones and nucleosomes (Cairns, 2007; Hargreaves and Crabtree, 2011; Yoo and Crabtree, 2009).

The role of BAF complex in regulation of developmental processes

As described above, the diverse subunit composition of the BAF complex enables it to play various roles in a cell lineage dependent manner, with wide ranging implications for embryonic development and tissue formation (Lessard et al., 2007; Matsumoto et al., 2006; Nguyen et al., 2016; Tuoc et al., 2013a). Unsurprisingly, the BAF complex has also been implicated in numerous pathologies, such as developmental disorders and several forms of cancer (Alfert et al., 2019; Kadoch et al., 2017; Sokpor et al., 2017).

Over the last few years, several studies have investigated the involvement of BAF complex in neuronal development in more detail (Sokpor et al., 2017). The most telling illustration of its importance comes from phenotype analysis of conditional mutant mice in which BAF complex expression is entirely lost (Narayanan et al., 2015). This can be achieved by simultaneous deletion of BAF155 and BAF170, which causes the dissociation of the entire BAF complex, followed by ubiquitination and subsequent degradation of its constituent subunits, effectively obliterating any BAF-complex dependent remodeling of chromatin (Narayanan et al., 2015). When the loss of BAF complex is triggered in the telencephalon at E8.5, shortly before the onset of neurogenesis, the telencephalon entirely fails to develop (Narayanan et al., 2015). When activated at E10.5 in cortex, the deletion of BAF complex results in hypotrophic and underdeveloped cortical structures (Narayanan et al., 2015). These results highlight the importance of BAF complex integrity for proper brain development.

The role of BAF complex has also been studied with respect to cellular proliferation and differentiation during neurogenesis (Sokpor et al., 2017). Several reports indicate that NSCs (including NECs and RGCs) express a BAF complex variation whose composition is characteristic of their type, the NSC/neuronal progenitor - npBAF complex (Chen et al., 2012; Ho and Crabtree, 2010; Lei et al., 2015; Li et al., 2010; Meng et al., 2018; Oh et al., 2008). Among the subunits composing this cell-type specific BAF complex, BRG1, BAF45A/D, BAF53A and BAF55A are known to be indispensable for NSCs proliferation (Lessard et al., 2007; Matsumoto et al., 2006; Staahl et al., 2013). Furthermore, the composition of the BAF complex in RGCs determines whether these cells engage in direct or indirect modes of neurogenesis, that is, by directly generating neurons or by producing intermediate progenitors (Tuoc et al., 2013b). Two of the core subunits have been

implicated in this phenomenon, BAF170 and BAF155 (Tuoc et al., 2013b). More precisely, direct neurogenesis is favoured when BAF170 is incorporated into the BAF complex, whereas the dominance of BAF155 promotes indirect neurogenesis (Tuoc et al., 2013b). In addition, the BAF complex has been implicated in various other neurodevelopmental processes, such as neuronal migration, dendritic morphogenesis, neuronal subtype determination and even adult neurogenesis (Lessard et al., 2007; Ninkovic et al., 2013; Olave et al., 2002; Petrik et al., 2015; Tuoc et al., 2017; Wiegreffe et al., 2015; Woodworth et al., 2016; Wu et al., 2007).

Overall, these wide ranging effects of BAF complex on neural development clearly identify it as a potential molecular switch capable of orienting progenitors born at different places and time towards a common fate.

BAF complex in regulation of gliogenic switch and astrocyte differentiation

Although BAF complex is known to have a profound effect on neurogenesis, only few studies have investigated its involvement in astrogliogenesis. What studies exist have relied on deletion of a single BAF complex subunit, have investigated the effect of BAF complex outside of the forebrain, or during adult gliogenesis rather than in embryonic development. As a result the interpretation of these studies in the context of embryonic forebrain astrogliogenesis is haphazard at best.

For example, Matsumoto and colleagues have investigated the effects of *Nestin*-Cre driven deletion of BRG1 on embryonic astrogliogenesis in the cortex and spinal cord (Matsumoto et al., 2006). The loss of BRG1 caused an apparent loss of astrogliogenesis. This was possibly due to a precocious exhaustion of the progenitor pool. Another study examined the role of BRG1 deletion in adult neurogenesis. Surprisingly the study found that deletion of BRG1 in adult NSCs abolishes production of neurons and directs differentiation towards astroglia (Ninkovic et al., 2013). These contradictory findings raise the possibly that BRG1 plays different roles in embryonic versus adult astrogliogenesis. Finally, a previous study from our laboratory (Tuoc et al., 2017) investigated the role of BAF170 in adult neurogenesis and found that deletion of this subunit from adult NSCs in dentate gyrus (DG) leads to the depletion of their pool, and promotes terminal differentiation towards astrocytes.

Although these studies are insufficient to establish what role the BAF complex as a whole plays in embryonic astrogliogenesis, some hints can be found elsewhere in the literature. For example, it has been suggested that BAF complex interacts with the nuclear corepressor complex (N-CoR) through some of its subunits (Underhill et al., 2000). N-CoR was shown to repress astrogliogenesis: indeed, NSCs deprived of N-CoR are unable to proliferate *in vitro*, and their differentiation to GFAP-expressing astroglial cells is enhanced (Hermanson et al., 2002). Furthermore, another chromatin remodeler, the polycomb repressive complex (PcR) has been shown to repress neurogenesis, and thus indirectly enabling astrogliogenesis (Hirabayashi et al., 2009). Interestingly, it is known that BAF

complex can evict PcR from its binding site on chromatin, through which it could potentially antagonize its repression of neurogenesis and putative enhancement of astrogliogenesis (Hirabayashi et al., 2009; Kadoch et al., 2017).

Overall, the existing literature on the involvement of BAF complex on astrogliogenesis is scarce and insufficient to come to a satisfying conclusion. However, the importance of BAF complex on neurogenesis, and the evidence described here led us to anticipate that BAF complex potentially also exerts a powerful regulatory effect on astrogliogenesis.

1.5 Aims and approaches

The literature reviewed so far clearly indicates that astrocytes play indispensable roles in the function of the CNS. Because astrocytes form a connected network, it is crucial that they are generated in appropriate numbers during development to ensure full coverage of the cerebral parenchyma as well as minimal overlap between individual astrocytic domains. These requirements are challenging and imply that the number of astrocytes generated must keep pace with the number of neurons born previously, as neurogenesis typically precedes astrogliogenesis. Adding to that complexity, we have described that cells of the astroglial lineage are born at various locations (MGE, LGE and cortical VZ), both pre- and postnatally, and yet this diverse developmental landscape must culminate in the establishment of an integrated network of mature astrocytes. These observations raise the question of the molecular events guiding astroglial development and led us to wonder about the existence of a unique molecular regulator capable of guiding progenitors born at various time and places towards a common fate as well as ensuring the formation of an appropriate number of mature astrocytes with respect to the existing neuronal population. Such a molecular mechanism may involve the powerful chromatin remodeling BAF complex, which is already known to exert control over proliferation and differentiation in the neural lineage.

Therefore, in the present thesis, we investigated the role of BAF complex in astroglial and neuronal lineages. To this end, we first investigated the expression of several BAF subunits (namely; BRG1, BAF155, BAF170, BAF60a and BAF250a) in both lineages using immunohistochemistry in distinct areas of perinatal brain tissue. Progenitors of the astroglial lineage were identified by combined expression of NFiA and GLAST together with careful analysis of their localization with respect to known germinal zones. This approach enabled us to identify unique BAF subunit expression dynamics characteristic of astroglial cells, which clearly differed from the neuronal lineage.

Subsequently, we investigated the function of BAF complex in astrogliogenesis. To this end, we used a double conditional knockout (dcKO) mouse model in which expression of BAF155 and BAF170 was lost. As described above, the loss of these two core subunits is sufficient to abolish the complete BAF

complex within affected cells. Cre-dependent BAF subunit deletion was driven by the *hGFAP* promoter, enabling us to target late cortical neurogenesis and dorsal and ventral astrogliogenesis. Using a combination of immunohistochemistry, EdU incorporation assay, *in utero* electroporation and RNA sequencing, we describe the impact of BAF complex depletion in both neuronal and astroglial lineages, finding a profound numerical imbalance between these populations.
Finally, we sought to identify the molecular pathways that BAF complex could potentially influence to exert its effects on the abundance of astroglial cells. To this end, we used RNA sequencing and RNA *in situ* hybridization to single out a molecular factor known to be involved in astroglial proliferation which was massively upregulated in our dcKO model. By means of pharmacological inhibition, we then provide the first recorded evidence of the interaction of this molecular factor with the BAF complex in this cell lineage.

The results described herein provide convincing evidence of the role of BAF complex in regulating the proliferation, differentiation and number of cells of the astroglial lineage. Based on this novel evidence, we propose an original model of BAF complex function, whereby a cell lineage-dependent BAF complex subunit composition acts as a guardian of the balance between neuronal and astroglial populations in the developing mouse brain.

Chapter 2

Materials and Methods

2.1 Animals and animal procedures

All animal procedures described in the present doctoral thesis were carried out in accordance with Directive 2010/63/EU of the European Parliament and the Council on the protection of animals used for scientific purposes and with the German Animal Protection Law.
All mice were housed with a 12 hours (h) light/dark circadian cycle with freely accessible food and water. The highest efforts were made to refine housing conditions and reduce the numbers of animals used for the experimental procedures.
For all studies carried out on embryonic stages the day of detection of vaginal plug (at noon) is equivalent to the embryonic day (E) 0.5. For experiments involving postnatal stages the day of birth was considered as postnatal day (P) 0.

Investigated animals

Transgenic colonies

By means of Cre/loxP system (Sauer, 1998), five different BAF155/BAF170 mutant mouse lines were generated and used for the experiments presented in this study;

- *BAF155_BAF170*dcKO_*hGFAP* line (genotype: *BAF155*$^{fl/fl}$, *BAF170*$^{fl/fl}$, Cre+) carrying *hGFAP* promoter driven, Cre dependent BAF155 and BAF170 dcKO, henceforth referred to as either *hGFAP*-Cre dcKO or dcKO;
- *BAF155_BAF170*dcKO_tdTomato_*hGFAP* reporter line (genotype: *BAF155*$^{fl/fl}$, *BAF170*$^{fl/fl}$, *ROSA*$^{+/-}$, Cre+) exhibiting *hGFAP* promoter driven, Cre dependent BAF155 and BAF170 dcKO coupled with tdTomato (tdTOM) red fluorescent protein expression, also referred to as either *hGFAP*-Cre dcKO tdTomato or dcKO.

Because of mutation severity, animals from both of the above described dcKO lines were dying 3-4 days after birth.

- *BAF155_BAF170*Het_tdTomato_*hGFAP* reporter line (genotype: *BAF155*$^{fl/+}$, *BAF170*$^{fl/+}$, *ROSA*$^{+/-}$, Cre+) with *hGFAP* promoter driven, Cre dependent heterozygous loss of BAF155 and BAF170 coupled with tdTOM red fluorescent protein expression, henceforth described either as *hGFAP*-Cre Het tdTomato or as Het;
- *BAF170*cKO_*hGFAP* line (genotype: *BAF170*$^{fl/fl}$, Cre+) carrying Cre dependent conditional loss of BAF170 driven by *hGFAP* promoter, henceforth referred to as BAF170KO;
- *BAF155_BAF170*dcKO_*Olig2* line (genotype: *BAF155*$^{fl/fl}$, *BAF170*$^{fl/fl}$, Cre+) with *oligodendrocyte transcription factor 2* (*Olig2)* promoter driven, Cre dependent BAF155 and BAF170 dcKO, further described as *Olig2*-Cre dcKO; because of mutation severity animals from this line were dying at birth.

Generation of mouse lines

Transgenic colonies were obtained by crossing previously described parental colonies: *BAF155*$^{fl/fl}$ (Choi et al., 2012), *BAF170*$^{fl/fl}$ (Tuoc et al., 2013b), *hGFAP*-Cre (Zhuo et al., 2001), *Olig2*-Cre (Zawadzka et al., 2010) and *ROSA*-tdTomato (Ai9 Cre reporter allele) (Madisen et al., 2010). All mice were maintained in a C57BL6/J genetic background.

In brief, *BAF155_BAF170*dcKO_*hGFAP* and *BAF170*cKO_*hGFAP* animals were obtained by crossing 2 intermediate lines: *BAF155*$^{fl/fl}$_*BAF170*$^{fl/fl}$ (line with homozygous flox of *BAF155* and *BAF170* alleles) and *BAF155*$^{fl/+}$_ *BAF170*$^{fl/fl}$_*hGFAP* (line with heterozygous flox of *BAF155* allele, homozygous flox of *BAF170* allele and Cre expression under control of *hGFAP* promoter). The *BAF155*$^{fl/fl}$_*BAF170*$^{fl/fl}$ line was initially generated by crossing *BAF155*$^{fl/fl}$ line with *BAF170*$^{fl/fl}$ animals. The resulting *BAF155*$^{fl/+}$_ *BAF170*$^{fl/+}$ mice were crossed together and animals with homozygous flox of *BAF155* and *BAF170* alleles were chosen for the final steps of *BAF155_BAF170*dcKO_*hGFAP* line generation. For the creation of the intermediate *BAF155*$^{fl/+}$_ *BAF170*$^{fl/fl}$_*hGFAP* line, *BAF155*$^{fl/fl}$_*BAF170*$^{fl/fl}$ animals were crossed with *hGFAP*-Cre line. The resulting mice heterozygous for *BAF155* and *BAF170* flox (*BAF155*$^{fl/+}$_ *BAF170*$^{fl/+}$) and positive for Cre expression (*BAF155*$^{fl/+}$_ *BAF170*$^{fl/+}$_*hGFAP*) were crossed to each other for the final generation of *BAF155*$^{fl/+}$_*BAF170*$^{fl/fl}$_ *hGFAP* line or *BAF170*cKO_*hGFAP* line.

*BAF155_BAF170*dcKO_tdTomato_*hGFAP* reporter line was created through the final crossing of 2 intermediate lines: *BAF155*$^{fl/fl}$_*BAF170*$^{fl/fl}$_*Rosa*$^{+/+}$ (line with homozygous flox of *BAF155* and *BAF170* alleles and homozygous for *ROSA*) and the previously described *BAF155*$^{fl/+}$_ *BAF170*$^{fl/fl}$_*hGFAP*. In order to generate *BAF155*$^{fl/fl}$_ *BAF170*$^{fl/fl}$_*Rosa*$^{+/+}$ line, mice from above characterized *BAF155*$^{fl/fl}$_ *BAF170*$^{fl/fl}$ line were crossed to *ROSA*-tdTomato animals. The generated *BAF155*$^{fl/+}$_*BAF170*$^{fl/+}$_

ROSA$^{+/-}$ mice were crossed to each other and the resulting individuals with homozygous flox of *BAF155* and *BAF170* alleles and homozygous for *ROSA* were chosen for final crossings in order to obtain *BAF155_BAF170*dcKO_ tdTomato_*hGFAP* line.

*BAF155_BAF170*Het_tdTomato_*hGFAP* reporter line was generated by crossing above described *BAF155*$^{fl/+}$_ *BAF170*$^{fl/+}$_*hGFAP* mice to *ROSA*-tdTomato mice.

*BAF155_BAF170*dcKO_*Olig2* mutation was achieved by crossing of 2 intermediate lines: the previously described *BAF155*$^{fl/fl}$_*BAF170*$^{fl/fl}$ and *BAF155*$^{fl/+}$_ *BAF170*$^{fl/+}$_*Olig2* (line with heterozygous flox of *BAF155* allele, homozygous flox of *BAF170* allele and Cre expression under control of *Olig2* promoter). The animals of *BAF155*$^{fl/+}$_ *BAF170*$^{fl/+}$_*Olig2* intermediate line were generated by crossing *BAF155*$^{fl/fl}$_ *BAF170*$^{fl/fl}$ mice to *Olig2*-Cre animals.

Experimental and control individuals

Animals were genotyped by PCR as described in (Madisen et al., 2010; Narayanan, 2017; Tuoc et al., 2013b). *BAF155_BAF170*dcKO_*hGFAP* (genotype: *BAF155*$^{fl/fl}$, *BAF170*$^{fl/fl}$, Cre+), *BAF155_BAF170* dcKO_tdTomato_*hGFAP* (genotype: *BAF155*$^{fl/+}$, *BAF170*$^{fl/+}$, *ROSA*$^{+/-}$ Cre+), *BAF170*cKO_*hGFAP* (genotype: *BAF170*$^{fl/fl}$, Cre+) and *BAF155_BAF170*dcKO_*Olig2* (genotype: *BAF155*$^{fl/fl}$, *BAF170*$^{fl/fl}$, Cre+) were used as the test specimens whereas the sibling animals of *BAF155_BAF170*dcKO_*hGFAP,* which did not exhibit the Cre recombinase mutation (regardless of *BAF155* and *BAF170* alleles being floxed) as well as *BAF170*$^{fl/fl}$ mice served as controls and are henceforth referred to as wild type (WT). Because of tdTOM tracing purposes in a few exceptional cases *BAF155_BAF170*Het_tdTomato_ *hGFAP* mice were used as control probes (whenever stated). Both genders of embryos and pups were subjected to the embryonic and early postnatal studies. Only male mice were selected for stereotaxic cortical stab experiments.

Ethynyl deoxyuridine (EdU) thymidine analogue injection

EdU thymidine analogue injection was performed for the purpose of labelling proliferative cells, as previously described in (Chehrehasa et al., 2009; Flomerfelt and Gress, 2016; Vega and Peterson, 2005). EdU powder (ThermoFisher Scientific) was dissolved in phosphate buffered saline (PBS) with a pH of 7.2 (ThermoFisher Scientific) for a final concentration of 1mg/ml. The solution was pre-warmed to 37^{o}C prior to animal application. P3 mouse pups were administered a single intraperitoneal (IP) EdU injection with a final dosage of 3 mg/kg of mouse body weight. Animals were sacrificed 30 minutes (min) after injection. Collected brain tissues were subsequently analyzed for EdU incorporation (see: Chapter 2. Materials and Methods. 2.4).

GLI antagonist (GANT61) inhibitor injection

We performed GANT61 injections in order to effectively block glioma associated oncogene 1 (GLI1) mediated transcription in treated mice. GANT61 was used as GLI1 antagonist as previously described in (Lauth et al., 2007). The protocol of injection was modified from (Huang et al., 2014; Samanta et al., 2015). The GANT61 (Enzo Life Sciences) was prepared at the concentration of 0.5mg/ml in sterile dimethyl sulfoxide (DMSO) (Merck) with constant mixing for 2h to accomplish an effective dissolution. The inhibitor solvent DMSO alone was used as a vehicle in sham injections. Mice crossed for the purpose of breeding dcKO and WT were daily injected IP with vehicle (250 µl) or inhibitor (250 µl; 8.5mg/kg of mouse body weight). The injections were started at E15.5 stage of gestation and the experiment was terminated after 4 consecutive days of drug administration. Late E18.5 brain tissues were collected, fixed and further analyzed by immunohistochemical methods (described in: Chapter 2. Materials and Methods. 2.4).

***In utero* electroporation**

The method of *in utero* DNA injection and electroporation was adapted from (Saito, 2006; Saito and Nakatsuji, 2001). The purpose of the experiment was to trace the postnatal location of cells differentiating from late cortical RGCs.

Injected DNA

As in (Minocha et al., 2015), the plasmid encoding for the enhanced green fluorescent protein (EGFP) expression under the control of cytomegalovirus early enhancer/chicken β actin (*CAG*) promoter - *pCAG*-IRES-EGFP (kindly provided by Dr. Francois Guillemot) served as an injection DNA. For the purpose of amplification the plasmid was transformed to *E. coli* DH5α strain competent bacteria (K 12 strain, Invitrogen). In short, following 10min incubation on ice, 10ng of plasmid were mixed with 200µl of competent bacteria. After 30min of incubation on ice, the bacteria were subjected to 45 seconds (sec) heat shock performed at 42^{o}C. After that, the mixture was rapidly chilled on ice, enriched with 500µm of super optimal catabolite (SOC) medium (ThermoFisher Scientific) and incubated with shaking for 1h at 37^{o}C. Subsequently bacteria were plated on lysogeny broth (LB) agar screening plates containing ampicillin (50µg/ml of ampicillin (Sigma Aldrich) in LB-agar medium: 0.5% Yeast extract (Roth), 1% Peptone (Roth), 1% sodium chloride (NaCl) (Roth), 1.5% Agar (Roth) in deionized water (dH2O), pH 7.0) and incubated overnight at 37^{o}C. Single colonies of bacteria isolated from the plate were afterwards subjected to an overnight culture in ampicillin supplemented LB medium (50µg/ml of ampicillin in 0.5% Yeast extract, 1% Peptone, 1% NaCl in

dH2O, pH 7.0) with constant shaking at 37°C. Following the mini scale preparation (QIAprep Miniprep kit, Qiagen) performed according to the manufacturer instructions, the isolated plasmid was assessed by the control restriction digestion (with NotI (New England BioLabs) and SalI (New England BioLabs) restriction enzymes, following manufacturers protocol) and the bacterial glycerol stock was prepared (600µl of bacteria mixed with 200µl of autoclaved 80% glycerol (Roth)) and frozen at -80°C. For the purpose of purification of higher quantity and better quality DNA desired for the *in utero* injection, the plasmid was amplified during an overnight culture inoculated from the previously prepared glycerol stock and subsequently maxi scale purified with the purification kit (EndoFree Plasmid Purification Kit, Qiagen) according to the manufacturer's instructions. Plasmid DNA was dissolved in TE buffer (EndoFree Plasmid Purification Kit, Qiagen) to the final concentration of 2.5µg/µl. For the purpose of visualizing the injection site, right before surgery, the endotoxin free plasmid solution (2.5µg/µl) was mixed with 10% Fast Green (FG) (Fast Green FCF, Sigma Aldrich) ((w/v) in PBS) in the proportion of 2:1.

Injected animals

Late E16.5-timed pregnant mice crossed for the *BAF155_BAF170*dcKO_*hGFAP* mutation (*BAF155*$^{fl/fl}$_*BAF170*$^{fl/fl}$ crossed to *BAF155*$^{fl/+}$_*BAF170*$^{fl/fl}$_*hGFAP* (cre+)) were used for this surgical procedure.
Perioperative analgesia was achieved by subcutaneous injection of Carprofen (5mg/kg mouse body weight, Rimadyl, Pfizer). After approximately 30min the mouse was transferred to a sealed container where anesthesia was initiated by inhalation of 5% isoflurane (Forene, Abbvie) in pure oxygen. Once sedated, the animal was quickly placed in a supine position on a 37°C warm thermostatic heating pad (ATC 1000, World Precision Instruments) where anesthesia was maintained with 1.5-2.5% isoflurane in pure oxygen (flow speed: 0.8L/min) inhaled through a snout mask (Kopf Instruments). The depth of anesthesia and analgesia was assessed through the whole time of surgical procedure by monitoring of the rate of breathing and checking paw-pinch reflexes (Adams and Pacharinsak, 2015). Ointment (Bepanthen, Bayer) was applied to protect the eyes from desiccation. The abdominal skin was disinfected with an antiseptic (Kodan, Shülke) and subsequently incised along the midline for a length of about 2.5cm (Figure 2). The abdomen was covered with sterile gauze (Nobatop 8, Nobamed) with a small opening hole manually excised to access the site of the surgery. A cut of about 2cm through the *linea alba* and peritoneum allowed access to the abdominal cavity. The embryos were gently pulled out on gauze. The gauze, exposed internal organs and the uterine horns containing the embryos were continuously moisturized with sterile and pre-warmed 0.9% sodium chloride (NaCl) (NaCl 0.9%, B. Braun). Tapered capillaries pre-pulled from borosilicate glass (GB150F-8P, Science Products) served as injection pipettes. The capillaries were heated and pulled actively by a micropipette puller (P-97, Sutter Instruments) with the conditions depending on

specific batch of used borosilicate glass. Before used, the capillaries were cut under the microscope (Axioscope 2 mot+, Zeiss) to a tip diameter of around 20µm. One µl of plasmid/FG solution (2:1) was pressure injected into the lateral ventricle of the right hemisphere of each embryo (Figure 2), using a pedal-controlled microinjector (PDES-02DX picospritzer, Npi). The head of each embryo was subsequently clasped with tweezer-like 5mm circular electrodes (CUY650P5, Nepa Gene) and the cathode was placed to the side of the developing somatosensory cortical area (Figure 2). Five 50ms long pulses of 35mV separated by 900ms intervals were delivered to each embryo. The electric field was generated by the pedal controlled electroporator (NEPA21, Nepa Gene). Afterwards the embryos were moisturized with sterile and pre-warmed 0.9% NaCl and subsequently returned into the peritoneal cavity. The abdominal muscles were sutured with the polyester surgical thread (Ethibond excel 6951H, Ethicon) and the skin wound was closed by clipping (AutoClip staple system, FST) (Figure 2). The animal was placed in the pre-warmed cage allowing for recovery. For analgesic and anti-inflammatory post-surgical care Carprofen was subcutaneously injected every 24h for 2 consecutive days and Metamizol (1.5g/ml, Novaminisulfon, Zentiva) was given in drinking water.

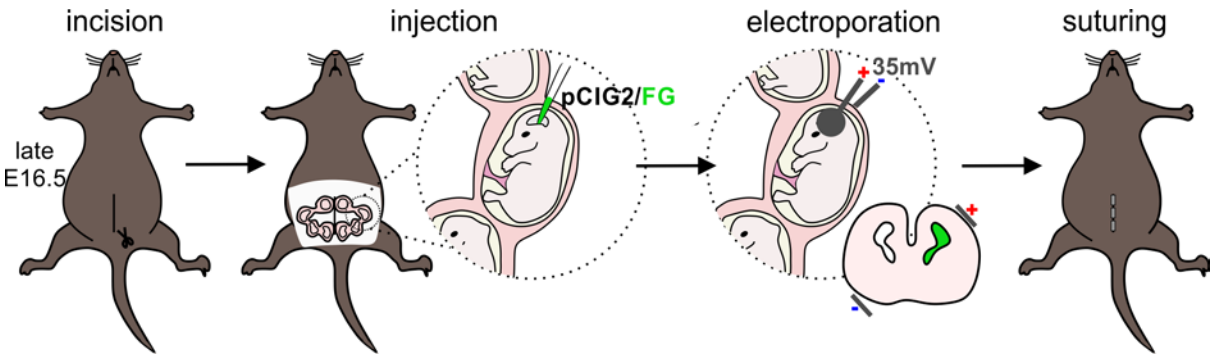

Figure 2 | Scheme depicting the procedure of *in utero* plasmid injection and electroporation. The abdomen of E16.5–time pregnant mouse was incised. The pCIG2/FG solution was injected to the lateral ventricle of each embryo. The specific orientation of electrodes allowed for the electroporation of the ventricle surface of the somatosensory area. After returning the embryos into abdominal cavity the mouse was sutured and allowed to recover. Adapted and modified from (Manfredsson, 2016). FG, Fast Green; pCIG2, *pCAG*-IRES-EGFP.

Embryos were left *in utero* till delivery. Electroporated brain tissue was collected from P3 pups and the EGFP expression was assessed prior-fixation by epifluorescent stereomicroscope (SM21500, Nicon). Only EGFP positive brains were chosen for fixation, sectioning and further immunostaining analysis (protocols described in: Chapter 2. Materials and Methods. 2.2 and 2.4).

Stereotaxic cortical stab injury

A blade stab lesion procedure was performed in order to induce reactive astrocytes (Figure 3) in adult animals (Allahyari and Garcia, 2015).

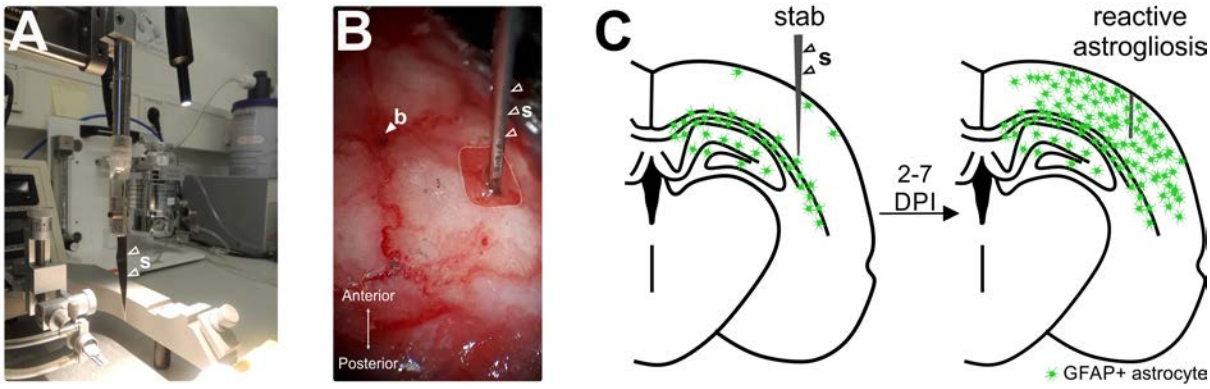

Figure 3 | Scheme depicting the procedure and experimental paradigm of stereotaxic cortical stab injury. (A) Surgical scalpel blade (indicated by empty arrows) attached to the operator arm of stereotaxic frame. (B) Small craniotomy over the area of somatosensory cortex. Full arrow indicates Bregma, empty arrows indicate lowered scalpel blade. The anterior and posterior directions are indicated by a two headed arrow. (C) Experimental paradigm illustrating the generation of GFAP positive reactive astrocytes after 2-7 days from stab injury operation. b, Bregma; DPI, day post-injury; s, surgical scalpel blade.

Stabbed animals

P60 male mice (*BAF170*$^{fl/fl}$ with C57BL6/J background) were used for this surgical procedure.

Perioperative analgesia was achieved by subcutaneous injection of Carprofen (5mg/kg mouse body weight, Rimadyl, Pfizer). After approximately 30min from analgesic administration the mouse was transferred to the secure lid container and exposed to the inhalant mixture of 5% isoflurane (Forene, Abbvie) in pure oxygen for the purpose of the initiation of anesthesia. The sedated animal was rapidly placed on a 37°C warm thermostatic heating plate (ATC 1000, World Precision Instruments) and the head was fixed in the small animal stereotaxic frame (Kopf Instruments). The anesthesia was continued by the administration of 1.5-2.5% isoflurane in pure oxygen (flow speed: 0.8L/min) via snout mask (Kopf Instruments). The depth of anesthesia was assessed by the monitoring of the rate of breathing and checking paw-pinch reflexes (Adams and Pacharinsak, 2015). The eyes were prevented from dehydration by the direct ointment application (Bepanthen, Bayer). The head was shaved, disinfected with an antiseptic (Kodan, Shülke) and subsequently administered to the local analgesia by subcutaneous lidocaine injection (2% Xylocaine, AstraZeneca). The scalp was opened by a small incision carried in parallel to anterior posterior axis. The periosteum tissue was removed and

the somatosensory area was delineated following the coordinates of -1.5 to -2mm caudal and 3.5 to 4mm medial from Bregma (Paxinos and Franklin, 2001). A small craniotomy was performed over the barrel cortex and a surgical scalpel blade (No. 11, Martor) was slowly lowered into the brain to a depth of 3mm using the arm of stereotaxic frame (Figure 3A and B). After retraction of the blade the surface of the brain was moisturized with a few drops of a pre-warmed and sterile 0.9% NaCl. Occasionally occurring bleedings were stopped by hemostatic gel sponge (Gelasypt, Sanofi). Afterwards the scalp was surgically stitched by polyamide surgical suture (6.0/697H, Ethilon) and the animal was placed in the pre-warmed cage allowing for recovery.

For analgesic and anti-inflammatory post-surgical care Carprofen was subcutaneously injected every 24h and Metamizol was administered in drinking water (1.5g/ml, Novaminisulfon, Zentiva). Stabbed animals were perfused at 2, 4 and 7 days post injury (DPI). The isolated brain slices were used for immunohistochemical stainings. Protocols for perfusion and immunohistochemical analysis are described below (see: Chapter 2. Materials and Methods. 2.2 and 2.4).

2.2 Tissue fixation and processing

Embryonic and early postnatal tissue

E13.5–P3 brain tissues were used for the purpose of the embryonic and early postnatal studies.

Following the opening of the skull, E15.5-P3 brains were extracted in chilled diethyl pyrocarbonate (DEPC) treated PBS (0.1% (v/v) DEPC/PBS) (PBS/DEPC). Because of small size and fragility the skull dissection step was omitted for E13.5 stages and the whole embryo head was used for further steps of this protocol. Residual blood was removed by rinsing with chilled PBS/DEPC. Collected tissues were transferred to ice-cold 4% paraformaldehyde (PFA) (w/v) in 0.1M phosphate buffer (PB) pH 7.4 (4% PFA/PB) for: 4h (for E13.5 stage), 2h (for E15.5 stage), 2.5h (for E17.5 stage), 3h (for E18.5 and P0 stages) or 3.5h (for P3 stage) allowing for immersion fixation. Fixed tissues were rinsed with chilled PBS/DEPC and dehydrated by an overnight incubation in 25% sucrose (w/v) in PBS/DEPC at 4^{o}C. The following day, the tissues were placed in embedding medium for cryopreservation (O.C.T. Compound, Sakura) and stored at -20^{o}C until sectioning.

For brain coronal sections preparation, cryopreserved tissues were cut to a thickness of 14µm (for embryonic brains) or 18µm (for postnatal brains) with a cryostat (CM 3050S, Leica). Brain slices were collected on adhesion microscope slides (Superfrost Plus, ThermoFisher Scientific) and used for stainings (see: Chapter 2. Materials and Methods. 2.4).

Adult brains

Adult brains were used for the reactive astrogliogenesis investigation or BAF complex subunits expression pattern studies. P60 non-injured and stab injured mice were perfused before the brain tissue dissection. At the day of experiment termination, mice were subjected to an overdose of Ketamine (10%, Medistar) injected IP. Once immobility and sedation were achieved, animals were transcardially perfused with 10% sucrose solution ((w/v) in dH_2O) for 10min and subsequently with 4% PFA/PB for 30min. Pre-fixed brains were isolated from the skull and subjected to an overnight fixation in 4%PFA/PB at 4°C. Afterwards fixative was removed, the brains were placed in sodium azide-containing PB (0.05% sodium azide (v/v) PB) and stored at 4°C until sliced.
Containing somatosensory cortex medial regions of perfused brains were isolated and sliced through the lesions area (and corresponding areas for non-injured mice) into 30µm thick consecutive coronal sections using a vibratome (VT1200S, Leica). Prepared slices were collected in sodium azide treated PB and stored at 4°C until free floating immunohistochemical analysis (described in: Chapter 2. Materials and Methods. 2.4).

2.3 Tissue preservation

E17.5 and P3 embryonic and early postnatal cortical tissue as well as P3 tissue of basal ganglia area were isolated and cryopreserved for the purpose of further transcriptome and protein investigations. Cortex and basal ganglia were separated according to the protocols described in (Beaudoin et al., 2012; Schildge et al., 2013).
Briefly, following decapitation E17.5 and P3 brains were dissected in chilled PBS/DEPC. The meninges, olfactory bulbs, thalamus and cerebellum were removed and the hemispheres were separated from each other. Subsequently following anatomical differences the cortical structure was removed from the basal ganglia. Isolated tissues were frozen in liquid nitrogen and stored at -80°C until used. E17.5 cortex was isolated chiefly by Linh Pham.

2.4 Staining methods

Fluorescent immunohistochemistry (on slide)

The following protocol was used for immunohistochemical analyses performed on cryosectionned embryonic and early postnatal brain slices collected on microscope slides and preserved at -20°C.

Primary antibodies

The following monoclonal (mAb) and polyclonal (pAb) primary antibodies were used in this protocol (corresponding dilutions and commercial sources shown in brackets): anti-ACSBG1 rabbit pAb (1:500, ab65154, Abcam), anti-BAF60a mouse mAb IgG_{2a} (1:200, 611728, BD Biosciences), anti-BAF155 mouse mAb IgG_1 (1:100, sc-48350, Santa Cruz Biotechnology), anti-BAF170 mouse mAb IgG_1 (1:100, sc-17838, Santa Cruz Biotechnology), anti-BAF250a mouse mAb IgG_1 (1:100, sc-32761, Santa Cruz Biotechnology), anti-BLBP rabbit pAb (1:200, ABN14, Merck Millipore), anti-BRG1 mouse mAb IgG_1 (1:100, sc-17796, Santa Cruz Biotechnology), anti-CLEAVED CASPASE-3 rabbit pAb (1:200, #9661, Cell Signaling), anti-GFAP mouse mAb IgG_1 (1:500, G3893, Sigma Aldrich), anti-GFAP rabbit pAb (1:400, Z0334, DakoCytomation), anti-GLAST guinea pig pAb (1:500, Af-1000-1, Frontier Institute), anti-GS mouse mAb IgG_{2a} (1:200, MAB302, Merck Millipore), anti-Ki67 mouse mAb IgG_1 (1:20, NCL-L-Ki67-MM1, Leica Biosystems), anti-NFiA rabbit pAb (1:200, HPA006111-100UL, Sigma Aldrich), anti-SATB2 mouse mAb IgG_1 (1:200, ab51502, Abcam), anti-SOX9 rabbit pAb (1:1000, AB5535, Merck Millipore).

Secondary antibodies

All secondary antibodies used in this protocol were diluted to 1:400. The list of applied secondary antibodies is as follows (corresponding commercial sources shown in brackets): goat anti-mouse IgG_1 Alexa Fluor 488 (A-21121, Invitrogen), goat anti-mouse IgG_{2a} Alexa Fluor 488 (A-21131, Invitrogen), goat anti-mouse IgG_1 Alexa Fluor 568 (A-21124, Invitrogen), goat anti-mouse IgG_1 Alexa Fluor 647 (A-21240, Invitrogen), goat anti-mouse IgG_{2a} Alexa Fluor 633 (A-21136, Invitrogen), goat anti-rabbit Alexa Fluor 488 (A-21042, Invitrogen), goat anti-rabbit Alexa Fluor 568 (A-11011, Invitrogen), goat anti-rabbit Alexa Fluor 647 (A-21244, Invitrogen), goat anti-guinea pig Alexa Fluor 488 (A-11073, Invitrogen), goat anti-guinea pig Alexa Fluor 568 (A-11075, Invitrogen), goat anti-guinea pig Alexa Fluor 633 (A-21105, Invitrogen).

Staining procedure

Fourteen and 18µm thick cryopreserved sections (see: Chapter 2. Materials and Methods. 2.2) were thawed and washed with 0.01M PBS. Potential non-specific antibodies binding sites were blocked and the cell membranes were permeabilised by an 1h incubation with 5% normal goat serum (Biozol) and Triton X 100 (Roth) in PBS (0.1% (v/v) Triton X 100/PBS) (blocking solution). Next, primary antibodies diluted in blocking solution were applied and incubated overnight at 4°C. The following day the sections were thoroughly washed with 0.01M PBS and subsequently incubated at the room temperature (RT) for 2h with fluorophore-conjugated secondary antibodies diluted in blocking solution. After that, slides were rinsed with 0.01M PBS and the nuclei of cells were

counterstained by 5min incubation with 0.1% 4' 6-diaminodino-2-phenylindole (DAPI) (Molecular Probes) (v/v) in blocking solution. Ultimately, the slides were washed with 0.01M PBS, drained and closed by mounting the coverslips (Menzel, ThermoFisher Scientific) with an aqueous mounting medium (Aqua-Poly/Mount, Polysciences). Immunostained slides were stored at 4^{o}C until described further in this section fluorescence signal acquisition.

Fluorescent immunohistochemistry (free floating)

Free floating fluorescent immunohistochemistry was used for the detection of GFAP expression in 30µm thick coronal sections of perfusion fixed (see: Chapter 2. Materials and methods. 2.2) adult brains so as to examine reactive astrogliogenesis. Additionally we used this procedure to investigate the expression of BAF complex subunits in protoplasmic astrocytes of adult (P60) WT animals.

Primary antibodies

The following monoclonal (mAb) and polyclonal (pAb) primary antibodies were used in this protocol (corresponding dilutions and commercial sources shown in brackets): anti-ACSBG1 rabbit pAb (1:500, ab65154, Abcam), anti-BAF60a mouse mAb IgG_{2a} (1:200, 611728, BD Biosciences), anti-BAF170 mouse mAb IgG_1 (1:100, sc-17838, Santa Cruz Biotechnology), anti-BAF250a mouse mAb IgG_1 (1:100, sc-32761, Santa Cruz Biotechnology), anti-BRG1 mouse mAb IgG_1 (1:100, sc-17796, Santa Cruz Biotechnology), anti-GFAP mouse mAb IgG1 (1:500, G3893, Sigma Aldrich) and anti-GFAP rabbit pAb (1:400, Z0334, DakoCytomation).

Secondary antibodies

All secondary antibodies used in this protocol were diluted to 1:500. The list of applied secondary antibodies is as follows (corresponding commercial sources shown in brackets): goat anti-mouse IgG1 Alexa Fluor 488 (A-21121, Invitrogen), goat anti-mouse IgG1 Alexa Fluor 568 (A-21124, Invitrogen), goat anti-mouse IgG_1 Alexa Fluor 647 (A-21240, Invitrogen), goat anti-mouse IgG_{2a} Alexa Fluor 633 (A-21136, Invitrogen), goat anti-rabbit Alexa Fluor 488 (A-21042, Invitrogen).

Staining procedure

The 4^{o}C stored slices were successively washed with 0.01M PB (pH 7.4), 0.0005M Tris buffer (Sigma Aldrich) (TB) (pH 7.6), 0.05M TB containing 0.9%NaCl (TBS) (pH 7.6) and Triton X 100 treated TBS (0.5% (v/v) Triton X 100/TBS, pH 7.6) (TBST) 2 times 15min each at RT. After that, the slices were subjected to the 1.5h blocking of non-specific antigens with 10% normal goat serum in bovine serum albumin (BSA, Sigma Aldrich) treated TBST (0.25% (v/v) BSA/PBS) (blocking solution) on a shaking

plate. Subsequently, the tissues were incubated overnight at 4°C with constant shaking with primary antibodies diluted in blocking solution. The following day the slices were washed 5 times with TBST buffer and subsequently incubated with the fluorophore-conjugated secondary antibodies diluted 1:500 in TBST at RT for 2h. For the purpose of nuclei visualization stained slices were treated with DAPI (Molecular Probes) diluted 1:1000 in TBS buffer for 5min at RT. Following the successive steps of rinsing with TBS buffer (1 time) and TB buffer (3 times), the immunostained slices were mounted and coverslipped with mounting medium (Aqua-Poly/Mount, Polysciences). The slides were stored at 4°C until microscopy.

EdU detection

The experiment of EdU detection was performed on cryopreserved embryonic and early postnatal slices isolated from animals subjected to the analogue injection. EdU was stained by means of EdU detection kit (Click-IT plus EdU Alexa Fluor 647 Imaging Kit, ThermoFisher Scientific). The experimental procedure was carried out according to manufacturer's protocol. Once stained for EdU, the sections were subjected to immunohistochemical analysis so as to perform colocalization studies.

Chromogenic *in situ* hybridization

The chromogenic *in situ* hybridization experiment was carried out in order to stain Gli1 transcripts by means of their detection with digoxigenin (DIG)-labelled Gli1 specific complementary (c) RNA probes (riboprobes). The experiment was performed on embryonic and early postnatal brain slices collected on microscope slides following cryosectioning and cryopreservation. The protocol was adapted from (Wagener et al., 2010).

In order to minimize the risk of RNA degradation all possible steps were taken to remove RNA-digesting RNAses from the experimental environment. All solutions used for this procedure were treated with DEPC (to the final concentration of 0.1% of DEPC) and subsequently autoclaved. All glassware and slide holders were baked for 4h in 180°C heated laboratory oven (Memmert, 400) one day before use. The experiment was carried out in RNAse free conditions from the moment of *in vitro* transcription reaction on.

DIG-labelled probe generation

Gli1 specific single strand antisense and sense DIG-labelled riboprobes were generated from the pBluescript vector containing the insert of 1266bp long fragment of mouse Gli1 cDNA (pm-Gli1)

kindly provided by Prof. Heidi Hahn and Dr. Anja Uhmann (Pelczar et al., 2013). As for the previously described *pCAG*-IRES-EGFP (see: Chapter 2. Materials and Methods. 2.1), the plasmid was amplified in *E. coli* DH5α strain competent bacteria and subsequently maxi scale purified by means of a purification kit (Plasmid Maxi Kit, Qiagen). Isolated circular pm-Gli1 plasmid DNA was subsequently subjected to linearization carried out by an enzymatic digestion with the adequate restriction enzymes (NotI and HindIII (ThermoFisher Scientific); NotI digested plasmids were used for the antisense probe generation whereas plasmid linearized with HindIII served further for the sense probe preparation). Restriction digestion reactions were run following the instructions provided by the enzyme producer. After the completion of enzymatic reaction the digestion mix was loaded onto a 1.5% agarose gel (1.5% agarose (Roth) in Tris /Borate/ Ethylenediaminetetraacetic acid (EDTA, MP Biomedicals LLC) (TBE) buffer). Following a short electrophoresis (performed at 90V), linearized forms of plasmid were extracted by purification kit (NucleoSpin Gel and PCR Clean-up, Maherey-Nagel). For the purpose of DIG-labeled sense and antisense probe preparation, purified linearized pm-Gli1 plasmid forms were subjected to an *in vitro* transcription procedure in RNAse free conditions. For the antisense Gli1 probe generation the *in vitro* transcription reaction was performed with the T3 polymerase (Roche). For the purpose of the sense Gli1 probe preparation the linearized plasmid was transcribed with the T7 polymerase (Roche). The *in vitro* transcription reactions were carried out according to manufacturer's instruction and labeling was achieved using DIG-labelled nucleotides (DIG RNA Labeling Mix, Roche). Once transcribed, the DIG-labelled sense and antisense probes were isolated by precipitation. The precipitation reaction was carried out with a pre-cooled (-20^{o}C) solution containing 4M Lithium Chloride (LiCl) and 100% ethanol (EtOH) in 0.2M EDTA and allowed to run for 2h at -80^{o}C. Obtained pellets were washed with 70% EtOH and subsequently dried by the incubation at 37^{o}C. The precipitated DIG-labelled riboprobes were dissolved in autoclaved and DEPC treated dH_2O (0.1% (v/v) DEPC/ dH_2O) and the quantity and quality was assessed by a fluorometer (Qubit 2.0, ThermoFisher Scientific). Prepared probes were stored at -80^{o}C until used for *in situ* hybridization experiment. Shh riboprobes were kindly provided by Dr. Joanna Pyczek.

Chromogenic *in situ* hybridization (on slide)

Cryopreserved sections (see: Chapter 2. Materials and Methods. 2.2) were thawed and subsequently subjected to 20min of post-fixation with 4%PFA/PB on ice. Once post-fixed the sections were rinsed 2 times with 0.01M PBS 10min each. To block the endogenous peroxidase activity and therefore minimize the background staining, the tissues were incubated for 15min with 1% hydrogen peroxide (Roth) (v/v) in methanol (Roth). After that, slides were washed 2 times for 2min with 0.01M PBS and then subjected to 0.2M hydrochloric acid (HCl, Merck) for 8min for the purpose of tissue permeabilization and protein extraction. Following 2min wash with 0.01M PBS, the permeabilization

step was continued by 3min of incubation with proteinase K-containing solution (Sigma Aldrich, 20µg/ml in 1M TB buffer, pH7.5, 0.0005M EDTA, pH 8.0). Subsequently, the slides were rinsed for 5min with 0.01M PBS. Tissue integrity was preserved by means of subsequent 20min incubation on ice with 4%PFA/PB. To further minimize background, slices were incubated in a solution containing 0.1M triethanolamine hydrochloride with 0.2% acetic anhydride and then washed once with 0.01M PBS and once with 2x saline sodium citrate (SSC) buffer, pH 7.0 ((diluted with DEPC/ dH_2O from 20x SSC: 0.3M NaCl, 0.03M sodium citrate (Sigma Aldrich)) for 5min each. Following successive steps of dehydration with 30% EtOH, 50% EtOH (20sec each), 70% EtOH (1min), 80% EtOH, 95% EtOH, twice 100% EtOH (20sec each), the tissues were incubated with the hybridization buffer (HB) ((50% formamide (Roth) (v/v), 4×SSC (diluted with DEPC/ dH_2O from 20x SSC), 250 µg/ml DNA, MB-grade from the fish sperm (Roche), 100 µg/ml tRNA (Roche), 5% dextran sulfate (D8906-109, Sigma Aldrich) (v/v), 1% Denhardt's solution (D9905, Sigma Aldrich) (v/v)) for 1h at 55°C and finally hybridized with DIG-labeled Gli1 or Shh sense and antisense probes diluted in HB to the final concentration of 200 ng/ml overnight at 55°C. The following day the tissues were subjected to high-stringency consecutive washings with 5xSSC (diluted with DEPC/ dH_2O from 20x SSC) for 1min at 65°C, 50% formamide (v/v) in 2xSSC (diluted with DEPC/ dH_2O from 20x SSC) for 30min at 65°C, 50% formamide (v/v) in 1xSSC (diluted with DEPC/ dH_2O from 20x SSC) for 30min at 65°C and 0.1xSSC (diluted from 20x SSC) for 30min at 65°C. After that, the slices were washed 3 times with TBS pH 7.5 at 30°C, 2min each and subsequently treated with 1% blocking reagent (Roche) (v/v) in TBS pH 7.5 for 30min at RT. Following blocking step the tissues were incubated overnight at 4°C with anti-DIG alkaline phosphatase (AP) conjugated antibody (Anti-Digoxigenin-AP, Roche) diluted in blocking buffer in the proportion of 1:500. After that, the sections were successively rinsed with TBS pH7.5 (2 times, 10min each) and with the reaction buffer ((0.1M Tris-HCl, 0.1M NaCl pH 9.5, 0.05M magnesium chloride (MgCl2) (Roth)) 1 time for 10min. The AP signal was developed by incubation with a developing solution composed of a mixture of 4-Nitro blue tetrazolium chloride (NBT, Roche) and 4-toluidine salt (BCITP, Roche) in the reaction buffer. The developing solution was prepared following producer's instructions. The intensity of developing signal was assessed by a microscopic control (Axioscope 2 mot+, Zeiss). After obtaining a satisfying signal quality, the reaction was interrupted by washing with TBS buffer. The slides were then coverslipped (Menzel, ThermoFisher Scientific) following mounting with Kaiser's glycerol gelatine medium (Merck). The sections hybridized with sense probes were considered as a negative control (no signal observed after the development step) whereas sections hybridized with antisense probe were considered as stained for Gli1/Shh transcripts. The developed slides were stored at 4°C until microscopic signal acquisition (described in: Chapter 2. Materials and Methods. 2.5).

2.5 Image acquisition and processing

Bright field microscopy

The bright field micrographs of the coronal sections stained for Gli1 mRNA expression were captured by means of 25x objective (LCI Plan-Apochromat, Zeiss) of an Axio Imager 2 light microscope (Zeiss). The microscope was controlled by the Neurolucida software (MBF Bioscience) and the images were digitized with a CCD camera (Retiga 2000R, Qimaging). The final bright field images of the brain sections, as they appear in figures, are minimum intensity projections of the image stacks acquired with 1µm z-step size.

The overview bright field images of the P3 WT and dcKO brains were acquired with a light stereomicroscope (M205FA, Leica) operated by a Leica application suite X software platform (LAS X, Leica).

Fluorescence microscopy

The fluorescence images were acquired with the following confocal scanning laser microscopes:

- TCS SP2 (Leica) with a 20x objective (HC PL APO 20x/0.70 IMM, Leica), the microscope was controlled by Leica confocal software (LCS, Leica) and the table motor was controlled by the arivis software (arivis Vision4D, arivis AG);
- TCS SP5 (Leica) with the use of a 40x objective (HCX PL APO CS 40.0x1.25 OIL UV, Leica) and 63x objective (HCX PL APO CS 63×/1.40-0.60 OIL, Leica), the microscope was operated by Leica application suite advanced fluorescence software (Las AF, Leica);
- TCS SP8 (Leica) with the use of a 20x objective (HC PL APO CS2 63x/1.40 OIL, Leica) and 63x objective (HC PL APO CS2 63x/1.40 OIL, Leica), the microscope was controlled by LASX software (LAS X, Leica).

The fluorescent images presented in the figures 4-11 and 15-17 are single plane acquisitions. The other micrographs are maximum intensity projections of the acquired image stacks (stacks with 1µm z-step size acquired with 40x as well as 63x objectives; stacks with 3.5µm z-step size acquired with 20x objectives).

The confocal microscopy with TCS SP5 and TCS SP8 was carried out at the Facility for Innovative Light Microscopy (FILM) at the Max Planck Institute for Biophysical Chemistry, Göttingen.

Image processing

The images were processed according to their signal, background and noise magnitude. Adequate corrections of colour levels, colour range and noise as well as pseudo colour applications were done by means of Photoshop software (Photoshop CS6, Adobe) and LAS X software (LAS X, Leica). Image stack acquisitions of fluorescent micrographs were projected for maximal intensity with LAS X software. Minimal intensity projections of bright field image stacks were achieved by means of Neurolucida software (Neurolucida, MBF Bioscience). Multiple frame acquisitions obtained with TCS SP2 or TCS SP5 confocal microscopes were manually stitched by use of arivis software (arivis Vision4D, arivis AG) or Adobe Photoshop. Multiple frame micrographs acquired by TCS SP8 confocal microscope were automatically merged by LAS X software.
CorelDraw X6 (CorelDRAW Graphics Suite X6, Corel) served as a software for manual drawing of schematics or final figure arrangements.

2.6 Cell quantifications and statistical analysis

Quantifications and measurements

All cell quantifications presented in this thesis were performed manually by means of Neurolucida software (MBF Bioscience).

Cells with fluorescence signal

Cells expressing analyzed marker detected by immunofluorescence and positive for nuclear DAPI staining were manually registered along the z axis of the acquired confocal image stacks. Cells were quantified from the region of interest chosen before immunostaining (Paxinos et al., 2006) and imaged accordingly. The quantifications were made from the total area of the acquired micrographs. Images of cortex were stitched before quantification in order to analyze the entire cortical thickness. Additionally the absolute number of cells in the quantified area was measured by manual quantifications of DAPI counterstain positives. In the majority of cases, the final numbers of marker-expressing cells were normalized to the absolute numbers of DAPI positives in the quantified area.

Cells with chromogenic signal

Gli1 positive cells detected by chromogenic *in situ* hybridization were manually counted directly under the microscope (Axioscope 2 mot+, Zeiss). The areas of interest (cortex and VP) were delineated manually based on the comparisons to the reference brain coronal sections taken from

(Paxinos et al., 2006). The surface area of regions of interest was calculated by Neurolucida software. The final numbers presented in the figures are densities of Gli1 positive cells in defined regions of interest.

Immunofluorescence intensity (FI) measurements

Semi-automated FI measurements were performed on the 40x confocal image stacks of immunofluorescent stainings of BAF complex subunits. The purpose of this analysis was to assess the BAF complex subunits expression levels in astrocytic RGCs as well as in AGPs and CP cells, and to compare it to the BAF complex subunit expression levels found in other cell types in the section under scrutiny.

Briefly, first all of BAF subunit positive cells were manually marked using the Neurolucida software. The software marker was placed directly over the most brightly fluorescent spot of the cell. Another Neurolucida marker was used to register NFiA positive/GLAST positive AGPs and placed in the same manner. In cortical areas, NFIA positive/GLAST positive cells of the CP were registered separately from those located in the VZ. The delineation of CP and VZ was estimated visually from the DAPI staining and with help from (Paxinos et al., 2006). NFIA positive/GLAST positive cells in the CP were considered to be AGPs, whereas those in the VZ were considered as astrocytic RGCs.

After that the coordinates of manually placed markers were exported and used together with corresponding stack images for the automated FI measurements in ImageJ (Fiji, NIH). There, a custom written script automatically measured the average FI within a radius of 5µm from each marker. FI measurements were taken only from the channel containing the BAF immunostaining. The ImageJ script was written by Pavel Truschow.

This procedure resulted in large datasets, where one FI value was assigned to every manually placed marker. These values were subsequently normalized to the highest FI value in the dataset.

Normalized data were represented as Beeswarm plots (plot spread points) generated by the plotSpread function, downloaded from www.mathworks.com and modified accordingly in Matlab (r2010b, Mathworks). Additionally FIs of individual BAF subunits stainings revealed for each investigated cortical cellular population of WT P0 mice (astrocytic RGCs, AGPs and CP cells) were averaged in Excel spreadsheet (Excel 2013, Microsoft) and subsequently represented by scatterplot generated in Sigma Plot 12 (Systat) and arranged in CorelDraw X6 (CorelDRAW Graphics Suite X6, Corel).

Density plots

Distribution density plots of cells expressing any given marker (GLAST, BLBP or Gli1) were generated for 2 analyzed cortical areas (M2 and S1BF) in E17.5 and P3 WT and dcKO animals.

Briefly, the marker of interest was registered manually along the z axis of the analyzed stack (as described above) and within manually delineated columns. Columns were covering the full cortical thickness (from the VZ (E17.5)/deep cerebral white (DW) (P3) up to the PS). Because of anatomical differences the thickness of the columns differed between WT and dcKO. The size of columns was assessed with the quick measure line function of the Neurolucida software. The relative distance of each registered individual cell to the PS was calculated based on Neurolucida markers' coordinates with NeurolucidaExplorer (MBP Bioscience). Columns were divided into 16 equally sized bins (from the PS to the VZ/DW) and the density of cells in each bin was calculated per mm^3. The calculations were made in Excel spreadsheet (Excel 2013, Microsoft) and the final density plots were generated in Sigma Plot 12 (Systat) and arranged in CorelDraw X6 (CorelDRAW Graphics Suite X6, Corel).

Anatomical size assessment

The medio-lateral (M-L) and rostro-caudal (R-C) extent as well as the cortical thickness of P3 WT and dcKO brains were measured by the quick measure line function of the Neurolucida software.

Statistical analysis

Datasets were processed in Excel for calculation of final means and standard deviations.
Statistical analysis was done by means of Sigma Plot 12 (Systat). The statistical difference between the analyzed groups was assessed on the basis of student's t-test and Mann-Whitney Rank-Sum test. The Mann-Whitney Rank-Sum test was used whenever data were not normally distributed, and normality of distribution was tested using Shapiro-Wilk or equal variance tests. The difference between the input groups was not considered significant if the resulting p-value exceeded 0.05. The scale of significance levels in figures is as follows: *p≤0.05, **p ≤0.01, *** p≤0.001, **** p≤0.0001.
All graphs shown in this thesis were generated by Sigma Plot and subsequently arranged in CorelDraw X6 (CorelDRAW Graphics Suite X6, Corel).

2.7 Protein isolation and Western blot (WB)

WB was used to compare the levels of BAF155 and BAF170 protein expression in cortex of dcKO and WT E17.5 mice.

Extraction of proteins

E17.5 cortical tissues cryopreserved at -80°C (see: Chapter 2. Materials and Methods. 2.3) were thawed on ice and subsequently mixed with 2x non-reducing sample buffer (Pierce Lane Marker,

ThermoFisher Scientific). Following 2 cycles of tissue sonication using an ultrasonic homogenizer (Sonoplus, Bandelin Electronics) the proteins were subjected to reduction with 5% β-mercaptoethanol (2-Mercaptoethanol, Sigma Aldrich) and subsequently denaturated at 95°C for 5min. The concentration of isolated proteins was assessed by spectrophotometric measurements of the absorbance at 280nm performed with NanoDrop (NanoDrop2000, ThermoFisher Scientific). Extracted protein samples were stored at -80°C until use.

Western blot

Cryopreserved protein samples were thawed on ice and subsequently subjected to molecular weight-dependent protein separation facilitated by sodium dodecyl sulfate (SDS)-polyacrylamide gel (PAGE) electrophoresis. Briefly, 150µg of proteins of each isolated sample (3 WT and 3 dcKO) were loaded on previously prepared SDS-polyacrylamide gel (10% resolving gel: Acrylamide (Roth), 1.5M Tris pH 8.8, 10% SDS (w/v) in H_2O (Sigma Aldrich), 10% ammonium persulfate (APS) (Sigma Aldrich), tetramethylethylenediamine (TEMED) (Sigma Aldrich) in dH_2O; 4% stacking gel: Acrylamide, 0.5M Tris pH 6.8, 10% SDS (w/v) in H_2O, 10% APS, TEMED in dH_2O; poured immediately after mixing between 2 glass plates (Mini-protean , Bio-Rad), the 10 well comb (Mini-protean, Bio-Rad) was placed accordingly after pouring). After that the proteins were separated in an electric field of 100V for 1.5h.

Following SDS-PAGE electrophoresis proteins were subjected to polyvinylidene difluoride (PDVF) membrane (Immobilon-P, Merck) transfer by wet-blotting at 150A for 1.5h. The PDVF membrane was pre-treated with 100% methanol (for 15sec) and the blotting chamber was filled with transfer buffer (2.9% (w/v) Glycine, 6% (w/v) Tris, 20% (v/v) Methanol and 0.04% (v/v) SDS in H_2O). Afterwards the membrane was into 3 parts (1 containing proteins of the size of ≥170kDa, second containing proteins of the size between 160 and 50kDa and third containing proteins with the molecular weight ≤50kDa), washed with 0.01M PBS for 10min and subsequently blocked for 1h with 5% milk powder (w/v) in 0.01M PBS (blocking solution) on a rocking plate. Once blocked, the membranes were incubated overnight on a rocking plate at 4°C, with the adequate primary antibodies: anti-BAF170 rabbit pAb (1:500, ab64853, Abcam); anti-BAF155 mouse mAb IgG1 (1:200, sc-48350, Santa Cruz Biotechnology) and anti-GAPDH mouse mAb IgG1 (1:2000, TA802519, OriGene) diluted in blocking solution in corresponding proportions. The following day the membranes were rinsed 2 times with 0.2% (v/v) Tween 20 (Roth) in 0.01M PBS (PBST) and then incubated for 2h at RT with the corresponding horseradish peroxidase (HPR) conjugated secondary antibodies (goat anti-mouse (115-035-003, Dianova) and goat anti-rabbit (111-035-003, Dianova)) diluted in blocking solution in the proportion of 1:2000. After that the immunoblots were rinsed with PBST 3 times 15min each. The HRP derived signal was then developed by means of a Western Blotting Detection

Kit (ECL, Amersham) following the manufacturers instruction. The chemoluminescent signal was detected with the Fluorchem Q (FluorChem Q system, Protein simple) and the signal intensity was measured by ImageJ (Fiji, NIH).

2.8 RNA isolation and RNA sequencing (RNA-seq)

RNA isolation and subsequent RNA-seq experiment was performed in order to reveal and compare the dorsal pallium (DP) and/or ventral pallium (VP) transcriptome of E17.5 and P3 WT and dcKO mice. In total 4 control and 4 mutant E17.5 or P3 DP as well as 4 control and 4 mutant P3 VP transcriptomes were sequenced.

RNA isolation

The cryopreserved E17.5 and P3 tissues (see: Chapter 2. Materials and Methods. 2.3) were subjected to the total RNA extraction by use of the RNA purification kit (RNeasy Plus Mini, Qiagen) following manufacturer's protocol. All of the steps of the purification were performed in RNAse free conditions. Isolated RNA was stored at -80^{o}C until sequencing.

RNA sequencing

RNA-seq (cDNA library preparation, quality control assessment, sequence reads and transcriptome assembly) were carried out in collaboration with Prof. André Fischer's laboratory (with help of Dr. Cemil Kerimoglu and Susanne Burkhardt, University Medical Center (UMG), German Center for Neurodegenerative Diseases (DZNE)). In brief, cDNA libraries were generated by means of Library Prep Kit (TruSeq RNA Library Prep Kit v2, Illumina) following manufacturer's instructions. Subsequently the quality of prepared DNA was assessed by Agilent 2100 Bioanalyzer. FASTQ conversions and base calling were performed by use of Illumina scripts as described in (Halder et al., 2016). The transcriptome was assembled by mapping of the reads to the mm10 mouse reference genome by means of STAR aligner v2.3.0 as previously described in (Djebali et al., 2012) and subsequent differential expression studies were performed by DESeq2, Bioconductor as previously described in (Love et al., 2014). Gene ontology (GO) Enrichment Analysis (ToppGene; http://geneontology.org/) (Chen et al., 2009) allowed for revealing the mutant enriched transcriptome pathways. Minor transcriptome analysis e.g. enriched glioma transcripts or downregulated late born neuron transcripts were performed on the basis of literature screening. The graphs were prepared in Sigma Plot 12 (Systat), RStudio (CRAN.R-project) as well as Matlab (r2010b, Mathworks) and subsequently arranged in CorelDraw X6 (CorelDRAW Graphics Suite X6, Corel).

Chapter 3

Results

3.1 Dynamic expression pattern of BAF complex subunits during astrocytogenesis

The aim of this study was to elucidate the impact of BAF complex on astrocytes development. We started our investigation from the analysis of BAF complex expression pattern within the astroglial lineage during the initial steps of forebrain astrogliogenesis. As astrocytes specification sets on within RGCs at later stages of mouse brain development (Rowitch and Kriegstein, 2010), a first step towards our goal was to assess BAF subunits expression within this particular cell lineage.

BAF subunits expression in astrocytic RGCs

Primarily forebrain astrocytes arise from astrocytic RGCs that reside in VZ of the perinatal cortex, LGE and MGE (Bayraktar et al., 2014; Minocha et al., 2015; Tsai et al., 2012). This developmental feature guided our choice of areas for investigation. Furthermore it is known that cortical astrogliogenesis starts during the late phase of embryonic development, around gestational stage E17.5 (Minocha et al., 2015; Mission et al., 1991; Rowitch and Kriegstein, 2010). However the exact time point of the initiation of astrogliogenesis within ventral (residing in MGE and LGE) RGCs remains unclear (Minocha et al., 2017). Because the astrogliogenic potential of perinatal ventral germinal zones has been described (Bayraktar et al., 2014; Gallo and Deneen, 2014; Minocha et al., 2015; Tsai et al., 2012) we therefore focused our investigation of astrocytic RGCs of MGE and LGE on the E17.5 developmental time point. Additionally, regardless of embryonic stage of development, RGCs exhibit the set of hallmarks typical for astroglial lineage, expressing *inter alia* astrocyte specific markers like GLAST (Chaboub and Deneen, 2012; Malatesta et al., 2000; Shibata et al., 1997). Hence the exact identification of the astroglial switch within RGCs is highly hindered by their durable expression of astroglial characteristics. This aspect impedes the choice of a proper cellular marker of astrocytic RGCs. Several lines of evidence indicate *de novo* induction of NFiA within the RGCs residing in the VZ

during the initiation of the gliogenic period (Chaboub and Deneen, 2013; Deneen et al., 2006; Gallo and Deneen, 2014; Rowitch and Kriegstein, 2010). However, due to the broad range of cells expressing NFiA through the full thickness of the perinatal cortex (Bunt et al., 2017), this marker could not be used as an exclusive indicator of astrocytic RGCs. Thus we chose to identify RGCs committed to astrocyte lineage by their simultaneous expression of NFiA and GLAST (Deneen et al., 2006; Kang et al., 2012).

Considering these points, expression of BAF complex subunits was immunohistochemically assessed in NFiA/GLAST positive astrocytic RGCs from the areas of MGE, LGE and cortical VZ of WT E17.5 murine brains. BAF complexes consist of different assemblies of numerous subunits (Kadoch and Crabtree, 2015; Sokpor et al., 2017; Son and Crabtree, 2014). We investigated expression of 5 BAF subunits, including a catalytic ATPase subunit - BRG1, two invariable scaffolding subunits: BAF155 and BAF170 (Narayanan and Tuoc, 2014b; Phelan et al., 1999; Ronan et al., 2013; Yoo and Crabtree, 2009), and two randomly chosen variant subunits; the actin dependent regulator of chromatin - BAF60a (Chen et al., 2012; Meng et al., 2018; Oh et al., 2008) and the AT-rich interaction domain containing - BAF250a (Lei et al., 2015; Li et al., 2010).

Overall the BAF subunits analyzed exhibited ubiquitous expression in many regions of stained brain tissues (data not shown). The gradual staining throughout the full cortical thickness allowed for the discrimination of the group of cells residing in VZ with only few BAF subunit positive cells found in the adjacent SVZ (Figure 4 and 11). Unlike in cortex, the ventral telencephalon staining for most of the BAF subunits investigated did not highlight a clear distinction of VZ residing cells (in LGE and MGE) (Figure 5 and 6).

All of the analyzed BAF complex subunits were detected in astrocytic RGCs of E17.5 WT murine cortex (Figure 4A-E), LGE (Figure 5A-E) and MGE (Figure 6A-E) VZs. Quantitatively, more than 80% of NFiA/GLAST positive astrocytic RGCs analyzed in all 3 astrocytic germinal zones exhibited expression of each investigated BAF complex subunit (Figure 4-6, F). The immunoreactivities towards BRG1, BAF155, BAF60a and BAF250a were close to 100% (97.8±0.97%, 99.8±0.15%, 98.6±0.79% and 98.0±0.92% of cortical astrocytic RGCs; 98.3±0.56%, 99.7±0.3%, 98.8±0.56% and 98.2± 0.45% of LGE astrocytic RGCs and 98.3±0.75%, 99.9±0.12%, 99.0±0.57% and 98.1±0.46% of MGE RGCs positive for BRG1, BAF155, BAF60a and BAF250a respectively). Given that the high level of colocalization between BAF subunits and NFiA/GLAST positive astrocytic RGCs did not show sizeable variations between single investigated animals (for BRG1 in cortex VZ: n=6, in LGE VZ: n=5 and in MGE VZ: n=5, for the rest of subunits in all investigated regions: n=4), the expression of BRG1, BAF155, BAF60a and BAF250a emerges as the perpetual ubiquitous feature of astrocytic RGCs. Strikingly the expression of BAF170 subunit seemed to deviate from this trend (Figure 4-6C and F). In all examined areas at least 10% of astrocytic RGCs did not exhibit immunohistochemically detectable levels of BAF170 subunit

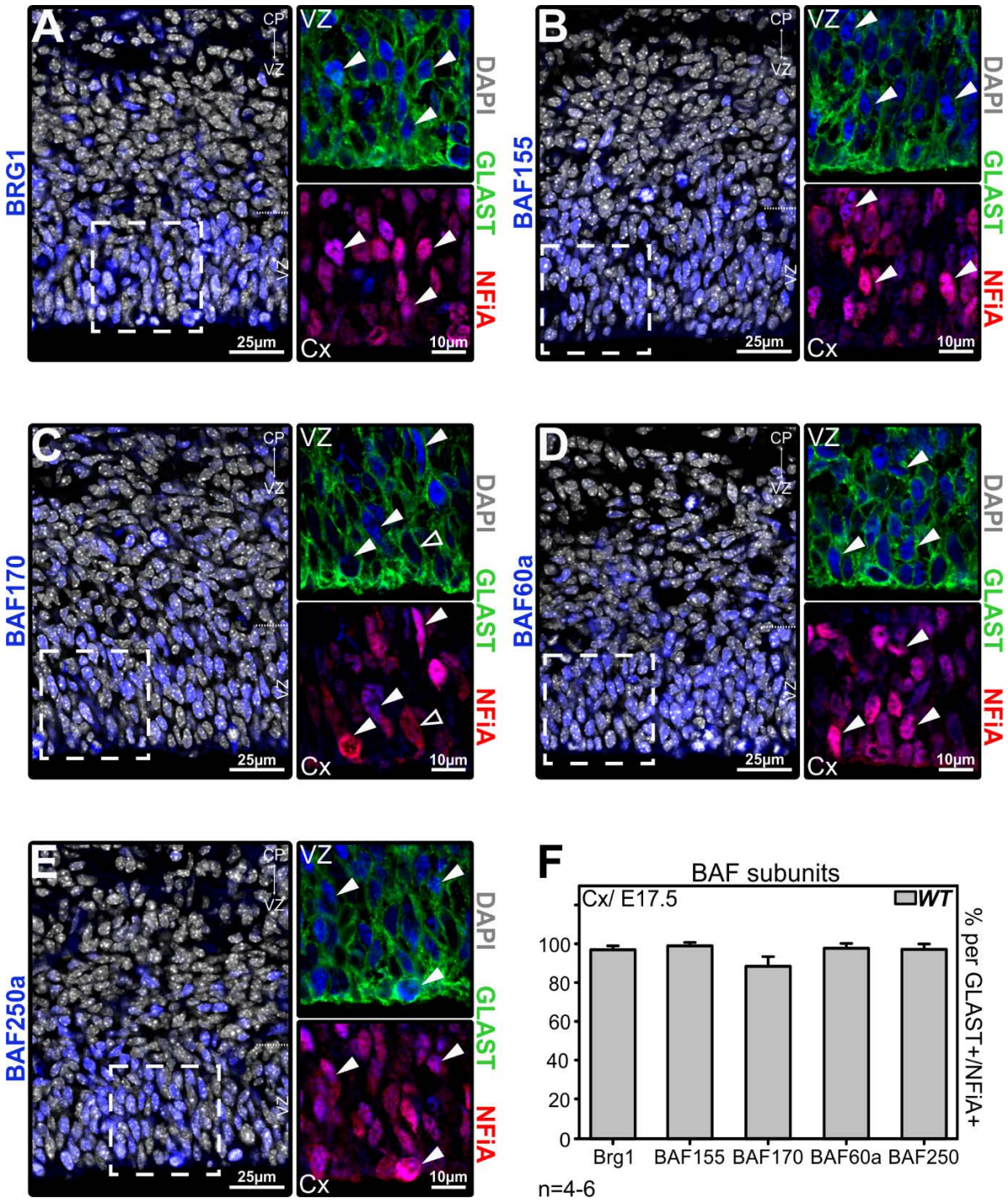

Figure 4 | Expression of BAF complex subunits in murine astrocytic cortical RGCs. (A-E) Staining of E17.5 cortical WT sections for astroglial progenitor markers; GLAST (green), NFiA (red) as well as BAF subunits (pseudo coloured in blue): BRG1 (A), BAF155 (B), BAF170 (C), BAF60a (D) and BAF250a (E). DAPI staining is gray (pseudo coloured). Cells expressing GLAST and NFiA located in VZ are astrocytic RGCs. Directions to VZ and CP pointed by two headed arrow, the border between VZ and IZ marked by dashed line. Right boards of (A-E) are magnifications of delineated VZ areas. Full arrowheads indicate astrocytic RGCs expressing BAF subunit, empty ones point to lack of expression. (F) Percentages of BAF subunit positive cells per total GLAST/NFiA positive VZ RGCs. Data are averages ± σ of n=4-6 replicates (BRG1: n=6, BAF155, BAF170, BAF60a and BAF250a: n=4). Cx, cortex; CP, cortical plate; VZ, ventricular zone; WT, wild type.

(89.2±3.7%, 87.1±1.6% and 84.4±1.8% of astrocytic RGCs positive for BAF170 staining in the area of cortical, LGE and MGE VZ respectively). This finding may indicate a potential gradual decline of BAF170 scaffolding subunit within a small population of astrocytic RGCs. Interestingly the astrocytic RGCs from the area of MGE shown the lowest rate of the colocalization with stained BAF170 subunit (84.4%, Figure 6F). MGE VZ has been reported as an area where astrogliogenesis may start earlier than typical for cortex day E17.5 (Minocha et al., 2017; Minocha et al., 2015). Thus the decrease of the amount of cells exhibiting immunohistochemically detectable BAF170 expression within astrocytic RGCs seems to be correlated with the level of the advancement of the astroglial development within the germinal zones analyzed.

Furthermore, considering that cell specific BAF complexes function as multimeric assemblies of at least 15 different subunits (Lessard et al., 2007; Narayanan et al., 2015; Sokpor et al., 2017; Wu et al., 2007), the immunostaining approach seems insufficient for the evaluation of the entire BAF complex presence within astrocytic RGCs. However the final assembly and functionality of the cell type specific BAF complex depends on the presence of the common core and scaffolding subunits (Phelan et al., 1999; Sokpor et al., 2017). Thus taking into account the fact that BAF155 and BAF170 belong to the group of the BAF complex core and scaffolding proteins (Phelan et al., 1999; Sokpor et al., 2017), we could extrapolate the existence of the entire astrocytic RGCs complex. Additionally the analysis of the expression of the BRG1 ATPase protein, a main core catalytic subunit for the majority of known nervous system BAF complexes (Kadoch and Crabtree, 2015; Trotter and Archer, 2008; Yoo and Crabtree, 2009), confirms the soundness of the chosen approach. Accordingly, the distinct variant subunits integrate to the core and scaffolding proteins assembling the final complexes (Narayanan and Tuoc, 2014b; Ronan et al., 2013). Therefore the expression of the BAF60a and BAF250a within astrocytic RGCs that possess ATPase and scaffolding proteins may be taken as indication that the entire BAF complex assembles properly and includes the subunits we analyzed here.

Overall, based on our immunostaining and quantifications, we conclude that the perinatal astrocytic RGCs residing in the VZ of cortex, LGE and MGE (all known astroglial germinal zones) express protein subunits: BRG1, BAF155, BAF170, BAF60a and BAF250a, which together indicates proper assembly of the BAF chromatin remodeling complex.

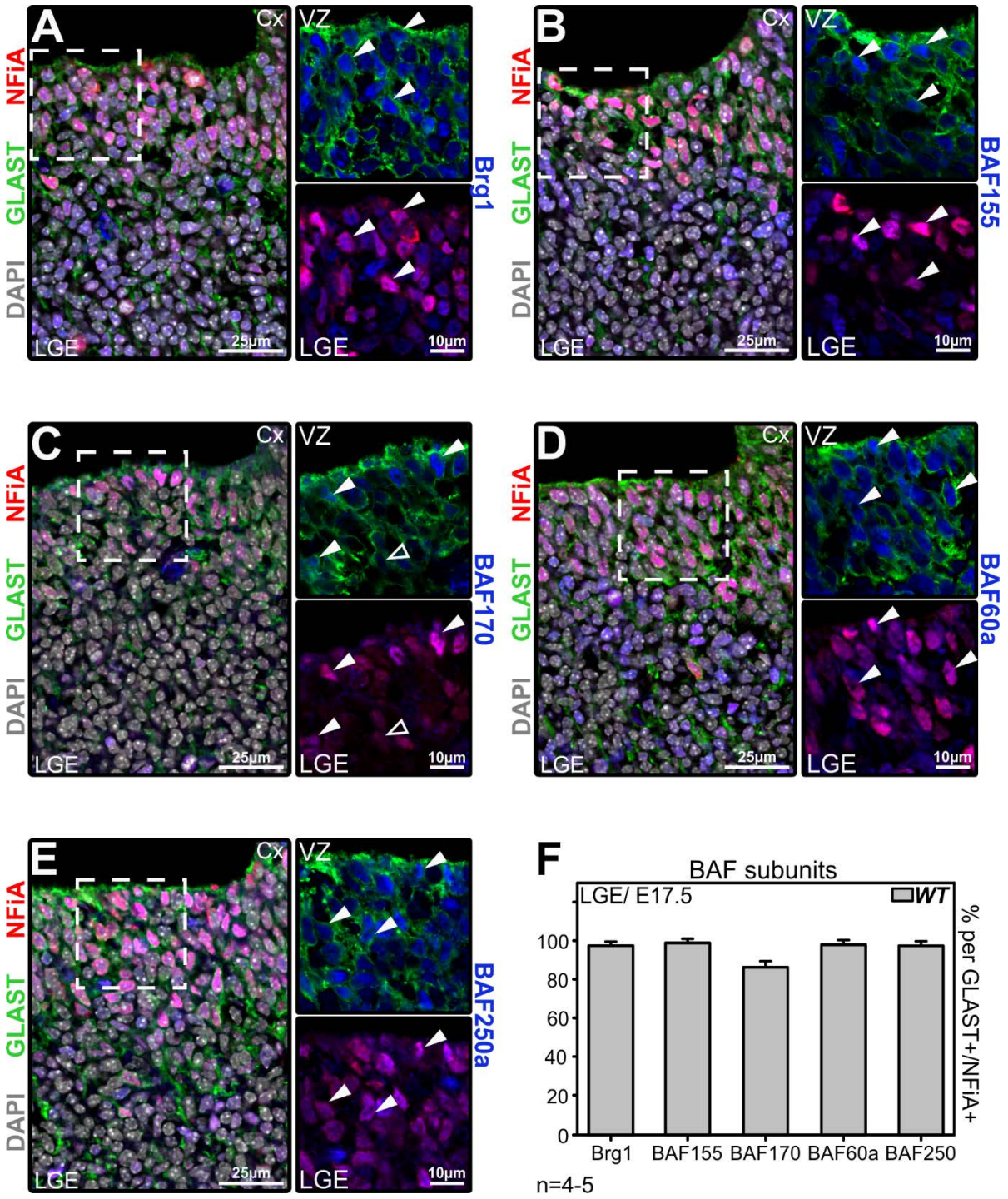

Figure 5 | Expression of BAF complex subunits in RGCs of murine LGE. Immunostaining of mouse E17.5 LGE WT sections for astroglial progenitors markers; GLAST (green), NFiA (red) as well as BAF complex subunits (in blue, pseudo coloured): BRG1 (A), BAF155 (B), BAF170 (C), BAF60a (D) and BAF250a (E). The nuclear DAPI staining is grey (pseudo coloured). Cells expressing GLAST and NFiA located in VZ of LGE are astrocytic RGCs. Right boards of each (A-E) are magnified insets of delineated VZ areas. Full arrowheads indicate astrocytic RGCs expressing investigated BAF complex subunit, empty arrowheads indicate lack of expression. Quantitative analysis of the percentages of BAF subunit positive cells per total GLAST/NFiA positive VZ RGCs (F). Data are averages ± σ of n=4-5 animals (BRG1: n=5, BAF155: n=4, BAF170: n=4, BAF60a: n=4, BAF250a: n=4). LGE, lateral ganglionic eminence; VZ, ventricular zone; WT, wild type.

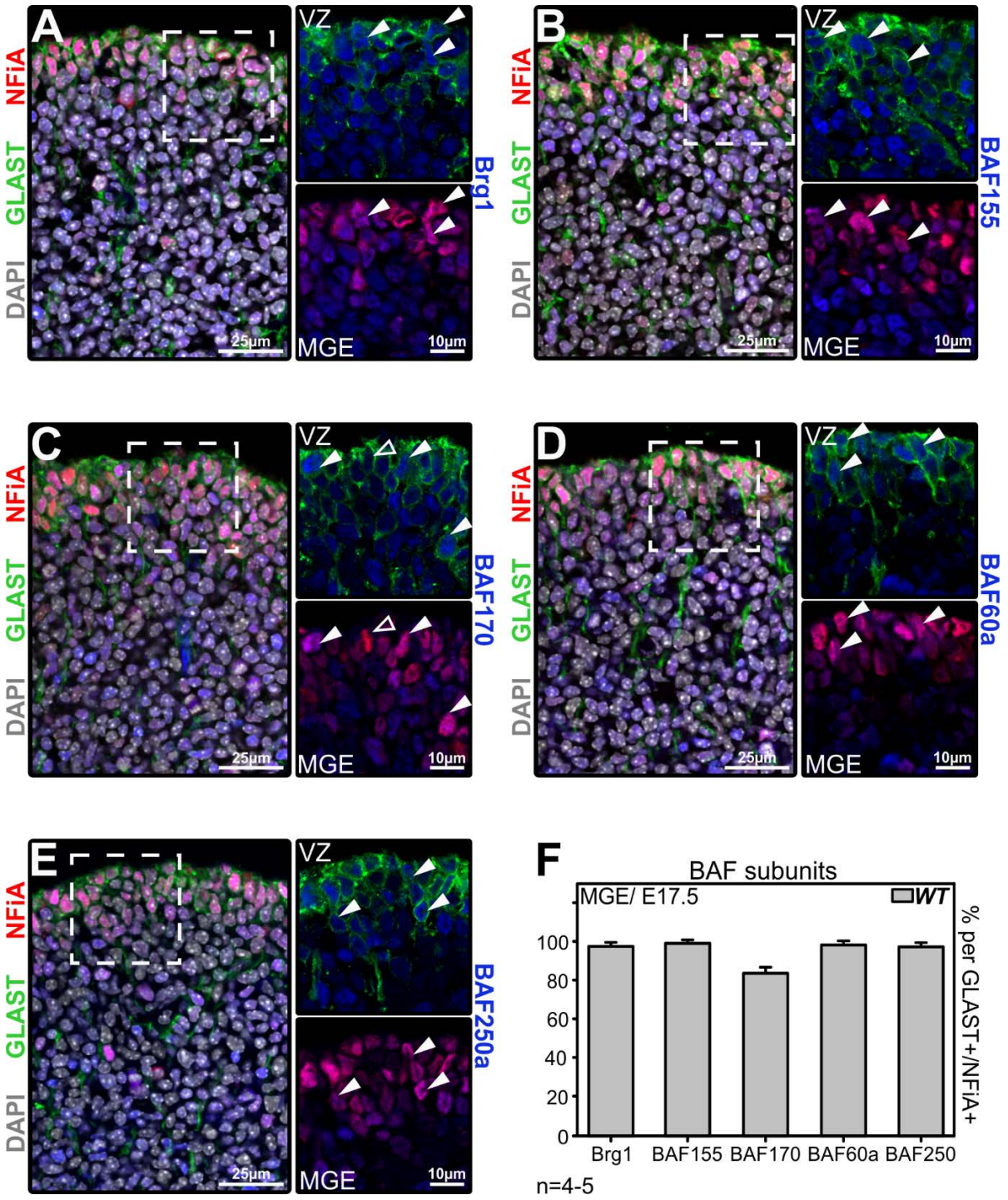

Figure 6 | Expression of BAF complex subunits in RGCs of murine MGE. (A-E) Immunostaining of mouse E17.5 MGE WT sections for astroglial progenitors markers; GLAST (in green) and NFiA (in red) as well as BAF complex subunits (in blue, pseudo coloured): BRG1 (A), BAF155 (B), BAF170 (C), BAF60a (D) and BAF250a (E). The nuclear DAPI staining is gray (pseudo coloured). Cells expressing GLAST and NFiA located in VZ of MGE are astrocytic RGCs. Right boards of each (A-E) are magnified insets of delineated VZ areas. Full arrowheads indicate astrocytic RGCs expressing BAF complex subunit, empty arrowheads indicate lack of expression. (F) Percentages of BAF subunit positive cells per total GLAST/NFiA positive VZ RGCs. Data are averages ± σ of n=4-5 animals (BRG1: n=5, BAF155: n=4, BAF170: n=4, BAF60a: n=4, BAF250a: n=4). MGE, medial ganglionic eminence; VZ, ventricular zone; WT, wild type.

Differential expression of BAF subunits in astrocytic precursor cells

The findings described above suggest the presence of BAF complex in the astrocytic RGCs, an initial progenitor cell lineage that further sequentially differentiates towards astrocytes (Gray and Sanes, 1992; Molofsky and Deneen, 2015; Rowitch and Kriegstein, 2010). At the onset of astroglial differentiation, some of the astrocytic RGCs detach from the surface of the VZs and translocate their cellular bodies outside of germinal zones (Cameron and Rakic, 1991; Guillemot, 2007; Marshall and Goldman, 2002; Minocha et al., 2015; Mission et al., 1991; Molofsky and Deneen, 2015; Rowitch and Kriegstein, 2010). These cells, AGPs, undergoing transient amplification (Ge and Jia, 2016; Ge et al., 2012) transform into astrocytes after reaching their final destinations (Ge et al., 2012; Kriegstein and Alvarez-Buylla, 2009; Molofsky and Deneen, 2015). Given that many studies indicate that reshuffling of the subunit composition of the BAF complex has a profound impact on the process of cellular differentiation (Bachmann et al., 2016; Kadoch and Crabtree, 2015; Lessard et al., 2007; Tuoc et al., 2013b; Vogel-Ciernia and Wood, 2014; Wu et al., 2007), we next evaluated the expression of previously investigated subunits within AGPs. Accordingly, we immunohistochemically assessed the expression of BRG1, BAF155, BAF170, BAF60a and BAF250a within NFiA/GLAST expressing AGPs that migrated towards the pia mater (as the derivatives of cortical VZ astrocytic RGCs (Bayraktar et al., 2014; Tsai et al., 2012), Figure 7A-E) or deeper into the striatum (caudate putamen (CPu) or central amygdala nucleus (CANu) areas as the derivatives of LGE and MGE VZ astrocytic RGCs (Bayraktar et al., 2014; Tsai et al., 2012), Figure 8A-E). We identified AGPs by their combined expression of NFiA and GLAST. We chose double immunostaining approach over single marker investigation because cells exhibiting solely GLAST or NFiA immunoreactivity could be mistaken for non-astrocytic cells, as GLAST is widely expressed by non-astrocytic outer radial glial progenitors (oRGPs) (Heng et al., 2017) and a broad range of cells express NFiA (Bunt et al., 2017)). In order to track the dynamics of the subunit changes we opted for analysis in the cortical and striatal regions of brain tissues isolated form WT mice at the gestational stages of E17.5 and P0 (Figure 7 and 8).

The percentages of E17.5 cortical and striatal AGPs expressing BRG1, BAF170, BAF60a and BAF250a visibly differ from that of astrocytic RGCs (Figure 4-8F). The E17.5 NFiA/GLAST positive AGPs exhibited lowered staining affinity towards these BAF complex subunits (Figure 7 and 8). As depicted in colour coded matrixes, the expression pattern of BAF170 in AGPs showed the most dramatic changes (Figure 7C, F and 8C, F). A quantitative analysis indicated that in E17.5 brains only 19.3±1.3% of cortical and 12.8±1.2% striatal AGPs exhibited immunohistochemically detectable levels of BAF170 protein (Figure 7F and 8F). Interestingly, the reduction in the amount of NFiA/GLAST positive AGPs exhibiting BRG1, BAF60a or BAF250a staining progressed in time. The number of 88.2±1.8% of cortical AGPs expressing BRG1 at E17.5 significantly declined to 77.9±6.7% at P0 (Figure 7A and F). The difference in BRG1 expression within striatal AGPs emerges as more striking (Figure 8A and F). In

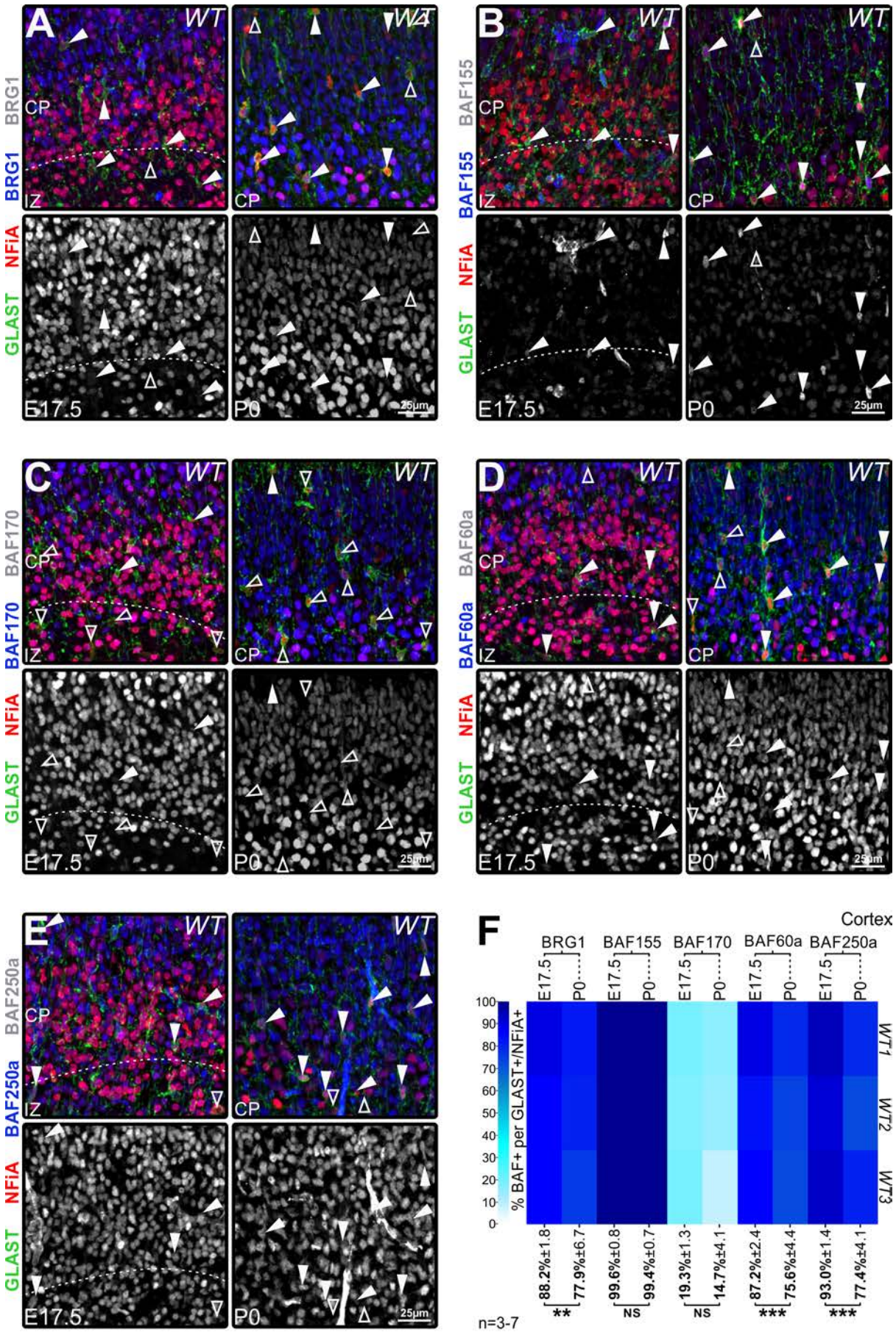
A
WT
BRG1
CP
IZ
NFiA
GLAST
E17.5
P0
25µm
B
BAF155
C
BAF170
D
BAF60a
E
BAF250a
F
Cortex
E17.5
P0
% BAF+ per GLAST+/NFiA+
WT1
WT2
WT3
88.2%±1.8
77.9%±6.7
99.6%±0.8
99.4%±0.7
19.3%±1.3
14.7%±4.1
87.2%±2.4
75.6%±4.4
93.0%±1.4
77.4%±4.1
**
NS
NS
***
***
n=3-7

Figure 7 | BAF complex subunits exhibit time dependent differential expression pattern within cortical AGPs. (A-E) Immunofluorescence staining of E17.5 (left panels of each) and P0 (right panels of each) WT coronal cortical sections (AuCx area) detecting the expression of GP/ AGP markers; GLAST (in green) and NFiA (in red) as well as BAF complex subunits (in blue and gray): BRG1 (A), BAF155 (B), BAF170 (C), BAF60a (D) and BAF250a (E). Cells co-expressing GLAST and NFiA found outside of VZ are AGPs. For each, the lower boards are single channel gray scale images of analyzed BAF subunit. Full arrowheads indicate AGPs positive, whereas empty arrowheads point to AGPs negative for immunohistochemical detection of corresponding BAF complex subunit. In each E17.5 section the border between IZ and CP is outlined with dashed line. Overview pictures of P0 brains stained for BAF155 or BAF170 are shown in Appendix, Figure 42 (provided here pictures were taken in regions delineated by dashed line (1)) (F) Quantitative analysis of the amount of BAF subunit positive GLAST/NFiA positive cortical AGPs. Colour coded matrix shows the percentage share of cortical AGPs expressing analyzed BAF complex subunit in 6 investigated WT animals harvested at 2 different time points: E17.5 (WT1, WT2 and WT3) and P0 (WT1, WT2 and WT3). Dark blue indicates high whereas light blue colour indicates low percentage of AGPs with immunohistochemically detectable expression of BAF complex subunit. Numbers stated under each matrix column are average percentage data ± σ for n=3-7 experimental replicates (BRG1/E17.5: n=7, BRG1/P0: n=5, BAF155/E17.5: n=4, BAF155/P0: n=4, BAF170/E17.5: n=4, BAF170/P0: n=4, BAF60a/E17.5: n=4, BAF60a/P0: n=6, BAF250a/E17.5: n=4, BAF250a/P0: n=3). Statistically significant reduction in AGPs exhibiting staining for corresponding BAF complex subunit marked by stars; **p≤0.01, ***p≤0.001, NS not significant (for BAF170) in t student test, for BAF155: NS not significant in Mann Whitney Rank Sum test (P<0.05 in Normality Shapiro-Wilk test). Quantifications performed in full cortical column (excluding VZ/DW) of S1BF and AuCx areas. CP, cortical plate; IZ, intermediate zone; NS, not significant; WT, wild type.

E17.5 striatum 90.3±2.2% AGPs stained for BRG1, however in P0 murine striatal regions only 70.9±3.8% NFiA/GLAST positive AGPs expressed detectable levels of BRG1 (Figure 8F). Similarly the fraction of 87.2±2.4% of cortical or 86.0 ±1.7% striatal AGPs exhibiting staining for BAF60a significantly decreased to 75.6±4.4% or 58.1±4.1% respectively (Figure 7D, F and 8D, F). Likewise, in case of BRG1 and BAF60a the number of BAF250a positive cortical and striatal AGPs significantly declined from 93.0±1.4% and 92.7±3.3% in E17.5 to 77.4±4.1% and 71.9±4.1% in P0 cortical and striatal areas respectively (Figure 7E, F and 8E, F). Previously described BAF170 expression pattern within E17.5 cortical and striatal AGPs did not significantly vary by comparison to the neonatal stage of development (Figure 7C, F and 8C, F). Intriguingly, among all analyzed BAF complex subunits, only BAF155 exhibited a high degree of colocalization with NFiA/GLAST positive AGPs (for E17.5 cortical AGPs: 99.6±0.8%, for E17.5 striatal AGPs: 98.3±0.2%), which did not significantly change over the time (for P0 cortical AGPs: 99.4±0.7%, for P0 striatal AGPs: 97.9±0.7%, Figure 7B, F and 8B, F). Overall we could observe a significant downregulation of the percentages of the cortical and striatal AGPs positive for BRG1, BAF170, BAF60a and BAF250a staining during the course of murine brain development. This however does not apply to BAF155, which was present in predominant fraction of NFiA/GLAST positive cortical and striatal AGPs (close to 100%).

Even though some of AGPs did not stain for the investigated BAF complex subunits, a variable fractions of these cells were labelled, indicating expression of the targeted subunits (Figure 7-8A-E).

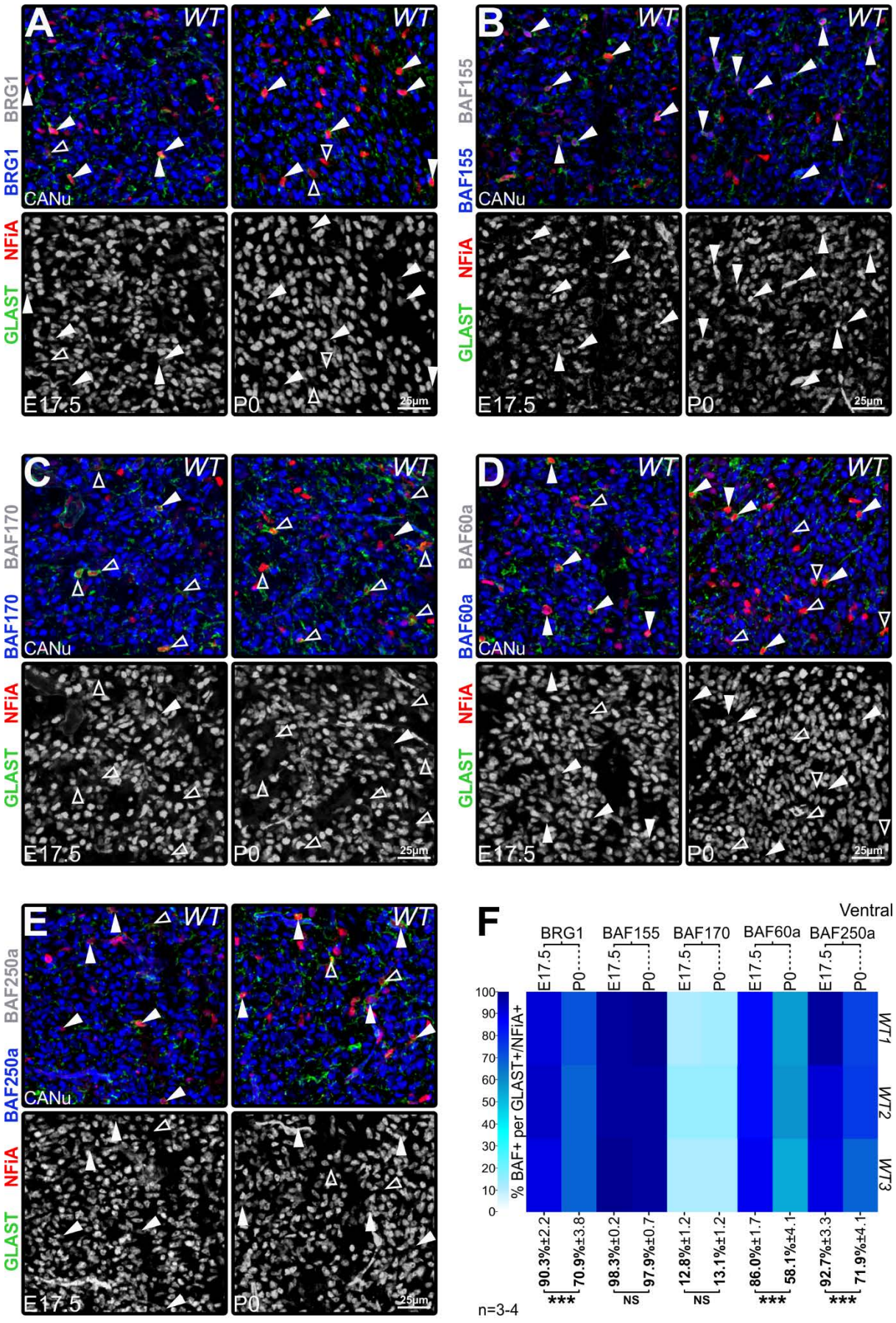
A
WT
BRG1
NFiA
GLAST
CANu
E17.5
P0
25µm
B
BAF155
C
BAF170
D
BAF60a
E
BAF250a
F
Ventral
E17.5
P0
WT1
WT2
WT3
% BAF+ per GLAST+/NFiA+
90.3%±2.2
70.9%±3.8
98.3%±0.2
97.9%±0.7
12.8%±1.2
13.1%±1.2
86.0%±1.7
58.1%±4.1
92.7%±3.3
71.9%±4.1
***
NS
n=3-4

Figure 8 | BAF complex subunits exhibit time dependent differential expression pattern within ventral AGPs. (A-E) Immunofluorescence staining of E17.5 (left panels of each) and P0 (right panels of each) WT coronal VP sections (CANu area) detecting the expression of GP/ AGP markers; GLAST (in green) and NFiA (in red) as well as BAF complex subunits (in blue and gray): BRG1 (A), BAF155 (B), BAF170 (C), BAF60a (D) and BAF250a (E). Cells expressing GLAST and NFiA are AGPs. For each, down boards are single channel gray scale images of analyzed BAF complex subunit. Full arrowheads indicate AGPs positive, whereas empty arrowheads point AGPs negative for immunohistochemical detection of corresponding BAF complex subunit. Overview pictures of P0 brains stained for BAF155 or BAF170 are shown in Appendix, Figure 42 (provided here pictures were taken in regions marked by 2). (F) Quantitative analysis of the amount of BAF subunit positive ventral AGPs expressing GLAST/NFiA. Colour matrix shows the percentage share of ventral AGPs expressing analyzed BAF complex subunit in 6 investigated WT animals harvested at 2 different time points: E17.5 (WT1, WT2 and WT3) and P0 (WT1, WT2 and WT3). Dark blue colour relates to high whereas light blue colour relates to low percentage share of AGPs with immunohistochemically detectable expression of BAF complex subunit. Numbers stated under each column of matrix are average percentage data ± σ for n=3-4 WT animals (BRG1/E17.5: n=4, BRG1/P0: n=4, BAF155/E17.5: n=4, BAF155/P0: n=4, BAF170/E17.5: n=3, BAF170/P0: n=4, BAF60a/E17.5: n=3, BAF60a/P0: n=4, BAF250a/E17.5: n=4, BAF250a/P0: n=3). Statistically significant reduction between investigated developmental stages in AGPs exhibiting staining for corresponding BAF complex subunit marked by stars; ***p≤0.001, NS not significant in t student test. Quantifications performed in the areas of CANu and CPu. CANu, central amygdala nucleus; NS, not significant; WT, wild type.

Thus as a next step we decided to investigate the exact levels of BAF complex subunits expressed by AGPs and evaluate them with reference to their global expression pattern. Accordingly, we measured the average FI of examined BAF complex subunits for each cell exhibiting subunit positive staining within P0 murine cortex (Figure 9) and striatum (Figure 10). The FI of corresponding BAF subunit was subsequently evaluated within AGPs found in the same cortical or striatal region. All of the FIs acquired for a single evaluated section were then normalized to the highest value registered within the entire group of analyzed cells (the highest FI=1, see Chapter 2. Materials and Methods. 2.6).

As represented in beeswarm plots (Figure 9 and 10 A'-E'), the cells expressing given BAF subunit showed a broad range of staining intensities (blue colour data points, considered as 'BAF subunit expression levels'). Strikingly the FIs measured for BRG1, BAF170 and BAF60a within cortical and striatal AGPs were among the lowest acquired and usually amounted to 20-30% of the highest registered value (Figure 9 and 10 A'-E'). The FI of BAF250a expressed by cortical AGPs tended to be minimally elevated by comparison to that of above described subunits (many of cells exhibited fluorescence as high as 60% of the highest value). However striatal AGPs showed equally low BAF250a FIs (comparing to striatal AGPs FI measured for BRG1, BAF170 and BAF60a). As previously described and unlike other investigated subunits, the vast majority of AGPs stained for BAF155. Strikingly, as shown in Figure 9B, B' and 10B, B', these AGPs did not exhibit FIs that could be easily classified as 'high' or 'low'. To the contrary, some of AGPs exhibited the highest BAF155 FIs found among all investigated cells, whereas other shown rather low levels of staining (well presented in Figure 10B, cells pointed by white arrows). The diverse and widely fluctuating FIs of BAF155 subunit

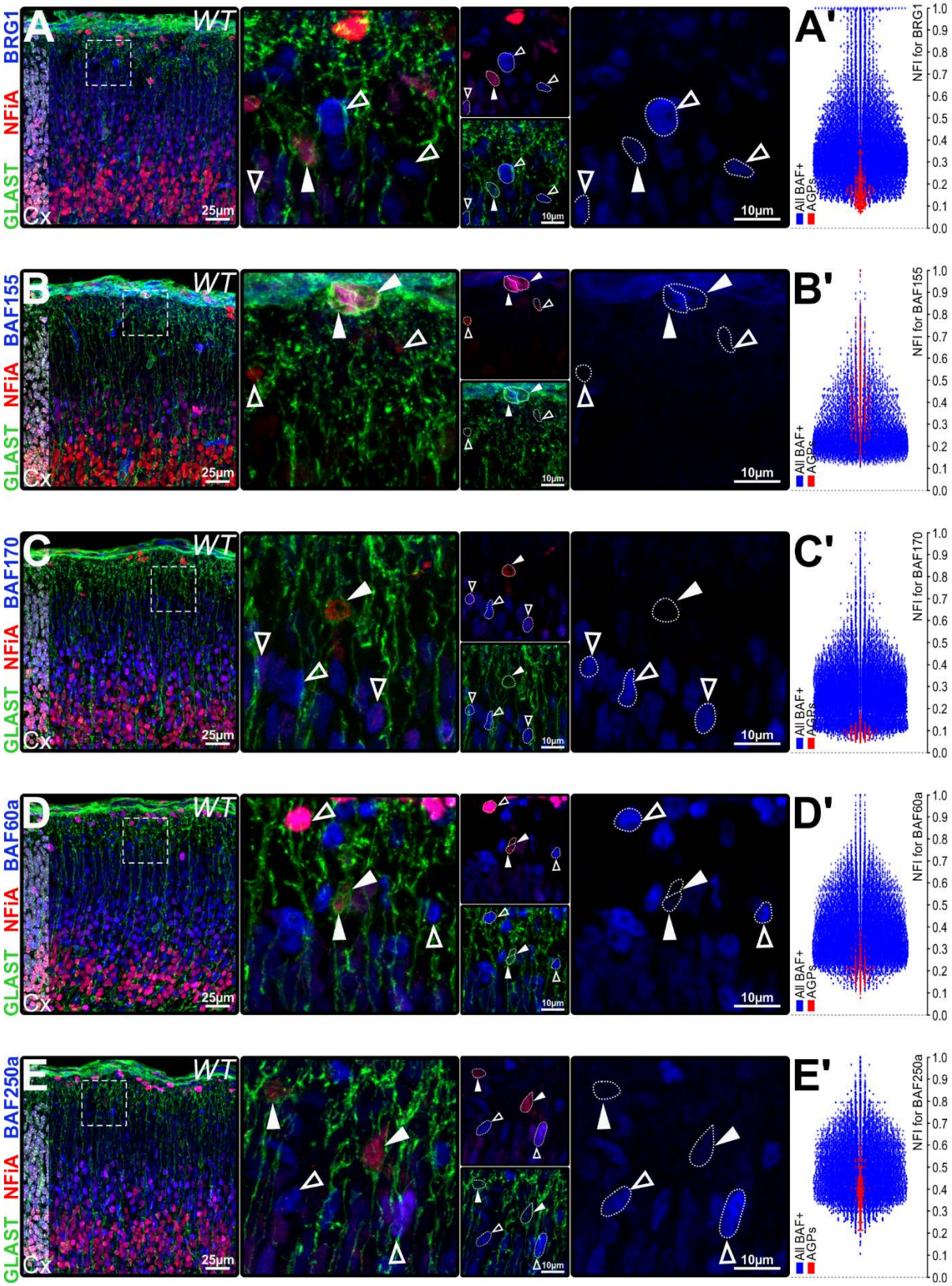

Figure 9 | Diminished expression levels of BAF complex subunits in AGPs of murine cortex. (A-E) Coronal tissue sections through WT murine P0 cortex (AuCx area) stained with antibodies to AGP markers; GLAST (in green) and NFiA (in red) together with antibodies detecting BAF complex subunits (in blue, pseudo coloured): BRG1 (A), BAF155 (B), BAF170 (C), BAF60a (D) and BAF250a (E). The nuclei of cells stained with DAPI (in pseudo colour gray). Cells simultaneously expressing GLAST and NFiA are AGPs.

Second, third and fourth panel of each shows magnified insets of delineated areas. The rightmost boards are single channel images of immunofluorescence signal for adequate BAF complex subunit. Full arrowheads point to AGPs and their expression of corresponding BAF complex subunit, empty arrowheads point to non-astrocytic cells and their expression of adequate BAF complex subunit. Cell bodies of indicated AGPs outlined with dashed line. Overview pictures of P0 brains stained for BAF155 or BAF170 are shown in Appendix, Figure 42 (provided here pictures were taken in regions marked by 1). (A'-E') FI analysis of P0 cortical sections (S1BF and AuCx for each) stained with antibodies to BAF complex subunits: BRG1 (A'), BAF155 (B'), BAF170 (C'), BAF60a (D') and BAF250a (E'). Beeswarm plots represent readouts of FIs for given BAF subunit staining normalized to the highest value of readout among all analyzed cells (=1) for all BAF subunit positive (blue data points) and AGPs (red data points). Data points are single readouts of BAF FIs from cortical areas of n=3 animals (results for WT1 plotted as data points in shape of star, results for WT2 plotted as dots, results for WT3 plotted as data points in shape of cross). AGPs, astroglial progenitors; Cx, cortex; NFI, normalized fluorescence intensity; WT, wild type.

expressed by AGPs may indicate highly dynamic changes in BAF155 abundance within this cell type. It was described that changes in expression levels of certain BAF proteins exert an influence on the expression of other complex subunits (Chen and Archer, 2005; Panamarova et al., 2016; Tuoc et al., 2013b). In particular, it has been shown that the abundance of BAF155 depends on the amount of BAF170. Indeed, the knockout (KO) of BAF170 increases BAF155 expression (Tuoc et al., 2013b). Thus the elevated expression levels of BAF155 reflected in high FIs could be initially caused by a reshuffle of the BAF complex composition within AGPs, where we found a substantially reduced abundance of BAF170 (Figure 7C-10C). On the other hand the observed decreased FIs of BAF155 within some of the investigated AGPs (Figure 9B' and 10B') may suggest that initially elevated (as described above, by the diminished abundance of BAF170) expression levels of BAF155 start to be downregulated, as in case of other investigated subunits. Thus overall we assume that AGPs can be described as cells exhibiting declining levels of BAF subunits expression.

In the course of brain development, RGCs differentiate to various neural cell types (Chojnacki and Weiss, 2008; Gotz and Barde, 2005). It is well established that cortical RGCs differentiate towards neurons initially (E10.5-E16.5/E17.5) and astrocytes later (approximately from E17.5) (Gotz and Barde, 2005; Kriegstein and Alvarez-Buylla, 2009; Rowitch and Kriegstein, 2010). To globally compare the differences in BAF complex subunits expression during RGCs differentiation towards astrocytic and non-astrocytic cells (neurons) we evaluated the FIs of BAF complex subunits within three populations of perinatal murine neural cells: RGCs, AGPs and CP residing cells. We chose to investigate the FIs of all cells found in CP assuming that the majority of these were neurons (thus considering the averaged readouts for CP as neuronal). As in the FI measurements described above, we averaged FIs of each examined BAF complex subunit for every cell exhibiting a positive staining within the full cortical thickness of developing S1BF area of P0 mouse brains. The FIs for the corresponding BAF subunit were subsequently evaluated within AGPs, RGCs and cells residing in CP

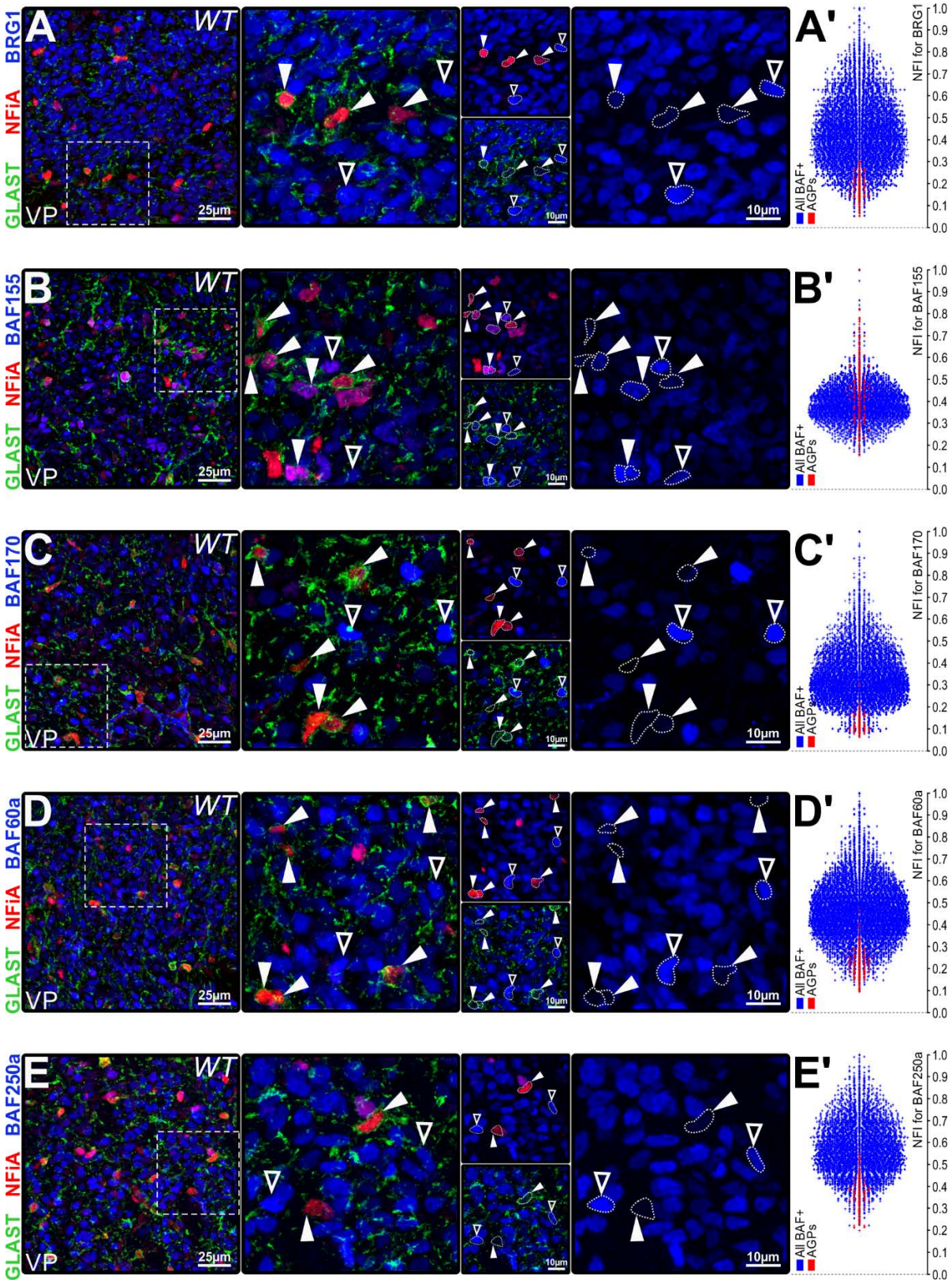

Figure 10 | Diminished expression levels of BAF complex subunits in AGPs of murine VP. (A-E) Coronal tissue sections through WT murine P0 VP (CANu/CPu area) stained with antibodies to AGP markers; GLAST (in green) and NFiA (in red) together with antibodies detecting BAF complex subunits (in blue, pseudo coloured): BRG1 (A), BAF155 (B), BAF170 (C), BAF60a (D) and BAF250a (E). The nuclei of cells stained with DAPI (in pseudo colour gray). Cells simultaneously expressing GLAST and NFiA are AGPs.

Second, third and fourth panel of each shows magnified insets of delineated areas. The right most boards are single channel images of immunofluorescence signal for adequate BAF complex subunit. Full arrowheads point to AGPs and their expression of corresponding BAF complex subunit, empty arrowheads point to non-astrocytic cells and their expression of corresponding BAF complex subunit. Cell bodies of indicated AGPs outlined with dashed line. Overview pictures of P0 brains stained for BAF155 or BAF170 are shown in Appendix, Figure 42 (provided here pictures were taken in the regions marked by 2). (A'-E') FI analysis of P0 VP sections (CANu/CPu area) stained with antibodies to BAF complex subunits: BRG1 (A'), BAF155 (B'), BAF170 (C'), BAF60a (D') and BAF250a (E'). Beeswarm plots represent readouts of FI for adequate BAF subunit staining normalized to the highest value of readout among all analyzed cells (=1) for all BAF subunit positive (blue data points) and AGPs (red data points). Data points are single readouts of BAF FI from VP of n=3 animals (results for WT1 plotted as data points in shape of star, results for WT2 plotted as dots, results for WT3 plotted as data points in shape of cross). AGPs, astroglial progenitors, NFI, normalized fluorescence intensity; WT, wild type.

(found in the same cortical region). Like previously, all of the FIs acquired for a single evaluated section were then normalized to the highest value registered within the entire group of the analyzed cells (see Chapter 2. Materials and Methods. 2.6).

The results of measurements are presented in Figure 11A-E. As depicted by violin plots and visible in corresponding micrographs the majority of investigated CP cells exhibited relatively high expression levels of BRG1, BAF170, BAF60a and BAF250a. As previously stated, RGCs also stained for these BAF subunits but with lower average FIs than CP cells (Figure 11A, C-E). Strikingly the FIs of BRG1, BAF170, BAF60a and BAF250a measured in AGPs (light blue colour violin plots) were even lower than in RGCs. As predicted and in agreement with the results described above, the FIs acquired for BAF155 stained cells revealed diverse expression levels within AGPs and RGCs (Figure 11B).

We then asked what the changes in subunits expression that occur as RGCs differentiate towards neurons or AGPs are. In order to address this question we normalized average BAF FIs of CP cells and AGPs to the average RGCs FIs of the corresponding analyzed subunit (RGCs FI=1, Figure 11F, marked by gray dashed line). As shown in Figure 11F, cells residing in the CP (considered as neurons) exhibited elevated average FI of BRG1, BAF170, BAF60a and BAF250a (dark blue data points) staining compared to RGCs. To the contrary, AGPs featured a downregulation of average FIs (light blue data points) relative to RGCs. Importantly the FI measurements for each set of the compared RGCs, AGPs and CP cells were performed on the same acquired micrographs. Like previously, BAF155 stood as an exceptional case with CP cells exhibiting downregulated FIs of the staining with respect to the enriched with BAF155 FIs RGCs (Figure 11B, F). Additionally, we did not notice major differences in averaged FIs of BAF155 staining between AGPs and RGCs.

In summary, we observed a significant downregulation of the percentages of the cortical and striatal AGPs positive for BRG1, BAF170, BAF60a and BAF250a immunostaining during the course of murine brain development. Moreover the remaining AGPs expressing detectable levels of the tested BAF

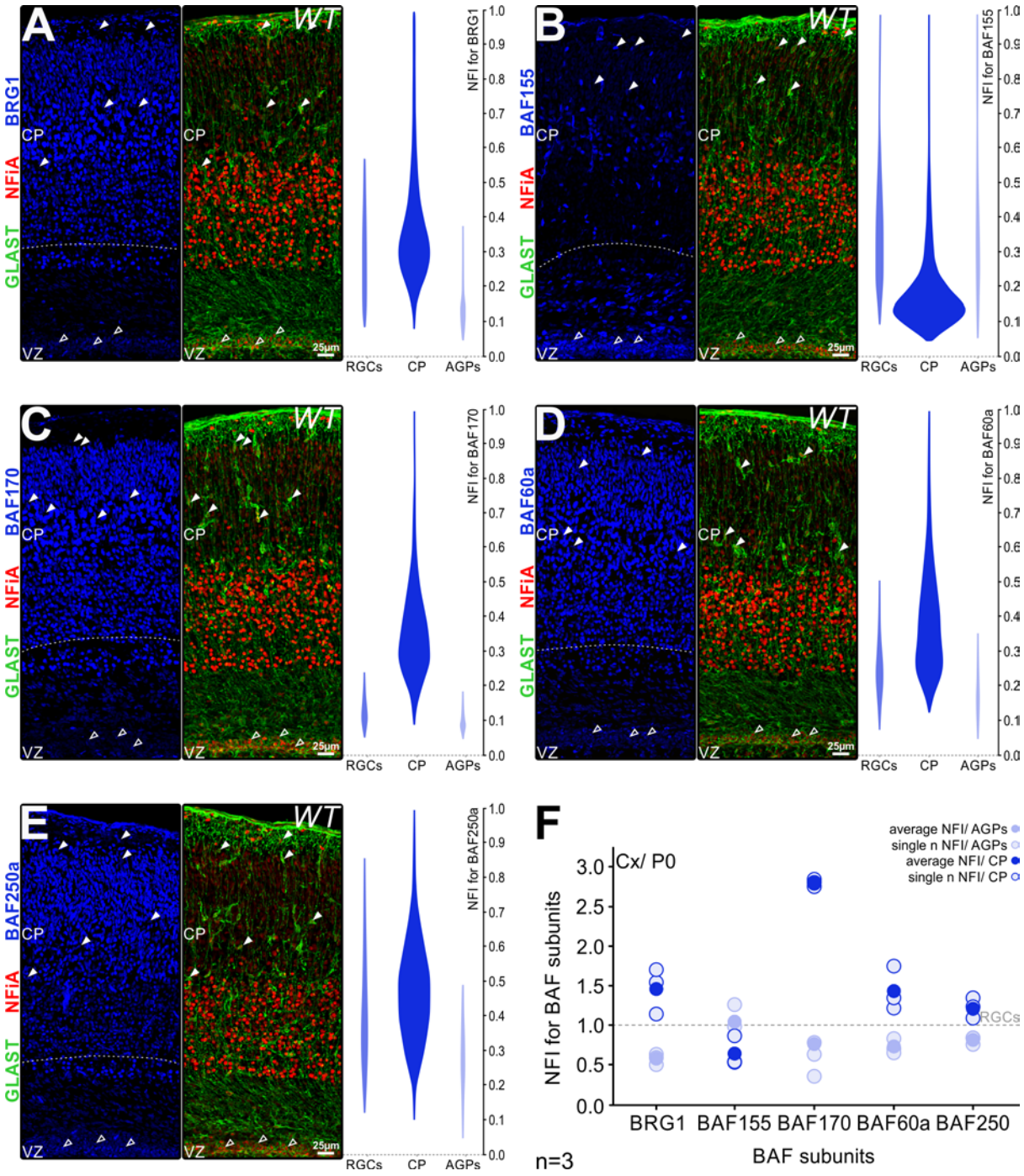

Figure 11 | Distinct neural cortical populations exhibit different expression levels of BAF complex subunits. (A-E) Coronal sections through WT S1BF cortical area of P0 mice stained with antibodies to AGP markers; GLAST (in green) and NFiA (in red) together with antibodies detecting BAF complex subunits (in pseudo colour blue): BRG1 (A), BAF155 (B), BAF170 (C), BAF60a (D) and BAF250a (E). Cells simultaneously expressing GLAST and NFiA are AGPs. Overview pictures of P0 brains stained for BAF155 or BAF170 are shown in Appendix, Figure 42 (provided here pictures were taken in regions marked by 3). The left most boards of each are single channel images of immunofluorescence signal for adequate BAF complex subunit. Full arrowheads point to example AGPs and their expression of given BAF subunit. The extreme right panels are violin plots representing quantitative FIs analysis for the adequate BAF subunit staining. Each single readout was normalized to the highest FI value among all analyzed cells (=1). Violin plots represent normalized FI surveys for n=3 animals for all BAF subunit positive cells located in CP (dark blue plots), BAF subunit positive RGCs (blue plots) and AGPs (light blue plots). (F) Average FI in CP cells and

AGPs relative to average FI of RGCs measured in P0 WT S1BF cortical area. Full data points represent average for n=3 animals. Average FI for given population of single animal showed by empty data points. Dark blue colour corresponds to the results acquired for CP whereas light blue to the readouts for AGPs. AGPs, astroglial progenitors; CP, cortical plate; NFI, normalized fluorescence intensity; RGCs, radial glial cells; VZ, ventricular zone; WT, wild type.

subunits exhibited a clear downregulation of these subunits staining affinity, resulting in declined FIs (refered to as 'expression levels'), also with respect to CP residing cells ('neurons') and cortical VZ RGCs. Importantly, P0 CP cells among which neurons constitute a vast majority (Tiberi et al., 2012) showed elevated FIs of BRG1, BAF170, BAF60a and BAF250a staining. It indicates a difference in expression of these BAF subunits between astrocytic and non-astrocytic (presumably neuronal) cell lineages. This phenomenon nonetheless did not apply to BAF155, which was broadly expressed by AGPs. However, assuming that the high ratio of BAF155 expressed by AGPs relates to its BAF170-dependent stoichiometry (as described above) and decreases with time (other interpretations are discussed in: Chapter 4. Discussion. 4.1), it seems that the expression levels of BAF complex elements decrease as astrocytic RGCs detach from the VZ and transform to AGPs.

3.2 Enforced BAF complex loss in astrocytic RGCs - dcKO approach

Having established that the expression of BAF subunits ubiquitous in neurons and astrocytic RGCs tends to cease within AGPs, we investigated the impact of BAF complex depletion on astrocytic RGCs. We took this step to determine whether the loss of the BAF complex would cause that astrocytic RGCs detach from the VZ and translocate as proliferative AGPs.

We addressed this question *in vivo* by means of BAF complex deletion targeted to late RGCs. To this end, we generated a transgenic mutant mouse model with human glial fibrillary acidic protein (*hGFAP*) promoter-driven dcKO of BAF155 and BAF170 (*hGFAP*-Cre dcKO) (Narayanan et al., 2015; Nguyen et al., 2018; Zhuo et al., 2001).

hGFAP promoter driven recombination

First, by means of ROSA-tdTomato system (Madisen et al., 2010) used in heterozygous (Het) mice (see Chapter 2. Materials and Methods. 2.1) we traced the activity of *hGFAP* promoter within astrocytic RGCs. As presented in Figure 12 the choice of *hGFAP* promoter as a driver of recombination allowed us to affect all known dorsal and ventral forebrain astrocytic germinal zones (Bayraktar et al., 2014; Minocha et al., 2015; Tsai et al., 2012). In agreement with the literature (Anthony and Heintz, 2008), we found that *hGFAP*-Cre driven recombination starts in hippocampal and medial cortical VZ (Figure 12 A), later propagating to all areas of DP as development proceeds

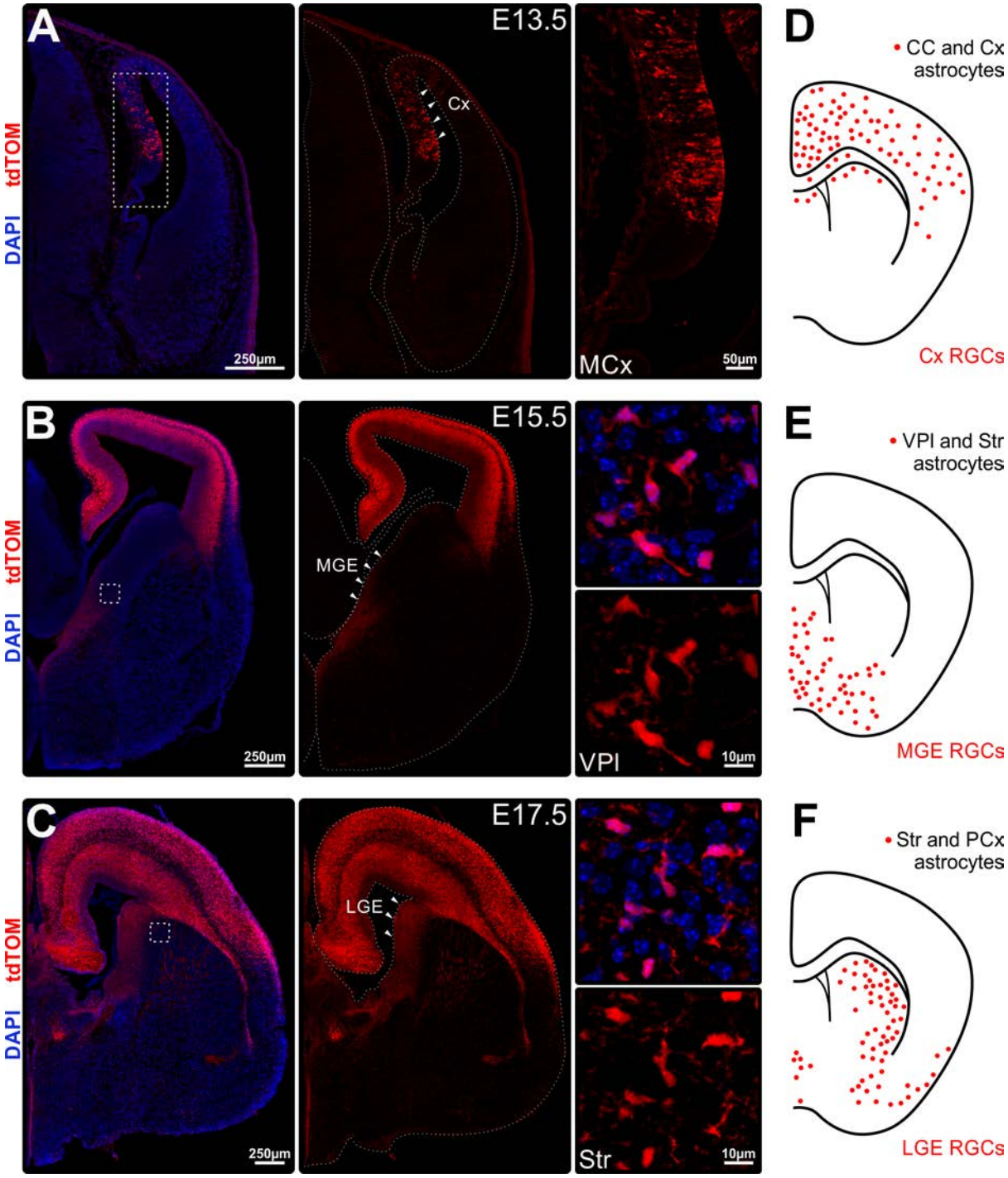

Figure 12 | *hGFAP* promoter drives recombination in all astrocytic germinal zones of murine forebrain. (A-C) Coronal sections of brains of *hGFAP*-Cre Het tdTomato mice at: E13.5 (A), E15.5 (B) and E17.5 (C). tdTomato (tdTOM) signal in red, DAPI in blue. A-C, middle: single channel tdTOM images. Arrowheads indicate astrocytic germinal zones with recombination detected at given stage in: Cx VZ (A), MGE VZ (B) and LGE VZ (C). A-C, right: are magnified pictures of tdTOM positive cells in given areas. (D-F) Schematics showing adult forebrain astrocytes born in embryonic astrocytic germinal zones affected by recombination: (D) CC and Cx astrocytes descend from Cx RGCs (E) these of VPI and Str from MGE RGCs and (F) Str and PCx astrocytes from LGE RGCs. Graphics prepared based on (Bayraktar et al., 2014; Tsai et al., 2012). CC, corpus callosum; Cx, cortex; MGE, medial ganglionic eminence; MCx, medial cortex; LGE, lateral ganglionic eminence; RGCs, radial glial cells; PCx, piriform cortex; Str, striatum; VPl, ventral pallidum.

(Figure 12A, B). Interestingly the activity of *hGFAP* promoter within ventral astrocytic germinal zone of MGE started to emerge later than that of DP and was observed around E15.5 (Figure 12B). The astrocytic RGCs affected latest were these of LGE where the recombination occurred around E17.5 (Figure 12C).

Based on previously published tracing studies (Tsai et al., 2012), we could indicate forebrain astrocyte populations, progenitors (astrocytic RGCs) of which exhibited *hGFAP*-Cre driven recombination (thus will be affected by introduced BAF complex dcKO). Accordingly, it is known that astrocytes of cortex and corpus callosum originate from cortical astrocytic RGCs (recombination within cortical VZ starts as early as E13.5, Figure 12D). At the same time astrocytes populating striatum and ventral pallidum as well as striatum and piriform cortex were shown to be derivatives of astrocytic RGCs of MGE (affected at E15.5, Figure 12E) and LGE respectively (affected at E17.5, Figure 12F).

Overall performed tracing studies confirmed that *hGFAP* promoter allows for targeting of all known dorsal and ventral astrocytic RGCs populations, thereby allowing us to affect different forebrain astrocyte populations.

Expression of BAF complex subunits in *hGFAP*-Cre dcKO forebrain

It has been previously established that dcKO of BAF155 and BAF170 results in a complete deletion of the entire BAF complex from the affected cells (Narayanan et al., 2015).

To assess the efficacy of this process within our *hGFAP*-Cre dcKO system (further referred to as dcKO for simplicity), we first compared the protein expression levels of BAF155 and BAF170 in WT and mutant E17.5 DP. The choice of this area allowed a proper evaluation of protein levels, as the cortical recombination in dcKO starts relatively early (around E13.5, Figure 12A), thus only a small fraction of tissue should contain KO unaffected cells.

Western blot (WB) analysis of E17.5 DP lysate proteomes (Figure 13) revealed a massive reduction in BAF155 and BAF170 protein abundance within dcKO cortex compared to WT (Figure 13A). Quantitatively, the average levels of BAF155 and BAF170 expression in dcKO cortex amounted to 35-40% and 32-35% of these of WT (=100%), respectively (Figure 13F).

The observation of residual BAF155/BAF170 levels in dcKO prompted us to investigate the possible cellular sources of these proteins. Using immunochemistry, we evaluated BAF155 and BAF170 expression in E17.5 coronal sections of Het (used as control) and *hGFAP*-Cre dcKO tdTomato mice (Figure 13B). As expected, both BAF complex subunits were depleted in dcKO astrocytic germinal zones (Figure 13B and C) exhibiting *hGFAP* promoter activity (tdTOM tracing). A faint signal was observed in the LGE of dcKO (indicated by arrow head in Figure 13B). We conjectured that this was

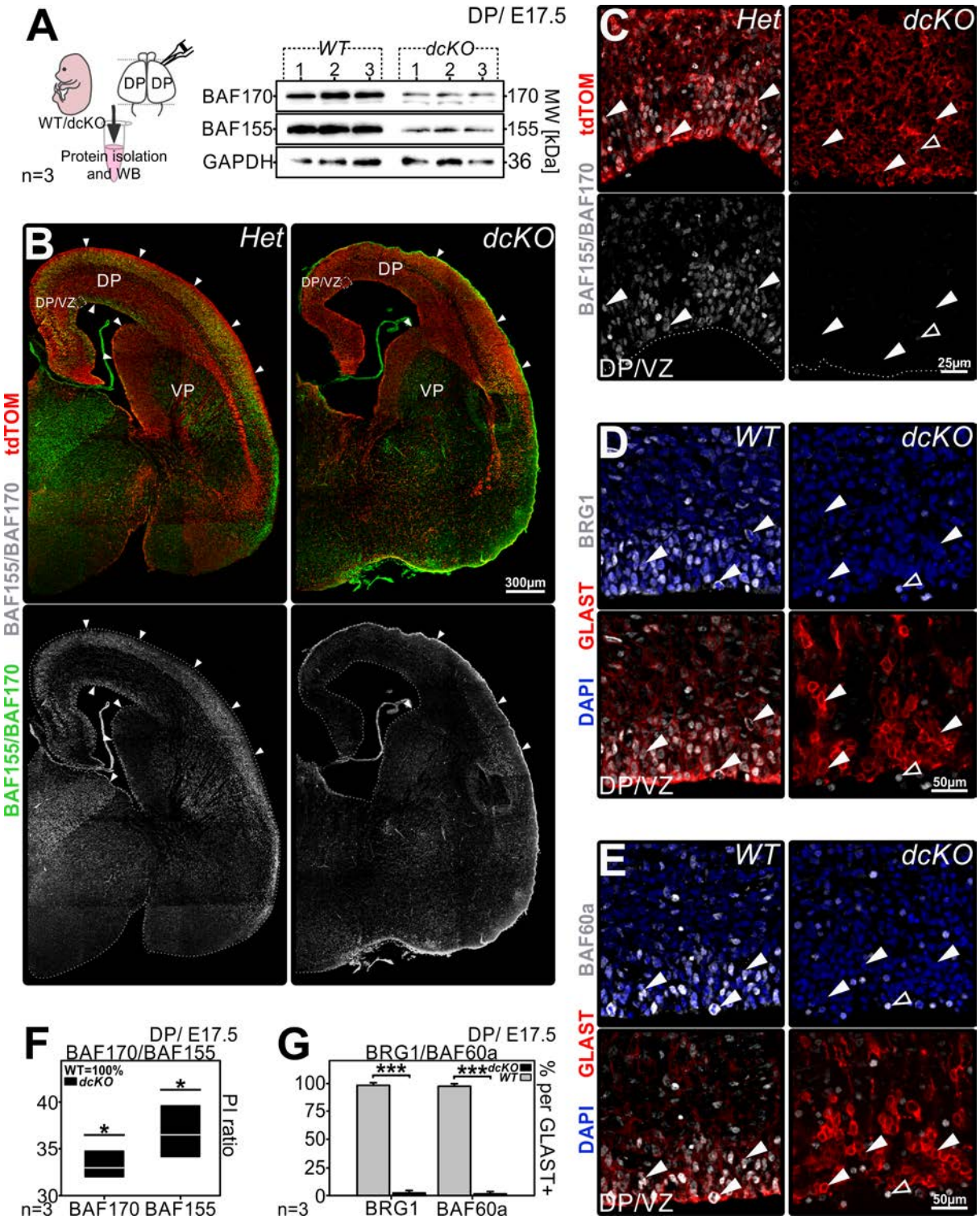

Figure 13 | Loss of BAF complex subunits in astrocytic cortical RGCs affected by *hGFAP*-Cre dcKO. (A) BAF155 and BAF170 protein expression analysis in WT and dcKO murine E17.5 DP tissues. Left panel shows a schematic explanation of experimental principle. E17.5 WT/dcKO embryos were subjected to DP dissection, subsequent protein isolation and WB analysis. Right board shows representative blots indicating expression of BAF170 (MW~170kDa, upper blot), BAF155 (MW~155kDa, middle blot) and GAPDH (housekeeping gene, MW~36kDa, lower blot) in 3 independent WT (right panel) and 3 independent dcKO (left panel) E17.5 DPs after WB experiment. The molecular weight of proteins (in kDa) marked on the right side of each blot. Quantitative representation of WB analysis shown in F. (B-C) E17.5 Het and dcKO coronal sections stained with antibodies to BAF155/BAF170 (in green and grey).

Endogenous tdTOM signal is red. (B) Overview pictures of Het (used as control) and dcKO medial area brain slices. For each down panels are single channel grey scale images. Regions exhibiting BAF155/BAF170 expression indicated with arrowheads. (C) Magnified insets of DP VZ (from the region of future M2 area, indicated in overview pictures by dashed line) showing downregulated expression of BAF155/BAF170 in the region of VZ in dcKO animals by comparison to WT. The surface of the VZ marked with dashed line. (D-E) Immunofluorescence analysis of mouse E17.5 WT and dcKO DP VZ coronal sections stained with antibody to astroglial progenitor marker – GLAST (in red) together with antibodies detecting BAF complex subunits (in grey): BRG1 (D) and BAF60a (E). Nuclear DAPI staining in blue. Immunohistochemical analysis shown depletion of BRG1 and BAF60a in GLAST positive astrocytic RGCs of dcKO animals. For C, D and E full arrowheads indicate cells positive for given BAF complex subunit, empty arrowheads indicate cells lacking BAF subunit expression. (F) Box plot representing dcKO BAF170 and BAF155 PI shown as ratio of WT results measured from the blot for 3 independent animals. WB analysis indicated significantly reduced amount of BAF155 and BAF170 in E17.5 dcKO DP by comparison to WT. (G) Percentages of given BAF subunit positive per total GLAST positive astrocytic RBCs in the DP of E17.5 WT and dcKO mice. Data are averages ± σ of n=3 animals. For F and G ***p≤0.001, *p≤0.05, in t student test. dcKO, double knockout; DP, dorsal pallium; Het, heterozygous; MW, molecular weight; PI, pixel intensity; VP, ventral pallium; VZ, ventricular zone; WB, Western blot WT, wild type.

due to the relatively late initiation of *hGFAP* promoter activity within this region, as described above. In addition and importantly protoplasmic astrocytes found within ventral regions of postnatal dcKO brains were deprived of BAF complex subunits, indicating for the efficient dcKO within ventral astrocytic germinal zones (Appendix, Figure 43).

Our previous study indicated that dcKO of BAF155 and BAF170 in ESCs, cultured neurons and early cortical development results in a complete deletion of the entire BAF complex from the affected cells (Narayanan et al., 2015). We therefore determined whether astrocytic RGCs of dcKO mice express BAF subunits (Figure 13C-E). Accordingly, we immunohistochemically assessed GLAST positive astrocytic RGCs of cortex VZ of E17.5 dcKO (that presumably did not stain for BAF155/BAF170, Figure 13C) and Het cortical for the expression of 2 BAF complex subunits: BRG1 (Figure 13D) and BAF60a (Figure 13E). Strikingly, cortical VZ of dcKO (shown to be deprived of BAF155 and BAF170) exhibited staining for both, BRG1 and BAF60a. However, as indicated in Figure 13D, E and G numbers of GLAST positive E17.5 dcKO cortical astrocytic RGCs expressing BRG1 or BAF60a were highly reduced comparing to control animals (Figure 13G), indicating BAF complex degradation within these cells.

Thus we confirm the full elimination of BAF complex from astrocytic RGCs achieved by means of *hGFAP*-Cre driven dcKO of BAF155 and BAF170.

BAF complex depleted mice - initial severity assessment

The *post-partum* mortality of generated dcKO animals was sorely high, limiting their average lifespan to P3-4. The external appearance of P3-4 mutant mouse body did not differ from WT or Het

littermates, apart from their slightly smaller size. However a striking anatomical difference was observed between the brains of WT and dcKO mice (Figure 14A-D).

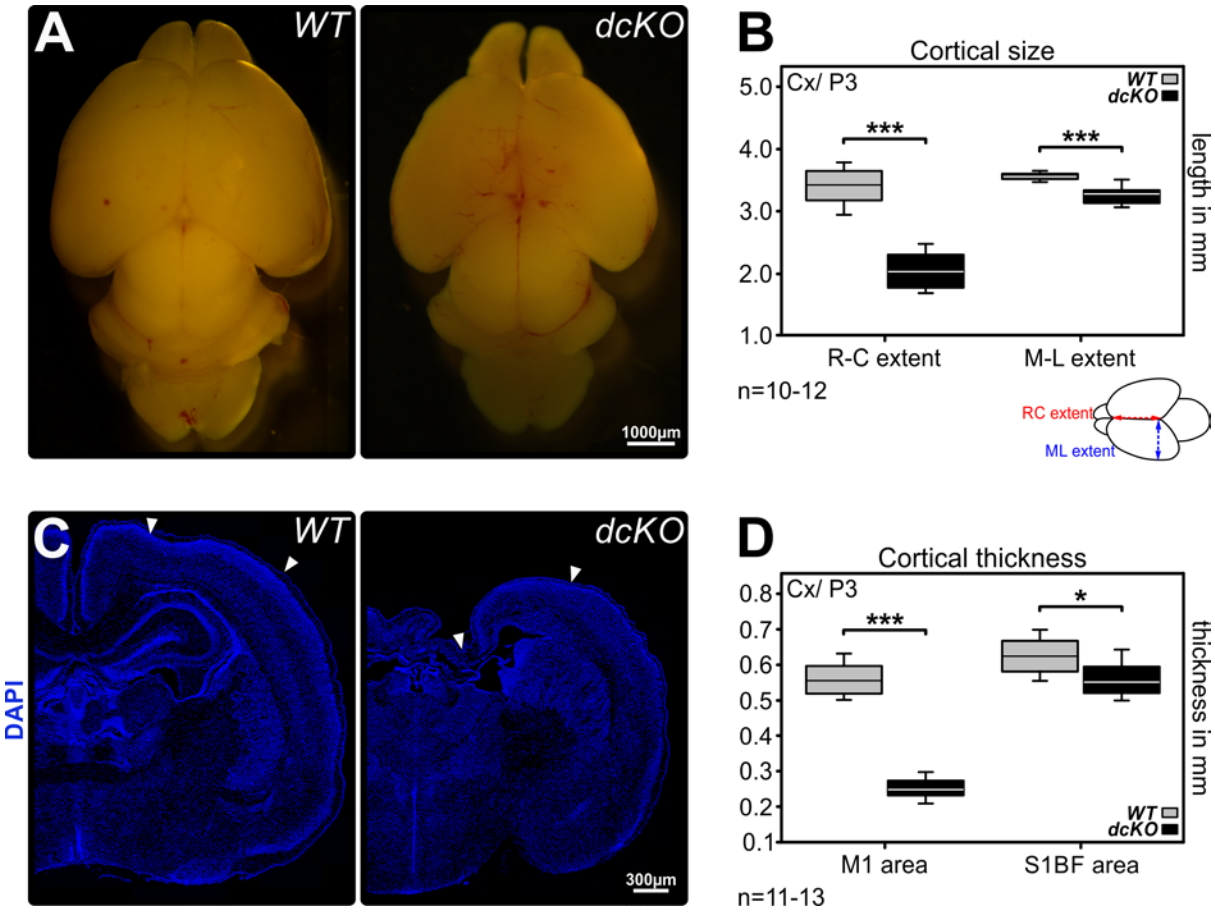

Figure 14 | Reduced cortical size of BAF complex depleted postnatal mouse brains. (A) Bright field images of WT and dcKO brains of P3 mice. (B) Box plot representing differences between R-C and M-L extent in WT and dcKO brains. The cartoon below indicates the dimensions measured. (C) DAPI staining of WT and dcKO coronal P3 murine brain slices showing visible anatomical differences. (D) Cortical thickness differences between M1 and S1BF areas of P3 WT and dcKO mouse brains. Horizontal lines within each bar indicate average value for (A) n=10-12 experimental replicates (WT RC/ML extent: n=10, dcKO RC/ML extent: n=12), (D) n=11-13 experimental replicates (WT M1 area: n=11, WT S1BF area: n=12, dcKO M1 area: n=13, dcKO S1BF area: n=12); for (B) R-C extent ***p≤0.001 in t-student test, for (B) M-L extent ***p≤0.001 in Mann-Whitney Rank Sum test, for (D) M1 area ***p≤0.001 in Mann-Whitney Rank Sum test and for (D) S1BF area *p≤0.05 in t-student test. dcKO, double knockout; M1, primary motor cortex; M-L, medio-lateral; R-C, rostro-caudal; S1BF, primary somatosensory barrel cortex; WT, wild type.

The undeveloped P3 dcKO brain displayed an atrophied cortex and cerebellum (Figure 14A). Noticeable changes to the cortex were in its rostro-caudal and medio-lateral extents, which were measurably smaller (Figure 14B). Notably, as shown in Figure 14C, dcKO brains did not develop a hippocampal structure and featured a significantly reduced cortical thickness, particularly in medial

areas. Quantitatively, measurements of primary motor cortex (M1) thickness indicated an almost 2.5 fold reduction compared to WT (Figure 14D). Strikingly, in more lateral areas, the thickness of cortex tended to normalize, with only minimal discrepancies between genotypes in S1BF area (Figure 14D).

Foreword to astroglial phenotype assessment

The purpose of this study was to elucidate the role of BAF complex in astrocytes development. As explained above, having generated transgenic mutant mouse model with specific *hGFAP*-Cre driven dcKO of BAF155 and BAF170, we were capable of targeting all 3 astrocytic germinal zones and eliminating BAF complex from astrocytic RGCs. Because our model featured high juvenile mortality, we could not assess astrogliogenesis beyond P3. As a result, the analysis presented henceforth will mostly focus on this developmental postnatal stage. We also evaluated the initial steps of cortical astroglia formation on E17.5 dcKO and WT tissues.

3.3 Cortical phenotype

It has been established that in rodents forebrain, astrocytes arise from dorsal and ventral germinal zones, however the most exhaustive surveys of astrocyte development concern cortical astrogenesis (Bayraktar et al., 2014; Miller and Gauthier, 2007; Minocha et al., 2017; Minocha et al., 2015). Thus despite the limited general knowledge about astrocyte developmental processes, the timing of the generation of cortical astroglia has been soundly examined and estimated to be around E17.5 (Cameron and Rakic, 1991; Minocha et al., 2015; Mission et al., 1991). Interestingly our *hGFAP*-Cre dcKO mouse model showed a loss of BAF complex subunits *inter alia* within cortical astrocytic RGCs allowing for a peculiar mimicking of the reduction in BAF expression observed for WT AGPs (as described in Chapter 3. Results. 3.1). It was evident from visual inspection that the cortex of postnatal dcKO mice was markedly reduced in size, both in its extents and thickness, indicating wide-ranging consequences of *hGFAP*-Cre induced mutation. Taken together, these observations prompted us to investigate the potential cortical astroglial phenotype of dcKO mice.

From RGCs to AGPs – initial steps of cortical embryonic astrogenesis in dcKO mice

Asking whether the generation of cortical astrocytes would be altered by loss of BAF complex, we first evaluated the general pool of astroglial precursors (astrocytic RGCs and AGPs) in dcKO and control cortex. Thus by means of immunostaining we assessed the expression of BLBP (Brunne et al., 2010; Gotz et al., 2015), GLAST (Brunne et al., 2010; Shibata et al., 1997) and SOX9 (Kang et al., 2012; Nagao et al., 2016) in coronal sections of Het/WT (control) and dcKO brain tissues harvested at E17.5 (Figure 15A-E).

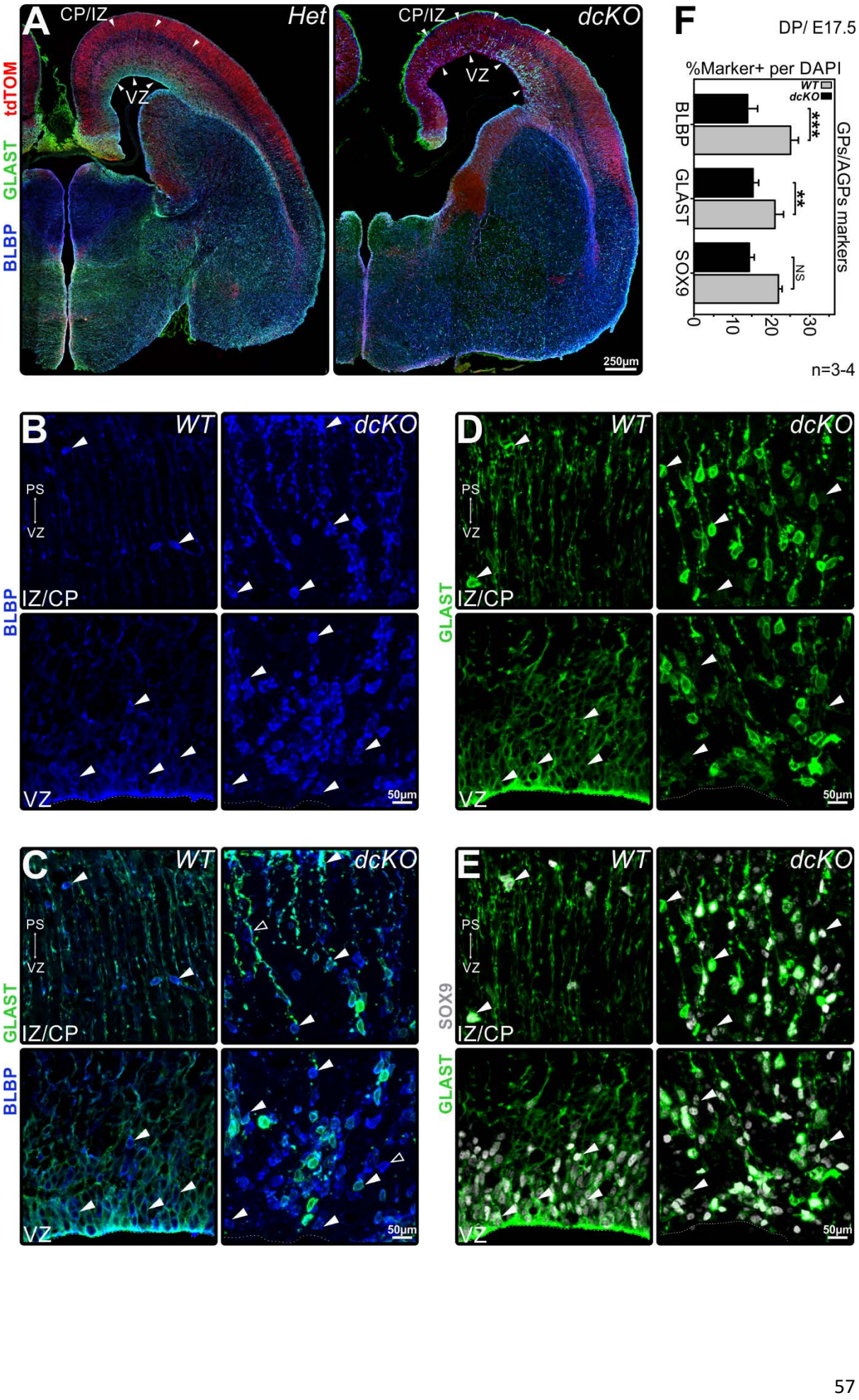
A
CP/IZ
Het
VZ
tdTOM
GLAST
BLBP
CP/IZ
dcKO
VZ
250μm
F
DP/ E17.5
%Marker+ per DAPI
WT
dcKO
BLBP
GLAST
SOX9
***
**
NS
GPs/AGPs markers
0
10
20
30
n=3-4
B
WT
dcKO
PS
VZ
IZ/CP
BLBP
VZ
50μm
D
WT
dcKO
PS
VZ
IZ/CP
GLAST
VZ
50μm
C
WT
dcKO
PS
VZ
GLAST
IZ/CP
BLBP
VZ
50μm
E
WT
dcKO
PS
VZ
SOX9
IZ/CP
GLAST
VZ
50μm

Figure 15 | Embryonic murine DP affected by BAF complex KO exhibits elevated numbers of cells expressing astrocytic RGCs and AGP markers. (A-E) Immunofluorescence staining of Het, WT and dcKO E17.5 mouse medial coronal brain sections showing expression of astrocytic RGCs/AGP markers: (A-C) BLBP (in blue), (A,D-E) GLAST (in green) and (E) SOX9 (in gray). The endogenous tdTOM signal is red (only for A). (A) Overview pictures of Het (used as control) and dcKO medial area brain slices. Cortical regions of CP/IZ and VZ control and dcKO brains exhibiting differences in evaluated markers expression indicated with arrowheads. (B-E) Magnified insets of MCx (developing M2 area, for B and C) and LCx (developing S1 areas, for D and E) regions of IZ/CP and VZ showing elevated expression of astrocytic RGCs/AGP markers in dcKO by comparison to WT. For each IZ/CP image the directions towards PS and VZ are indicated by two-headed arrow. For B, D and E full arrowheads indicate AGP/astrocytic RGCs positive for given marker. For C full arrowheads indicate AGP/astrocytic RGCs positive for GLAST and BLBP, empty arrowheads indicate cells positive only for BLBP. (E) Percentages of AGP marker positive cells per DAPI positive cells in the DP of E17.5 WT and dcKO mice. Data are averages ± σ of n=3-4 animals (BLBP/WT: n=4, BLBP/dcKO: n=3, GLAST/WT: n=3, GLAST/dcKO: n=3, SOX9/WT: n=3, SOX/dcKO: n=3); ***p≤0.001, **p≤0.01, in t student test, for SOX9: NS, not significant in Mann Whitney Rank Sum test. Manual quantifications of DAPI positive cells expressing given AGP marker and all DAPI positive cells performed in full cortical columns of 3 different regions of DP (developing M1, M2 and S1 areas) and summed up for each individual n. AGPs, astroglial progenitors; CP, cortical plate; dcKO, double knockout; DP, dorsal pallium; GPs, glial progenitors; Het, heterozygous; PS, pial surface; VZ, ventricular zone; WT, wild type.

As indicated in Figure 15A, BLBP and GLAST positive astroglial precursors were highly altered in the dcKO DP affected by *hGFAP*-Cre driven recombination (tdTOM positive cortical regions) compared to the Het control. Furthermore, the micrographs of VZ and CP/intermediate zone (IZ) areas and corresponding quantitative analysis indicated that the total amount of BLBP positive cells (manually quantified and then compared to that of all DAPI positive cells registered in the same area) in dcKO DP significantly (***p≤0.001) outnumbered that of WT (where 24.9±1.6% and 13.8±2.3% of DAPI positive cells were BLBP expressing progenitors in dcKO and WT respectively; Figure 15A-C and E). Similarly, dcKO DP showed elevated numbers of GLAST (significantly, **p≤0.01; Figure 15A, C-F) and SOX9 (not significantly, p>0.05; Figure 15E and F) expressing precursors. Quantitatively, in dcKO 20.9±1.9% and 21.8±0.8% of all DP DAPI positive cells expressed GLAST and SOX9 respectively (Figure 15E). In WT, GLAST positive progenitors constituted 15.2±1.1% whereas SOX9 expressing cells accounted for 14.3±0.8% (analyzing per all DAPI stained cells). Interestingly, the percentages of upregulated precursor cells positive for BLBP, GLAST and SOX9 in investigated dcKO DP differed between each other (Figure 15F). This distinguished astrocytic precursors of dcKO from that of WT, in which all markers were mostly co-expressed by the same group of cells (Figure 15C and E). Thus, as shown in Figure 15C, WT astrocyte precursors stained simultaneously for both astroglial proteins: BLBP and GLAST, however dcKO precursor cells positive for BLBP to a large degree did not exhibit GLAST expression (which was pronounced in lower dcKO GLAST positive cellular count compared to that of dcKO BLBP, Figure 15F). This very interesting feature did not apply to GLAST positive dcKO astrocytic precursors which commonly expressed BLBP (Figure 15C, indicated by full arrowheads). Notably, this feature appeared to be dependent on the area of investigation. As shown in Figure

15A, the number of GLAST cells was increasing the more lateral the area (detailed analysis presented further in this subsection). Strikingly GLAST and SOX9 were present in the same cell populations of WT as well as dcKO DP. These observations show the predominance of BLBP expression among E17.5 dcKO precursor cells.

Heretofore we have found that the loss of BAF complex in astrocytic RGCs causes massive increase in the abundance of cells expressing astrocyte precursor (astrocytic RGCs or AGPs) related proteins. However, in view of our finding that the expression levels of BAF subunits in WT mice decrease as astrocytic RGCs transform to AGPs, another crucial question had emerged: are these numerous cells observed in dcKO cortex astrocytic RGCs or AGPs?

As previously stated, astrocytic RGCs express a set of astrocyte specific markers (Hartfuss et al., 2001). The expression of these markers (e.g. BLBP, GLAST and SOX9) persists in AGPs (Chaboub and Deneen, 2013; Molofsky et al., 2012), hampering discrimination between these two populations (Chaboub and Deneen, 2013). However, it has been well established that the onset of astroglial differentiation corresponds to the VZ surface detachment of the differentiating astrocytic RGCs and their subsequent migration as AGPs outside of germinal zones (Cameron and Rakic, 1991; Ge et al., 2012; Guillemot, 2007; Marshall and Goldman, 2002; Minocha et al., 2015; Mission et al., 1991; Molofsky and Deneen, 2015; Rowitch and Kriegstein, 2010). Thus, we next investigated the spatial distribution of GLAST or BLBP positive cells through the cortical thickness of dcKO and WT E17.5 cortex. It has been already visible in Figure 15 that unlike in control conditions, many BLBP, GLAST and SOX9 positive cells could be found in dcKO IZ/CP. However, as indicated in Figure 15A, the distribution and abundance of investigated cells appeared to be dependent on cortical region of dcKO murine brains. Noticing that GLAST and BLBP positive cells quantity and cortical location differs in medial and lateral cortical areas, we focused our next analysis on 2 cortical regions: developing M1 (refered to as medial region (MCx)) and S1 (refered to as lateral region (LCx)) areas (overview in Figure 15). Additionally, in order to illustrate the localization of GLAST and BLBP positive cells localization, we generated distribution density plots (Figure 16A and D, see Chapter 2. Materials and Methods. 2.6). As indicated in Figure 16 A and D, most GLAST and BLBP positive cells in the medial and lateral areas of WT E17.5 cortex populated the cortical VZ, with only single positive found outside, in other cortical areas. Notably, the distribution of GLAST and BLBP positive cells greatly differed in dcKO MCx and LCx. Overall, GLAST and BLBP expressing cells of developing dcKO M1 area tended to detach from the VZ, not allowing for preservation of the AS (Figure 16A and D, indicated by arrowheads in dcKO images). As depicted in the corresponding density line graphs (solid line), both GLAST and BLBP expressing cells were present in VZ of dcKO cortex. However, their densities within this area were visibly lower than these of WT. In addition, great numbers of GLAST and BLBP

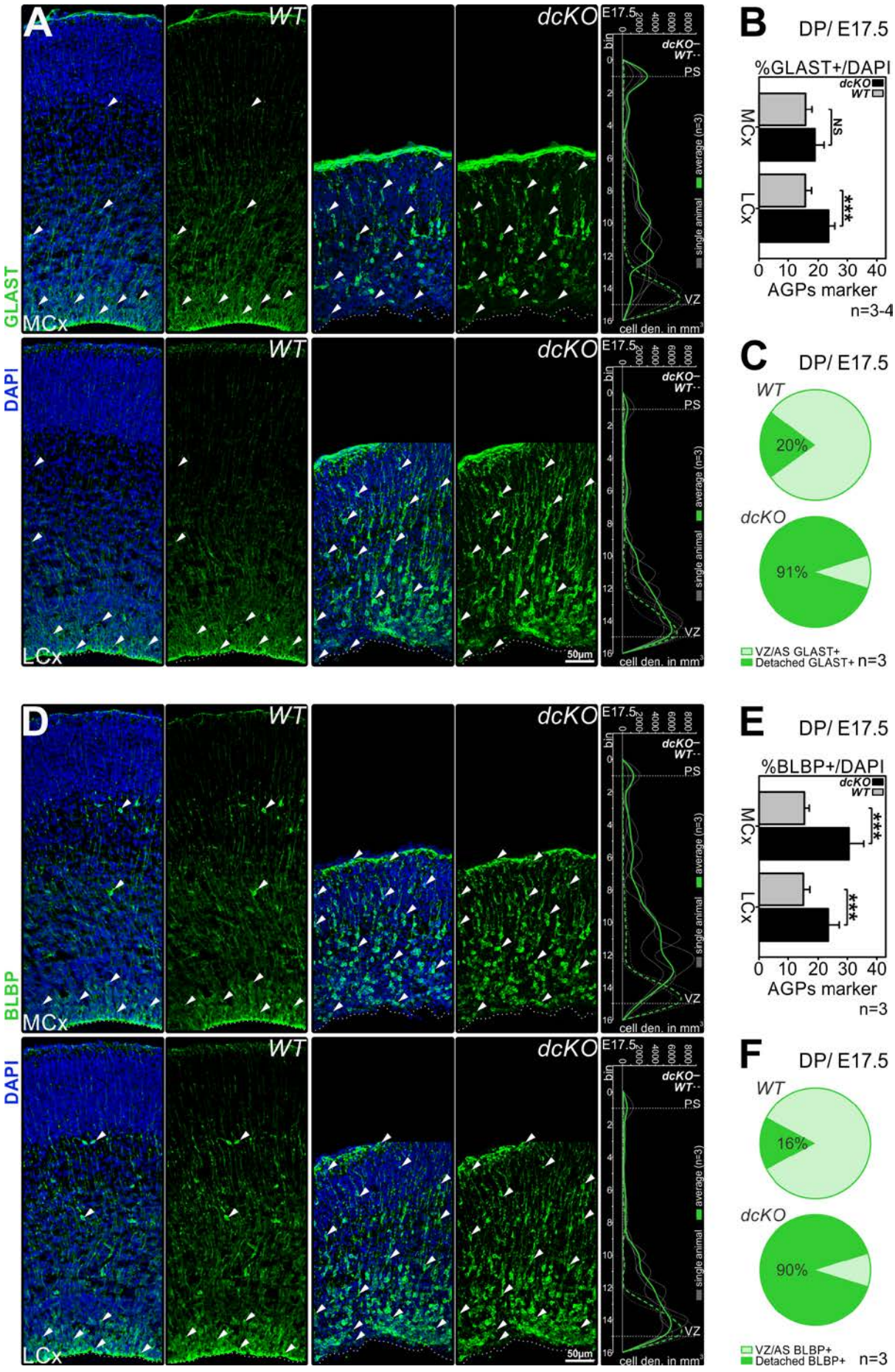
A
WT
dcKO
E17.5
GLAST
DAPI
MCx
LCx
PS
VZ
50µm
cell den. in mm²
B
DP/ E17.5
%GLAST+/DAPI
dcKO
WT
NS
***
AGPs marker
n=3-4
C
DP/ E17.5
20%
91%
VZ/AS GLAST+
Detached GLAST+
n=3
D
BLBP
E
%BLBP+/DAPI
F
16%
90%
VZ/AS BLBP+
Detached BLBP+

Figure 16 | Loss of RG features and delamination of cells expressing AGP markers in BAF complex deficient embryonic DP suggests their AGPs cell fate commitment. (A, D) Immunofluorescence analysis of coronal brain sections through WT and dcKO E17.5 murine MCx (future M1 area) and LCx (future S1 area) stained with antibodies to astroglial progenitor markers (in green); GLAST (A) and BLBP (D). The nuclei of cells visualized by DAPI intercalation (in blue). Overview pictures provided in Figure 15. Cells expressing GLAST and BLBP densely packed in the region of VZ with the preserved AS are astrocytic RGCs, delamination of cells expressing GLAST and BLBP from the VZ suggests the AGPs cell fate commitment of astrocytic RGCs. Full arrowheads indicate astrocytic RGCs (when attached to the AS and located in VZ)/ AGPs (when delaminated from VZ) expressing GLAST and BLBP. The surface of the VZ (for WT brains corresponds with AS) marked with dashed line. Line graphs represented in the extreme right boards of each (MCx and LCx for A and D) are distribution density plots generated for given marker in whole cortical column (divided in 16 equally sized bins) of given cortical area for WT (dashed line) and dcKO (solid line) animals (average plots for n=3 animals shown as thick green colour lines, plots for individual animals shown as thin gray colour lines). Each graph represents bin no. (0-16) juxtaposed with corresponding cell density in cubic millimeters. PS area corresponds to bin no. 1, VZ area corresponds to bin no. 15 (both marked with dashed lines). Distribution of GLAST/BLBP expressing cells in the WT MCx and LCx shows a clear peak in VZ area, whereas GLAST/BLBP positive cells in dcKO exhibited distribution scattered across the cortical column particularly visible in MCx. (B, E) Percentages of AGP marker positive cells: GLAST (B) and BLBP (D) per DAPI positive cells in the regions of MCx (future M1 area) and LCx (future S1 area) of E17.5 WT and dcKO mice. Data are averages ± σ of n=3-4 animals (for WT: GLAST/MCx: n=4, GLAST/LCx: n=4, BLBP/MCx: n=3, BLBP/ LCx: n=3; for dcKO: GLAST/MCx: n=3, GLAST/LCx: n=3, BLBP/MCx: n=3, BLBP/ LCx: n=3); ***p≤0.001, NS, not significant in t student test. (C, F) Pie charts showing the degree of VZ AS delamination of GLAST (C) and BLBP (F) positive cells in WT (upper panel) and dcKO (lower panel) E17.5 DP. Light green colour indicates percentages of marker positive cells residing in VZ attached to the AS, dark green colour indicates percentages of marker positive cells detached from VZ AS. Data are averages of n=3 animals (for WT: GLAST+/detached=20.3, GLAST+/AS=79.7±5.1%; BLBP+/detached=15.7, BLBP+/AS=84.3±6.5%; for dcKO: GLAST+/detached=90.6, GLAST+/AS=9.4±6.3%; BLBP+/detached=90.5, BLBP+/AS=9.5±4.6%). AGPs, astroglial progenitors; AS, apical surface; dcKO, double knockout; den. , density; DP, dorsal pallium; MCx, medial cortex (refers to the future M1 area); NS, not significant; LCx, lateral cortex (refers to the future S1 area); PS, pial surface; VZ, ventricular zone; WT, wild type.

positive cells were found outside of the germinal zone, in the intermediate regions of dcKO MCx. The loss of AS in S1 area of dcKO brain was not as remarkable as in MCx (Figure 16A-D, LCx). However, we still could observe a substantial amount of GLAST and BLBP positive cells in cortical areas other than dcKO VZ.

Interestingly, the percentages of DAPI positive cells expressing GLAST and BLBP (Figure 16B and E) revealed striking region dependent differences. In M1 area of dcKO, BLBP expressing cells significantly (***p≤0.001) outnumbered those of WT (with 30.5±4.3% and 15.4±1.1% of DAPI positive cells were BLBP expressing progenitors in dcKO and WT respectively). The same analysis for GLAST positive cells did not indicate significant differences between genotypes (p>0.05; 18.9±2.6% of dcKO and 15.8±1.6% of WT DAPI positive cells exhibited GLAST staining). This difference in cell abundance was obvious from the density plots generated for dcKO M1 area, with a reduced density of GLAST positive cells compared to BLBP (Figure 16A and D). However, regardless of their amount, the dcKO GLAST expressing cells still exhibited a scattered distribution, omitting the VZ (Figure 16 A and D; density plots). Surprisingly, these differences between genotypes did not appear in LCx

regions. In S1 area the percentages of DAPI positive cells expressing GLAST or BLBP found in dcKO brains were significantly higher than these of WT, with similar marker to DAPI ratios (***p≤0.001 for both analyzed markers; in WT 15.7±1.8% and 15.1±2.0%; in dcKO 23.6±1.5% and 23.4±3.2% of DAPI positive cells expressed GLAST and BLBP respectively). Thus, in dcKO DP, GLAST and BLBP positive cells differ in their abundance relative to WT (more BLBP and GLAST positive cells in dcKO cortex) as well as in their distribution (GLAST and BLBP positive cells were present in comparable amounts in the MCx and LCx of WT, while in dcKO, BLBP positive cells were more numerous in MCx than in LCx, with the opposite being true for GLAST positive cells).

In order to show the total degree of astrocytic RGCs delamination we further quantified the amount of all GLAST or BLBP positive cells found in VZ (tightly packed and directly creating the AS, as well as connected to the cells building the AS) and compared them to the numbers of cells that were delaminated. As indicated in Figure 16C and F, 80% of GLAST and 84% of BLBP positive cells in M1 and S1 (results were pooled) were residing in WT VZ attached to the AS. Thus, only 20% of GLAST and 16% of BLBP expressing cells were found to be detached and scattered throughout other cortical regions of WT brain. To the contrary, dcKO GLAST and BLBP positive cells showed a strong delamination with only 9% of GLAST and 10% of BLBP exhibiting cells facing the VZ surface. Accordingly, 91% of GLAST and 90% of BLBP expressing cells detached from VZ AS and migrated outside the germinal zone (Figure 16C and F; dcKO), indicating a tremendous delamination of BAF complex depleted astrocytic RGCs.

Altogether, our immunohistochemical analyses and quantifications show that the *hGFAP*-Cre driven loss of BAF complex within E17.5 cortical astrocytic RGCs causes their massive detachment from the surface of the VZ. This observation indicates a premature onset of astrocytic RGCs differentiation to AGPs in the brains of dcKO mice. Additionally, astrocyte precursors were more numerous in dcKO cortex than in WT, however their abundance and distribution varied depending on cortical area, with pronounced difference between medial and lateral regions. Finally, these results seem to confirm our previous assumption that a reduction in the abundance of BAF complex subunits causes the transformation of astrocytic RGCs to AGPs (see Chapter 3. Results. 3.1).

AGPs in postnatal cortex – dcKO versus WT phenotype

It is well know that the majority of astrocytic RGCs finish to differentiate into AGPs shortly after birth (Ge et al., 2012). This implies that in the early postnatal DP of WT mice the abundance of AGPs will increase compared to that of E17.5 cortex. Accordingly, this process may blur the difference between WT and dcKO astroglial phenotypes described above. In order to address this issue we decided to examine the abundance of AGPs and their distribution in P3 WT and dcKO cortex. Bearing

in mind the above described divergent AGPs phenotype of dcKO DP, we decided to again investigate GLAST and BLBP expressing cells within medial (developing M1 area) and lateral (developing S1 area) regions of postnatal cortex. For this purpose immunostaining analysis of GLAST and BLBP expression was conducted in WT and dcKO brain coronal sections isolated from P3 murine pups (Figure 17A and D). Additionally, we generated spatial distribution density plots (Figure 17A and D) as previously described (Chapter 2. Materials and Methods. 2.6) and the GLAST or BLBP positive cell numbers were manually registered and related to total cellular numbers (DAPI positive) within selected areas of cortex (Figure 17B and E). The percentages of markers positive cells found in the DW or scattered through the cortical thickness are shown in Figure 17C and F.

Overall, GLAST and BLBP positive cells were found through the full thickness of WT as well as dcKO cortex (Figure 17A and D, indicated by arrowheads). In WT M1 and S1 areas (MCx and LCx), as indicated in micrographs and density plots, a substantial amount of GLAST and BLBP expressing AGPs resided in DW (former VZ). However, the abundance of AGPs found scattered across these cortical areas was visibly higher than that of E17.5 (Figure 16A and D, Figure 17A and D). Even though the absolute numbers of GLAST and BLBP expressing cells appeared to not to deviate from these assessed for E17.5 M1 and S1 area (Figure17B and E, Figure 17 B and E), 60% of GLAST and 56% of BLBP positive cells were found outside of DW (Figure 17C and F), indicating an increase in AGPs abundance. As previously, expression pattern of GLAST and BLBP positive cells assessed in dcKO MCx and LCx greatly differed from that of WT. First of all, the abundance of GLAST and BLBP positive cells found in MCx of P3 dcKO DP was significantly greater comparing to WT (***$p \leq 0.001$ for both analyzed markers). Interestingly, the amount of GLAST expressing cells in MCx area of P3 mutant brain was elevated compared to E17.5 (for P3: 26.0±3.9%, for E17.5: 18.9±2.6% of DAPI positive cells expressing GLAST). However, the abundance of BLBP positive cells found in M1 area appeared not to differ between E17.5 and P3 (for P3: 32.3±5.4%, for E17.5: 30.5±4.3% of DAPI positive cells expressing BLBP). Therefore, the most parsimonious and straightforward explanation of this finding is that we observe the reconstitution of GLAST expression among MCx residing AGPs. Similarly to M1 area, the GLAST and BLBP positive cells of S1 LCx area of dcKO significantly outnumbered WT cells (***$p \leq 0.001$ where 23.4±2.1% and 9.5±1.3% of DAPI positive expressed GLAST and **$p \leq 0.01$ where 27.9±5.2% and 12.7±1.3% of DAPI positive expressed BLBP in dcKO and WT LCx respectively). Additionally, in agreement with E17.5 data, only 10% of all GLAST and 12% of all BLBP positive cells could be found at the surface of VZ (dcKO animals did not develop DW structure) of the M1 and S1 areas (Figure 17C and F; pie chart, dcKO). Accordingly, 90% of total GLAST expressing population and 88% of total BLBP expressing population were found to be scattered across the cortical thickness omitting the VZ surface. This phenomenon is visible in spatial distribution plots where high densities of GLAST and BLBP positive cells were obvious outside of dcKO DW (Figure 17A and D). Strikingly, the

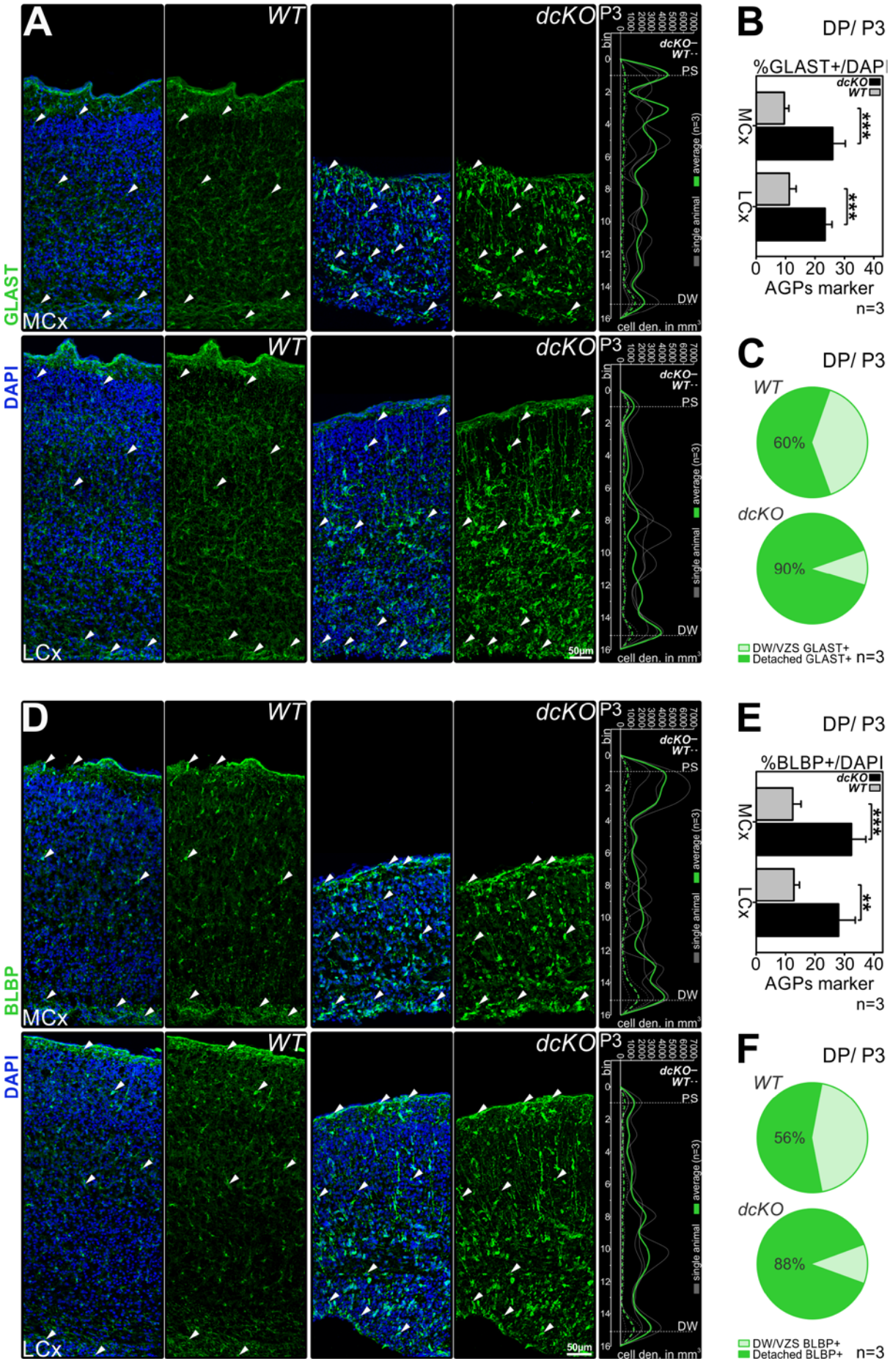
A
WT
dcKO
P3
GLAST
MCx
DAPI
LCx
50μm
cell den. in mm²
PS
DW
single animal
average (n=3)
dcKO
WT
B
DP/ P3
%GLAST+/DAPI
MCx
LCx
***
0 10 20 30 40
AGPs marker
n=3
C
DP/ P3
WT
60%
dcKO
90%
DW/VZS GLAST+
Detached GLAST+
n=3
D
BLBP
E
%BLBP+/DAPI
**
F
56%
88%
DW/VZS BLBP+
Detached BLBP+

Figure 17 | Numerous AGPs markers expressing cells scattered through the cortical column of BAF complex KO postnatal DP. (A, D) Immunofluorescence analysis of coronal brain sections through WT and dcKO P3 murine MCx (M2 area) and LCx (S1BF area) stained with antibodies to astroglial progenitor/astrocyte markers (in green); GLAST (A; overview in Figure 20) and BLBP (D, overview in Appendix, Figure 45A). The nuclei of cells stained by DAPI (in blue). Line graphs represented in the extreme right (MCx and LCx for A and D) are distribution density plots generated for a given marker in the whole cortical column (for each divided for 16 the same size bins) of a given cortical area for WT (dashed line) and dcKO (solid line) animals (average plots for n=3 animals shown as thick green colour lines, plots for individual animals shown as thin gray colour lines). Each graph represents bin no. (0-16) juxtaposed with corresponding cell density found in cubic millimeters. PS area corresponds with bin no. 1, DW area corresponds with bin no. 15 (both marked with dashed lines). Distribution of GLAST/BLBP expressing cells in the WT MCx and LCx shows clear peak in DW area with several cells found in CP and IZ, whereas GLAST/BLBP positive cells in dcKO were scattered across the cortical column without a single peak corresponding to the area of DW. (B, E) Percentages of AGP/astrocyte marker positive cells: GLAST (B) and BLBP (D) per DAPI positive cells in the regions of MCx (M2 area) and LCx (S1BF area) of P3 WT and dcKO mice. Data are averages ± σ of n=3 animals; ***p≤0.001, **p≤0.01 in t student test. (C, F) Pie charts showing the degree of DW detachment of GLAST (C) and BLBP (F) positive cells in WT (upper panel) and dcKO (lower panel) P3 DP. Light green colour indicates percentages of marker positive cells residing in DW (in WT)/attached to the VZS (in dcKO), dark green colour indicates percentages of marker positive cells outside DW. Data are averages of n=3 animals (for WT: GLAST+/detached=60.9, GLAST+/DW=39.1± 7.6%; BLBP+/detached=56.0, BLBP+/DW=56.0±5.4%; for dcKO: GLAST+/detached= 89.8, GLAST+/VZS= 10.2±4.2%; BLBP+/detached=88.8, BLBP+/VZS=11.2 ±5.27%). AGPs, astrocytic progenitors; dcKO, double knockout; den., density; DP, dorsal pallium; DW, deep cerebral white; MCx, medial cortex (refers to the M1 area); LCx, lateral cortex (refers to the S1 area); PS, pial surface; VZS, ventricular zone surface; WT, wild type.

spatial distribution of the cells evaluated in dcKO M1 and S1 areas seemed to differ from that of E17.5 (Figure 16A and D, Figure 17A and D). The comparison of dcKO density plots generated for E17.5 and P3 GLAST and BLBP expressing cells found in MCx and LCx indicated a tendency for P3 dcKO GLAST and BLBP positive AGPs to reside closer to the PS.

In summary, we conclude that despite the visibly advanced differentiation of astrocytic RGCs towards AGPs in early postnatal WT DP, higher AGPs abundance suggests that the astrogliogenic processes are much more advanced in cortex affected by BAF complex depletion.

Astroglial identity of upregulated progenitors

Previous studies from our group showed that the loss of BAF155 subunit evokes delamination of RGCs from the cortical VZ and subsequent generation of oRGPs (Narayanan et al., 2018). These progenitors exhibit several characteristics of AGPs. They are lacking apical junctions and thus reside outside the VZ, and express some common astrocyte markers such as GLAST or BLBP (Heng et al., 2017; Narayanan et al., 2018; Pollen et al., 2015). Regardless of their AGPs – like features, oRGPs do not produce astrocytes, and in primates they are believed to generate the majority of cortical neurons, to the point that they were suggested to be responsible for cortical expansion and folding

(Dehay and Kennedy, 2007; Hansen et al., 2010; Lui et al., 2011; Pollen et al., 2015).

In order to confirm the astroglial identity of the upregulated progenitors found in dcKO cortex we decided to immunohistochemically investigate the NFiA expression within upregulated GLAST positive cells (Figure 18; see Chapter 3. Results. 3.3). We chose NFiA to identify astroglia because of its well-known role in astrocyte differentiation, reprogramming and maintenance (Caiazzo et al., 2015; Deneen et al., 2006; Kang et al., 2012; Molofsky et al., 2012). Additionally NFiA RNA was not found to be present in the group of astroglial transcripts enriched within oRGPs (in contrast to e.g. Ptprz1, Blbp or Tnc) (Pollen et al., 2015). However, due to the broad range of cells exhibiting NFiA staining through the cortex (Bunt et al., 2017), this marker could not be used as an exclusive marker of astroglial fate. Thus we chose to confirm the astroglial nature of the elevated progenitors by their simultaneous expression of NFiA and GLAST (Deneen et al., 2006; Kang et al., 2012).

We therefore assessed co-expression of GLAST and NFiA by immunostaining performed on P3 brain coronal sections isolated from WT and dcKO mouse pups. Due to the distinct GLAST phenotype of medial or lateral cortical regions of dcKO brain (previously described), the expression of the markers selected was further analyzed in developing M1 (MCx) and S1 areas (Figure 18).

The NFiA staining showed strong enrichment in WT MCx and LCx, prominently marking DW and layer V located cells with single positives scattered across the cortical thickness (Figure 18 A-C; WT). To the contrary, numerous NFiA expressing cells found in dcKO MCx and LCx areas exhibited rather dispersed location eschewing grouping in LV (Figure 18 A-C; dcKO). Interestingly, the percentages of all DAPI positive cells exhibiting NFiA staining were significantly upregulated in medial (M1) as well as lateral (S1) areas of dcKO cortex (**$p \leq 0.01$; 25.7±4.9% and 47.9±3.9% of DAPI positive cells found in MCx as well as 31.7±4.8% and 46.1±2.5% of DAPI positive cells found in LCx of WT and dcKO respectively, Figure 18D). Increased numbers of NFiA positives may indicate a massive promotion of glial fate cells that do not necessarily express other astroglial markers (e.g. GLAST or BLBP). This interpretation appears legitimate when considering the critical role of NFiA in gliogenesis initiation (Kang et al., 2012) as well as the loss of GLAST and BLBP within early RGCs affected by BAF complex depletion (Nguyen et al., 2018). However, a massive upregulation of NFiA within dcKO cortex revealed by quantitative study could be due to the reduced cortical thickness and misinterpreted glial/neuronal fate of counted NFiA positive cells (Bunt et al., 2017).

Importantly, double immunohistochemical analysis revealed that the majority of WT as well as dcKO GLAST positive cells co-expressed NFiA (indicated by full arrowheads). As typical AGPs, GLAST/NFiA positive cells could be localized across the cortical thickness of M1 and S1, near PS, in CP and in DW of both WT and dcKO brains (Figure 18B and C). Additionally, several GLAST positive cells found in CP (empty arrowheads) of WT and dcKO mice did not express NFiA, suggesting that their fate is not to become AGPs. These cells could be oRGPs however, more experiments need to be done in order to

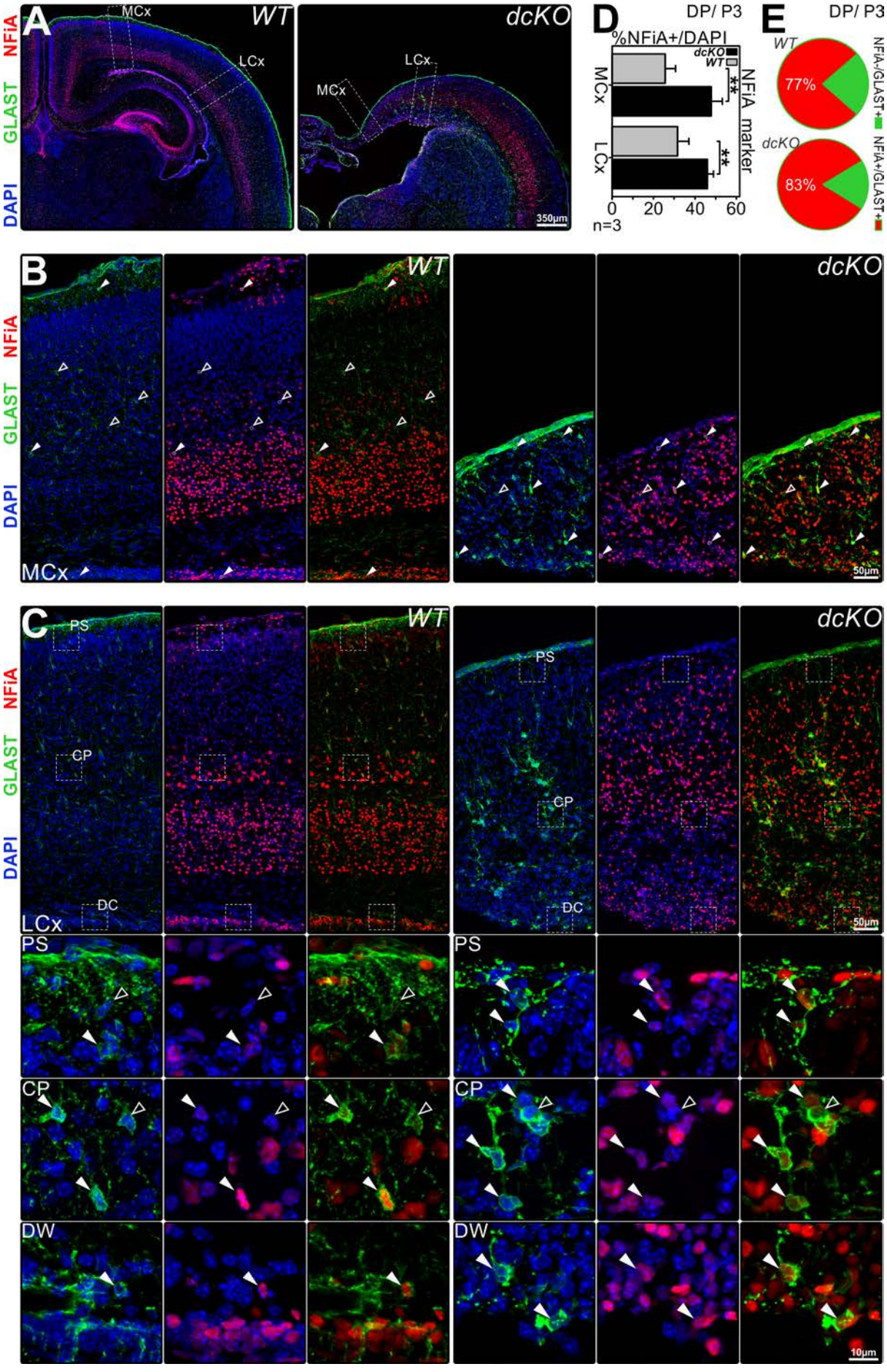
A
WT
dcKO
MCx
LCx
NFiA
GLAST
DAPI
350μm
D
DP/ P3
%NFiA+/DAPI
dcKO
WT
MCx
LCx
NFiA marker
**
**
0
20
40
60
n=3
E
DP/ P3
WT
77%
dcKO
83%
NFiA-/GLAST+
NFiA+/GLAST+
B
WT
dcKO
MCx
50μm
C
WT
dcKO
PS
CP
DC
LCx
50μm
PS
CP
DW
10μm

Figure 18 | Astroglial identity of GLAST positive cortical progenitors in BAF complex deficient DP. (A-C) Coronal sections through P3 brains of WT and dcKO mice stained with antibodies to astroglial progenitor markers; GLAST (in green) and NFiA (in red). The nuclear DAPI staining is blue. Cells expressing GLAST and NFiA are AGPs. GLAST positive cells lacking expression of NFiA are (possibly) oRGPs. (A) Overview pictures of WT and dcKO DP areas. (B-C) Magnified insets of (B) MCx (developing M1 area) and (C) LCx (developing S1 area) delineated in (A). Full arrowheads indicate AGP expressing GLAST and NFiA, empty arrowheads indicate progenitors expressing only GLAST. For (C) lower panels of magnified LCx view are enlarged insets of delineated areas of PS, CP and DW. For (B) nuclei of arrow indicated cells outlined with dashed line. (D) Percentages of NFiA positive GP per total number of DAPI positive cells in the regions of MCx (M1 area) and LCx (S1BF area) of P3 WT and dcKO DP. Data are averages ± σ of n=3 animals; **p≤0.01, in student's t-test. (E) Pie charts showing the degree of colocalization between GLAST and NFiA in WT (upper graph) and dcKO (lower graph) P3 DP. Red colour indicates percentages of GLAST positive cells expressing NFiA, green colour indicates percentages of GLAST positive cells negative for NFiA. Data are averages of n=5-6 experimental replicates (for WT: n=5, GLAST+/NFiA+=77.09%, GLAST+/NFiA-=22.9±8.1%; for dcKO: n=6, GLAST+/NFiA+=82.6%, GLAST+/NFiA-=17.4%±4.7%). CP, cortical plate; dcKO, double knockout; DP, dorsal pallium; DW, deep cerebral white; MCx, medial cortex (refers to M1 area); LCx, lateral cortex (refers to S1BF area); PS, pial surface; WT, wild type.

prove this assumption (Fietz et al., 2010; Narayanan et al., 2018; Wang et al., 2016a). The quantitative study of GLAST/NFiA co-expression revealed that 83% of GLAST positive cells found in DP of dcKO brains exhibited NFiA expression (Figure 18E). Similarly, 77% of GLAST positive progenitors registered in WT DP expressed NFiA. Only 17% of dcKO and 23% of WT GLAST staining cells could potentially be considered as oRGPs, as they did not exhibit NFiA staining. Thus the majority of GLAST positive cells found in cortex of P3 WT and dcKO mice were AGPs.

In summary, we could confirm that the increased abundance of GLAST expressing cells in DP of dcKO mouse brains was related to active astroglial processes presumably evoked by *hGFAP*-Cre driven BAF complex depletion within astrocytic RGCs.

Aberrant gene expression profile of dcKO affected DP

Beyond a mere immunohistochemical investigation of protein expression, the analysis of the transcriptome may help us reveal and understand the changes evoked by *hGFAP*-Cre driven BAF complex depletion. Thus, as a next step we decided to examine and compare the gene expression profiles of WT and dcKO murine DP isolated from E17.5 embryos and P3 pups. We focused our analysis on these two distinct developmental stages because of two particular reasons. First of all, we wanted to inquire whether dcKO evoked DP transcriptome changes increase over the time. Secondarily, we wished to capture these transcriptome aberrations that persist in developing dcKO DP. We chose the E17.5 stage as murine cortical astrogliogenesis starts approximately at this gestational day (Cameron and Rakic, 1991; Minocha et al., 2015). The selection of P3 as another time point was dictated by necessity, as the lifespan of dcKO mice did not exceed 3-4 days *post-partum*. In order to assess the expression profiles of the selected genes, RNA was isolated from E17.5 and P3

WT and dcKO DP tissue lysates and subsequently subjected to sequencing analysis (see Chapter 2. Materials and Methods. 2.8). RNA-seq experiment was conducted in collaboration with Prof. André Fischer.

The analysis of the transcriptome revealed massive gene expression aberrations found within DP of E17.5 and P3 dcKO mice (Figure 19). As indicated by volcano plots, 623 and 3199 transcripts were significantly downregulated in E17.5 and P3 dcKO DP, respectively ($p \leq 0.01$, -Log $p \geq 2$, Figure 19A and B, blue colour). Accordingly, in E17.5 dcKO DP 533 transcripts were significantly upregulated (Figure 19A, in red colour). The number of aberrantly upregulated genes increased to 2804 transcripts found in DP of P3 dcKO mice (Figure 19B, in red).

Thus the loss of BAF complex in cells of DP targeted by *hGFAP*-Cre evoked massive aberrations in gene expression profiles that amplified over developmental time.

Next, in order to inquire whether transcriptome aberrations persist in developing dcKO DP, we compared the transcripts significantly up and downregulated found in DP of E17.5 and P3 mice (Figure 19C and D). As shown by means of Venn diagrams, 440 transcripts (blue colour diagrams) were found to be significantly downregulated in DP of both analyzed developmental stages. Similarly, in DP of E17.5 and P3 dcKO 284 transcript were upregulated at both developmental stages (red colour diagrams). This analysis indicated the existence of a subset of genes whose normal expression was permanently disrupted following BAF complex depletion.

After finding that substantial transcriptome changes persist in developing dcKO DP, we decided to classify the aberrant down and upregulated transcripts according to their biological functionality using GO enrichment analysis (http://geneontology.org/). As shown in Figure 19E, transcripts found to be highly downregulated in DP at both developmental stages (E17.5 and P3) were known regulators of neurogenesis, responsible *inter alia* for neuronal maturation and differentiation, axonogenesis or dendrite development. Importantly, the transcriptome changes were enhanced in DP of P3 dcKO mice, suggesting that deficits in neuronal development were possibly already present at E17.5 (at least at the transcriptome level) and could not be rescued at later developmental stages (indicating that abundant GLAST/BLBP progenitors observed in dcKO did not differentiate to neurons). A similar enrichment analysis performed for the transcripts significantly upregulated in E17.5 and P3 dcKO DP indicated a durably increased expression of genes positively regulating cell proliferation (Figure 19F). Additionally, it was found that stem cell proliferation transcripts, prominent at E17.5, tended to decline in postnatal dcKO DP in favour of transcripts related to proliferation of other cell types. Unfortunately GO analysis did not reveal a common pool of transcripts related to gliogenic processes and modulated at both developmental stages, however as indicated by white-red heat map, some of transcripts upregulated in DP of E17.5 dcKO could be related to glial cell fate commitment. Similarly, a group of upregulated transcripts found in DP of P3

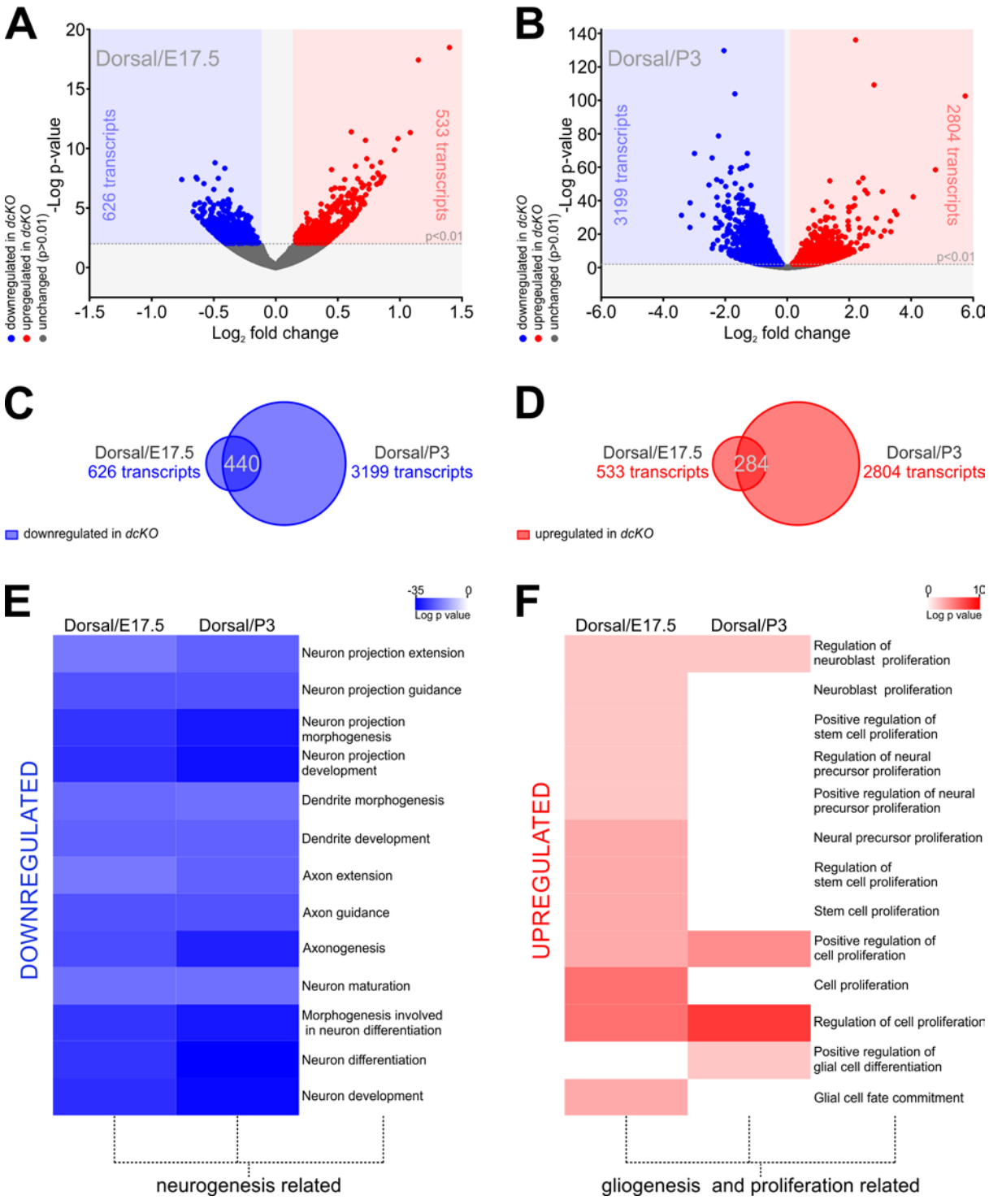

Figure 19 | Aberrant gene expression profile in BAF complex depleted embryonic and postnatal DP. (A-B) Transcriptome of (A) E17.5 and (B) P3 *hGFAP*-Cre dcKO versus WT DP. Volcano plots represent Log_2 fold change of transcript abundance together with –Log of corresponding p value for all significantly upregulated (in red) and downregulated (in blue) transcripts. Gray colour indicates transcripts with insignificant changes (p>0.01). The exact number of down and upregulated transcripts is noted in blue and red respectively. (C-D) Venn diagrams illustrating overlap between (C) downregulated and (D) upregulated transcripts of E17.5 and P3 *hGFAP*-Cre dcKO DP. Numbers in gray indicate exact amount of transcripts down- (C) and upregulated (D). (E-F) Examples of biological processes significantly down- (E) and upregulated or unchanged (F) in E17.5 and P3 *hGFAP*-Cre dcKO DP. Heat maps show Log of p value for corresponding analyzed GO pathway. Dendrograms depict existing relation between downregulated

(neurogenesis related) and upregulated (gliogenesis and proliferation related) pathways. Data are averages of n=3-4 animals (E17.5 DP; *hGFAP*-Cre dcKO: n=3, WT: n=4; P3 DP; *hGFAP*-Cre dcKO: n=4, WT: n=4). For all investigated transcripts p≤0.01. In GO pathway enrichment analysis Bonferroni-corrected for p<0.05. Transcriptome results stating about neurogenesis and proliferation at E17.5 have been already published in (Nguyen et al., 2018). dcKO, double conditional knockout.

dcKO was described as positive regulators of glial cell differentiation (Figure 19F). Thus, this analysis indicated advanced gliogenic processes visible in the revealed transcriptome aberrations of dcKO DP.

In summary, the data presented here constitute elegant evidence for massive changes in DP gene expression profiles evoked by *hGFA*P-Cre driven BAF complex loss. Some of these changes could be classified as neurogenesis related, in case of transcripts significantly downregulated in BAF depleted tissues, as well as gliogenesis and proliferation related, for transcripts of which BAF complex loss caused significant upregulation. Overall, our transcriptome analysis revealed two important features of the BAF-depleted cortex: impaired neurogenesis and enhanced gliogenesis and proliferation.

Production of neurons or AGPs? Neuronal deficits in dcKO postnatal cortex

Given that the initial analysis of dcKO evoked transcriptional changes indicated a massive impairment of neurogenesis, as a next step we decided to gain further insight into neuronal deficits in BAF complex depleted P3 DP (Figure 20). In view of our previous observations that BAF subunits are upregulated in neurons (see Chapter 3. Results. 3.1), the neuronal development of BAF depleted progenitors appeared especially intriguing. Importantly, we decided to investigate dcKO impact on late born neurons (upper layers neurons), as these are the last to be developed before neurogenesis ceases and astrogenesis takes over (Miller and Gauthier, 2007).

In order to evaluate the abundance of upper layer neurons we first decided to assess the expression of the late born neuron marker - special AT-rich sequence-binding protein 2 (SATB2) in DP coronal sections of WT and dcKO P3 pups by immunostaining (Britanova et al., 2008; Georgala et al., 2011). Additionally, for the purpose of comparing neuronal and astroglial phenotypes, we also assessed these sections for the expression of the AGPs enriched marker – GLAST (Zhao et al., 2014). Like previously, due to the distinct astroglial phenotype in medial and lateral cortical regions, as well as because of the reduced cortical thickness of dcKO brain (described in Chapter 3. Results. 3.2), the expression of the markers chosen was evaluated in developing M1 (MCx) and S1 (LCx) areas (Figure 20A-E).

In agreement with transcriptome data, double SATB2/GLAST immunostaining analysis of P3 DP revealed a massive reduction in SATB2 expressing neuronal pool in favour of GLAST positive AGPs (Figure 20A). Importantly, similarly to the astroglial phenotype described earlier, the abundance and

cortical position of SATB2 positive late born neurons exhibited regional differences with distinct phenotypes found in medial and lateral cortical areas of dcKO mice (Figure 20A-C). As presented in Figure 20B and C (pointed by empty arrowheads), SATB2 staining was visibly enriched in upper layers of developing WT M1 (MCx) and S1 (LCx) cortical areas. Interestingly, as shown in bar graphs presented in Figure 20D and C, SATB2 positive cells constituted around 50% of all DAPI cells found in the regions of MCx and LCx of P3 WT pups. Thus, SATB2 staining data indicated that advanced and proper neurogenesis processes take place in WT DP. Strikingly, the expression of SATB2 within P3 dcKO MCx was significantly (***p≤0.001) reduced compared to that of WT, with few SATB2 positive cells scattered across the cortical thickness (Figure 20B and D, empty arrowheads).

The same antibody staining of dcKO LCx area appeared to be more prominent (Figure 20C), however, still significantly reduced (**p≤0.01) compared to WT S1 (Figure 20 E). In addition, in contrast to the MCx region, stained dcKO SATB2 positive neurons preferentially populated upper cortical areas of LCx exhibiting specific medio-rostral gradient of enrichment (Figure 20A).

As described previously, dcKO DP exhibited highly elevated levels of GLAST expressing cells that were found to be spread throughout the full cortical thickness (Figure 20A-C, examples indicated by full arrowheads). Interestingly, in dcKO MCx the percentages of DAPI positive cells expressing GLAST appeared to be higher than these of DAPI cells expressing SATB2 (Figure 20D). This was not the case in dcKO LCx (Figure 20E). Importantly, the depletion of late born neurons in P3 dcKO DP could be confirmed by our RNA-seq data. Screening the literature allowed us to identify 15 late born neurons specific genes characteristic for mouse neocortex (Molyneaux et al., 2007). We searched our transcriptome sequencing data for the expression of these genes. As indicated in the bar graph in Figure 20H, these late born neurons related transcripts (Molyneaux et al., 2007) were significantly downregulated in P3 DP of dcKO. Importantly, the reduction of SATB2 (Figure 20A-E) described above was found to be significant as well at the RNA level (Figure 20H). Additionally, it is known that BRN2 is one of the crucial regulators of late neurogenesis (Dominguez et al., 2013) and it is largely due to its suppression by NFiA and SOX9 that the molecular processes within RGCs switch from neurogenic to astroglial (Nagao et al., 2016). Importantly Brn2 was one of the late born neuron related transcripts found to be downregulated in dcKO DP, suggesting the promotion of astrogenesis and suppression of late born neurons development in dcKO DP.

Bearing in mind that the *hGFAP*-Cre driven recombination starts earlier than the late neurogenesis processes (see Chapter 3. Results. 3.2) we then decided to inquire about the scale of total neuronal depletion investigating how many of significantly downregulated transcripts (found in dcKO P3 DP by RNA-seq; described above) would be related to neuronal development, morphology and physiology. For this purpose, by means of GO analysis we sorted all of significantly downregulated transcripts

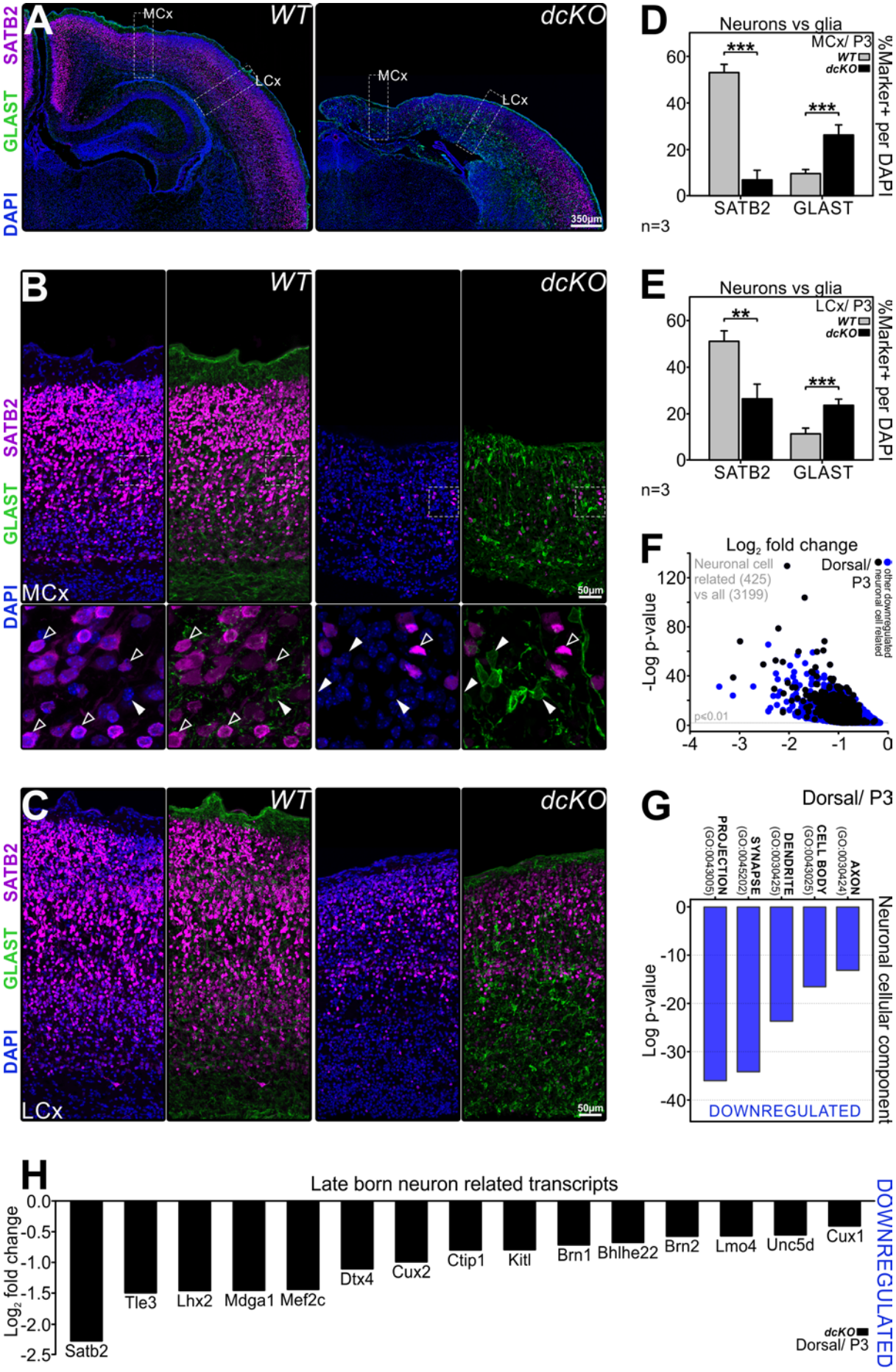
A
WT
dcKO
MCx
LCx
SATB2
GLAST
DAPI
350µm
B
MCx
50µm
C
LCx
50µm
D
Neurons vs glia
MCx/ P3
WT
dcKO
%Marker+ per DAPI
***
***
SATB2
GLAST
n=3
E
Neurons vs glia
LCx/ P3
**
***
n=3
F
Log2 fold change
Neuronal cell related (425) vs all (3199)
Dorsal/ P3
other downregulated
neuronal cell related
-Log p-value
p≤0.01
G
Dorsal/ P3
PROJECTION (GO:0043005)
SYNAPSE (GO:0045202)
DENDRITE (GO:0030425)
CELL BODY (GO:0043025)
AXON (GO:0030424)
Log p-value
Neuronal cellular component
DOWNREGULATED
H
Late born neuron related transcripts
Log2 fold change
Satb2
Tle3
Lhx2
Mdga1
Mef2c
Dtx4
Cux2
Ctip1
Kitl
Brn1
Bhlhe22
Brn2
Lmo4
Unc5d
Cux1
DOWNREGULATED
dcKO
Dorsal/ P3

Figure 20 | Postnatal murine DP affected by BAF complex KO exhibits severe neuronal deficits favouring AGPs production. (A-C) Immunofluorescence analysis of P3 WT and dcKO murine cortical coronal sections stained with antibody to upper layer neurons marker – SATB2 (in magenta) together with antibody to AGPs marker – GLAST (in green). The nuclei of cells visualized by DAPI intercalation (in blue). (A) Overview pictures of WT and dcKO cortical areas. (B-C) Magnified insets of (B) MCx (M1 area) and (C) LCx (S1 area) delineated in (A). For (B) lower panels of each are enlarged views of outlined areas. Full arrowheads indicate AGPs expressing GLAST, empty arrowheads indicate neurons expressing SATB2. (D-E) Bar graphs showing percentage share of SATB2 positive cells and GLAST positive cells in all DAPI positive cells of P3 WT and dcKO mouse (D) MCx and (E) LCx. Data are averages ± σ of n=3 animals; ***p≤0.001, **p≤0.01 in t student test. (F) Expression profile of significantly downregulated neuronal cell related transcripts (in black) juxtaposed with all significantly downregulated transcripts (in blue) in DP of P3 *hGFAP*-Cre dcKO versus WT mice. Scatter plot represents Log_2 fold change of transcript abundance together with –Log of corresponding p value for all significantly downregulated transcripts. The exact transcripts numbers noted in brackets. (G) GO cellular component enrichment analysis indicating groups of genes related to neuronal cellular elements significantly downregulated in P3 DP *hGFAP*-Cre dcKO. Exact GO ID numbers shown in brackets. Bar graph represents –Log of corresponding p value for each indicated cellular component category. (H) Bar graph representing Log_2 fold change of late born neuron related transcripts abundance in DP of P3 dcKO animals. Transcriptome data are averages of n=4 animals. For all investigated transcripts p≤0.01. In GO pathway enrichment analysis Bonferroni corrected for p<0.05. dcKO, double knockout; MCx, medial cortex (refers to M1 area); LCx, lateral cortex (refers to S1 area); WT, wild type.

(3199 blue colour data points, Figure 20F) into two groups: neuronal cell related and unrelated. Strikingly, 425 transcripts out of all 3199 could be classified as neuronal cell related. Importantly, as shown by scatterplot (Figure 20F), many of neuron-related transcripts were strongly downregulated with high significance (black data points). Additionally, GO cellular component enrichment analysis revealed groups of transcripts related to neuronal cellular elements significantly downregulated in P3 DP (Figure 20G). Among them the 5 most aberrant were these related to neuronal projection, synapse, dendrite, cell body and axon. All of the transcripts assigned to these 5 groups were highly and significantly downregulated in P3 dcKO DP comparing to that of WT (e.g. the amount of transcripts related to neuronal projections was over 35 times lower in dcKO DP than in WT; Figure 20G).

Taken together, these results indicate that *hGFAP*-Cre driven BAF complex loss manifests itself as severe neuronal deficits in postnatal DP. Additionally, the data suggests that BAF complex plays a decisive role in balancing cortical neurogenesis and astrogenesis, as its depletion leads to the promotion of astroglia (AGPs) production and suppresses late born neurogenesis.

Proliferation of BAF complex depleted cortical AGPs

During the first postnatal weeks, the abundance of rodent astroglia increases up to 8-fold (Bandeira et al., 2009). Exciting reports of 2 - photon imaging and bromodeoxyuridine (BrdU) pulsing experiments indicated locally proliferative AGPs as a major source for astroglia expansion (Chaboub

and Deneen, 2013; Ge et al., 2012; Tien et al., 2012). However, little is known about the molecular underpinnings controlling this process. Considering that the gliogenesis and proliferation related transcripts were significantly upregulated in embryonic as well as postnatal DP of dcKO murine brain, a further goal of our project was to determine whether highly numerous BAF complex depleted AGPs found in P3 cortex exhibit elevated proliferation capacities.

For this purpose two types of experiments addressing cellular proliferation were performed. The first involves immunohistochemistry of the proliferation marker – Ki67 (Scholzen and Gerdes, 2000) within BLBP positive AGPs (Figure 21). The second consists of the labelling and identification of the fraction of the proliferative cells by IP injected thymidine analogue - EdU (Chehrehasa et al., 2009; Flomerfelt and Gress, 2016; Vega and Peterson, 2005) and subsequent recognition of proliferative cells by immunostaining analysis (Figure 22A).

Accordingly, by means of immunofluorescence analysis, we assessed the expression of AGPs enriched marker – BLBP together with proliferation marker – Ki67 (Figure 21C). We performed this immunostaining on coronal sections of developing M1 (MCx) and S1 (LCx) cortical areas of WT and dcKO P3 brains (Figure 21A and B).

As indicated in Figure 21A and B, some of WT BLBP expressing cells found in MCx and LCx areas did exhibit Ki67 staining (full arrowheads) indicating active local proliferation of AGPs in postnatal DP. Quantitatively these WT proliferative AGPs accounted for 15.2±2.5% of all BLBP positive (the results of manual quantifications performed in both stained areas of cortex were pulled together; bar graph presented in Figure 21D). Strikingly, the BLBP enriched cells found in MCx and LCx of dcKO DP frequently exhibited Ki67 expression. Quantitatively 26.7±5.4% of dcKO BLBP positive cells stained for Ki67, significantly outnumbering Ki67 expressing BLBP positive cells found in WT (*$p \leq 0.05$; Figure22 A, B and D).

Further, as explained above, we decided to investigate the proliferation of BLBP positive cells by another method - EdU labeling. For this purpose EdU was injected into WT/dcKO P3 pups 30 minutes before brain isolation (Figure 22A). As EdU incorporates to DNA during the S phase of cell cycle, this method allowed us to label the fraction of cells that were proliferative at the time of tissue collection. Next, we detected BLBP and EdU by immunostaining (Figure 22B). Overall, BLBP stained cells that incorporated EdU were found in cortex of WT and dcKO (Figure 22B, full arrowheads). However, the fraction of BLBP expressing cells exhibiting EdU labelling was significantly higher in dcKO compared to that of WT (**$p \leq 0.01$; in WT 12.9±1.8% whereas in dcKO 19.1±1.3% of all BLBP stained for EdU). Additionally, a substantial amount of WT BLBP/EdU positive cells was found in DW area of cortex (Figure 22B DW; full arrowheads) indicating their astrocytic RGCs fate rather than AGPs (Tramontin et al., 2003). To the contrary, dcKO BLBP/EdU stained cells were scattered through the full cortical thickness, which suggests that these were proliferative AGPs. Considering this

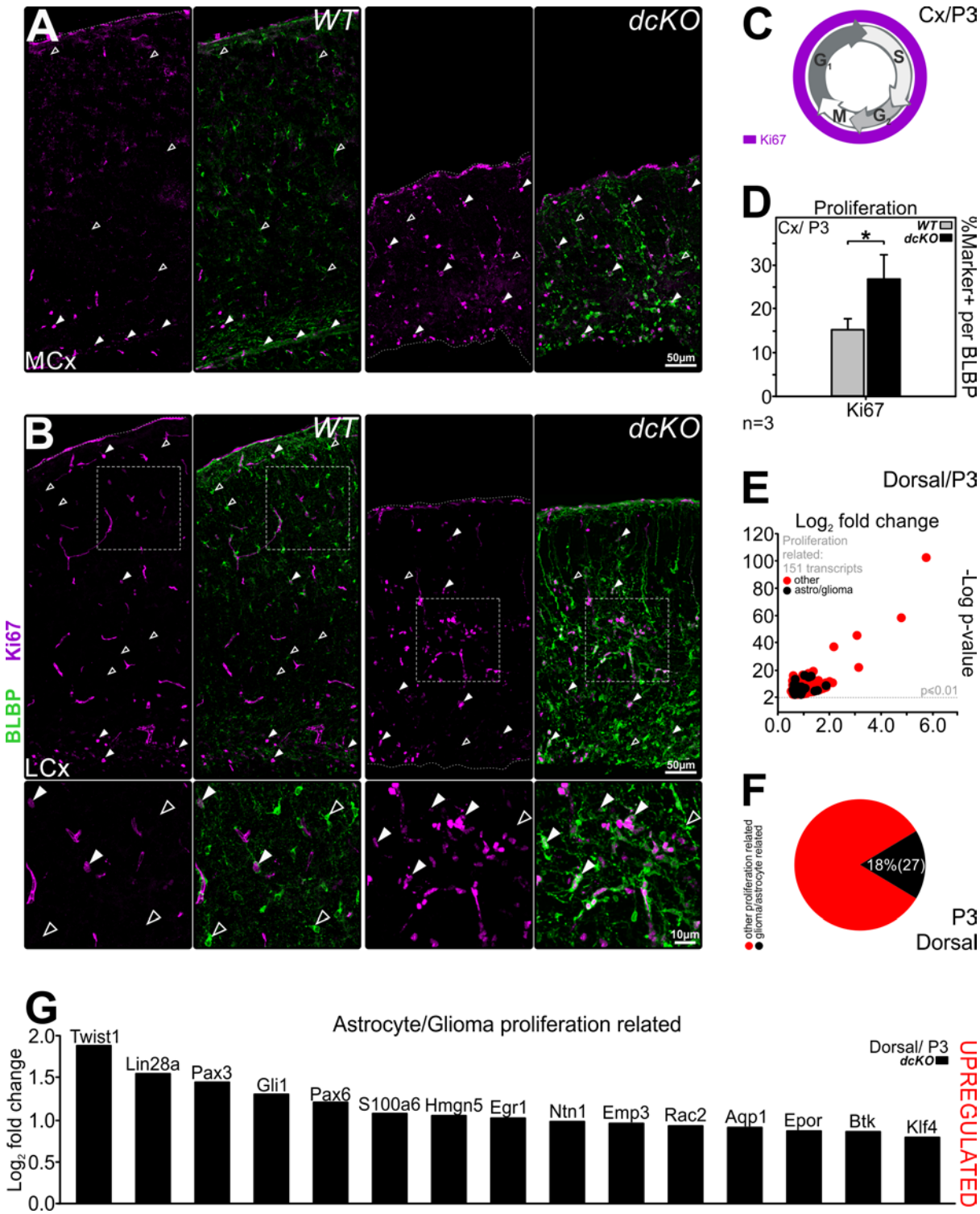

Figure 21 | High proliferation capacities of BAF complex depleted dorsal AGPs (I). (A) Coronal tissue sections through WT and dcKO P3 mouse MCx (developing M1 area) and LCx (developing S1 area) stained with antibody detecting AGPs enriched marker - BLBP (in green) together with proliferation marker Ki67 (in magenta). The nuclear DAPI staining is blue. Cells expressing BLBP together with Ki67 are proliferative AGPs. For (B) lower boards of each are magnified insets of delineated areas. Full arrowheads indicate proliferative AGPs, empty arrowheads indicate non-proliferative AGPs. (C) Scheme explaining the principle of proliferation analysis by Ki67 staining. Ki67 (magenta) is expressed during all active phases of the cell cycle. (D) Percentages of proliferative AGPs found among all BLBP expressing cells, registered in

the total cortex (MCx and LCx) of P3 WT and dcKO mice. Data are averages ± σ of (A) n=3 experimental replicates; *p≤0.05 in t- student test. (E) Expression profile of significantly upregulated glioma/astrocyte proliferation related transcripts (in black) juxtaposed with all cell proliferation related transcripts (in red) upregulated in DP of P3 *hGFAP*-Cre dcKO versus WT mice. Scatter plot represents Log_2 fold change of transcript abundance together with –Log of corresponding p value for all significantly upregulated proliferation related transcripts. The Log_2 fold change level of upregulation as well as names of glioma/astrocyte proliferation related transcripts represented as black dots in scatter plot are shown in G. (F) Pie chart showing the percentage of glioma/astrocyte proliferation related transcripts among all significantly upregulated proliferation associated transcripts. The exact transcript number shown in brackets. For E and F black colour refers to the glioma/astrocyte proliferation related transcripts, red colour refers to other upregulated proliferation related transcripts. Transcriptome data are averages of n=4 animals. For all investigated transcripts p≤0.01. In GO pathway enrichment analysis, used for proliferation related transcripts detection, Bonferroni-corrected for p<0.05. Cx, cortex; dcKO, double knockout; MCx, medial cortex (refers to the developing M1 area); LCx, lateral cortex (refers to the developing S1area); WT, wild type.

observation we then asked how many of BLBP expressing cells labelled by EdU could be found scattered through the cortical thickness in WT and dcKO and which fraction of these resided in DW. Since mutant animals did not develop DW structure we decided to count the number of BLBP/EdU positives found at the surface of dcKO VZ. As presented in pie charts (Figure 22D) only 15% of WT BLBP expressing cells that incorporated EdU could be found in the areas of cortex different than DW. In contrast to WT, 98% of dcKO EdU labelled BLBP positive cells were detached from the VZ surface and scattered across the full cortical thickness. This implies that the majority (98%) of dcKO BLBP/EdU stained proliferative cells may classify as AGPs. The same classification applies to the smaller fraction of WT EdU labelled BLBP expressing cells, which accounted only for 15%.
Thus, our Ki67 immunostaining/EdU incorporation experiments confirmed the elevated proliferation capacities of BAF complex depleted BLBP positive AGPs.

Another line of evidence supporting this conclusion could be drawn from transcriptome sequencing data. Given that the initial GO analysis of dcKO revealed transcriptional changes indicative of a massive upregulation of proliferation related transcripts, we next investigated the involvement of these transcripts in astrocyte or glioma proliferation regulation (Figure 21E-G, Table 1). Screening the literature for information on the 151 proliferation related transcripts that were upregulated in dcKO DP, we found that 27 of these (18%, Figure 21F) were related to the proliferation of astrocyte and/or glioma. The relation between these two groups is shown by scatterplot in Figure 21E. The level of upregulation (Log_2 fold change of given transcript abundance) of all proliferation related (red data points) as well as astrocyte and/or glioma related (black data points) is plotted together with the significance (with –Log of corresponding p value). Additionally, the Log_2 fold changes of 15 genes related to astrocyte and/or glioma proliferation, whose expression was most upregulated, are shown in bar graph of Figure 21G (detailed description of these provided in Table 1). As described in

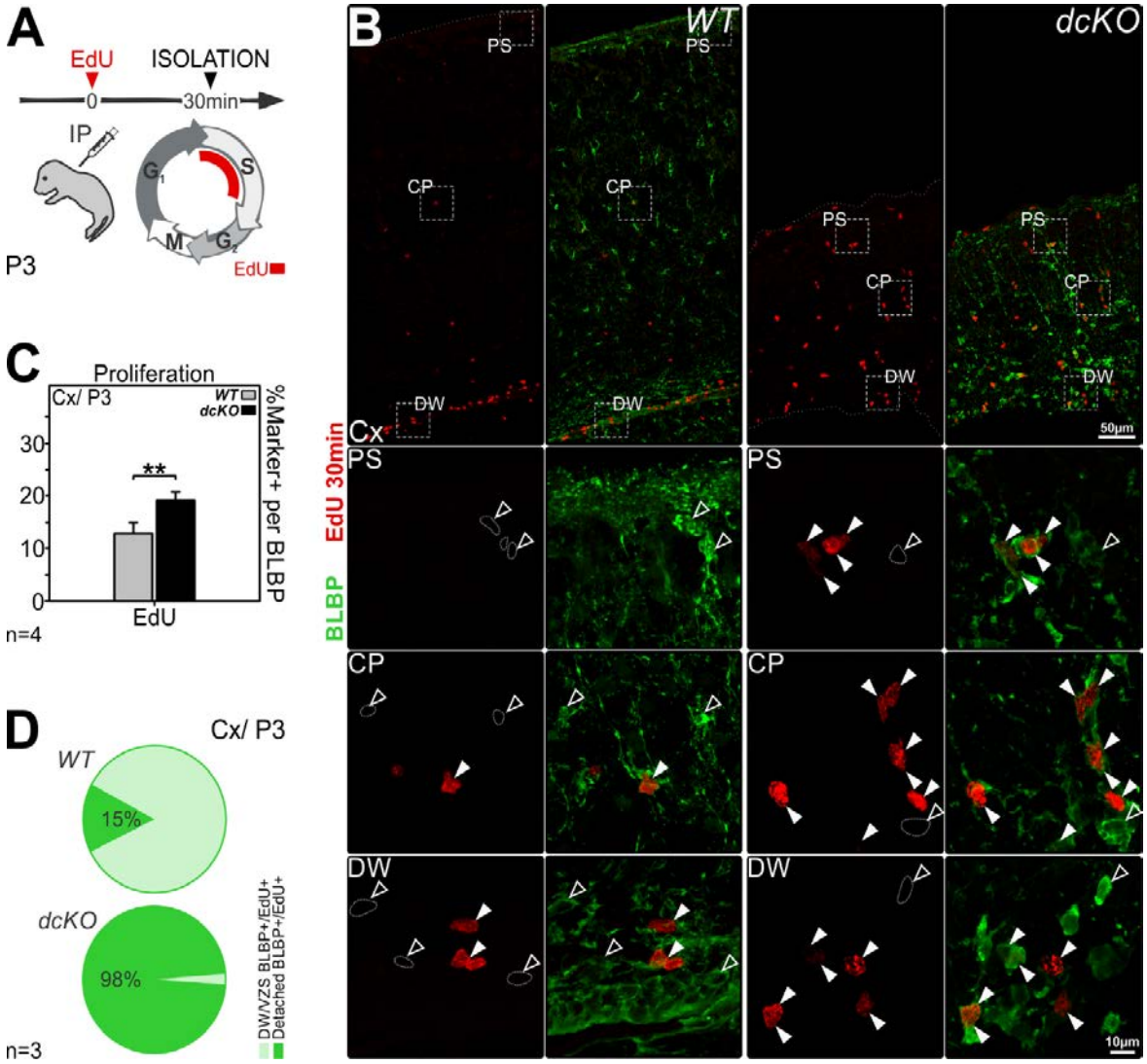

Figure 22 | High proliferation capacities of BAF complex depleted dorsal AGPs (II). (A) Scheme explaining the principle of proliferation analysis by thymidine analogue (EdU) injection. IP injected EdU (red colour) incorporates to DNA during the S phase of cell cycle allowing for the labelling of the fraction of proliferative cells. (B) Immunofluorescence analysis of mouse P3 cortex (M1 area) WT and dcKO sections detecting BLBP positive AGPs (in green) and EdU (in red) that incorporated into DNA of cells after 30 minutes from IP injection. Cells expressing BLBP positively stained for EdU are proliferative AGPs (scattered through cortex) or astrocytic RGCs (residing in DW). Lower boards of each are magnified insets of delineated areas of PS, CP and DW. Full arrowheads indicate EdU positive cells expressing BLBP, empty arrowheads indicate examples of EdU negative/BLBP positive cells. Cell bodies of some of BLBP expressing cells negative for EdU outlined with dashed line. (C) Percentages of proliferative BLBP positive cells registered in P3 WT and dcKO murine cortex. Bar graph indicates the percentage of BLBP expressing cells positive for EdU 30 minutes after injection. Data are averages ± σ of n=4 experimental replicates; **p≤0.01 in t- student test. (D) Pie charts showing the degree of DW detachment of BLBP/EdU positive cells in WT (upper panel) and dcKO (lower panel) P3 DP. Light green colour indicates percentages of BLBP/EdU positive cells residing in DW, dark green colour indicates percentages of these cells found outside DW. Data are averages of n=3 animals (for WT: BLBP+/EdU+ detached=15.2, BLBP+/EdU+ DW=84.8±2.4%; for dcKO: BLBP+/EdU+ detached= 97.7, BLBP+/EdU+ DW=2.3±0.8%). CP, cortical plate; Cx, cortex; dcKO, double knockout; DW, deep cerebral white; IP, intraperitoneal injection; PS, pial surface; WT, wild type.

NAME	LOG_2 FOLD CHANGE	P VALUE	ASTROCYTES/GLIOMA PROLIF. RELATED	REFERENCES
Twist1	1.88	2.75E-09	astrocytes and glioma	(Elias et al., 2005; Wasilewski et al., 2017)
Lin28a	1.54	1.10E-05	glioma	(Mao et al., 2013)
Pax3	1.44	3.06E-05	glioma	(Su et al., 2016; Xia et al., 2013)
Gli1	1.30	3.19E-16	astrocytes and glioma	(Clement et al., 2007; Garcia et al., 2010; Pitter et al., 2014)
Pax6	1.20	1.79E-15	glioma	(Liu et al., 2012)
S100a6	1.07	2.58E-07	astrocytes and glioma	(Yamada and Jinno, 2012, 2014)
Hmgn5	1.04	8.97E-17	glioma	(Cao et al., 2017)
Egr1	1.02	4.22E-07	astrocytes	(Mayer et al., 2009)
Ntn1	0.97	1.09E-06	glioma	(Sanvoranart et al., 2016)
Emp3	0.95	8.62E-05	glioma	(Jun et al., 2017)
Rac2	0.92	2.00E-08	glioma	(Lai et al., 2017)
Aqp1	0.90	0.008705	glioma	(Hayashi et al., 2007)
Epor	0.86	0.000601	glioma	(Peres et al., 2011)
Btk	0.85	0.001167	glioma	(Yue et al., 2017)
Klf4	0.79	0.000114	glioma	(Tang et al., 2016)
Jag1	0.76	6.77E-09	astrocytes	(LeComte et al., 2015)
Id4	0.73	4.78E-08	astrocytes	(Lee et al., 2011)
Hmox1	0.71	7.82E-09	glioma	(Ghosh et al., 2016)
Sox2	0.68	6.58E-14	glioma	(Annovazzi et al., 2011)
Tspo	0.67	0.009165	glioma	(Werry et al., 2015)
Ccnd1	0.67	4.64E-10	glioma	(Cao et al., 2017)
Hpse	0.66	0.002486	glioma	(Kundu et al., 2016)
Ptch1	0.66	1.02E-07	glioma	(Clement et al., 2007)
Cdc7	0.63	3.97E-07	glioma	(Erbayraktar et al., 2016; Li et al., 2018a)
Hdac1	0.63	0.000456	glioma	(Li et al., 2018b)
Tgfβ3	0.60	4.39E-06	glioma	(De Falco et al., 2007)
Wwtr1	0.58	1.22E-09	glioma	(Qiu et al., 2016)

Table 1 | Astrocyte/glioma proliferation related transcripts upregulated in DP of P3 dcKO mice. The table describes 27 transcripts related to astrocyte/glioma proliferation significantly upregulated in DP of P3 dcKO stating the level of upregulation (log_2 fold change), significance (p value), involvement in astrocyte and/or glioma proliferation (astrocytes/glioma prolif. related) and corresponding literature source (references). Prolif. , proliferation.

Table 1 the majority of the genes selected was related to glioma proliferation, where out of 27 only 5 are proven to regulate astrocyte proliferation. According to recent literature, these were Twist1 (Wasilewski et al., 2017), Gli1 (Garcia et al., 2010; Pitter et al., 2014) , S100a6 (Yamada and Jinno, 2012, 2014), Jag1 (LeComte et al., 2015) and Id4 (Lee et al., 2011). In addition, all of these regulators are known to be involved in reactive astrocyte proliferation induction rather than in postnatal multiplication of AGPs (except for Gli1 and S100a6). This creates the impression of a lack of upregulation of 'real' astrocyte proliferation regulators. However, the process of astrocyte proliferation has not been widely investigated and key informations about its molecular regulation are missing. Thus, the possibility of a deep analysis of our transcriptome data was frustrated by the lack of literature describing the molecular control of astrocyte proliferation.

In summary, BAF complex depleted AGPs of postnatal DP are highly proliferative. Additionally, the proliferation processes evoked by *hGFAP*-Cre driven BAF loss were accompanied by upregulation of several glioma related proliferation regulators.

The more AGPs – the less astrocytes? Maturating protoplasmic astrocytes in dcKO DP

Having established that the loss of BAF complex in astrocytic RGCs causes a massive increase in the abundance of AGPs we then asked whether this aberrant amount of progenitors affects the numbers of maturating astrocytes, which we expected to increase. Because the AGPs of dcKO were found to be scattered throughout the cortical thickness we turned our attention to maturating gray matter (protoplasmic) astrocytes, which normally exhibit a similar distribution pattern (Cahoy et al., 2008; Li et al., 2012; Oberheim et al., 2012). Using immunohistochemistry, we assessed the expression of the mature protoplasmic astrocyte marker - ACSBG1 (Cahoy et al., 2008; Chaboub and Deneen, 2013; Li et al., 2012) in coronal sections of WT and dcKO P3 brain tissue. The selection of this time point was dictated by our observation of the elevated abundance of AGPs in P3 mutant mice, as well as by the necessity of proper WT control experiment (E17.5 WT brain tissue did not exhibit ACSBG1 staining, Appendix, Figure 46). Additionally, due to the distinct AGPs cortical phenotype in medial and lateral regions of dcKO cortex (previously described), the expression of ACSBG1 was also assessed in developing M1 (MCx) and S1 areas (Figure 23A-C, E). The immunostaining showed ACSBG1 positive cells scattered through the full thickness of WT gray matter in MCx and LCx areas (Figure 23A-C,

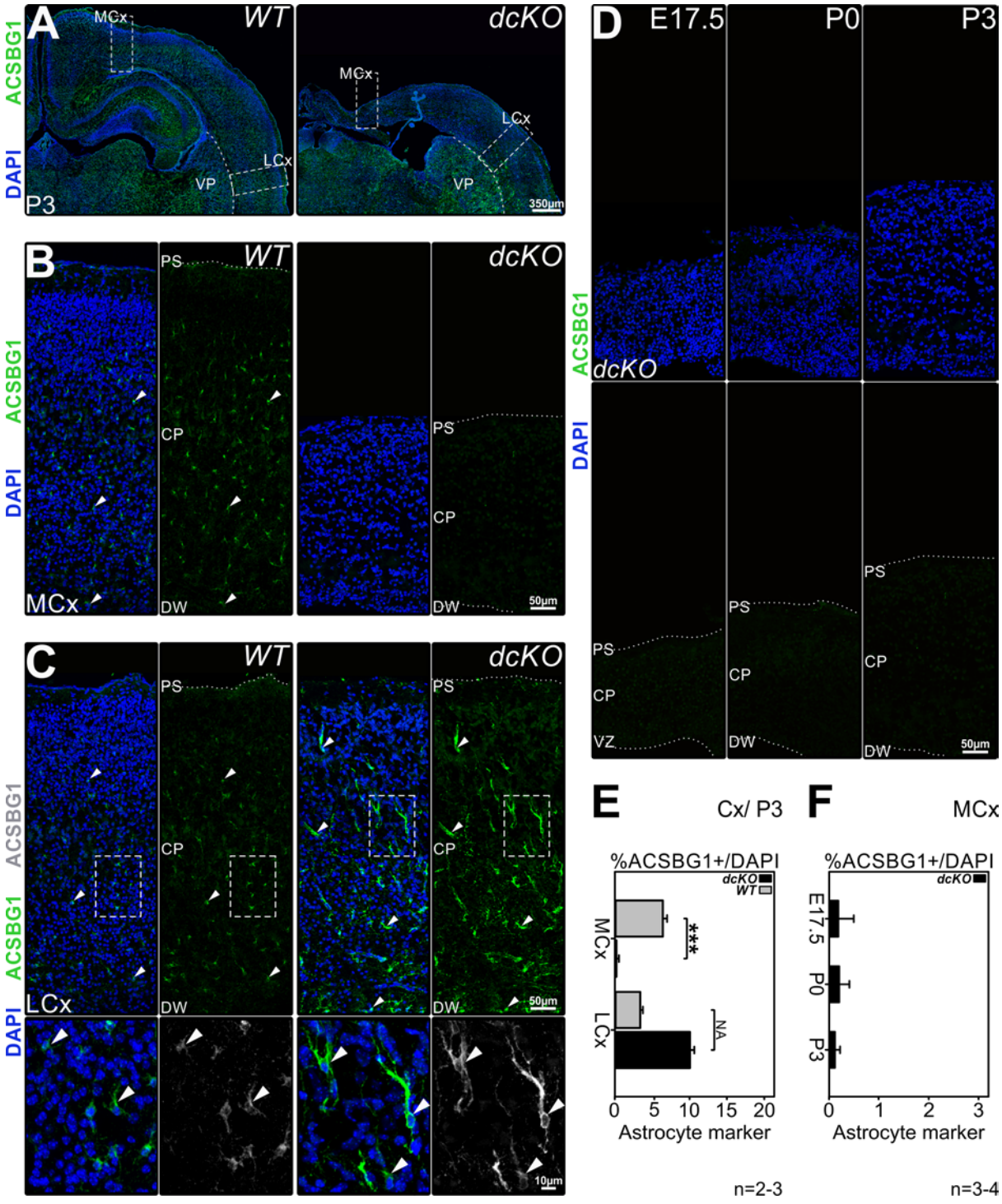

Figure 23 | Area dependent astrocyte differentiation in BAF complex depleted cortex of postnatal mice. (A-C) Immunofluorescence staining of coronal sections through P3 WT and dcKO murine DP regions detecting the expression of astroglial marker – ACSBG1 (in green and gray). The nuclei of cells visualized by DAPI intercalation (in blue). (A) Overview pictures of WT and dcKO cortical areas. (B-C) Magnified insets of (B) MCx (developing M1 area) and (C) LCx (developing S1 area) delineated in (A). For (B) lower panels of each are enlarged views of outlined areas (RGB and gray scale images). Full arrowheads indicate ACSBG1 positive astrocytes. (D) ACSBG1 immunostaining for MCx area of E17.5, P0 and P3 dcKO DP. Nuclear DAPI staining shown in blue. (E and F) Bar graphs representing percentage share of ACSBG1 positive cells in all DAPI positive cells in indicated areas of P3 WT and dcKO mouse DP (E) or in MCx area of E17.5, P0 and P3 dcKO mice (F). Data are averages ± σ of n=2-3 (E) or n=3-4 (F) experimental replicates;

***p≤0.001 in t student test, NA not applicable (n=2). CP, cortical plate; Cx, cortex; dcKO, double knockout; DW, deep cerebral white; MCx, medial cortex (refers to M1 area), LCx, lateral cortex (refers to developing S1 area); NA, not applicable; PS, pial surface; VP, ventral pallium; WT, wild type.

pointed by arrowheads), exhibiting a distribution pattern typical for protoplasmic astrocytes (Cahoy et al., 2008). Surprisingly MCx area of dcKO DP did not stain for ACSBG1 (Figure 23A and B). This was apparent in our quantifications, where among all DAPI cells found in M1 area of analyzed brain dcKO sections, less than 1% expressed ACSBG1. Thus, the dcKO MCx exhibited a strong reduction in the abundance of protoplasmic astrocyte compared to WT (***p≤0.001, Figure 23E). Interestingly, the same antibody staining of dcKO LCx area appeared to be more prominent (Figure 23C). Moreover, quantitatively, comparing to the developing WT S1 area, more dcKO DAPI positive cells expressed ACSBG1 (Figure 23A, C and E; percentage value of DAPI cells expressing ACSBG1). In addition, dcKO affected protoplasmic LCx astrocytes showed characteristic, hypertrophic morphologies with highly enriched cellular ACSBG1 staining comparing to that of WT (Figure 23C, magnified insets).

Overall, ACSBG1 positive astrocytes exhibited specific medio-rostral gradient of cortical distribution with diminished expression in medial and elevated expression in lateral areas (Figure 23A-C).

This striking phenomenon of lack of development of protoplasmic astrocytes in the medial areas of dcKO affected cortex prompted us to inquire about the reasons for this deficiency. As the premature embryonic differentiation of MCx AGPs to ACSBG1 positive protoplasmic astrocytes followed by e.g. apoptosis or migration could offer an elegant explanation to the above described gradient, we therefore decided to evaluate the expression of ACSBG1 in E17.5 and P0 M1 cortical sections of dcKO mice. As presented in Figure 23D, MCx areas of any developmental stage (E17.5, P0 and P3) of dcKO brain did not exhibit ACSBG1 positive cells (except for isolated cells that accounted for no more than 1% of DAPI positive cells, Figure 23F). Thus it is not due to the premature differentiation that MCx of dcKO is deprived of ACSBG1 positive astrocytes.

Possible apoptosis (programmed cell death) of AGPs affected by BAF complex depletion could serve as another explanation of lack of their differentiation to protoplasmic astrocytes in MCx of dcKO cortex. Thus, as a next step we sought to investigate the process of apoptosis in AGPs (Figure 24). For this purpose we immunohistochemically evaluated the expression of one of the final executor proteins of programmed cell death – CASPASE 3 (CASP3) (Porter and Janicke, 1999) in AGPs. We performed this study on coronal brain slices isolated from WT and dcKO mice at two developmental stages: E17.5 and P0. We chose to investigate tissues isolated at E17.5, as we wanted to test apoptosis at the beginning of the cortical astrogliogenesis. Additionally, we sought to check whether

the possible wave of apoptosis precedes the previously investigated P3 stage, therefore we also decided to assess CASP3 expression in P0 brain tissues. As shown in Figure 24A and B, cells found in MCx and LCx of E17.5 and P0 dcKO mice more frequently stained for CASP3 comparing to that of WT (indicated by empty and full arrowheads). Some of those found in dcKO as well as WT tissues, however not all, were apoptotic GLAST positive AGPs (pointed by full arrowheads). Quantitatively, in MCx of E17.5 dcKO mice 1.9±0.9% of GLAST stained cells as well as 1.0±0.4% of DAPI positive cells expressed CASP3 (pointed by full and empty arrowheads respectively) (Figure 24C and D). A similar analysis performed in LCx of E17.5 dcKO indicated that 2.0±0.8% of GLAST stained cells expressed CASP3 whereas globally 0.9±0.3% of DAPI stained cells exhibited positive staining for CASP3. As shown in bar graphs of Figure 25C and D, these percentage values of cells expressing CASP3 found in MCx and LCx of E17.5 dcKO significantly outnumbered the percentages quantified for the corresponding areas of E17.5 WT cortex (**$p \leq 0.01$; in WT MCx 0.1±0.03% of DAPI and 0.3±0.2% of GLAST positive cells stained for CASP3 whereas in WT LCx 0.1±0.02% of DAPI and 0.3±0.2% of GLAST stained cells expressed CASP3; Figure 24C and D). Thus, we could observe elevated apoptosis in dcKO cortex harvested at the developmental stage corresponding to the time of early cortical astrogliogenesis. However, only a fraction of 53.0±15.9% of all apoptotic cells found in both analyzed E17.5 dcKO cortical areas was corresponding to the apoptotic GLAST positive AGPs (thus 47% of apoptotic cells were of another cell type). For comparison, 41.0±35.0% of apoptotic cells found in both analyzed areas of E17.5 WT cortex expressed GLAST. Similarly to E17.5, analysis of the abundance of apoptotic cells found in P0 dcKO and WT MCx and LCx, revealed increased percentages of dcKO DAPI and GLAST positive cells exhibiting CASP3 staining. Accordingly, in MCx of dcKO 1.4±0.3% of DAPI stained cells and 1.6±0.2% of GLAST positive cells expressed CASP3, whereas in dcKO LCx 1.3±0.05% of DAPI and 1.9±0.7% of GLAST expressing cells stained for CASP3 (Figure 24E and F). Comparing to the percentage values revealed for P0 WT MCx (0.05±0.02% of DAPI stained cells and 0.1±0.07% of GLAST positive cells expressed CASP3), as well as for P0 WT LCx (0.06±0.002% of DAPI stained cells and 0.2±0.03% of GLAST positive cells expressed CASP3), the apoptotic processes of P0 dcKO cortex seemed to be elevated (no statistical analysis due to the low numbers of investigated animals (for WT and dcKO n=2). Overall, these experiments indicated a slightly increased apoptosis in BAF complex depleted GLAST positive AGPs. However, even though elevated, the extent of the programmed cell death in dcKO AGPs was relatively low, as the percentage numbers of CASP3 positive found in dcKO at both investigated developmental stages did not exceed 2% of all GLAST expressing cells. Thus, we conclude that it is unlikely that the apoptosis of AGPs deprived of BAF complex led to the deficits in the protoplasmic astrocytes pool observed in medial areas of dcKO cortex.

Seeking for the answer we subsequently noticed that several literature reports indicated the

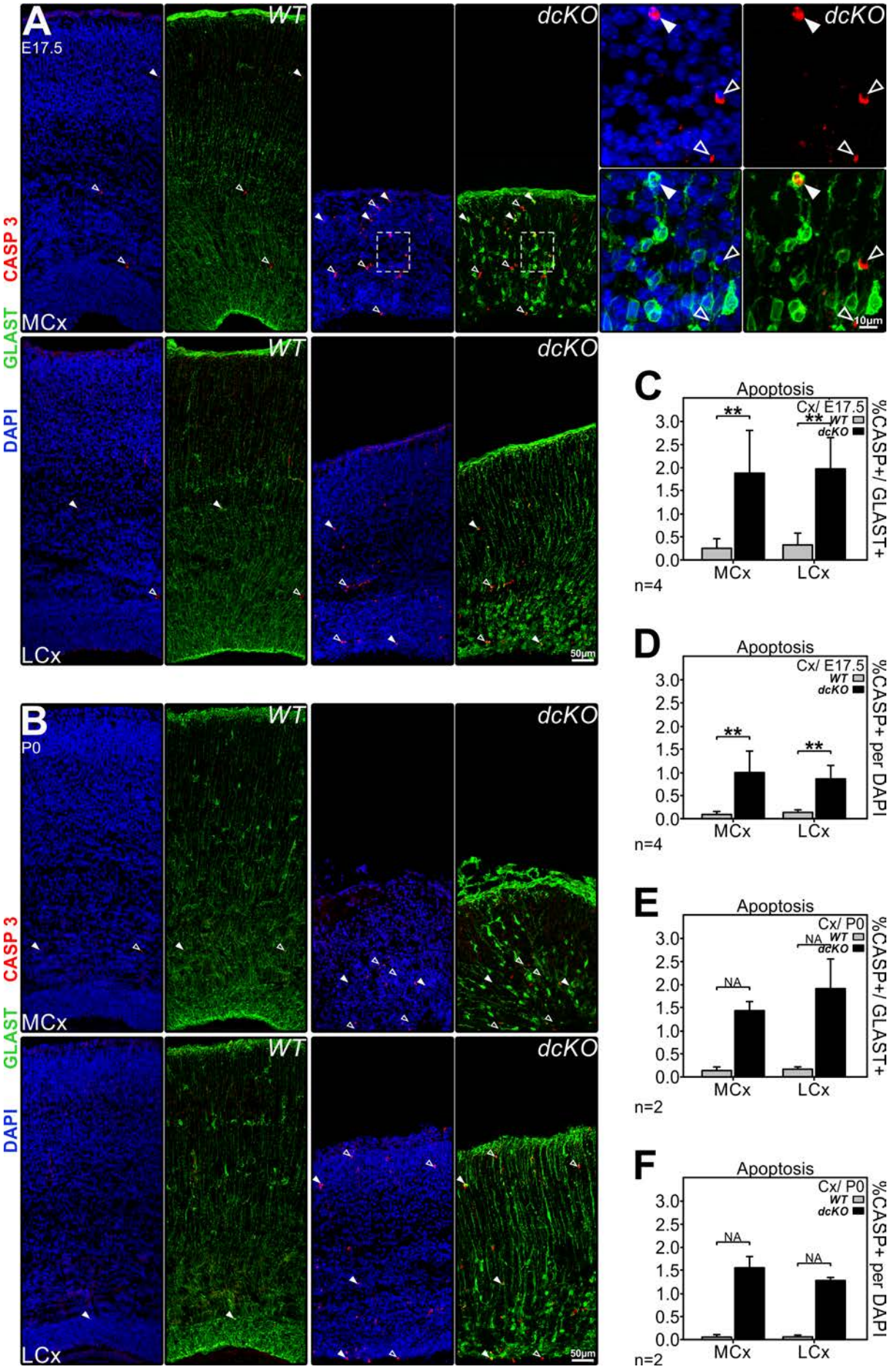
A
E17.5
WT
dcKO
dcKO
CASP 3
GLAST
MCx
10µm
DAPI
WT
dcKO
LCx
50µm
B
P0
WT
dcKO
CASP 3
GLAST
MCx
WT
dcKO
DAPI
LCx
50µm
C
Apoptosis
Cx/ E17.5
WT
dcKO
%CASP+/ GLAST+
3.0
2.5
2.0
1.5
1.0
0.5
0.0
**
**
MCx
LCx
n=4
D
Apoptosis
Cx/ E17.5
WT
dcKO
%CASP+ per DAPI
3.0
2.5
2.0
1.5
1.0
0.5
0.0
**
**
MCx
LCx
n=4
E
Apoptosis
Cx/ P0
NA
WT
dcKO
%CASP+/ GLAST+
3.0
2.5
2.0
1.5
1.0
0.5
0.0
NA
MCx
LCx
n=2
F
Apoptosis
Cx/ P0
WT
dcKO
%CASP+ per DAPI
3.0
2.5
2.0
1.5
1.0
0.5
0.0
NA
NA
MCx
LCx
n=2

Figure 24 | Slightly elevated apoptosis in murine DP affected by BAF complex KO. (A, B) Immunostaining analysis of coronal brain sections through WT and dcKO E17.5 (A) and P0 (B) murine MCx (developing M1 area) and LCx (developing S1 area) stained with antibody to AGPs marker - GLAST (in green) together with apoptosis marker - CASP3. The nuclei of cells stained by DAPI (in blue). Four zoom in pictures in (A) are magnified insets of delineated area of dcKO MCx. Full arrowheads indicate examples of GLAST positive AGPs positive for CASP3 staining, empty arrowheads indicate examples of CASP3 positive/ GLAST negative cells. (C-F) Percentages of CASP3 positive cells per: (C and E) total number of GLAST expressing cells analyzed at (C) E17.5 and (E) P0; (D and F) per total number of DAPI positive. All bar graphs show data collected in the regions of MCx (developing M1 area) and LCx (developing S1 area). Data are averages ± σ of n=2-4 animals; **p≤0.01, in t student test, NA not applicable (n=2). CASP, CASP3; Cx, cortex; dcKO, double knockout; MCx, medial cortex (refers to developing M1 area); LCx, lateral cortex (refers to developing S1 area); NA, not applicable; WT, wild type.

indispensable role of late born neuron derived cytokines in the activation of astrocytic genes within progenitor cells (Barnabe-Heider et al., 2005; Freeman, 2010; Miller and Gauthier, 2007). Thus, we reasoned that neuronal depletion occurring upon BAF KO could lead to impaired differentiation of cortical astrocytes (Figure 25). In order to investigate whether lack of development of ACSBG1 positive protoplasmic astrocytes within MCx of dcKO may be caused by neuronal aberrations, we decided to reanalyze and compare the P3 WT and dcKO cortical distribution of GLAST stained AGPs (described in Figure 17), SATB2 stained late born neurons (details in Figure 20) and above described ACSBG1 stained protoplasmic astrocytes (Figure 23). As presented in micrographs of Figure 25A and bar graph of Figure 25B, the medio-lateral cortical distribution of GLAST expressing AGPs seemed to be homogenous (indicated by evenly distributed arrowheads) with similar percentage values of DAPI cells expressing GLAST found in medial (M1) and lateral (S1) parts of P3 WT as well as dcKO cortex. Thus, it is not due to the difference in AGPs distribution that ACSBG1 positive astroglia are not developed in medial cortical areas. Additionally, cells expressing SATB2 or ACSBG1 found in WT cortex of P3 mice displayed a similarly regular distribution (Figure 25C-F; pointed by evenly distributed arrowheads). However, in the brain of P3 dcKO mice SATB2 expressing late born neurons as well as ACSBG1 stained protoplasmic astrocytes exhibited specific medio-lateral cortical gradient of distribution (Figure 25C and E; pointed by unevenly distributed arrowheads). Overall, both of these cellular populations were diminished in medial cortical areas (M1) of dcKO mice; SATB2 positive cell population to a lesser extent (Figure 25C and D), whereas ACSBG1 expressing astroglial population was not present at all (Figure 25E and F). In order to summarize, based on quantification data shown in bar graphs of Figure 25B, D and F, we generated a line graph (end of lines correspond to percentages of DAPI positive cells expressing given marker in MCx and LCx; Figure 25G) and corresponding scheme (gradient colour coded percentages of DAPI positive cells expressing given marker in MCx and LCx; Figure 25H) that allowed the comparison of the distribution of neurons vs glia in P3 dcKO cortex. Accordingly, in dcKO mouse brain GLAST positive AGPs were equally distributed through the cortex, whereas the amounts of SATB2 neurons and ACSBG1 astrocytes were

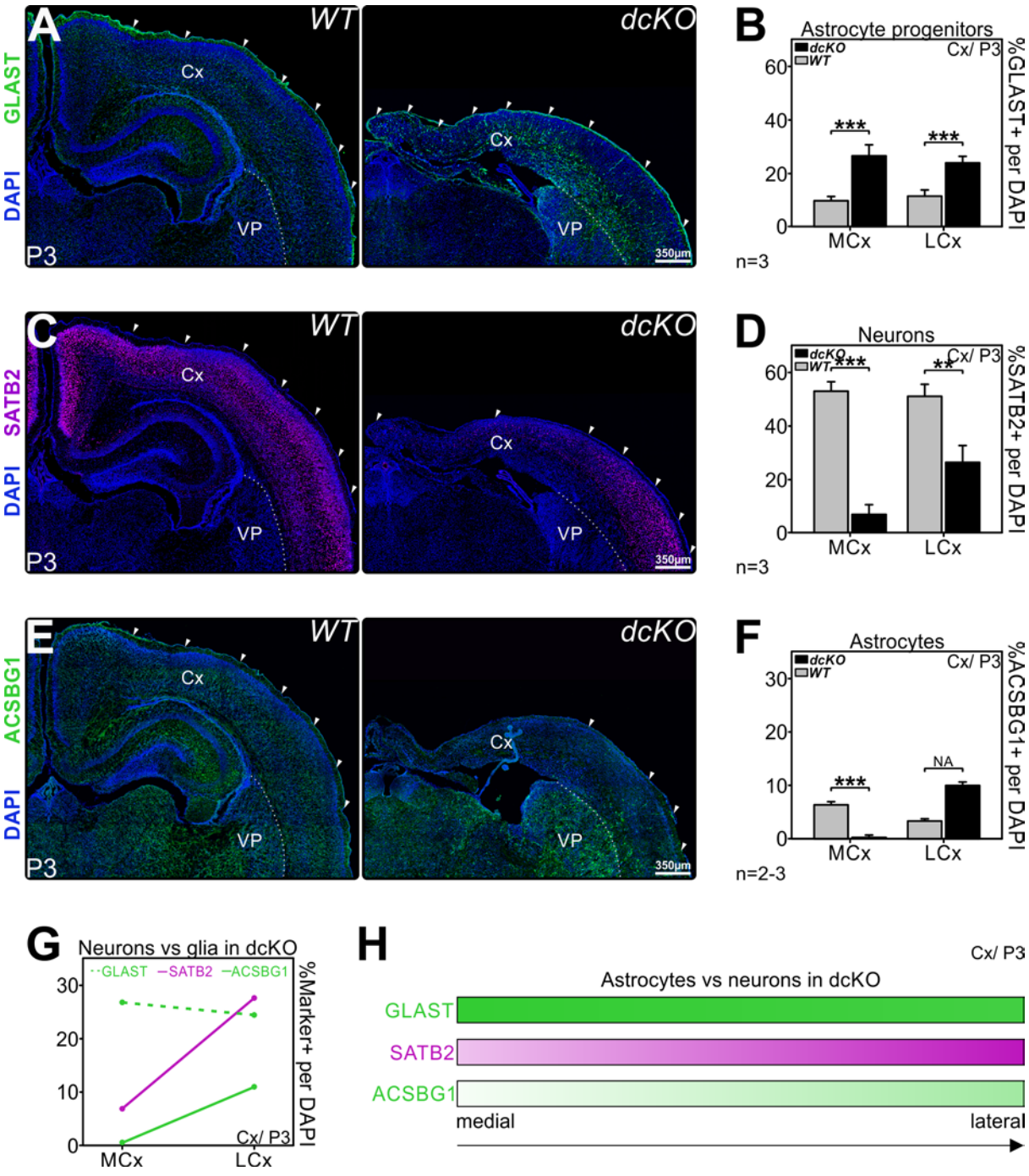

Figure 25 | Neuronal and astroglial distribution differs between and within cortex of WT and dcKO mice. Coronal sections through P3 cortex of WT and dcKO mice stained with antibodies against astroglial progenitor marker - GLAST (in green, A), late born neuron marker – SATB2 (in magenta, B) and protoplasmic astrocytes marker – ACSBG1 (in green, C). The nuclear DAPI staining is blue. Full arrowheads indicate the areas of registered positive staining for given marker. (B, D and F) Percentages of given marker positive cells per total number of DAPI positive in the regions of MCx (M1 area) and LCx (S1 area) of P3 WT and dcKO DP. Data are averages ± σ of n=2-3 animals; ***p≤0.001; **p≤0.01, in t student test, NA not applicable (n=2). (G) Line graph representation of values shown by bar graphs from B, D and F indicating dynamic changes in the abundance of: GLAST positive cells (dashed green line), SATB2 positive cells (magenta line) and ACSBG1 positive cells (green line) between the areas of medial (MCx) and lateral (LCx) part of the cortex. (H) Scheme depicting medio-rostral distribution of analyzed markers in dcKO cortex. GLAST expressing AGPs were equally distributed through the cortex whereas the amounts of

SATB2 neurons and ACSBG1 astrocytes were found to be reduced in MCx (lighter colour) and partially reconstituted in LCx (darker colour). Colour intensity proportional to the percentage values found in B, D and F. Cx, cortex; dcKO, double knockout; MCx, medial cortex (refers to developing M1 area); LCx, lateral cortex (refers to developing S1 area); VP, ventral pallium; WT, wild type.

found to be reduced in MCx and partially reconstituted in LCx. Thus, we found a correlation between the distributions of neurons and astrocytes, suggesting that low numbers of late born neurons may be responsible for the underdevelopment of protoplasmic astrocytes in medial areas of P3 dcKO mouse cortex, presumably through reduced concentration of late born neurons derived cytokines. This hypothesis will need to be confirmed in future experiments.

Last but not least, abnormal migration of cortical progenitors could also possibly explain the scarcity of protoplasmic astrocytes in MCx of dcKO mice. In order to address this issue, we first decided to analyze the results of GO pathway evaluation in P3 dcKO/WT DP. We focused our analysis on known pathways connected to the regulation of migration. As indicated in Figure 26D, several transcripts significantly upregulated in P3 dcKO DP were related to the cell locomotion and migration or to the movement of subcellular compartments, indicating enhanced migration-related processes in dcKO DP. Encouraged by this finding we further traced the localization of the progenies of cortical RGCs found in lateral VZ of WT and dcKO mice. We electroporated LCx VZ cells of perinatal embryos with a *pCAG*-IRES-EGFP plasmid, enabling expression of EGFP in electroporated cells and their progenies. Subsequently we analyzed the localization of EGFP positive cells at P3 developmental stage (Figure 26A). Unfortunately a mortality rate of 100% of embryos electroporated at E17.5 prevented us from tracing astrocytic RGCs and their progenies. Therefore we decided to trace daughter cells of intermediate (between neurogenic and astrogenic) RGCs from late E16.5 embryos. Furthermore, due to the fragile cortical structure of dcKO MCx we chose to electroporate LCx VZ cells instead. As indicated in Figure 26B and C, the progenies of WT RGCs electroporated at E16.5 mostly populated superficial layers of cortex (LII/III) postnatally (P3), indicating their neuronal fate. Additionally, a fraction of electroporated cells in WT was left behind still residing in VZ of LCx (as RGCs population) or migrating across the cortical layers (possibly as migrating neurons) towards the final destination. The distribution of EGFP traced cells of dcKO mice substantially differed from that of WT (Figure 26B and C). Only single EGFP expressing cells could be found close to the PS of LCx (arrowheads). However, the cellular morphology and distribution pattern of these cells was not similar to that of neurons. Additionally, some of the traced cells resided in the VZ of LCx. Since this area was electroporated, we assumed that these cells were RGCs. Besides, to our surprise, a substantial amount of EGFP expressing cells could be found in VP of dcKO, namely in the LGE and striatum (indicated by arrowheads). Importantly these observations stand true for 3 electroporated WT and 3 electroporated dcKO brains (visual evaluation, no statistical analysis). We also considered the

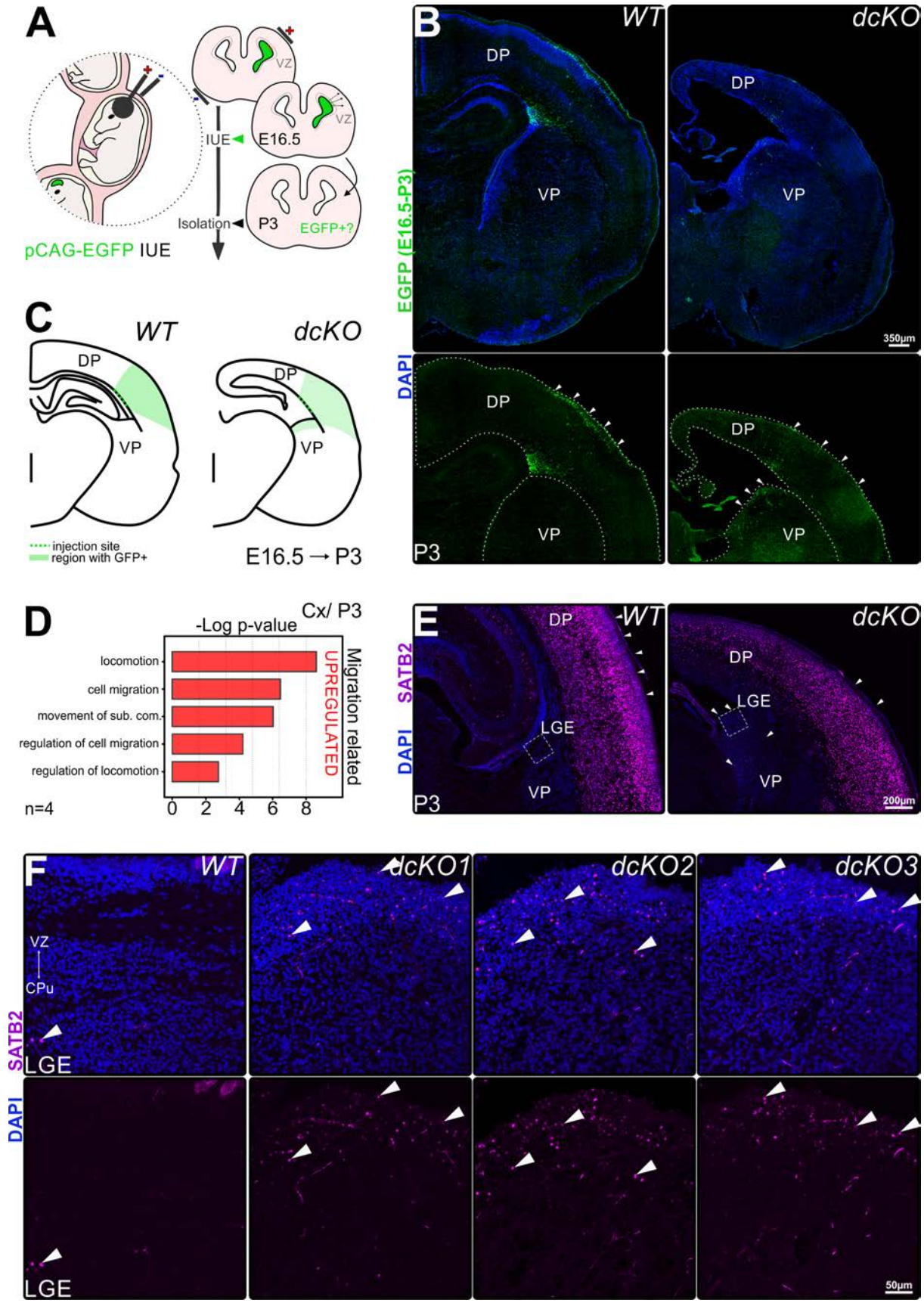

Figure 26 | The distribution of perinatal RGCs progenies differs between WT and dcKO brains. (A) Scheme explaining the principle of distribution studies conducted by means of EGFP plasmid *in utero*

injection and electroporation (IUE). Lateral ventricles of late E16.5 embryos were injected with *pCAG*-IRES-EGFP and subsequently electroporated, directing plasmid DNA towards LCx VZ. Electroporated brains were assessed for EGFP (in green) expression at P3 postnatal stage. (B) Endogenous EGFP signal in P3 WT and dcKO coronal brain slices prepared from electroporated brains. Nuclear DAPI staining is blue. Lower boards of WT and dcKO are single channel images of EGFP. Full arrowheads indicate approximate localization of EGFP positive cells. (C) Scheme of the areas of P3 WT and dcKO brains in which EGFP positive cells were found after IUE at 16.5. Dashed green line indicates the injection and electroporation site. Green coloured area indicates brain regions with EGFP positive cells. Shades of green represent the approximate quantity of EGFP positive cells. (D) GO molecular pathway enrichment analysis indicating groups of transcripts related to migration and significantly upregulated in P3 DP *hGFAP*-Cre dcKO (E, F). Immunofluorescence analysis of P3 WT and dcKO murine cortical coronal sections stained with antibody to upper layer neurons marker – SATB2 (in magenta). DAPI stained by intercalation (in blue). (E) Overview pictures of WT and dcKO coronal brain sections indicating (by arrowheads) the areas exhibiting positive staining for SATB2. Delineated areas of LGE show regions of which inset images presented in (F) were taken. (F) LGE and striatum areas of WT and 3 independent dcKO mice exhibiting staining for SATB2. Arrowheads indicate cells positive for SATB2. The directions towards VZ and CPu are indicated by two headed arrow. com., compartment; CPu, caudate putamen; dcKO, double knockout; DP, dorsal pallium; IUE, *in utero* electroporation; LGE, lateral ganglionic eminence; sub., subcellular; VP, ventral pallium; VZ, ventricular zone; WT, wild type.

influence of pronounced (at the stage of P3) anatomical differences in WT and dcKO brain architecture on the outcome of electroporation experiments. However comparing E16.5 brain structures of WT and dcKO mice we concluded that the degree of anatomical differences at this developmental stage is very low and unlikely to influence the results of electroporation (Appendix, Figure 47A and B). Thus, as presented in schemes of Figure 26C, RGCs of E16.5 WT LCx (Figure 26C, WT; dashed line) gave rise to progenies that postnatally resided in several areas of DP (Figure 26C, WT; green shade depicts areas of P3 WT brain in which EGFP positive cells were observed (n=3)). However, electroporated E16.5 dcKO LCx VZ cells (Figure 26C, dcKO; dashed line) and their progenies could be found in DP as well as VP of postnatal brain (Figure 26C, WT; green shade depicts areas of P3 dcKO brain in which EGFP positive cells were found (n=3)). These results seem to confirm our assumption that BAF depleted AGPs of DP may migrate out of the cortical areas to populate other regions of dcKO brain. Additionally, another line of evidence supporting this hypothesis comes from late born neurons studies. Careful investigation of SATB2 expression revealed a population of late born neurons that in dcKO brain resides in LGE and striatum (Figure 26E and F, arrowheads). This finding stands to the contrary of WT SATB2 positive cells distribution that solely populate upper layers of cortex with no single positive cell found in LGE or striatum (Figure 26F, arrowheads). As shown in Figure 26F, SATB2 positive cells could be found in LGE and striatum of 3 independent dcKO mice. In summary, it appears likely that BAF complex depleted AGPs of MCx are migrating towards presumably healthier ventral regions of dcKO brains and subsequently differentiate to ACSBG1 positive protoplasmic astrocytes (Appendix, Figure 47C further described in upcoming section 3.4).

Overall, we could observe that ACSBG1 positive gray matter astrocytes exhibit a specific medio-rostral gradient of distribution with lack of expression in MCx and elevated expression in LCx. This striking phenomenon in the medial areas of dcKO cortex could be due to the low numbers of late born neurons in this area and the ensuing impoverishment in cytokines promoting AGPs maturation. Lack of protoplasmic astrocytes in dcKO MCx could also be caused by aberrant migration of AGPs, prompting these to translocate from DP to LGE or striatum. It is less likely that lack of ACSBG1 expressing protoplasmic astrocytes in MCx of dcKO is due to the premature differentiation of AGPs or their apoptosis. However, these possible explanations of the medio-lateral gradient in protoplasmic astrocytes numbers in dcKO need to be verified by further experiments.

3.4 Ventral astroglial phenotype

A comprehensive survey of dcKO cortical phenotype of perinatal mice revealed several interesting aspects of astrocytogenesis evidently affected by the mutation. It is crucial, however, to keep in mind that the *hGFAP* promoter used in this study targets not only dorsal but also ventral astroglial germinal zones (Chapter 3. Results. 3.2), thereby affecting ventral astroglial populations (Bayraktar et al., 2014; Tsai et al., 2012). Therefore, *hGFAP*-Cre driven loss of BAF complex in ventral and dorsal astrocytic RGCs mimics the reduction in BAF expression commonly observed in WT striatal AGPs (as described in Chapter 3. Results. 3.1). Additionally, the cortical gradient of protoplasmic astrocytes distribution as well as our migration studies suggest that ventral forebrain astrocytes may also be altered upon *hGFAP*-Cre driven BAF complex depletion. Thus, we decided to investigate the ventral astroglial phenotype of dcKO mice forebrain. Prompted by our previous observations we analyzed the possible changes within the cellular population of ACSBG1 expressing protoplasmic astrocytes.

Maturating astrocytes in BAF complex deprived VP

Immunohistochemical analysis of ACSBG1 revealed an interesting cortical distribution pattern with diminished expression in medial and elevated expression in lateral parts of P3 dcKO cortex (Chapter 3. Results. 3.3). Because *hGFAP* promoter allows to target both ventral astrocytic germinal zones (MGE and LGE) potentially affecting different astroglial populations (astrocytes of piriform cortex, striatum and ventral pallidum; see Figure 12), to gain further insights into protoplasmic astrocytes phenotype of BAF complex depleted VP, we examined the forebrain distribution of ACSBG1 positive cells. For this purpose we immunohistochemically assessed the ASCBG1 expression in anterior and posterior coronal sections of P3 WT and dcKO brains. We used a custom-written Matlab routine to generate semi-quantitative heat maps (based on single sections) of WT and dcKO distribution of ACSBG1 positive cells. As shown in Figure 27 and 28, ACSBG1 positive astrocytes of WT mice were

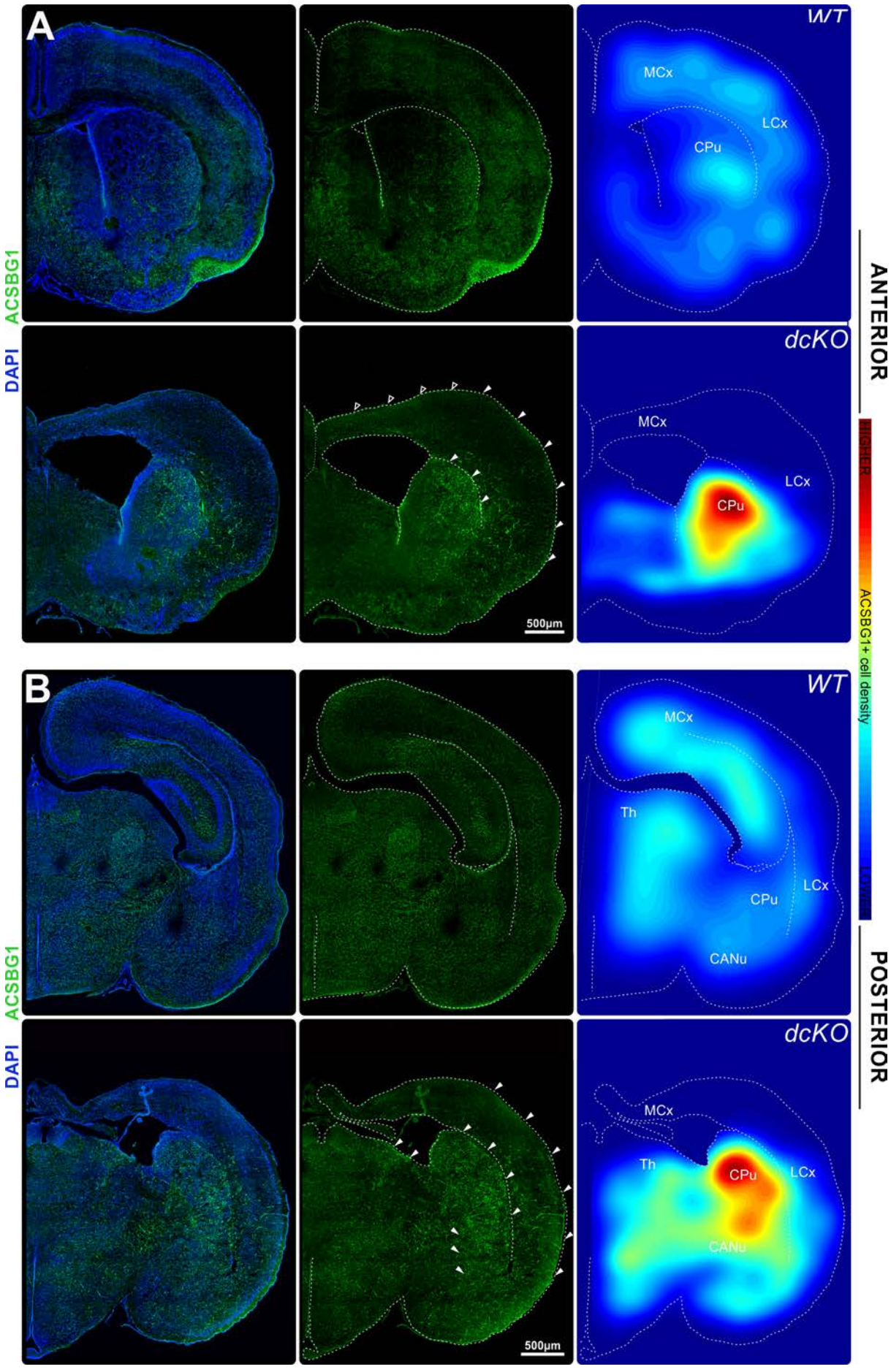
A
ACSBG1
DAPI
WT
MCx
LCx
CPu
dcKO
MCx
LCx
CPu
500µm
ANTERIOR
HIGHER
ACSBG1+ cell density
LOWER
POSTERIOR
B
ACSBG1
DAPI
WT
MCx
Th
LCx
CPu
CANu
dcKO
MCx
Th
CPu
LCx
CANu
500µm

Figure 27 | Highly elevated astrogliosis in BAF complex deprived VP and lateral pallium (LP) (I). (A, B) Immunostaining of ACSBG1 in coronal brain sections through P3 WT and dcKO murine brain (in green) in the rostro-medial (A, anterior) and medio-caudal (B, posterior) brain regions. The nuclei of cells visualized by DAPI intercalation (in blue). Middle panels of each are single channel images of ACSBG1 staining. Full arrowheads indicate the areas of dcKO brain exhibiting increased density of astrocytes expressing ACSBG1. Extreme right boards of each are semi-quantitative distribution maps generated based on manual labeling of ACSBG1 positive cells in a single representative section. As indicated by scale bar (arbitrary units), red colour corresponds to high density whereas blue colour corresponds to low density of ACSBG1 positive cells. CANu, central amygdala nucleus; CPu, caudate putamen; dcKO, double knockout; MCx, medial cortex; LCx, lateral cortex; Th, thalamus.

rather evenly scattered through anterior and posterior regions of brain. A slightly higher concentration of astrocytes could be observed in hippocampus and thalamus (Th) of posterior as well as in CPu of anterior WT sections (Figure 27A and B; distribution maps). A similar analysis performed for dcKO brain sections revealed several alterations in ACSBG1 expressing protoplasmic astrocytes distribution (Figure 27A and B; distribution maps, Figure 28A-E). First of all, we found a massive increase in ACSBG1 density (indicated in Figure 27 by arrowheads) in anterior and posterior regions of dcKO CPu (Figure 27A and B; distribution maps - red colour; Figure 28A) and LCx (Figure 27A and B; Figure 28D) as well as in CANu (Figure 27B; Figure 28B) and Th (Figure 27B; Figure 28C). As depicted in Figure 28E, 14.1±2.4% of DAPI positive cells of the region of dcKO CPu expressed ACSBG1. For WT CPu cells positive for ACSBG1 amounted to 5.7±1.0% of all DAPI stained cells. Importantly, as revealed by statistical analysis, the amount of ACSBG1 expressing astrocytes found in CPu of several dcKO individuals significantly outnumbered that of WT (**$p \leq 0.01$). Similarly, the fraction of DAPI stained cells exhibiting ACSBG1 staining was significantly higher in the areas of dcKO CANu and Th compared to the corresponding areas in WT (**$p \leq 0.01$; for CANu: in WT 5.2±0.9% whereas in dcKO 13.6±2.6% of all DAPI positive stained for ACSBG1; for Th: in WT 6.3±0.8% whereas in dcKO 12.6±2.1% of all DAPI positive stained for ACSBG1). Importantly, this observation seems to minimally support our previous assumption that BAF complex depleted cortical ACSBG1 positive cells preferentially reside in ventral regions of dcKO brains (Appendix, Figure 47C). Additionally, despite the quantitative differences, dcKO affected protoplasmic astrocytes also exhibited qualitative discrepancies. As shown in Figure 28B (in magnified insets), protoplasmic astrocytes of dcKO VP manifested hypertrophic morphologies with highly enriched cellular ACSBG1 staining what clearly distinguishes them from protoplasmic astrocytes residing in WT VP areas. Furthermore, ACSBG1 positive astrocytes found in enriched dcKO regions tended to group into clusters and were rarely found in isolation (Figure 28B, magnified insets). Overall, ACSBG1 immunostaining data indicated elevated amounts of protoplasmic astrocytes in VP of dcKO mice.

In order to confirm this finding we decided to search for WT/dcKO transcriptome differences that could indicate elevated astrogliosis in BAF complex depleted VP. We sequenced RNA isolated from

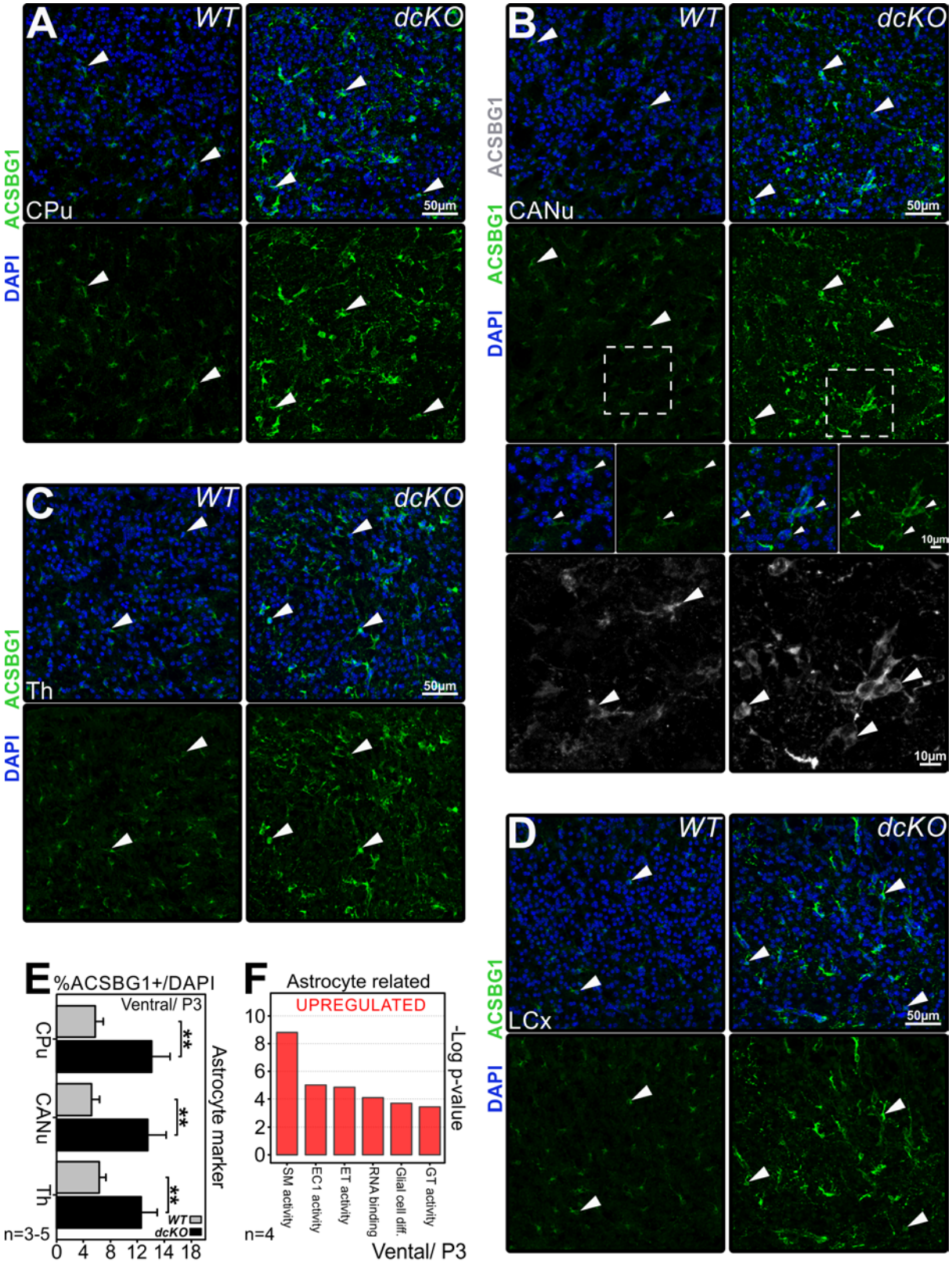
A
WT
dcKO
ACSBG1
CPu
DAPI
50µm
B
CANu
10µm
C
Th
D
LCx
E
%ACSBG1+/DAPI
Ventral/ P3
CPu
CANu
Th
**
Astrocyte marker
WT
dcKO
n=3-5
0 4 8 12 14 18
F
Astrocyte related
UPREGULATED
-Log p-value
SM activity
EC1 activity
ET activity
RNA binding
Glial cell diff.
GT activity
n=4
Ventral/ P3
G
Log2 fold change
Astrocyte related
n=4
Ventral/ P3
dcKO
UPREGULATED
Nkx6.1
Pamr1
Nkx2.1
Gli1
Id3
Acsbg1
Romo1
Vcam1
Nnat
Magoh
H3f3a
Dll1
Rfx4
Vim

Figure 28 | Highly elevated astrogliosis in BAF complex deprived VP and LP (II). (A-D) Immunostaining of coronal brain sections through WT and dcKO murine P3 VP (A-C) and LP (D) for ACSBG1 (in green and gray) in the following areas: CPu (A), CANu (B), Th (C) and LCx – S2 (D). Cell nuclei are visualized by DAPI (in blue). Lower boards of WT and dcKO are single channel images. Full arrowheads indicate astrocytes expressing ACSBG1. Magnified views of ACSBG1 positive astrocytes from delineated areas of WT and dcKO CANu shown as small panels and grayscale images in B. (E) Bar graph representing percentage share of ACSBG1 positive cells in all DAPI positive cells in indicated areas of P3 WT and dcKO mouse VP. Quantifications for D shown in Figure 19. Data are averages ± σ of n=3-5 experimental replicates (WT/CPu: n=5, dcKO/CPu: n=5, WT/CANu: n=5, dcKO/CANu: n=5, WT/Th: n=3, dcKO/Th: n=3); **p≤0.01 in Mann Whitney Rank Sum test. (F) GO analysis indicating groups of genes related to astrocyte function and differentiation, significantly upregulated in P3 VP *hGFAP*-Cre dcKO. Bar graph represents – Log of corresponding p value for each indicated GO category. (G) Bar graph representing Log_2 fold change of astrocyte related transcripts abundance in VP of P3 dcKO animals. Transcriptome data are averages of n=4 animals. For all investigated transcripts p≤0.01. In GO pathway enrichment analysis Bonferroni corrected for p<0.05. CANu, central amygdala nucleus; CPu, caudate putamen; dcKO, double knockout; diff, differentiation; EC1, oxidoreductase; ET, electron transfer; GT, glutathione transferase; LCx, lateral cortex (refers to S2 area); SM, structural molecule; WT, wild type.

P3 WT and dcKO VP tissue lysates (see Chapter 2. Materials and Methods. 2.8) and selected aberrantly upregulated genes for subsequent GO enrichment analysis. We then compared the outcome of the GO classification with the online available list of GO annotated astrocyte enriched molecular pathways (http://www.networkglia.eu (Cahoy et al., 2008; Doyle et al., 2008; Lovatt et al., 2007)). As indicated in Figure 28F, several molecular pathways upregulated in P3 dcKO were previously annotated as astrocyte specific. Accordingly, by means of this analysis we could reveal that VP of dcKO upregulated transcripts known to be elements of molecular pathway of: structural molecule activity (GO: 0005198), oxidoreductase activity (GO: 0016491), electron transfer activity (GO: 0009055), RNA binding activity (GO: 0003723) as well as glutathione transferase activity (GO: 0004364). All of these molecular pathways are typically enhanced in astroglial cells, which highlights the prominent astroglial phenotype of dcKO VP. In addition, several transcripts significantly elevated in P3 dcKO VP (**p≤0.01) were related to glial cell differentiation (GO: 0045687 and GO: 0045685), indicating enhanced glia development in dcKO VP compared to WT. Among those, Nkx6.1 as well as Nkx2.1 are known to induce astrocyte differentiation (Minocha et al., 2017; Minocha et al., 2015; Zhao et al., 2014). Furthermore, screening the literature for astrocytic markers allowed us to select 14 the most upregulated transcripts known to be astrocyte related. Figure 28G illustrates their levels of upregulation where Log_2 fold changes of chosen transcript correspond to its abundance compared to P3 WT VP). The relation of a given transcript to astroglial cell fate regulation is documented in Table 2. Importantly, the increase of ACSBG1 described above (Figure 27A-B and Figure 28A-E) was also apparent at the transcriptome level (Figure 28G).

Overall, our transcriptome studies together with the ACSBG1 immunohistochemistry prompted us to

NAME	FUNCTION	REFERENCES
Nkx2.6	Control of astrocyte specification and differentiation	(Zhao et al., 2014)
Pamr1	Unknown. Transcript upregulated in human and murine astrocytes. An extracellular matrix molecule.	(Molofsky et al., 2014; Zhang et al., 2016)
Nkx2.2	Control of astrocyte specification and differentiation	(Minocha et al., 2017; Minocha et al., 2015)
Gli1	Enhancement of astrocyte development	(Garcia et al., 2010)
Id3	Promotes astrocytic differentiation and negatively regulates neuronal differentiation	(Nakashima et al., 2001)
Acsbg1	Gray matter astrocyte marker	(Cahoy et al., 2008; Chaboub and Deneen, 2013)
Romo1	Unknown. Transcript upregulated in murine astrocytes.	(Zhang et al., 2016)
Vcam1	Unknown. Transcript upregulated in murine astrocytes.	(Zhang et al., 2016)
Nnat	Unknown. Transcript upregulated in murine astrocytes.	(Zhang et al., 2016)
Magoh	Unknown. Transcript upregulated in murine astrocytes.	(Zhang et al., 2016)
H3f3a	Unknown. Transcript upregulated in murine astrocytes. Often mutated in astrocytomas	(Michelucci et al., 2016; Zhang et al., 2016)
Dll1	Initiation of astrogliogenesis	(Freeman, 2010)
Rfx4	Unknown. Transcript upregulated in murine astrocytes.	(Zhang et al., 2014)
Vim	Astrocyte enriched protein	(Schnitzer et al., 1981)

Table 2 | Selected astrocyte related transcripts upregulated in VP of P3 dcKO mice. The table describes 14 transcripts considered as typical for astrocytes significantly upregulated in VP of P3 dcKO stating the function and corresponding literature source (references).

assume that unlike in DP, VP of P3 dcKO mice exhibits prominent mature astrocyte phenotype.

In order to confirm this assumption we decided to investigate the P3 VP expression of another protoplasmic astrocyte marker - GS (Anlauf and Derouiche, 2013) and compare it to that of ACSBG1. As shown in Figure 29A (overviews shown in Appendix, Figure 45B), immunostaining indicated a massive increase of the abundance of GS positive cells found in the area of LGE of dcKO VP. A quantification (Figure 29C) revealed that the fraction of DAPI stained cells exhibiting GS expression in

the LGE was significantly higher in dcKO than in WT (***p≤0.001; in WT 8.2±0.7% whereas in dcKO 14.9±1.9% of all DAPI found in LGE stained for GS). Surprisingly, this elevated amount of GS expressing astrocytes seemed to decline in deeper areas of dcKO VP (Figure 29A and C; CPu). Even though still significantly outnumbering WT CPu residing cells (**p≤0.01; Figure 29C), GS positive astrocytes of dcKO CPu were not as numerous as in LGE (in WT 5.5±0.9% whereas in dcKO 9.3±1.3% of all DAPI found in CPu stained for GS). However, considering the total area of VP, GS expressing astrocytes found in dcKO brains were significantly more numerous than those of WT (Figure 29C; ***p≤0.001; in WT 7.0±0.6% whereas in dcKO 12.7±1.3% of all DAPI found in VP stained for GS).

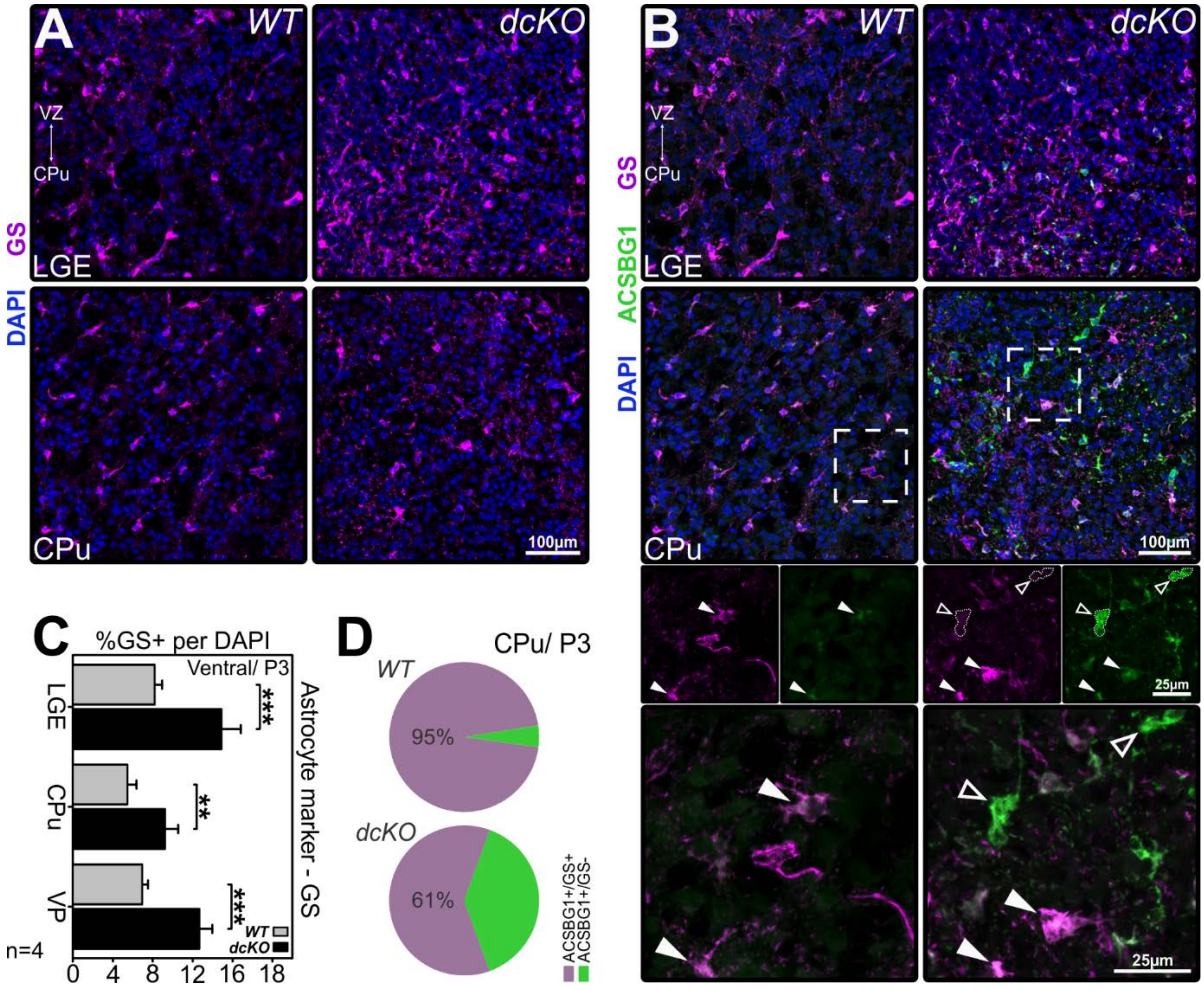

Figure 29 | Area dependent upregulation of GS expression in BAF complex depleted postnatal VP. (A-B) Coronal tissue sections through WT and dcKO P3 mouse LGE and CPu stained with antibodies detecting astroglial markers; (A) GS (in magenta) and (B) GS (in magenta) together with Acsbg1 (in green). DAPI staining is blue. For LGE the directions towards VZ and CPu are indicated by two headed arrow. For (B) lower panels of CPu are magnified insets of delineated areas. Full arrowheads indicate CPu astrocytes positive for GS and ACSBG1, emptyones indicate astrocytes positive only for ACSBG1. Cell bodies of ACSBG1 positive/GS negative astrocytes outlined with dashed line. (C) Percentages of GS positive astrocytes per DAPI positive cells in the areas of LGE, CPu and total VP of WT and dcKO mice. Data are

averages ± σ of n=4 experimental replicates; ***p≤0.001, **p≤0.01 in t- student test. (D) Pie charts showing the degree of colocalization between ACSBG1 and GS in WT (upper panel) and dcKO (lower panel) P3 CPu. Light purple colour indicates percentages of ACSBG1 positive cells expressing GS, green colour indicates percentages of ACSBG1 positive cells negative for GS. Data are averages of n=3 (for WT: ACSBG1+/GS+=95.3, ACSBG1+/GS-=4.6% ±2.8%; for dcKO: ACSBG1+/GS+=61.0, ACSBG1+/GS-=39%±4.3%). CPu, caudate putamen; dcKO, double knockout; LGE, lateral ganglionic eminence; VP, ventral pallium; VZ, ventricular zone; WT, wild type.

Furthermore, the ACSBG1/GS co-immunostaining indicated an interesting relationship between these two markers in dcKO CPu (Figure 29B). As indicated in Figure 29B (CPu; full arrowheads) and the pie chart (Figure 29D), the majority of ACSBG1 positive astrocytes of WT CPu exhibited GS staining (95% of all CPu ACSBG1 positive cells stained for GS). A Similar comparison of ACSBG1 and GS expression in dcKO mice indicated a reduced fraction of CPu ACSBG1 positive cells expressing GS (61% of all dcKO CPu ACSBG1 stained for GS, ACSBG1 positive that did not express GS indicated by empty arrowheads in Figure 29B). Importantly, several studies indicated that GS expression may not be confined to astrocytes and can be present in oligodendrocytes and common glial precursors (Cahoy et al., 2008; Derouiche and Rauen, 1995; Sun et al., 2017; Tansey et al., 1991). Thus, the highly enriched GS staining found in dcKO astroglial germinal zone (LGE) may indicate an increased production of common glial precursors. As expression of GS decays in deeper areas of dcKO VP (CPu) a visible decline in ACSBG1 positive cells may lead one to assume that GS positive dcKO glial precursors migrating out of the germinal zone loose GS expression and differentiate into astroglial cells (ACSBG1 was found to be exclusively enriched in astrocytes (Cahoy et al., 2008)). However, evidence supporting this is scarce and needs to be expanded by further experiments.

Together, data from our marker analyses and transcriptome studies indicate that *hGFAP*-Cre driven loss of BAF complex evokes a massive increase in astrocyte abundance in VP of P3 murine brain.

AGPs in postnatal VP – dcKO versus WT phenotype

As previously described, during WT mouse development expression of several BAF complex subunits decreased along with the transformation of astrocytic RGCs to AGPs. This stood true for cortical and striatal progenitors (see: Chapter 3. Results. 3.1). Accordingly, we showed that loss of BAF complex in astrocytic RGCs massively increases the abundance of cortical AGPs. However, it would be interesting to prove that the absence of BAF complex can positively influence the abundance of ventral AGPs. Having established that the amount of ventral protoplasmic astrocytes is increased in dcKO VP, we asked whether the numbers of ventral AGPs are also elevated upon BAF complex loss. Thus, using immunostaining we investigated the expression of the AGPs markers: NFiA, BLBP and GLAST (Chaboub and Deneen, 2013) (Figure 30). Because the highest numbers of GS and ACSBG1

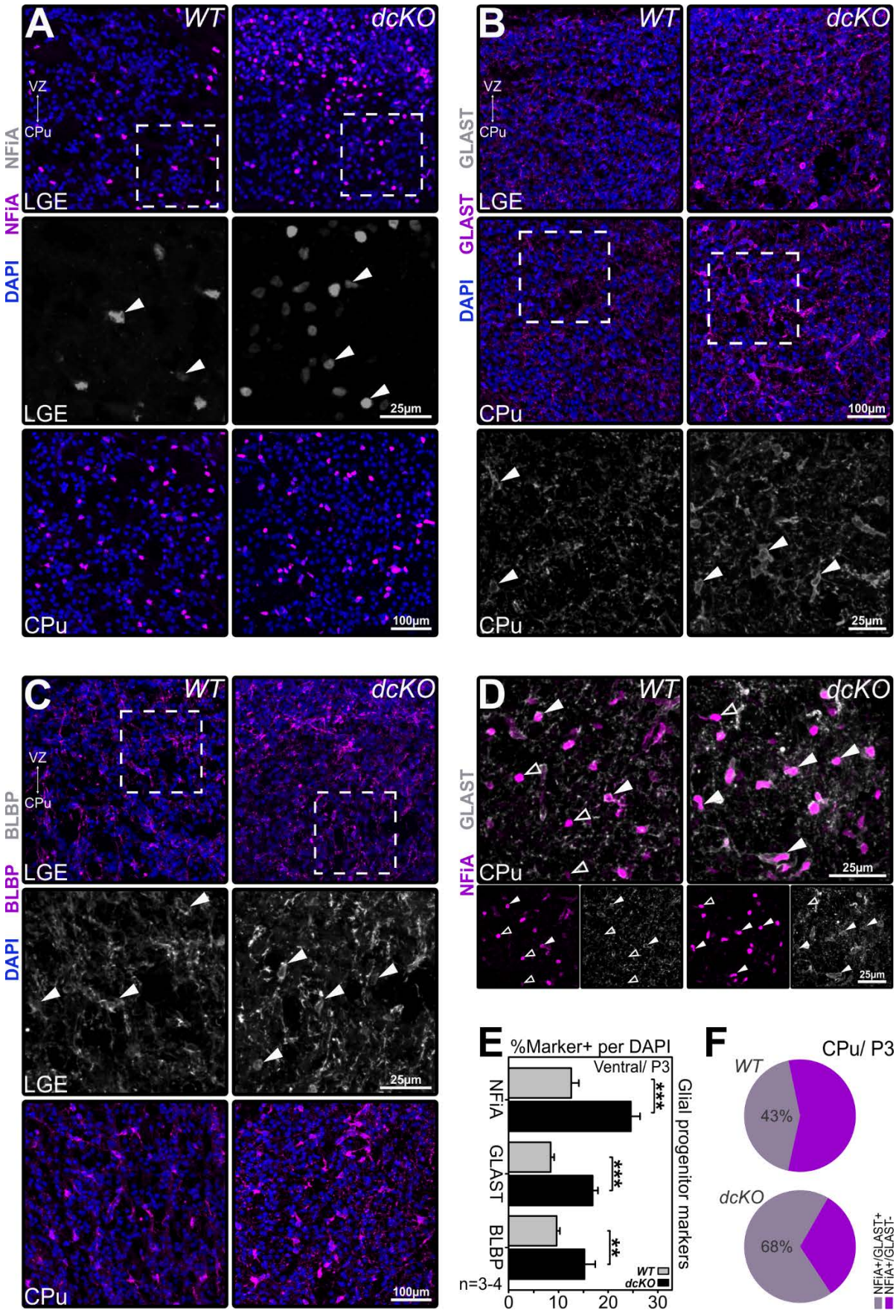
A
WT
dcKO
VZ
CPu
NFiA
LGE
DAPI
25µm
100µm
CPu
B
GLAST
C
BLBP
D
E
%Marker+ per DAPI
Ventral/ P3
Glial progenitor markers
n=3-4
WT
dcKO
0
10
20
30
F
CPu/ P3
43%
68%
NFiA+/GLAST+
NFiA+/GLAST-

Figure 30 | Deficiency in BAF complex results in highly elevated astrocytic GP generation in postnatal striatum. (A-D) Immunofluorescence staining of WT and dcKO P3 mouse LGE and CPu coronal sections showing expression of GP and astrocyte markers: (A) NFiA (in magenta and gray), (B) GLAST (in magenta and gray), (C) BLBP (in magenta and gray, overview in Appendix, Figure 45), (D) NFiA (in magenta) and GLAST (in gray, overview in Figure 18). The nuclear DAPI staining is blue. For LGE area the directions towards VZ and CPu are indicated by two headed arrow. For A-C grayscale images are magnified insets of delineated areas of: (A,C) LGE and (B) CPu. Full arrowheads indicate GP positive for given marker. Lower boards in D are single channel images of WT and dcKO CPu. Full arrowheads indicate CPu GPs positive for NFiA and GLAST, empty arrowheads indicate progenitors positive only for NFiA. (E) Percentages of astrocytic GP marker positive cells per DAPI positive cells in the area of striatum of P3 WT and dcKO mice. Data are averages ± σ of n=3-4 experimental replicates (NFiA/WT: n=4, NFiA/dcKO: n=3, GLAST/WT: n=3, GLAST/dcKO: n=3, BLBP/WT: n=3, BLBP/dcKO: n=3); ***p≤0.001, **p≤0.01 in t student test. (F) Pie charts showing the degree of colocalization between NFiA and GLAST in WT (upper panel) and dcKO (lower panel) P3 CPu. Light purple colour indicates percentages of NFiA positive cells expressing GLAST, magenta colour indicates percentages of NFiA positive cells negative for GLAST. Data are averages of n=2-3 animals (for WT: n=2, NFiA+/GLAST+=43.2, NFiA+/GLAST-=56.8 ±0.9%; for dcKO: n=3, NFiA+/GLAST+=67.7, NFiA+/GLAST-=32.3 ±11.2%). CPu, caudate putamen; dcKO, double knockout; LGE, lateral ganglionic eminence; VZ, ventricular zone; WT, wild type.

positive cells were observed in dcKO LGE and CPu, we decided to focus our analysis on these two areas of P3 VP. As showed in Figure 30A-C, compared to WT the LGE and CPu of dcKO P3 pups exhibited elevated staining for all investigated markers of AGPs. Accordingly, the quantifications performed for both analyzed areas (LGE and CPu pulled together and presented as VP; Figure 30E) indicated a significant increase in the amount of NFiA expressing cells found in VP of dcKO comparing to that of WT (***p≤0.001; in dcKO VP 24.7±1.7% of DAPI stained cells expressed NFiA, 12.6±1.4% in WT). Interestingly, despite the increased general cell numbers, the expression pattern of dcKO NFiA cells was similar to that of dcKO GS positive cells with elevated staining found in LGE area that further seemed to decay in deeper VP regions (here shown in CPu). However, as in the case of GS, the elevated NFiA staining found in dcKO astroglial germinal zone (LGE) may indicate an increased production of common glial precursors. This assumption is supported by the literature, as it was described that in gliogenesis, NFiA initiates the induction of an oligodendrocyte/astrocyte genetic program (Deneen et al., 2006). Furthermore, cortical neurons are known to express NFiA (Bunt et al., 2017). Because we have already shown that cortical cells migrate aberrantly in dcKO (see Chapter 3. Results. 3.3) we could also assume that some of the NFiA positive cells found in dcKO LGE may be of cortical neuronal fate. Thus, we could not accept NFiA as an exclusive marker of dcKO astroglia and therefore, we decided to co-stain for NFiA and GLAST in CPu of P3 WT and dcKO and evaluate their colocalization (Figure 30D). These experiments revealed cells exclusively expressing NFiA (indicated by empty arrowheads) and cells that co-expressed NFiA and GLAST (indicated by full arrowheads) in both genotypes. However, as indicated in Figure 30F, the percentage of NFiA positive cells expressing GLAST was higher in CPu of dcKO mice (68% in dcKO and 43% in WT). This indicates that a substantial fraction of NFiA positive cells found in dcKO VP are of AGP fate. Additionally,

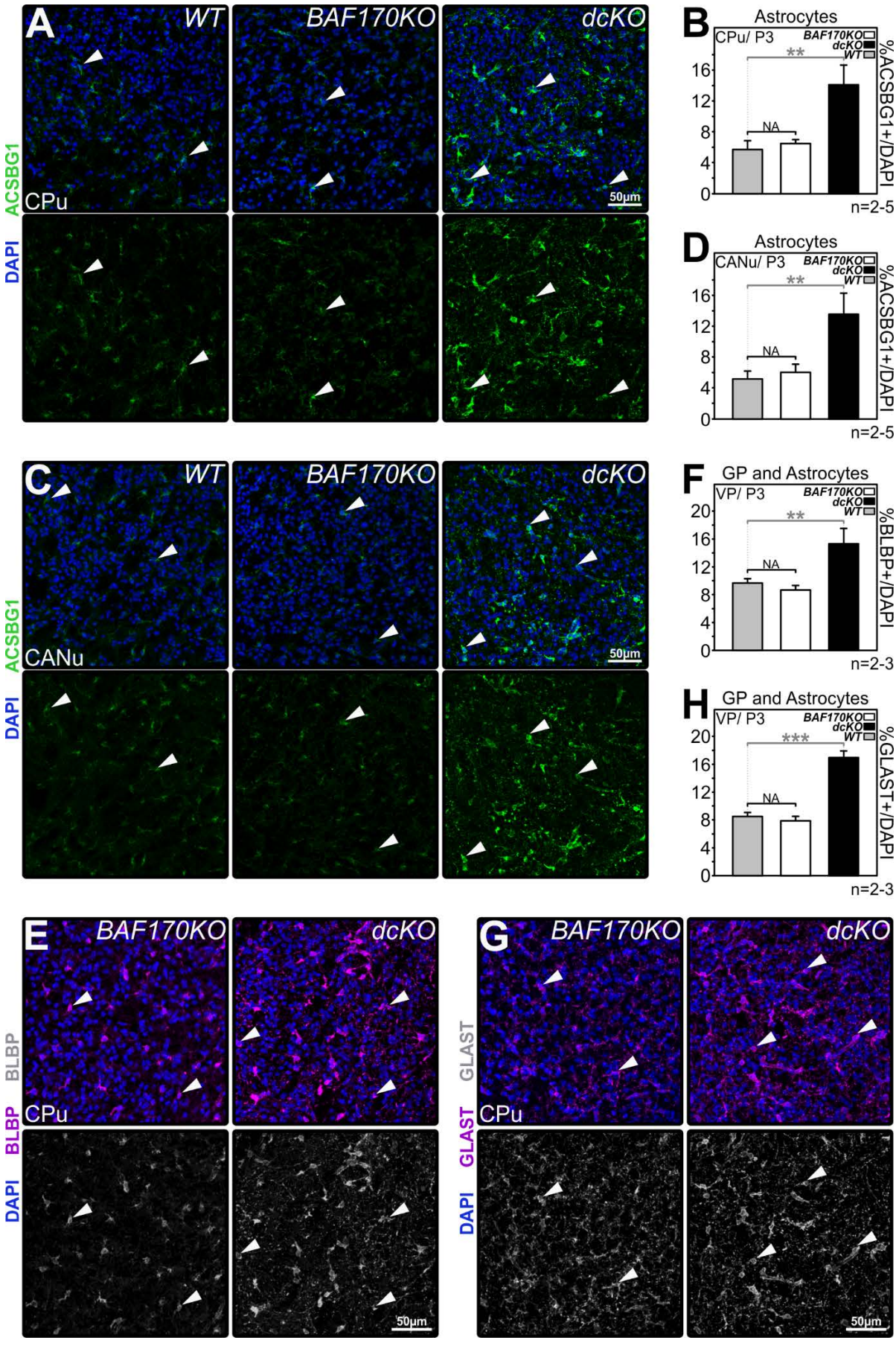
A
WT
BAF170KO
dcKO
ACSBG1
CPu
DAPI
50µm
B
Astrocytes
CPu/ P3
BAF170KO
dcKO
WT
**
NA
%ACSBG1+/DAPI
n=2-5
D
Astrocytes
CANu/ P3
BAF170KO
dcKO
WT
**
NA
%ACSBG1+/DAPI
n=2-5
C
WT
BAF170KO
dcKO
ACSBG1
CANu
DAPI
50µm
F
GP and Astrocytes
VP/ P3
BAF170KO
dcKO
WT
**
NA
%BLBP+/DAPI
n=2-3
H
GP and Astrocytes
VP/ P3
BAF170KO
dcKO
WT
***
NA
%GLAST+/DAPI
n=2-3
E
BAF170KO
dcKO
BLBP
CPu
DAPI
50µm
G
BAF170KO
dcKO
GLAST
CPu
DAPI
50µm

Figure 31 |Single BAF170 subunit KO does not lead to increased astrogliosis in postnatal VP. (A, C, E, G) Coronal sections through P3 VP areas (CPu in A, E and G, CANu in C) of WT (in A and C), BAF170KO and dcKO (in A, C, E and G) mice, stained with antibodies to astrocyte and GP markers; (A and C) astrocyte marker – ACSBG1 (in green), (E) GP and astrocyte marker – BLBP (in magenta and gray) and (G) GP and astrocyte marker – GLAST (in magenta and gray). Nuclei of cells stained with DAPI (in blue). Lower panels are single channel images of the corresponding marker. Full arrowheads indicate cells positive for a given marker. (B, D, F and H) Bar graphs indicating percentages of astrocyte/GP marker positive cells per all DAPI positive cells in the areas of; (B) CPu, (D) CANu and (F and H) total VP of P3 WT, BAF170KO and dcKO pups. Data are averages ± σ of n=2-5 experimental replicates (ACSBG1/WT/CPu: n=5, ACSBG1/BAF170KO/CPu: n=2, ACSBG1/dcKO/CPu: n=5, ACSBG1/WT/CANu: n=5, ACSBG1/BAF170KO /CANu: n=2, ACSBG1/dcKO/CANu: n=5, BLBP/WT: n=3, BLBP/BAF170KO: n=2, BLBP/dcKO: n=3, GLAST/WT: n=3, GLAST/BAF170KO: n=2, GLAST/dcKO: n=3); for B and D: **p≤0.01 in Mann Whitney Rank Sum test, for F and H: ***p≤0.001, **p≤0.01 in t student test. For all NA not applicable (n=2). BAF170KO, BAF170 knockout; CANu, central amygdala nucleus; CPu, caudate putamen; dcKO, double knockout; GP, glial progenitors; NA, not applicable; VP, ventral pallium; WT, wild type.

GLAST and BLBP positive cells of dcKO VP significantly outnumbered these of WT (Figure 30E; ***p≤0.001; in WT 8.5±0.5% whereas in dcKO 17.0±0.8% of all DAPI found in VP stained for GLAST; **p≤0.01; in WT 9.7±0.4% whereas in dcKO 15.3±1.9% of all DAPI found in VP stained for BLBP) thereby indicating elevated amount of AGPs within BAF complex depleted VP.

In summary, we showed that the loss of BAF complex in astrocytic RGCs causes a massive increase in the abundance of AGPs in cortex and striatum.

However, in P0 WT mice, BAF complex subunits of striatal AGPs, even though declining, exhibited different levels of downregulation (Figure 8 and 10). Strikingly, the decay of BAF170 in striatal AGPs seemed to be faster and more pronounced than that of other investigated BAF complex subunits (only ~13% of AGPs expressed detectable levels of BAF170, and positive cells had low NFI). This could indicate that the downregulation of BAF170 expression itself promotes AGPs production. In order to test whether astrocytic RGCs differentiate to AGPs due to the decline in BAF complex as a whole or because of the reduction in BAF170 expression alone, we compared the abundance of AGPs and protoplasmic astrocytes in VP of WT, dcKO and BAF170KO (exhibiting loss of single BAF complex subunit – BAF170 (Tuoc et al., 2013b)) P3 mice (both KO driven by *hGFAP*-Cre; see Chapter 2. Materials and Methods. 2.1). Using immunohistochemistry, we compared the expression of the AGPs markers GLAST and BLBP as well as the protoplasmic astrocyte marker ACSBG1 in VP tissues (CPu and CANu) of WT, BAF170KO and dcKO P3 pups. The results are shown in Figure 31. As previously described, CPu and CANu of dcKO exhibited prominent upregulation of all investigated markers with respect to WT. To the contrary, neither GLAST and BLBP positive AGPs nor ACSBG1 expressing protoplasmic astrocytes were upregulated in the corresponding ventral regions of BAF170KO brains. Moreover, the astroglial phenotype exhibited by CPu and CANu of BAF170KO mice

was similar to WT (Figure 31A and C), showing comparable percentage of DAPI stained cells positive for ACSBG1, BLBP and GLAST (Figure 31B, D, F and H). Additionally, astroglial cells found in BAF170KO VP showed a WT-like scattered distribution pattern (Figure 31A and C). Thus, these results demonstrate that in contrast to the elimination of complete BAF complex, KO of BAF170 alone does not evoke the differentiation of astrocytic RGCs to AGPs or protoplasmic astrocytes.

Altogether, we showed that the loss of the entire BAF complex forces astrocytic RGCs to differentiate to AGPs and to protoplasmic astrocytes in the developing mouse brain.

BAF complex controls genesis of astrocytes in a cell-autonomous mechanism

In order to trace the origin of the generated astrocytes in BAF complex deficit brain, we looked at the expression of ACSBG1 at different developmental stages (E17.5, P0 and P3) in *hGFAP*-Cre dcKO tdTomato mice (Chapter 2. Materials and Methods. 2.1).

As indicated in Figure 32A and B, elevated amounts of ACSBG1 positive cells could be detected already in E17.5 CPu of dcKO mice. Importantly, the corresponding area of E17.5 WT brain did not exhibit cells stained for ACSBG1. Thus the amount of dcKO ACSBG1 positive cells found in E17.5 brains significantly (**$p \leq 0.01$) outnumbered that of WT. Additionally, tracing experiments indicated that 99% of ACSBG1 expressing cells found in VP of E17.5 dcKO mice expressed tdTOM (upper most pie chart of Figure 32H). This suggests that these cells were affected by the mutation and possibly originated from *hGFAP*-Cre targeted astrocytic RGCs. The same experiment performed for CPu of P0 WT and dcKO pups revealed a massive increase in the amount of ACSBG1 expressing astrocytes found in mutant tissue (Figure 32C, D and G). Importantly, these elevated amounts of ACSBG1 positive cells significantly outnumbered that of WT (***$p \leq 0.001$). However the tracing analysis indicated that the fraction of ACSBG1 positive cells expressing tdTOM decreases to 91% (Figure 32C and H). This suggests that some of the protoplasmic astrocytes found in CPu of P0 dcKO originate from germinal zones unaffected by the mutation. Last but not least we subjected P3 CPu tissues of WT and dcKO brains to the same analysis. As shown in Figure 32E-G the amount of ACSBG1 positive astrocytes found in dcKO CPu was higher than that of P0 mutant mice or CPu (***$p \leq 0.001$). In addition 94% of ACSBG1 astrocytes stained in CPu of P3 dcKO mice exhibited tdTOM, demonstrating that they were affected by the mutation of the BAF complex (lowest pie chart of Figure 32H). Taken together, the numbers of ACSBG1 expressing astrocytes found in WT as well as dcKO CPu were escalating over developmental time (Figure 32G). Additionally, the amount of dcKO protoplasmic astrocytes always significantly exceeded that of WT. However, not all ACSBG1 positive cells found in CPu of postnatal dcKO mice were tdTOM positive, implying that a small fraction was not affected by BAF complex mutation. Still, the vast majority of ACSBG1 positive cells were, suggesting that the

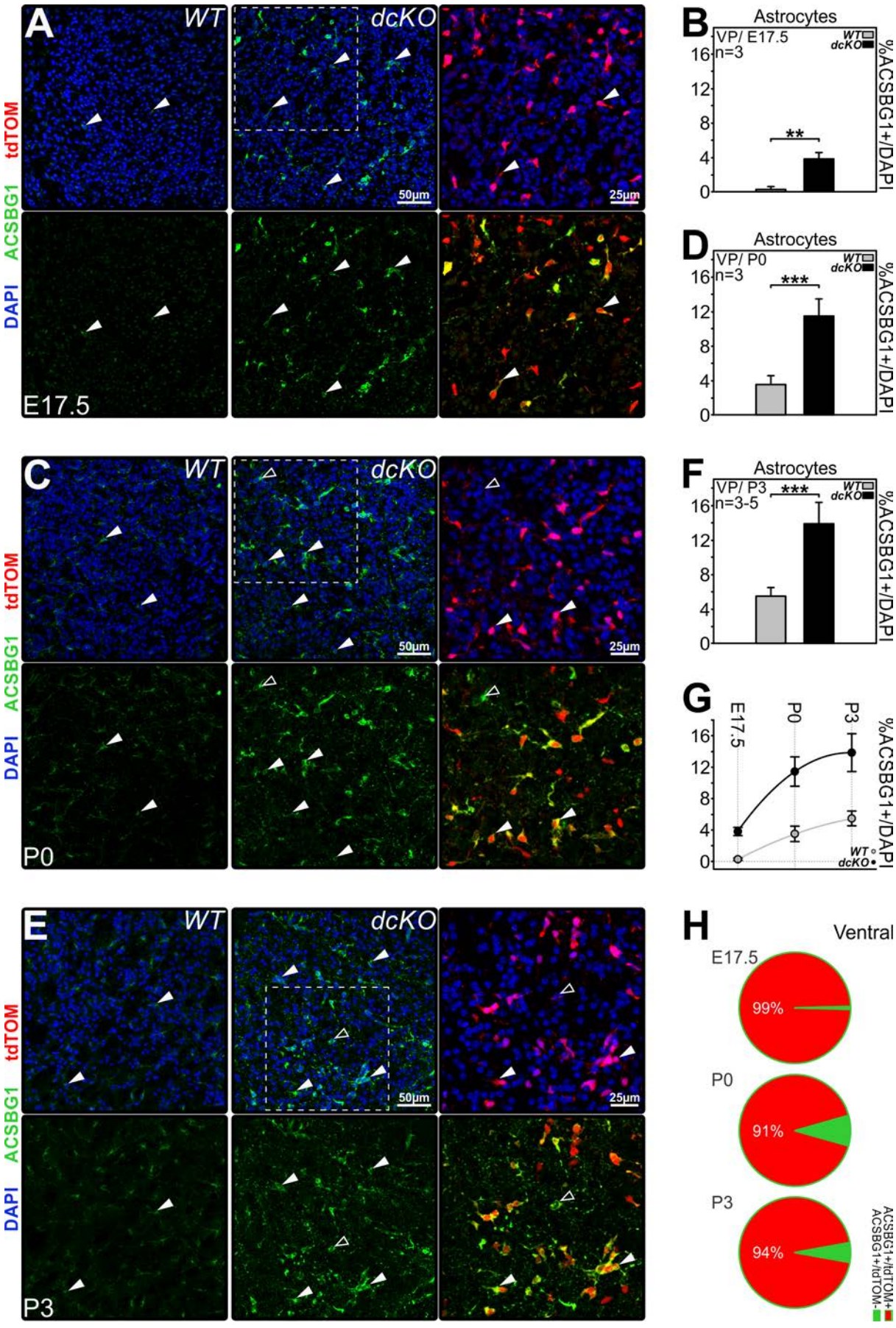
A
WT
dcKO
tdTOM
ACSBG1
DAPI
E17.5
50µm
25µm
B
Astrocytes
VP/ E17.5
n=3
WT
dcKO
%ACSBG1+/DAPI
**
D
Astrocytes
VP/ P0
n=3
***
C
P0
F
Astrocytes
VP/ P3
n=3-5
***
G
E17.5
P0
P3
%ACSBG1+/DAPI
E
P3
H
Ventral
E17.5
99%
P0
91%
P3
94%
ACSBG1+/tdTOM+
ACSBG1+/tdTOM-

Figure 32 | Deficiency in BAF complex leads to intensified VP astrocyte production during embryonic development and postnatally. (A, C, E) Immunofluorescence analysis of WT and dcKO (*hGFAP*-Cre dcKO tdTomato) mouse coronal sections of brain tissue isolated at: (A) E17.5, (C) P0, (E) P3 and immunostained for ACSBG1 (in green). The nuclear DAPI staining is blue, the endogenous tdTOM signal is red (only for dcKO sections). Overview of E17.5 sections stained for ACSBG1 provided in Appendix, Figure 46. Lower boards of WT and dcKO are single channel images of ACSBG1 staining. Right panels of dcKO are magnified views of ACSBG1 positive astrocytes from delineated VP areas of dcKO brains, shown together with an endogenous tdTOM signal. Cells expressing ACSBG1 and tdTOM are astrocytes with an active *hGFAP* promoter, presumably affected by BAF complex knockout. For WT and dcKO overview pictures full arrowheads indicate astrocytes positive for ACSBG1, for magnified panels full arrowheads indicate dcKO ACSBG1 positive astrocytes exhibiting endogenous tdTOM signal, empty arrowheads indicate dcKO ACSBG1 positive astrocytes negative for tdTOM expression. (B, D, F) Bar graphs representing percentages of ACSBG1 positive cells among all DAPI cells in WT and dcKO VP of (B) E17.5, (D) P0 and (F) P3 mice. (G) Scatter plots with polynomial regression lines juxtaposing the quantifications for all analyzed developmental stages represented in bar graphs in (B, D, F). Regression line for WT is gray, regression line for dcKO is black. For (B, D, F, G) data are averages ± σ of n=3-5 experimental replicates (E17.5/WT: n=3, E17.5/dcKO: n=3, P0/WT: n=3, P0/dcKO: n=3, P3/WT: n=3, P3/dcKO: n=5); for E17.5 and P3: **p≤0.01, ***p≤0.001 in Mann Whitney Rank Sum test, for P0: ***p≤0.001 in t student test. (H) Pie charts representing the degree of colocalization between ACSBG1 tdTOM in VP of dcKO brains harvested at; E17.5 (upper graph), P0 (middle graph) and P3 (bottom most graph). Red colour indicates percentages of ACSBG1 positive cells expressing tdTOM, green colour indicates percentages of ACSBG1 positive astrocytes negative for tdTOM. Data are averages of n=2 (for E17.5: ACSBG1+/tdTOM+=99.1, ACSBG1+/tdTOM-=0.9±1%; for P0: ACSBG1+/tdTOM+=91.1, ACSBG1+/tdTOM-=8.9±2.1%; for P3: ACSBG1+/tdTOM+=94.3, ACSBG1+/tdTOM-=5.7±1.4%). dcKO, double knockout; tdTOM, tdTomato; VP, ventral pallium; WT, wild type.

abundance of astrocytes is due to the BAF complex mutation.

Keeping in mind that *hGFAP*-Cre drives recombination in all astrocytic RGCs of the forebrain (Figure 12), we subsequently asked whether every astrocytic germinal zone serves as a source for the abundant astroglial cells found in dcKO. It is most likely due to the BAF complex KO within cortical germinal zone that the cortex of dcKO mice exhibits highly elevated numbers of AGPs. Additionally, based on our IUE experiments we may assume that at least a fraction of ACSBG1 positive astrocytes found in CPu of dcKO mice could originate from cortical astrocytic RGCs (see Chapter 3. Results. 3.3). This assumption seems to be supported by the observation of ACSBG1 positive astrocytes in dcKO CPu as early as at E17.5. As indicated by tracing experiments, the *hGFAP*-Cre driven recombination within ventral astrocytic RGCs starts relatively late comparing to cortex (E13.5, E15.5 and E17.5 for cortical VZ, MGE and LGE respectively). Thus, we decided to investigate whether depletion of BAF complex within ventral astrocytic RGCs alone would result in an increased amount of astrocytes as in *hGFAP-Cre* dcKO brains. Accordingly, we assessed the expression of ACSBG1 in *Olig2*-Cre driven dcKO and compare it to that of WT and *hGFAP*-Cre driven dcKO (Figure 33). We chose to use *Olig2*-Cre as a driver of dcKO mutation, as it is known to exclusively target ventral germinal zones in developing forebrain (Zawadzka et al., 2010). As *Olig2*-Cre dcKO animals were dying at birth, we were forced to

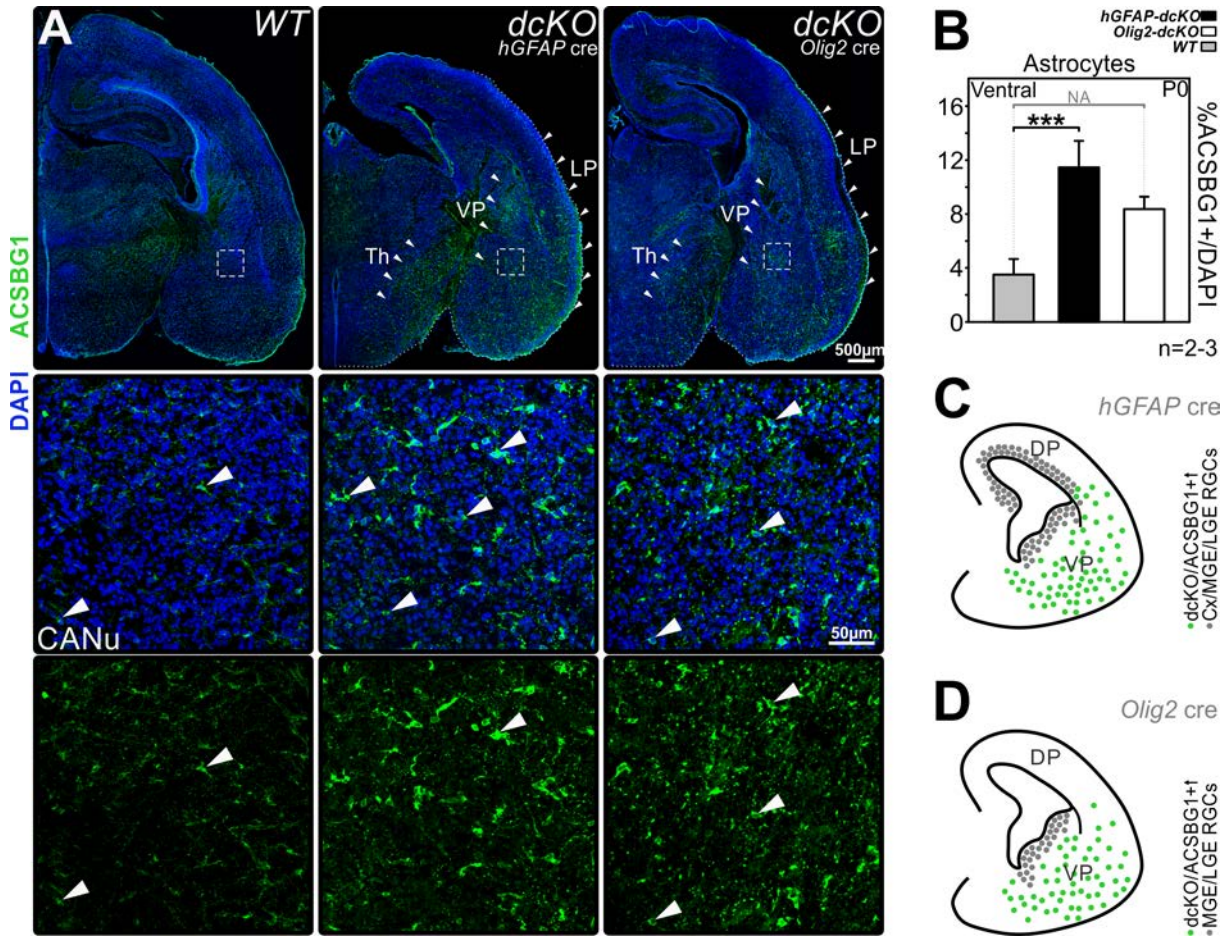

Figure 33 | *Olig2*-Cre congruous to *hGFAP*-Cre driven BAF complex KO leads to increased astrogliogenesis in affected LP and VP areas. (A) Immunofluorescence analysis of P0 WT as well as *hGFAP*-Cre and *Olig2*-Cre dcKO mouse brain sections stained with antibody to astroglial marker – ACSBG1 (in green). The nuclear DAPI staining is blue. First row represents overview brain pictures of WT (left panel), *hGFAP*-Cre dcKO (middle panel) and *Olig2*-Cre dcKO (right panel) animals. Full arrowheads indicate the areas of dcKO LP, Th and VP exhibiting increased amount of ACSBG1 signal. Second and third row show magnified views of ACSBG1 positive astrocytes from delineated in overview areas of WT, *hGFAP*-Cre dcKO and *Olig2*-Cre dcKO CANu. Full arrowheads indicate astrocytes expressing ACSBG1. (B) Percentages of ACSBG1 positive cells per total DAPI positive cells in VP of WT, *hGFAP*-Cre and *Olig2*-Cre dcKO mice. Data are averages ± σ of n=2-3 animals (WT: n=3, *hGFAP*-Cre dcKO: n=3, *Olig2*-Cre dcKO n=2); ***p≤0.001 in t student test, NA not applicable (n=2). (C-D) Sum up schematics showing astrocytic germinal zones affected by recombination (gray dots) together with the populations of ACSBG1 positive astrocytes (green dots) that differ from WT in the increase of amount in: (C) *hGFAP*-Cre dcKO and (D) *Olig2*-Cre dcKO P0 brains. CANu, central amygdala nucleus; dcKO, double knockout; DP, dorsal pallium; NA, not applicable; RGCs, radial glial cells; Th, thalamus; VP, ventral pallium; WT, wild type.

perform ACSBG1 immunostaining on brain slices of P0 mice. Immunohistochemistry revealed that the amount of ACSBG1 positive cells found in Th, VP and LP of both mutants was visibly elevated comparing to that of WT. However the quantitative analysis performed for the area of CANu indicated that the ACSBG1 positive cells found in *hGFAP*-Cre dcKO were more numerous than that of

Olig2-Cre dcKO (Figure 33B). Thus, despite the lack of statistical significance, this results suggests that *hGFAP*-Cre driven BAF complex depletion is more thorough. However, as indicated in summary schemes, the aberrant expression of ACSBG1 was found in VP regions of all brain sections from *hGFAP*-Cre dcKO and *Olig2*-Cre dcKO mice (Figure 33C and D, targeted RGCs shown in gray, aberrant protoplasmic astrocytes shown in green). The only observed difference was in the density and cortical localizations of cells, namely cells aberrantly expressing ACSBG1 found in *hGFAP*-Cre dcKO appeared denser, and in contrast to those in *Olig2*-Cre dcKO, they could often be found in S1 cortical area.

Taken together, our data indicate that the vast majority of the abundant astroglia found in dcKO derives from dorsal as well as ventral astrocytic RGCs affected by BAF complex depletion.

Proliferation of BAF complex depleted protoplasmic astrocytes of VP

Considering that BAF complex depleted AGPs of postnatal DP are highly proliferative, we next investigated the proliferation of astroglia in VP of dcKO mice.

We first evaluated proliferation by immunostaining of Ki67 within BLBP positive AGPs as well as ACSBG1 enriched protoplasmic astrocytes (Figure 34A-C) in P3 brains, focusing on the CPu. As indicated in Figure 34B and C, some of WT BLBP and ACSBG1 expressing cells found in CPu did exhibit Ki67 staining (pointed by full arrowheads), indicating active local proliferation of AGPs and maturating protoplasmic astrocytes in postnatal VP. Quantitatively, Ki67 was expressed by 18.6±1.2% of BLBP and 13.2±2.9% of ACSBG1 positive cells in P3 WT CPu (Figure 34E). Strikingly, the BLBP positive AGPs as well as ACSBG1 enriched protoplasmic astrocytes of dcKO CPu exhibited prominent staining for Ki67 as well. Quantitatively, 39.6±5.3% of BLBP positive AGPs and 59.0±4.6% of ACSBG1 enriched protoplasmic astrocytes stained for Ki67 in dcKO. These were significantly higher fractions than in WT (*$p \leq 0.05$ and ***$p \leq 0.001$ for BLBP and ACSBG1 respectively; Figure34E).

We next investigated the proliferation of ACSBG1 positive protoplasmic astrocytes by another method - EdU labeling. For this purpose EdU was IP injected into WT/dcKO P3 pups 30 min before brain collection (Figure 34A). In order to quantify ACSBG1 expressing protoplasmic astrocytes that incorporated EdU, coronal brain slices from injected mice were subjected to immunostaining of ACSBG1 and EdU (Figure 34D). Overall, large amounts of cells that incorporated EdU were found in CPu of WT as well as dcKO (Figure 34D full and empty arrowheads). However, in dcKO EdU mostly labelled ACSBG1 expressing cells whereas in WT EdU positive cells were commonly of other types. Moreover, the fraction of ACSBG1 expressing cells exhibiting EdU labelling was significantly higher in dcKO than in WT (**$p \leq 0.01$; in WT 6.5±1.5%; in dcKO 23.3±4.6% of all ACSBG1 stained for EdU). However, the numbers of mice in these experiments were quite low, and further repetitions should

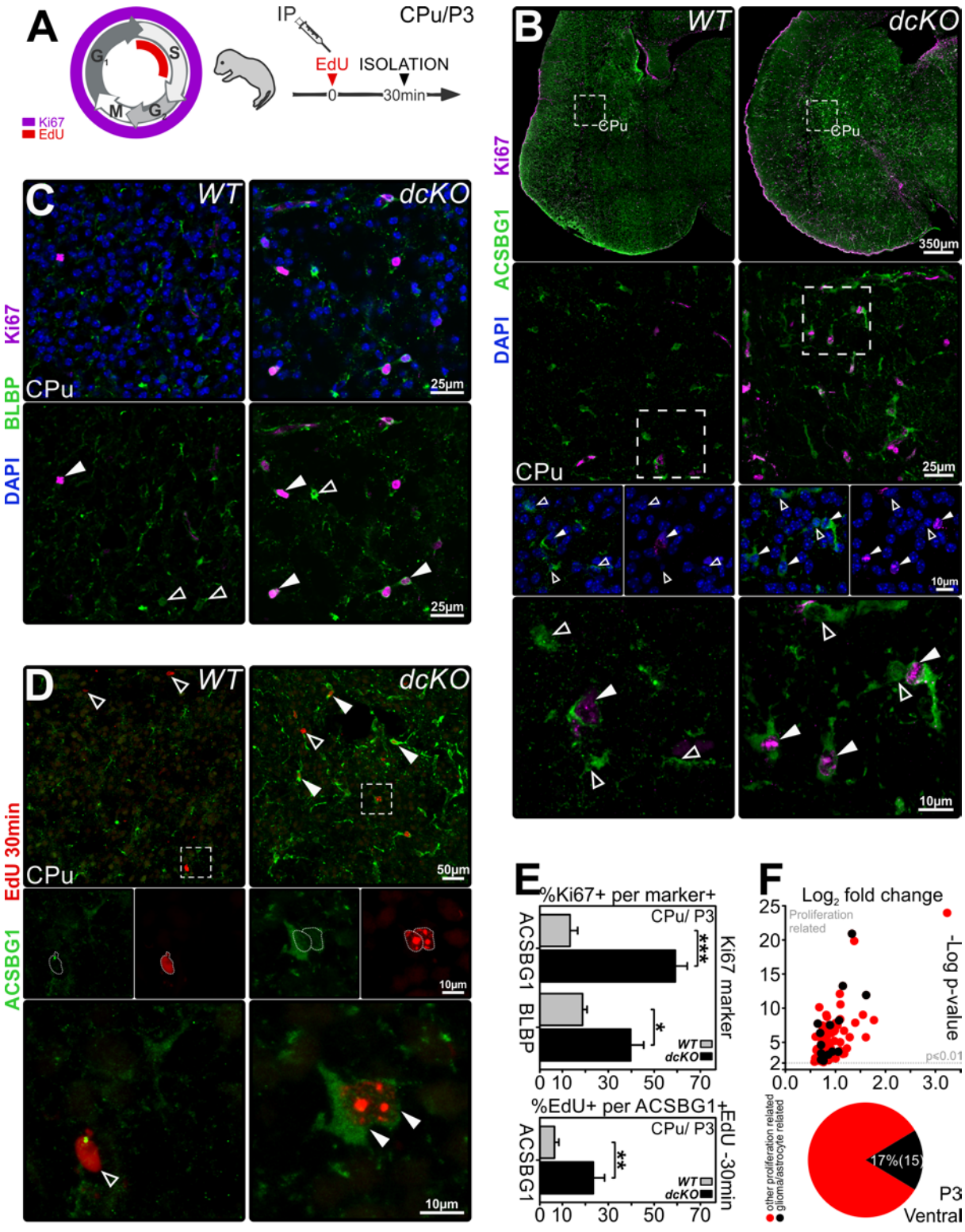
A
IP
CPu/P3
EdU
ISOLATION
0
30min
Ki67
EdU
B
WT
dcKO
Ki67
ACSBG1
DAPI
CPu
350µm
25µm
10µm
C
WT
dcKO
Ki67
BLBP
DAPI
CPu
25µm
D
WT
dcKO
EdU 30min
ACSBG1
CPu
50µm
10µm
E
%Ki67+ per marker+
CPu/ P3
ACSBG1
BLBP
Ki67 marker
WT
dcKO
***
*
0 10 30 50 70
%EdU+ per ACSBG1+
CPu/ P3
ACSBG1
EdU -30min
**
F
Log2 fold change
Proliferation related
-Log p-value
p≤0.01
other proliferation related
glioma/astrocyte related
17%(15)
P3
Ventral
G
Astrocyte/Glioma proliferation related
Log2 fold change
Ventral/ P3
dcKO
UPREGULATED
S100a6
Ccnd1
Hmgn5
Rac2
Fas
Btk
Gli1
Hpse
Ifitm1
Atf3
Syk
Hdac1
Fezf1
Cdc7
Spry1

Figure 34 | High proliferation capacities of BAF complex depleted ventral astrocytes. (A) Scheme explaining the principle of proliferation analysis by Ki67 expression investigation and thymidine analogue (EdU) injection. Ki67 (magenta) is expressed during all active phases of the cell cycle whereas IP injected EdU (red) incorporates to DNA during the S phase allowing for proliferative cells labelling. (B-C) Coronal tissue sections through WT and dcKO P3 mouse CPu stained with antibodies detecting astroglial markers; (B) ACSBG1 (in green) and (C) BLBP (in green) together with proliferation marker Ki67 (in magenta). The nuclear DAPI staining is blue. Cells expressing ACSBG1 or BLBP together with Ki67 are proliferative astrocytes. For (B) lower boards of each are magnified insets of delineated areas. For (C) lower panels of each are double channel images. Full arrowheads indicate proliferative astrocytes, empty arrowheads indicate non-proliferative astrocytes. (D) Immunofluorescence analysis of mouse P3 CPu WT and dcKO sections detecting ACSBG1 positive astrocytes (in green) and EdU (in red) that incorporated into DNA of cells after 30 minutes pulse IP injection. Cells expressing ACSBG1 positively stained for EdU are proliferative astrocytes. Lower boards of each are magnified insets of delineated areas. Cell bodies of EdU positive outlined with dashed line. Full arrowheads indicate EdU positive cells expressing ACSBG1, empty arrowheads indicate EdU positive/ACSBG1 negative cells. (E) Percentages of proliferative astrocytes in the areas of P3 WT and dcKO murine CPu. Upper graph illustrates percentages of ACSBG1 positive astrocytes and BLBP positive astrocytes expressing Ki67. Lower graph indicates the percentage of ACSBG1 expressing astrocytes positive for EdU after 30 minutes from injection. Data are averages ± σ of (A) n=4 experimental replicates; ***p≤0.001, *p≤0.05 in t- student test; (B) n=3 experimental replicates; **p≤0.01 in Mann-Whitney Rank Sum test. (F) Expression profile of significantly upregulated glioma/astrocyte proliferation related transcripts (in black) juxtaposed with all cell proliferation related transcripts (in red) upregulated in ventral pallium of P3 *hGFAP*-Cre dcKO versus WT mice. Scatter plot represents Log_2 fold change of transcript abundance together with –Log of corresponding p value for all significantly upregulated proliferation related transcripts. Pie chart shows the percentage of glioma/astrocyte proliferation related transcripts among all significantly upregulated proliferation associated transcripts. The exact transcript number shown in brackets. Black colour refers to the glioma/astrocyte proliferation related transcripts, red colour refers to other upregulated proliferation related transcripts. The Log_2 fold change level of upregulation as well as names of glioma/astrocyte proliferation related transcripts represented as black dots in scatter plot are shown in G. Transcriptome data are averages of n=4 animals. For all investigated transcripts p≤0.01. In GO pathway enrichment analysis, used for proliferation related transcripts detection, Bonferroni-corrected for p<0.05. CPu, caudate putamen; dcKO, double knockout; IP, intraperitoneal injection; WT, wild type.

be performed in the future. Still, taken together our Ki67 immunostaining and EdU incorporation experiments highlight the elevated proliferative capacities of BAF complex depleted, BLBP positive AGPs as well as ACSBG1 expressing protoplasmic astrocytes found in CPu of postnatal mice.

To confirm this finding we searched for transcriptome differences between genotypes that would indicate elevated proliferation in BAF complex depleted VP. Thus, we subjected all genes found to be aberrantly overexpressed in RNA-seq experiments of VP of P3 dcKO mice (see Chapter 3. Results. 3.4) to GO enrichment analysis. As this procedure highlighted several overexpressed genes from the group of proliferation regulators (regulation of cell proliferation - GO: 0042127; -Log –p value=3.1), we decided to investigate their involvement in astrocyte or glioma proliferation (Figure 34F and G, Table 3). Thus, as previously, we screened the literature for information on the precise function of 92 proliferation related transcripts that were upregulated in dcKO VP. We found that 15 of these (17%, Figure 34F) were related to the proliferation of astrocyte and/or glioma. The detailed results indicating significant upregulation of these transcripts are shown in scatter plot (Figure 34F).

NAME	LOG_2 FOLD CHANGE	P VALUE	ASTROCYTES/GLIOMA PROLIF. RELATED	REFERENCES
S100a6	1.61	1.27E-12	astrocytes and glioma	(Yamada and Jinno, 2012, 2014)
Ccnd1	1.33	1.26E-21	glioma	(Cao et al., 2017)
Hmgn5	1.15	5.88E-14	glioma	(Cao et al., 2017)
Rac2	1.07	6.66E-09	glioma	(Lai et al., 2017)
Fas	1.06	0.000251	glioma	(Barca et al., 2013; Bechmann et al., 2000; Runic et al., 1996)
Btk	0.94	0.000246	glioma	(Yue et al., 2017)
Gli1	0.89	3.15E-08	astrocytes and glioma	(Clement et al., 2007; Garcia et al., 2010; Pitter et al., 2014)
Hpse	0.85	0.000692	glioma	(Kundu et al., 2016)
Ifitm1	0.76	0.005193	astrocytes and glioma	(Arakelyan et al., 2014; Seyfried et al., 2008; Yu et al., 2011)
Atf3	0.75	0.003528	glioma	(Ma et al., 2015)
Syk	0.71	0.000436	glioma	(Moncayo et al., 2018)
Hdac1	0.71	2.55E-05	glioma	(Li et al., 2018b)
Fezf1	0.71	0.003581	glioma	(Yu et al., 2018)
Cdc7	0.70	4.52E-07	glioma	(Erbayraktar et al., 2016; Li et al., 2018a)
Spry1	0.65	1.93E-08	glioma	(Park et al., 2018; Walsh et al., 2015)

Table 3 | Astrocyte/glioma related transcripts upregulated in VP of P3 dcKO mice. The table describes 15 transcripts related to astrocyte/glioma proliferation significantly upregulated in VP of P3 dcKO stating the level of upregulation (log_2 fold change), significance (p value), involvement in astrocyte and/or glioma proliferation (astrocytes/glioma prolif. related) and corresponding literature source (references). Transcripts in red were also found to be upregulated in DP of P3 dcKO. Prolif., proliferation.

Additionally, the names and the Log_2 fold changes of all 15 genes related to astrocyte and/or glioma proliferation whose expression was upregulated are shown in Figure 34G and Table 3. As indicated in Table 3, only 3 of 15 selected genes were known to regulate astrocyte proliferation. These were: Gli1 (Garcia et al., 2010; Pitter et al., 2014), S100a6 (Yamada and Jinno, 2012, 2014) and Ifitm1 (Arakelyan et al., 2014). However, as mentioned previously, our transcriptome analysis was hindered by the scarcity of literature about the molecular control of astrocyte proliferation. In this context, even few upregulated transcripts may be considered as already sufficient proof supporting our immunostaining data. Additionally, several transcripts were also upregulated in DP of P3 dcKO brain

(Table 2, Table 3 - marked in red). This suggests that similar proliferative processes are at work in both areas of postnatal dcKO brain.

Taken together, these results indicate that BAF complex depleted AGPs and protoplasmic astrocytes found in postnatal VP as well as DP are highly proliferative. Additionally, proliferation evoked by *hGFAP*-Cre driven BAF loss were accompanied by upregulation of several glioma related proliferation regulators. Overall, taking into account the recent state of knowledge, we are one few scientific groups that could show a possible way of astrocyte proliferation regulation during early postnatal brain development.

The case of fibrous astrocytes and reactive astrogliosis

Our GO classification revealed that several inflammation related transcripts were upregulated in DP and VP of P3 dcKO animals (Figure 35A). Inflammation as well as neuronal degeneration triggers reactive astrogliosis (Anderson et al., 2014). Upon activation, reactive astrocytes become hypertrophic and highly proliferative (Robel et al., 2011; Sofroniew, 2015). Bearing this in mind, we asked whether the proliferative astroglial phenotype observed in DP and VP of postnatal dcKO mice is due to the activation of astrocytes rather than a loss of BAF complex. Importantly, the fibrous astrocytes marker, GFAP is considered as one of a hallmarks of reactive astrocytes (RAs) (Liddelow and Barres, 2017; Robel et al., 2011). Thus, as a next step we sought to assess the expression of GFAP in coronal brain slices isolated from P3 WT and dcKO mice by immunohistochemistry. As shown in Figure 35B, several regions of WT brain prominently expressed GFAP. By contrast, GFAP expression seemed to be reduced in P3 dcKO mice. In order to further assess the reactive astrogliosis of the abundant protoplasmic astrocytes of dcKO brains we performed co-immunostaining of GFAP and ACSBG1 in the developing S1 area of P3 WT and dcKO mice (ACSBG1 positive astrocytes were already reported to be upregulated in dcKO; see Chapter 3. Results. 3.3, Figure 23). The results of this staining are shown in Figure 35C. None of the ACSBG1 positive cells found in WT or dcKO CP of S1BF expressed GFAP (pointed by full arrowheads, empty arrowheads indicate another stained cells). Importantly, in order to confirm that our antibody against GFAP reliably stains RAs, we evoked reactive astrogliosis in S1BF area of adult mice (by stab injury, see Chapter 2. Materials and Methods. 2.1) and subsequently performed GFAP staining in stabbed brains. As indicated in Figure 35D and E, injured mice exhibited prominent GFAP staining at every investigated DPI. To the contrary and similarly to WT and dcKO P3 tissues, S1BF area (CP) of P60 control mouse (Figure 35D, extreme left images) rarely stained for GFAP.

Despite the morphological similarities between RAs and hypertrophic protoplasmic astrocytes of

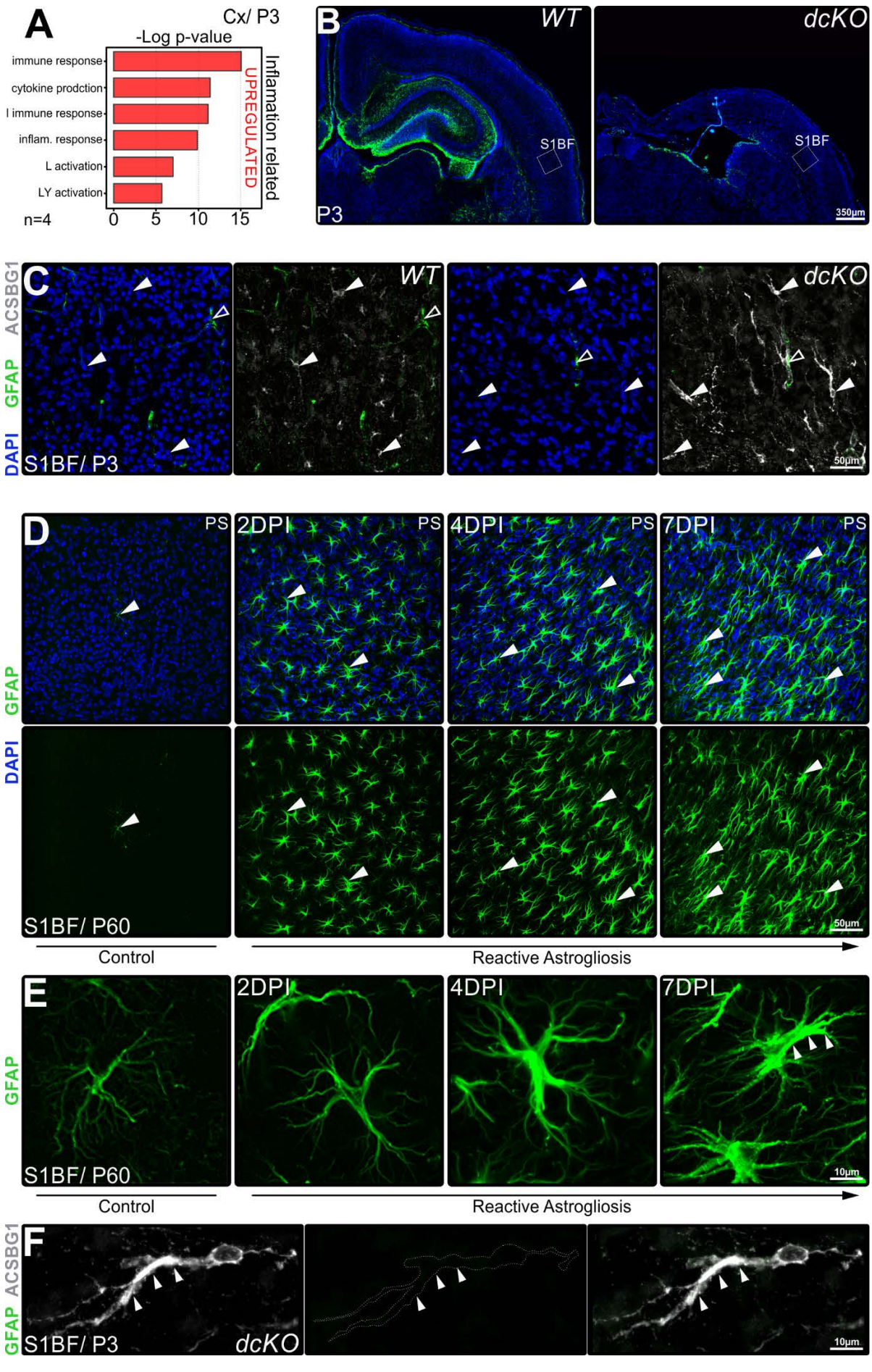
A
Cx/ P3
-Log p-value
immune response
cytokine prodction
I immune response
inflam. response
L activation
LY activation
n=4
0
5
10
15
UPREGULATED
Inflamation related
B
WT
dcKO
S1BF
S1BF
P3
350µm
C
ACSBG1
GFAP
DAPI
WT
dcKO
S1BF/ P3
50µm
D
PS
2DPI
PS
4DPI
PS
7DPI
PS
GFAP
DAPI
S1BF/ P60
50µm
Control
Reactive Astrogliosis
E
2DPI
4DPI
7DPI
GFAP
S1BF/ P60
10µm
Control
Reactive Astrogliosis
F
ACSBG1
GFAP
S1BF/ P3
dcKO
10µm

Figure 35 | Fibrous astrocytes and reactive astrogliosis in BAF complex depleted postnatal brain. (A) GO biological process enrichment analysis indicating groups of genes related to inflammation significantly upregulated in P3 Cx *hGFAP*-Cre dcKO. Bar graph represents –Log of corresponding p value for each indicated GO category. (A, B) Coronal tissue sections through WT and dcKO P3 mouse brain stained with antibodies detecting astroglial markers; (B) GFAP (in green) and (C) GFAP (in green) together with ACSBG1 (in pseudo colour gray) in the area of S1BF. The nuclear DAPI staining is blue. The pictures presented in C are magnified insets of areas delineated in B. Full arrowheads indicate cells positive for ACSBG1, empty arrowheads indicated other cells stained by GFAP antibody (D) Coronal tissue sections through healthy (control) and injured (at 2, 4 and 7 DPI) S1BF area of P60 WT mice stained with antibody to fibrous astrocytes – GFAP (in green). Nuclear DAPI staining is blue. Full arrowheads indicate examples of reactive astrocytes stained for GFAP. (E) Example morphologies of GFAP positive astrocytes found in healthy (control) and injured (at 2, 4 and 7 DPI) S1BF area of P60 WT mice. (F) Example morphology of ACSBG1 positive astrocyte found in S1BF area of P3 dcKO brain. Middle panel shows lack of GFAP expression in these astrocytes. Cell body delineated by dashed line. For E and F arrowheads indicate abnormally elongated process of astrocyte. Cx, cortex; dcKO, double knockout; DPI, days post injury; I, innate; inflam., inflammation; L, leucocyte; LY, lymphocyte; WT, wild type.

dcKO (Figure 35E and F) as well as the visibly increased inflammation processes, ACSBG1 expressing protoplasmic astrocytes of mutant mice did not express GFAP. We can thus conclude that astrocytes of dcKO mice were not proliferative because of their reactivity, but directly because of BAF complex depletion.

3.5 BAF dependent molecular trigger of astrocyte proliferation

One of the most important finding of this study is that BAF complex depleted AGPs and protoplasmic astrocytes exhibit elevated proliferative capacities, resulting in an increase in their numbers (see Chapter 3. Results. 3.3). In other words, the elimination of BAF complex de-represses certain factor(s) that trigger the proliferation of astroglia. Moreover, the upregulation of this (these) BAF-dependent factor(s) may be responsible for the generation of aberrant quantities of astrocytes, with implications for several neurological disorders (Alcantara Llaguno et al., 2009; Molofsky et al., 2012; Sofroniew and Vinters, 2010; Stiles and Rowitch, 2008). Thus, as a final step, we sought to find which molecular effector/pathway triggers abnormal astrocyte proliferation upon the BAF complex depletion.

Selection of the potential BAF dependent proliferation regulator

Previous studies from other groups have proposed that enhanced canonical WNT signaling, SHH/GLI signaling or NOTCH signaling may promote proliferation of astroglial cells (Alqudah et al., 2013; Araujo et al., 2014; Pierfelice et al., 2011; Pitter et al., 2014; Rush et al., 2010; Ugbode et al., 2017; Yang et al., 2012). The GO analysis performed on genes significantly overexpressed in DP of E17.5 dcKO mice (see Chapter 3. Results. 3.3) showed that all 3 signaling pathways were aberrantly

upregulated in BAF complex mutants at the onset of cortical astrogliogenesis (Figure 36A). As shown in Figure 36A and B, elements of WNT signaling pathway were most prominently overexpressed and constituted 25% of all proliferation related transcripts that were upregulated in DP of E17.5 dcKO mice. Among upregulated genes, 16 were involved in SHH/GLI signaling pathway, representing 20% of all overexpressed proliferation regulators (Figure 36B). Finally, only 5 elements of the NOTCH signaling pathway were upregulated in DP of E17.5 dcKO mice (6% of all proliferation related, Figure 36A and B). Having established that all these 3 pathways are upregulated in BAF complex depleted DP of E17.5 brains, we searched for the expression of their receptors/effectors that had previously been linked to astrocyte and glioma proliferation, namely β-catenin (CTNNB1; WNT signaling (Yang et al., 2012)), glioma associated oncogene 1 (GLI1; SHH/GLI1 signaling (Araujo et al., 2014; Clement et al., 2007; Garcia et al., 2010; Pitter et al., 2014)) and neurogenic locus notch homolog protein 3 (NOTCH3; NOTCH pathway (Alqudah et al., 2013; Pierfelice et al., 2011)). As indicated in Figure 36B, all 3 investigated effectors were present among the upregulated proliferation related transcripts. However, the level of upregulation of Gli1 was the highest and the most significant compared to the other 2 factors (relatively high Log_2 fold change of transcript abundance as well as –Log of p value, scatter plot, Figure 36B). In addition, the -Log of p values corresponding to the fold change of Ctnnb1 and Notch3 were rather low and close to the threshold of significance (**p≤0.01, indicated by dashed line). Nevertheless, we recognized these features insufficient for the selection of a final candidate that triggers abnormal astrocyte proliferation. Believing that the overexpression of the proliferation regulator must be initiated early but also must persist further in postnatal brain (as the high proliferative capacities of BAF depleted DP and VP astroglia have been confirmed for postnatal stages) we then expanded our analysis to the other upregulated proliferation related transcripts of DP and VP of P3 dcKO mice (see Chapter 3. Results. 3.3 and 3.4). To find proliferation regulators commonly upregulated in E17.5 and P3 dcKO brains, we compared the expression of all proliferation associated transcripts found to be significantly upregulated in at least 1 of all 3 locations of E17.5 and P3 brains: Dorsal E17.5, Dorsal P3 and Ventral P3 of dcKO brains. Thus, as indicated in Figure 36C, we generated a binomial colorimetric matrix illustrating the expression of proliferation related genes that were either significantly upregulated (in red) or unchanged (downregulated or exhibiting not significant changes, in blue) found in E17.5 DP, P3 DP and P3 VP of dcKO mice. It is worth stressing that each listed transcript was significantly upregulated at least in one of the analyzed locations. This analysis allowed us to select 15 proliferation related genes that were overexpressed in all 3 investigated locations (the top most transcripts of colorimetric matrix, red rectangle for all 3 investigated conditions). Importantly, Gli1 was present among these 15 transcripts (Figure 36C, bold names shown in red, Figure 36D). Notably, Ctnnb1 and Notch3, involved in WNT and NOTCH signaling pathways, were among the group of proliferation regulators overexpressed only in DP of

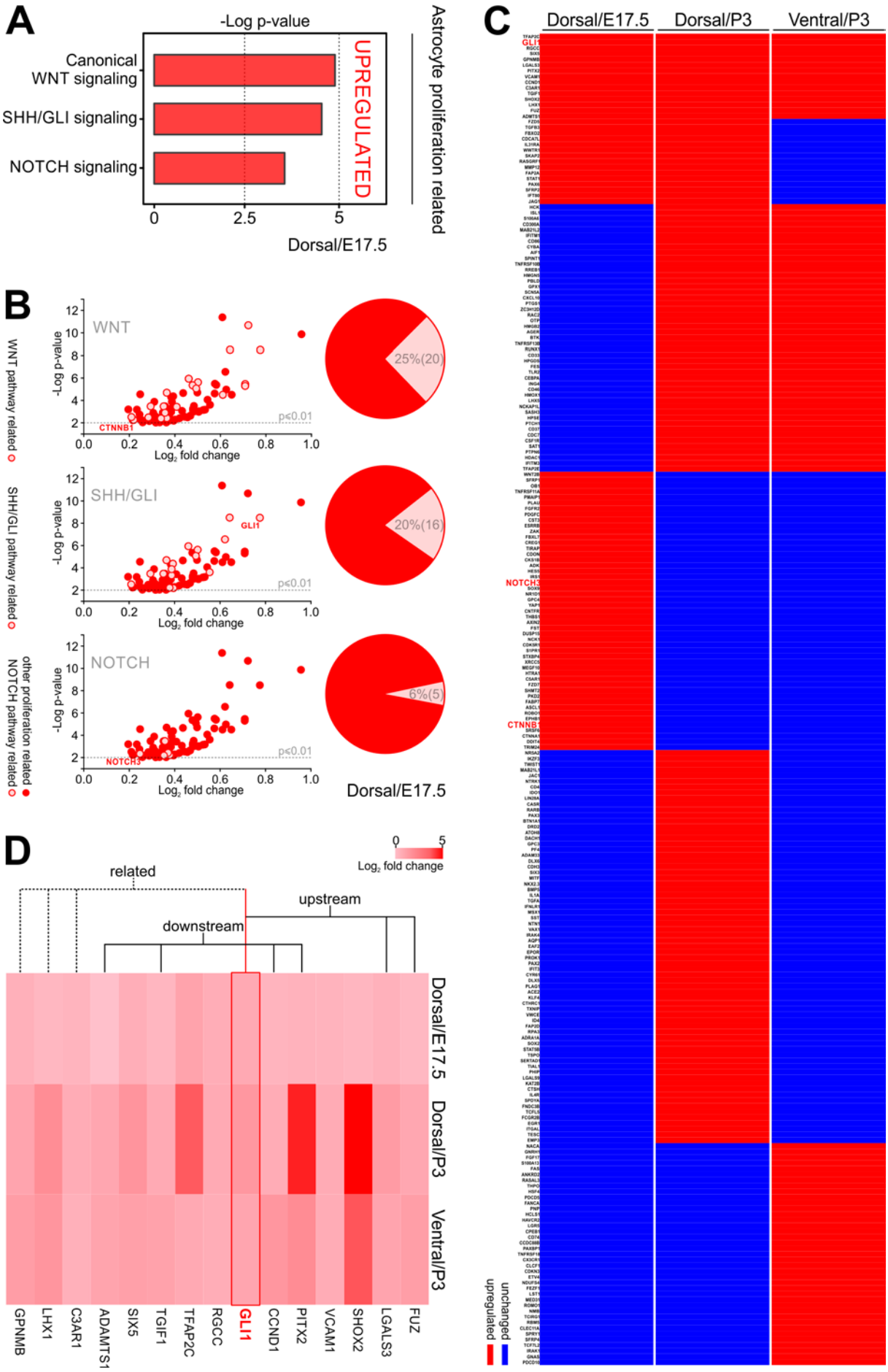
A
-Log p-value
Canonical WNT signaling
SHH/GLI signaling
NOTCH signaling
UPREGULATED
Astrocyte proliferation related
0
2.5
5
Dorsal/E17.5
B
WNT pathway related
SHH/GLI pathway related
other proliferation related
NOTCH pathway related
WNT
SHH/GLI
NOTCH
-Log p-value
Log2 fold change
p≤0.01
CTNNB1
GLI1
NOTCH3
25%(20)
20%(16)
6%(5)
Dorsal/E17.5
C
Dorsal/E17.5
Dorsal/P3
Ventral/P3
GLI1
NOTCH3
CTNNB1
upregulated
unchanged
D
related
upstream
downstream
0
5
Log2 fold change
Dorsal/E17.5
Dorsal/P3
Ventral/P3
GPNMB
LHX1
C3AR1
ADAMTS1
SIX5
TGIF1
TFAP2C
RGCC
GLI1
CCND1
PITX2
VCAM1
SHOX2
LGALS3
FUZ

Figure 36 | Astrocyte proliferation related gene expression profile of BAF complex depleted mouse brain. (A) Astrocyte proliferation inducing signaling pathways significantly upregulated in DP of E17.5 *hGFAP*-Cre dcKO versus WT transcriptome. (B) Expression profile of significantly upregulated WNT (upper panel), SHH/GLI (middle panel) and NOTCH (lower panel) pathway related transcripts associated with proliferation induction juxtaposed with all cell proliferation related transcripts upregulated in DP of E17.5 *hGFAP*-Cre dcKO versus WT mice. Scatter plots represent Log_2 fold change of transcript abundance together with –Log of corresponding p value for all significantly upregulated proliferation related transcripts. For each pathway, the regulator of astrocyte/glioma proliferation (CTNNB1, GLI1, NOTCH3) is highlighted in red. Pie charts show the percentages of the corresponding pathway related transcripts among all significantly upregulated proliferation associated transcripts. The exact transcripts numbers shown in brackets. Light red colour refers to the corresponding pathway related transcripts, dark red colour refers to other upregulated proliferation related transcripts. (C) Binomial expression profile analysis of all proliferation associated transcripts significantly upregulated at least in 1 of all 3 investigated *hGFAP*-Cre dcKO vs WT transcriptomes; E17.5 DP, P3 DP and P3 VP. Red colour refers to significantly upregulated expression level, blue colour refers to unchanged (downregulated or non-significantly upregulated) expression level. For each pathway from A and B the key astrocyte proliferation regulator (CTNNB1, GLI1, NOTCH3) is highlighted in red. (D) Dynamic expression profile of 15 proliferation related genes significantly upregulated in all 3 investigated *hGFAP*-Cre dcKO vs WT conditions. Heat map shows Log_2 fold change of transcript abundance. Dendrogram depicts existing relation between astrocyte proliferation regulator – GLI1 and other upregulated proliferation related transcripts. Data are averages of n=3-4 animals (E17.5DP; *hGFAP*-Cre dcKO: n=3, WT: n=4; P3 DP and VP; *hGFAP*-Cre dcKO: n=4, WT: n=4). For all investigated transcripts $p \leq 0.01$. In GO pathway enrichment analysis Bonferroni-corrected for $p<0.05$.

E17.5 dcKO (Figure 36C, bold names shown in red). Thus we excluded these two candidates from further analysis.

As indicated in Figure 36D (representing Log2 fold change of given transcript abundance), the selected transcripts exhibited a dynamic expression pattern with their abundance visibly increasing with time (for majority, comparing Dorsal E17.5 to Dorsal P3). Interestingly, the literature screening and online gene set enrichment analysis (Liberzon et al., 2015; Liberzon et al., 2011; Subramanian et al., 2005) about the pathway affiliation of these genes revealed that some of them may act upstream, downstream or be related to SHH/GLI1 signaling (Figure 36D). Accordingly, Fuz (Szabo-Rogers et al., 2010; Zhang et al., 2011) and Lgals3 (Kang et al., 2016) could act as upstream genes. Pitx2 (Satheesha et al., 2016; Subramanian et al., 2005), Ccnd1 (Kasiri et al., 2017; Mathew et al., 2014; Wang et al., 2016b), Tgif (Subramanian et al., 2005) and Adamts1 (Oliver et al., 2003; Subramanian et al., 2005) were indicated as possible downstream factors. And yet others were shown to be related to SHH/GLI1 signaling (C3ar1 (Pun et al., 2011), Lhx1 (Zhao et al., 2007) and Gpnmb (Zahreddine et al., 2014)) (Figure 36D).

In summary, we found that the proliferation regulator Gli1 was overexpressed in dorsal and ventral brain regions of perinatal and postnatal dcKO brains. The upregulation of Gli1 was accompanied by aberrant overexpression of other proliferation regulators related to the SHH/GLI signaling pathway. Thus, we decided to select GLI1 as a candidate trigger of astrocyte proliferation in dcKO mice.

De-repressed GLI1 as a candidate trigger of astrocyte proliferation in dcKO mice

Seeking further support for our choice, we evaluated the upregulation of Gli1 transcript by *in situ* hybridization. Using digoxigenin (DIG)-labelled probes, we detected Gli1 mRNA in brain tissues of E17.5 WT and dcKO mice. As shown in Figure 37A and C, the staining of WT cortex revealed low levels of Gli1 mRNA confined mostly to the VZ, with isolated cells found outside in CP (depicted by distribution plots). The VZ of WT VP also exhibited faint Gli1 mRNA staining (Figure 37A and B). To the contrary, the BAF complex deficient DP and VP showed prominent Gli1 mRNA labelling (Figure37 A-C). Additionally, as presented in distribution density plots, unlike in control, the Gli1 mRNA staining of dcKO DP exhibited scattered distribution reminiscent of that observed for GLAST or BLBP positive AGPs in dcKO cortex (see Chapter 3. Results. 3.3, Figure 16). Furthermore, quantitative studies performed for Gli1 mRNA stained tissues of E17.5 and P3 WT and dcKO animals (results of P3 *in situ* hybridization shown in Appendix, Figure 48) indicated a massive upregulation of the Gli1 transcript in dcKO mice of both developmental stages (Figure 37D-F).

Accordingly, the densities of Gli1 mRNA stained cells found in dcKO brains significantly exceeded these of WT (***p≤0.001, **p≤0.01), which held true in cortex (Figure 37F), VP (Figure 37E) as well as in the brain section as a whole (Figure 37D). Thus, our *in situ* hybridization confirms the upregulation of Gli1 mRNA in BAF complex depleted DP and VP.

Next, we asked whether the upregulation of Gli1 leads to the overexpression of its target genes. Therefore, using an online tools for TF binding site profiling (Lachmann et al., 2010; Liberzon et al., 2015; Liberzon et al., 2011; Subramanian et al., 2005; Yun et al., 2017) we found a list of all potential GLI1 target genes and inquired how many of these were upregulated in DP of E17.5 as well as DP and VP of P3 dcKO mice. The outcome of this analysis is shown in Figure 37I. We identified several GLI1 target genes whose overexpression level increased over developmental time (from Dorsal/E17.5 to Dorsal/P3). Importantly, VP and DP of P3 dcKO mice exhibited similar sets of upregulated GLI1 targets. This might indicate similarities in the molecular regulation of dorsal and ventral proliferative astroglial phenotype.

Having established that GLI1 and its targets are potently upregulated in BAF complex depleted perinatal and postnatal brains we asked whether the observed overexpression of Gli1 is directly evoked by BAF complex elimination. Previous studies showed that a BAF complex subunit, BRG1, binds to the regulatory regions of Gli1, directly repressing its transcription (Figure 37G) (Zhan et al., 2011). This may be taken as evidence that the observed upregulated Gli1 levels are due to the loss of BRG1 evoked by elimination of the entire BAF complex (see Chapter 3. Results. 3.2). However, it is well known that the expression of Gli1 can be triggered by the externally secreted morphogen SHH (Dahmane et al., 2001; Palma et al., 2005). Importantly, it has been shown that externally released SHH protein can trigger proliferation of astrocytes upon neurodegeneration (Ugbode et al., 2017). In

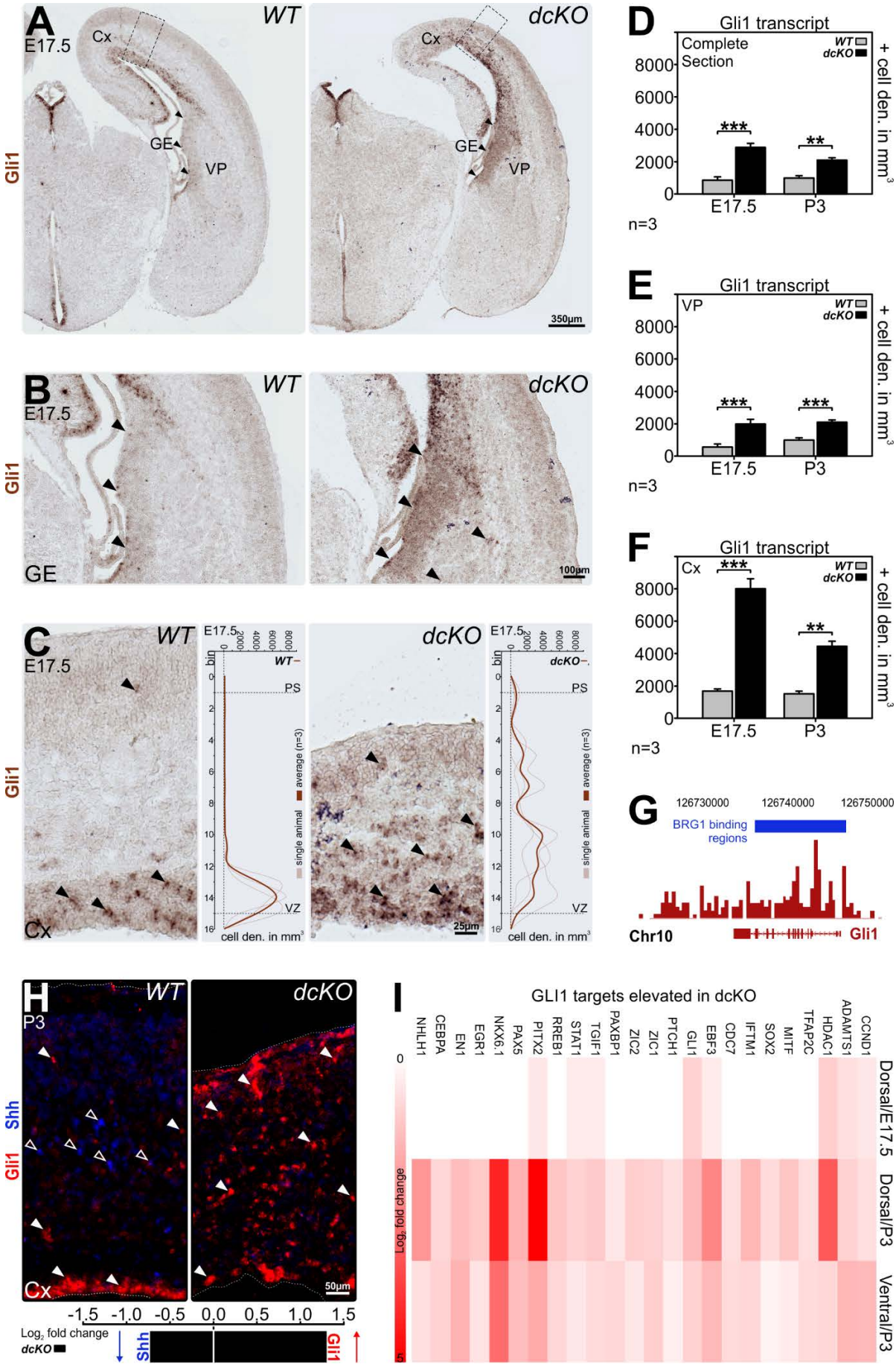
A
E17.5
WT
dcKO
Cx
GE
VP
Gli1
350µm
B
E17.5
WT
dcKO
GE
Gli1
100µm
C
E17.5
WT
dcKO
Cx
Gli1
PS
VZ
single animal
average (n=3)
cell den. in mm3
25µm
D
Gli1 transcript
Complete Section
WT
dcKO
+ cell den. in mm3
8000
6000
4000
2000
0
***
**
E17.5
P3
n=3
E
Gli1 transcript
VP
WT
dcKO
+ cell den. in mm3
***
***
E17.5
P3
n=3
F
Gli1 transcript
Cx
WT
dcKO
+ cell den. in mm3
***
**
E17.5
P3
n=3
G
126730000
126740000
126750000
BRG1 binding regions
Chr10
Gli1
H
P3
WT
dcKO
Shh
Gli1
Cx
50µm
-1.5 -1.0 -0.5 0.0 0.5 1.0 1.5
Log2 fold change
dcKO
Shh
Gli1
GLI1 targets elevated in dcKO
NHLH1
CEBPA
EN1
EGR1
NKX6.1
PAX5
PITX2
RREB1
STAT1
TGIF1
PAXBP1
ZIC2
ZIC1
PTCH1
GLI1
EBF3
CDC7
IFTM1
SOX2
MITF
TFAP2C
HDAC1
ADAMTS1
CCND1
Log2 fold change
0
5
Dorsal/E17.5
Dorsal/P3
Ventral/P3

Figure 37 | De-repression of Gli1 in embryonic and postnatal dcKO brains caused by elimination of BAF complex. (A, C) *In situ* hybridization of coronal brain sections through WT and dcKO E17.5 murine Cx (developing M1 area) stained Gli1 mRNA. (A) Overview pictures of WT and dcKO stained brain sections (B-C) Magnified insets of (B) ventral germinal zones of ganglionic eminence and (C) developing M1 area - delineated in (A). Full arrowheads indicate Gli1 mRNA positive cells. For (C) line graphs represented in the extreme right boards of each (WT and dcKO) are distribution density plots generated for Gli1 mRNA in whole cortical column (divided for 16 the same size bins). Average plots for n=3 animals shown as thick brown colour lines, plots for individual animals shown as thin beige colour lines). Each graph represents bin no. (0-16) juxtaposed with corresponding cell density found in cubic mm. PS area corresponds with bin no. 1, VZ area corresponds with bin no. 15 (both marked with dashed lines). Distribution of Gli1 mRNA expressing cells in the WT cortex shows clear peak in VZ area, whereas Gli1 mRNA positive cells in dcKO exhibited distribution scattered across the cortical column. (D-F) Densities of cells expressing Gli1 mRNA found in cubic mm of (D) complete brain slice, (E) VP and (F) cortex. Data are averages ± σ of n=3 experimental replicates; ***p≤0.001, **p≤0.01 in t student test. (G) BRG1 binding sites around the region of mouse Gli1 gene. Reproduced from Zhan et al., 2011. (H) *In situ* hybridization of coronal brain sections through WT and dcKO P3 murine Cx (developing M1 area) stained Gli1 mRNA (in red) and Shh mRNA (in blue). Pictures are pseudo-colored mergers of consecutive sections. Full arrowheads indicate cells expressing Gli1 mRNA, empty arrowheads indicate cells expressing Shh mRNA. Contours of brain tissues delineated with dashed lines. Bottom bar graph indicates Log_2 fold change level of downregulation of Shh and upregulation of Gli1 revealed by RNA-seq of DP transcriptome of P3 WT and dcKO mice (I) Dynamic expression profile of potential/confirmed GLI1 target genes unchanged (in white) or significantly upregulated in 3 investigated *hGFAP*-Cre dcKO vs WT conditions. Heat map shows Log_2 fold change of transcript abundance. Chr., chromosome; Cx, cortex; dcKO, double knockout; den., density; GE, ganglionic eminence; PS, pial surface; VZ, ventricular zone; WT, wild type.

order to exclude the possibility that the upregulated Gli1 levels found in dcKO brains are due to the external action of SHH we opted for *in situ* hybridization for Gli1 and Shh. We performed this analysis on cortical sections of P3 WT and dcKO brains. As shown in Figure 37H and in agreement with the literature, layer IV and layer V of WT cortex exhibited Shh mRNA staining (empty arrowheads, in blue) (Courchet and Polleux, 2012). At the same time, Gli1 mRNA was mostly present in DW with some positive cells scattered across the cortical thickness (full arrowheads, in red). To the contrary, the cortex of dcKO mice did not display any staining for Shh mRNA despite the prominent Gli1 labelling. These results were supported by RNA-seq data, which indicated a significant downregulation of Shh transcript DP of P3 dcKO mice. Thus Gli1 overexpression is not due to the SHH but rather to the elimination of the BAF complex.

In summary, our data confirmed that the elimination of BAF complexes causes de-repression of Gli1.

Restoration of WT-like phenotype by direct inhibition of GLI1 in dcKO mutants

In order to determine whether de-repressed GLI1 promotes astrocyte proliferation in dcKO mice we opted for a rescue experiment. We blocked GLI1 mediated transcription by administering an inhibitor (Figure 38). Starting from E15.5, pregnant mice were given daily IP injections of the GLI1 antagonist - GANT61 (Lauth et al., 2007). Injections were carried out for 4 consecutive days and the

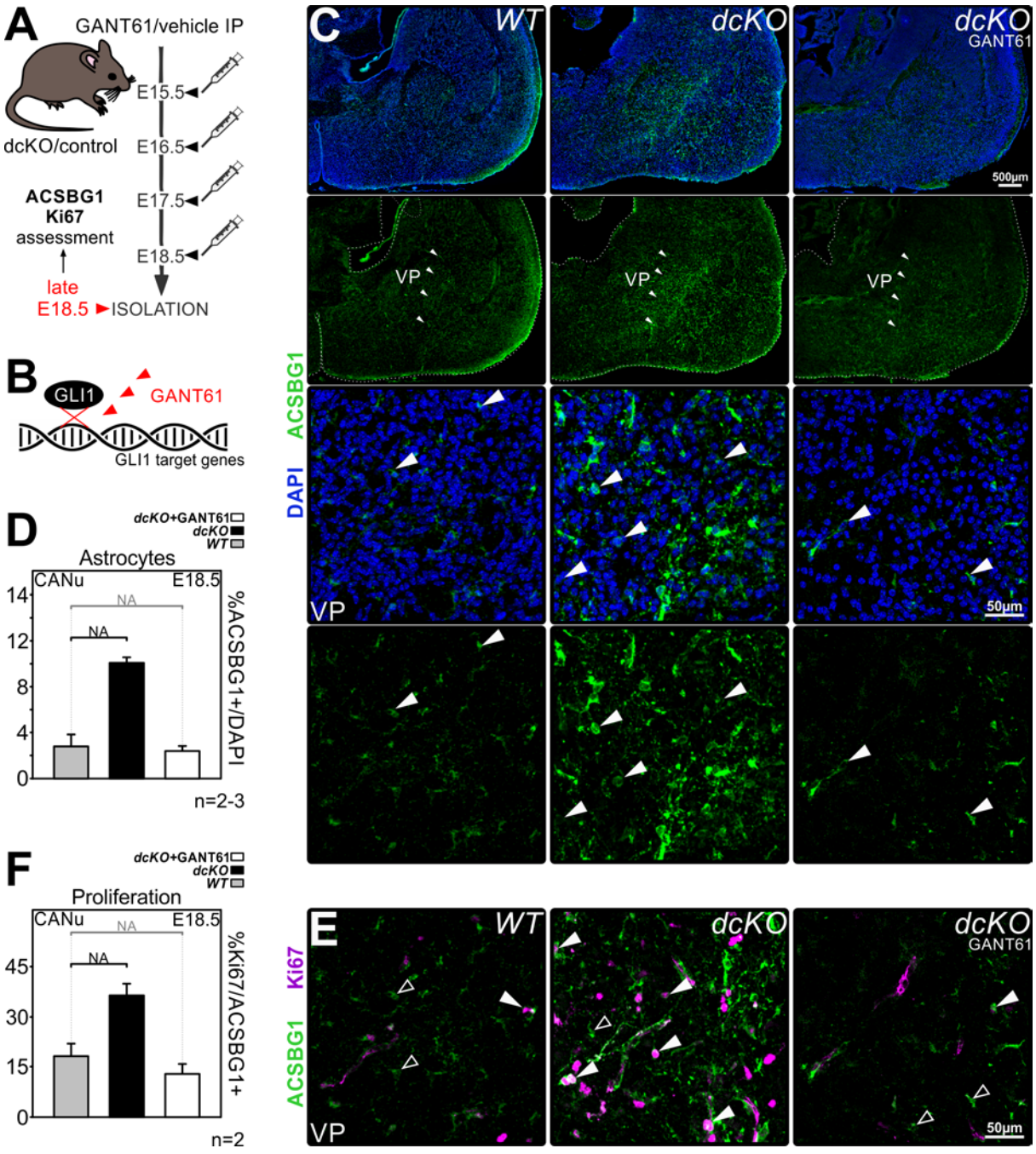

Figure 38 | Direct inhibition of GLI1 rescues proliferative astrocytic phenotype of BAF complex depleted VP. (A) Scheme explaining the experimental plan for GLI1 antagonist – GANT61 injection. Starting from E15.5, pregnant mice were administered a daily dosage of GANT61. The injections were carried for 4 consecutive days and the brain tissues were isolated at late E18.5. Isolated tissues were subsequently subjected to immunohistochemical analysis of ACSBG1 and Ki67 expression. (B) Scheme illustrating the way of GANT61 action. GANT61 antagonizes GLI1 blocking transcription of GLI1 target genes. (C, F) Coronal tissue sections through WT, dcKO and inhibitor treated dcKO E18.5 mouse brains stained with antibodies detecting: (C) ACSBG1 expressing protoplasmic astrocytes (in green) as well as (E) ACSBG1 expressing protoplasmic astrocytes (in green) together with proliferation marker Ki67 (in magenta). The nuclear DAPI staining is blue. Cells expressing ACSBG1 and Ki67 are proliferative astrocytes. For (C) top panels are overview pictures. Arrowheads point the area of VP with strongest ACSBG1 staining found in untreated dcKO animals. For magnified insets full arrowheads indicate ACSBG1 expressing astrocytes. For (E) full arrowheads indicate proliferative astrocytes, empty arrowheads point to astrocytes that were not

proliferative. (D, F) Percentages of: (D) DAPI cells expressing ACSBG1 and (E) proliferative astrocytes quantified in the areas of CANu of late E18.5 WT, dcKO and inhibitor injected dcKO mice. Data are averages ± σ of n=2 experimental replicates; NA, not applicable (n=2). CANu, central amygdala nucleus; dcKO, double knockout; NA, not applicable; WT, wild type.

brain tissues were isolated at late E18.5 (Figure 38A and B). Subsequently, we assessed the astroglial phenotype within treated and untreated dcKO and WT brain sections. First, by means of immunostaining, we investigated ACSBG1 positive protoplasmic astrocytes. As shown in Figure 38C, the VP of untreated dcKO mice exhibited prominent staining for ACSBG1 (middle panel images). Strikingly the VP phenotype of dcKO mice treated by GANT61 reverted to WT-like pattern (Figure 38C, extreme left and right panels). Accordingly, the ACSBG1 expressing protoplasmic astrocytes of injected dcKO mice were scattered throughout the brain tissue as single individuals and unlike these of untreated dcKO, did not tend to group into clusters of hypertrophic cells. Additionally, the amount of ACSBG1 positive cells found in VP of GANT61 treated animals was similar to that of WT and visibly lower than in untreated dcKO (Figure 38D).

Next, we sought to investigate the proliferation of the above described astrocytes. Using staining we analyzed the expression of the proliferation marker Ki67 in ACSBG1 positive protoplasmic astrocytes found in VP of treated and untreated dcKO as well as WT mice (Figure 38E). As expected, we found a prominent staining for Ki67 within numerous ACSBG1 positive astrocytes of untreated dcKO mice (pointed by full arrowheads). To the contrary and similarly to the WT condition, only few ACSBG1 expressing cells found in VP of GANT61 treated dcKO mice stained for Ki67. Moreover, the amount of ACSBG1 positive cells expressing Ki67 found in VP of treated dcKO mice was similar to that of WT and definitely lower than the fraction of ACSBG1 expressing cells exhibiting Ki67 staining found in VP of untreated dcKO mice (Figure 38F).

Taken together, these results indicate that direct inhibition of Gli1-dependent transcriptional activity rescues the abnormally proliferative astrocytic phenotype of BAF complex depleted VP. In other words, the elimination of BAF complex de-represses GLI1 that triggers proliferation within mutation affected astroglia. This confirms that BAF complexes control the proliferation of astrocytes by repressing GLI1 activity.

Chapter 4

Discussion

In the present study, we investigated the role of BAF complex in the development of neuronal and astroglial lineages. We found that the composition of the BAF complex depends on the cellular lineage as well as the developmental stage. Furthermore, the analysis of our *hGFAP*-Cre driven dcKO of BAF155 and BAF170 revealed that the loss of BAF complex results in a tremendous depletion of neurons and an abundance of massively overproliferative astroglia. Finally, we demonstrated that the overproliferation of astroglia was mediated by the mitogen GLI1, which was de-repressed in cells lacking BAF complex. In this chapter, we will discuss the interpretation and significance of these findings.

4.1 Dynamic expression pattern of BAF complex subunits during astrogliogenesis: lessons from brain development

BAF chromatin remodeling complexes utilize energy from the hydrolysis of ATP to orchestrate changes in the structure of chromatin (Cairns, 2007; Hargreaves and Crabtree, 2011; Sokpor et al., 2017). This chromatin altering activity endows BAF complexes with the capacity to execute transcriptional activation and/or repression (Sokpor et al., 2017; Wu, 2012). Functional competence of different BAF complexes has been attributed to their specific subunit composition (Ho and Crabtree, 2010). Precisely, the particular subunit assemblies of BAF complex determine which genomic areas it can target and its interaction with specific factors (Ho and Crabtree, 2010; Wu, 2012). Therefore, reshuffling the subunits of BAF complexes during development initiates unique transcriptional programs that regulate developmental events such as cellular proliferation or differentiation (Bachmann et al., 2016; Ho et al., 2009; Kadoch and Crabtree, 2015; Lessard et al., 2007; Mashtalir et al., 2018; Yoo et al., 2009). These processes are naturally involved in astrogliogenesis, from the initial astrocytic RGCs self-renewal, subsequent specification to AGPs,

transient amplification and final maturation to astrocytes (Kriegstein and Alvarez-Buylla, 2009; Molofsky and Deneen, 2015).

In this study we shed light on the BAF complex assemblies within astroglial cells. For the first time we showed that BAF complex expression pattern correlates not only with cell type (namely neurons *versus* astroglia) but also with different levels of specification within the astrocytic lineage (namely astrocytic RGCs *versus* AGPs).

Technical considerations

Our findings about BAF complexes were based chiefly on immunohistochemical assessment of the expression of 5 chosen BAF subunits (namely: BRG1, BAF155, BAF170, BAF60a and BAF250a). Considering that cell-specific BAF complexes are multimeric assemblies of at least 15 different subunits (Lessard et al., 2007; Narayanan et al., 2015; Sokpor et al., 2017; Wu et al., 2007), such an approach may at first glance appear insufficient to infer anything about the entire complex assembly. However, early studies describing BAF complex purification posited that all subunits must be incorporated into the complex (Chen and Archer, 2005; Doan et al., 2004; Goldberg, 2003; Kadoch and Crabtree, 2015; Wang et al., 1996). This implies that the presence of single subunits testifies to the assembly of the entire BAF complex. Our choice of method was grounded in this reasoning. On the other hand, it has been shown that under certain circumstances BAF subunits can be found as unbound to the complex. Accordingly, in destabilized BAF complex, some subunits degrade faster than other, hinting at differences in the temporal expression of free BAF elements (Sohn et al., 2007). Unbound subunits could also be found as maturating proteins adopting correct folding before their incorporation to the complex (Chen and Archer, 2005). Additionally, single subunits of BAF complexes were found in cells as monomeric fraction (Kadoch and Crabtree, 2015). It has been also proposed that the methylation of core subunits can destabilize entire BAF complex, suggesting the presence of solely methylated BAF elements (Panamarova et al., 2016). However, these findings were described only for 4 subunits out of 15 (BAF155, BAF57 as well as β-actin and BAF53a) (Chen and Archer, 2005; Kadoch and Crabtree, 2015; Sohn et al., 2007). Thus, on the whole, it does not seem unreasonable to extrapolate the state of the BAF complex from the co-expression of only 5 of its constituents.

Additionally, it is not without good reasons that we chose to investigate these particular 5 BAF subunits (BRG1, BAF155, BAF170, BAF60a and BAF250a). This choice was dictated by their functionality within the complex. Indeed, three of these subunits are elements of the core of BAF complex (one catalytic ATPase - BRG1, and two invariable scaffolding subunits: BAF155 and BAF170)

(Ho and Crabtree, 2010; Phelan et al., 1999). The remaining two are variant subunits: BAF60a and BAF250a. These were shown to be present within npBAF complex as well as neuronal - nBAF complex (Chen et al., 2012; Ho and Crabtree, 2010; Lei et al., 2015; Li et al., 2010; Meng et al., 2018; Oh et al., 2008). As the distinct variant subunits integrate into the core and scaffolding proteins (Mashtalir et al., 2018; Narayanan and Tuoc, 2014b; Ronan et al., 2013), this specific selection covered a broad range of subunit functions and therefore allowed us to infer the integrity of the complex.

In addition, it is obvious that coimmunoprecipitation under stringent conditions (Wang et al., 1996) followed by mass spectrometry measurements would provide more accurate evaluation of the complete complex assembly. However this experiment involves the purification of AGPs population which due to the lack of exclusive markers is not possible to this day (Schiweck et al., 2018). Thus, overall, our immunohistochemical approach seems reasonable given the current state of knowledge.

Dynamic expression of BAF subunits during astrogliogenesis

Our immunostaining studies have enabled us to reveal the spatio-temporal dynamics of BAF complex expression pattern within the astroglial lineage. We found that all tested BAF subunits were ubiquitously expressed in astrocytic RGCs of all astroglial germinal zones of developing forebrain. However, BAF170 alone stood as an exception to this rule. Indeed, a small fraction (~11-16%) of astrocytic RGCs in any area did not express this subunit. This loss of BAF170 may be a sign that the RGCs are transitioning towards a more advanced state of differentiation, that of AGPs. In support of this hypothesis, we observed that astrocytic RGCs that detach from the AS of VZ practically lose the expression of BAF170. It is well established that astrocytic RGCs delaminate as they differentiate towards AGPs (deAzevedo et al., 2003; Ge and Jia, 2016; Noctor et al., 2004; Voigt, 1989). It thus appears that changes within BAF170 expression and detachment from the VZ are two sides of the same coin. In fact, we suspect that the loss of BAF170 is causal to the detachment of astrocytic RGCs. Some support for this hypothesis comes from the observation that BAF170 depleted adult NSCs detach from the subgranular zone (SGZ) and mis-position to the outer layers of DG (Tuoc et al., 2017).

Once astrocytic RGCs have differentiated to AGPs, the composition of the BAF complex does not remain static but undergoes deep and characteristic changes. Our immunostaining studies have revealed that the expression of investigated subunits decreased within delaminated AGPs. A bold hypothesis hence leaped to our minds: the downregulation of BAF complex expression could be necessary for the initiation of some AGPs characteristics. One such characteristic is a high rate of

proliferation (Ge and Jia, 2016; Ge et al., 2012; Molofsky and Deneen, 2015). Several groups have described BAF complex as a proliferation limiting factor that inhibits mitogens e.g. GLI1 (Narayanan et al., 2015; Nguyen et al., 2018; Panamarova et al., 2016; Wu, 2012; Zhan et al., 2011). Thus one may speculate that the downregulation of BAF subunits abundance is causing or at least enabling AGPs proliferation.

Although compelling, this assumption was frustrated by the fact that unlike all other subunits, BAF155 expression levels remained high in AGPs. This does not suffice to disprove our hypothesis and can in fact be explained quite simply. Indeed, on the one hand it has been shown that the elimination of BAF170 increases the expression of BAF155 (Tuoc et al., 2013b). On the other hand, it is known that high levels of methylated BAF155 destabilize the BAF complex (Panamarova et al., 2016), possibly leading to downregulation of other subunits. It is therefore conceivable that the strong expression of BAF155 that we observed in AGPs corresponds to its less competent, methylated form, which has no bearing on our hypothesis. High levels of methylated BAF155 and low levels of BAF170 would exert a powerful destabilizing effect on the entire BAF complex (Narayanan et al., 2015; Panamarova et al., 2016; Poston et al., 2018), explaining the decrease in expression of other subunits that we have observed within AGPs. However, the experimental proof for this statement is parsimonious and further investigations (e.g. addressing methylation of BAF155) need to be performed in the future.

The final step of astrogliogenesis is differentiation of AGPs into postmitotic astrocytes (Kriegstein and Alvarez-Buylla, 2009; Tabata, 2015). Remarkably, our immunostaining confirmed the presence of 4 subunits absent from AGPs in adult astrocytes: BAF170, BRG1, BAF60a and BAF250a (Appendix, Figure 44). Alas we could not determine whether BAF155 was also present because we failed to successfully stain adult tissue; however, we presume that this was the case. It thus appears that the pattern of BAF subunit expression in adult astrocytes differs substantially from AGPs and recovers an astrocytic RGCs-like character. This result further supports the notion that BAF subunits expression levels may control the rate of astroglia proliferation. We hypothesize that downregulated levels of BAF complex enable AGPs (premature astroglia) proliferation while their elevation immobilizes the cell into a quiescent state.

Different expression levels of BAF subunits in cortical neurons and AGPs

In addition to the astroglial lineage we also investigated BAF subunit composition in cortical neurons and found marked differences with astrocytic RGCs and AGPs. Our immunohistochemical analysis revealed that BRG1, BAF170, BAF60a and BAF250a were highly expressed in neurons. BAF155 on the other hand was only present at low levels. In other words, the BAF subunit composition in neurons is

the mirror opposite of that in AGPs, where BAF155 was more strongly expressed than any other subunit. Thus, the BAF complex subunit composition is not only specific for a given stage of differentiation within a defined cellular lineage, but it is also cell type specific. From there, one can extrapolate that BAF complex influences cell fate specification in addition to its role in the regulation of proliferation.

Revealed pattern of BAF subunits expression - summary

In summary, our results indicate that the expression pattern of BAF subunits differs between various cells of astrocytic lineage as well as between neuronal and astroglial cell types (Figure 39A).

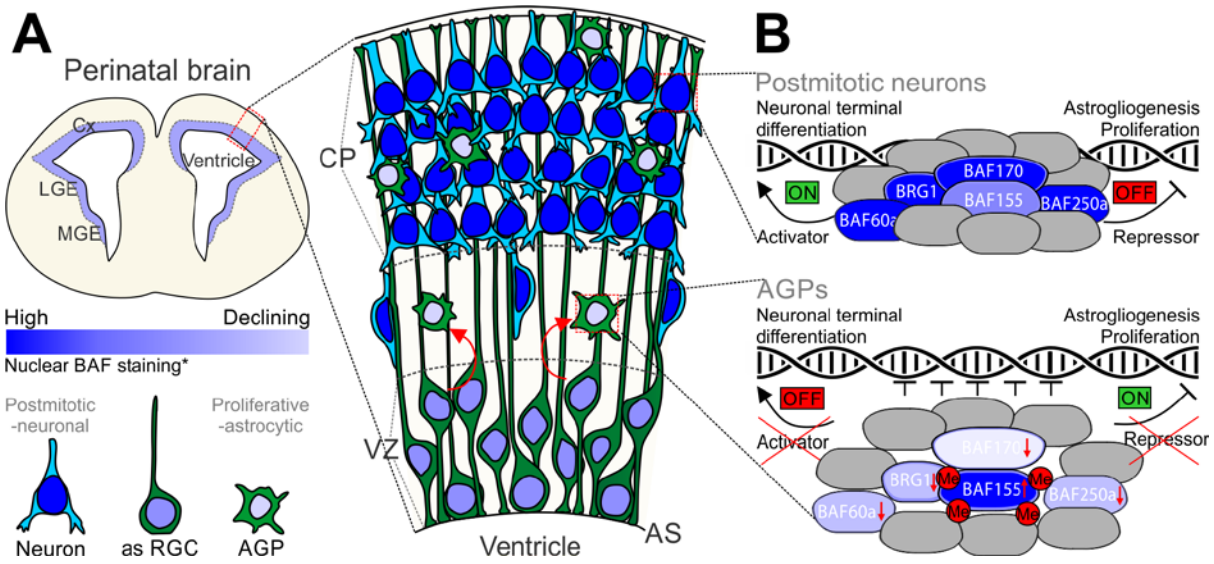

Figure 39 | Changes of BAF complex subunits composition in relation to various neural cell fates. (A) Scheme depicting our findings. The cartoon shows that astrocytic RGCs of all astrocytic germinal zones (VZ of Cx, LGE and MGE; indicated in the of drawing of perinatal murine brain section) assemble BAF complex and its expression tends to decline as they detach from the surface of VZ in the form of AGPs (process pointed by red arrow; this was showed for all subunits except for BAF155, expression of which was elevated). To the contrary, expression of subunits downregulated within AGPs was highly elevated in neurons populating CP (surpassing that of astrocytic RGCs as well; this was true for all subunits except BAF155, whose expression was lowered). The colour of the nuclei of a given cell population is proportional to the average expression levels of all tested subunits (*in (A) scale bar refers to the expression of all tested subunits except for BAF155, problem discussed above). (B) Proposed hypothetical model of described BAF composition reshuffles showed for postmitotic neurons (upper panel) and AGPs (lower panel). Postmitotic neurons expressed high levels of BRG1, BAF170, BAF60a and BAF250a. BAF155 expression was rather moderate (comparing to that of astrocytic RGCs and AGPs). This could be caused by high expression levels of BAF170 (discussed previously). High expression levels suggest assembly of BAF complex within postmitotic neurons and its action as activator of transcription of genes allowing for neuronal terminal differentiation. On the other hand postmitotic neuronal BAF complex can act as transcriptional repressor of genes coding for astrocytic marks and proliferation promotion. AGPs exhibited declining abundance of BRG1, BAF170, BAF60a and

BAF250a; however, levels of BAF155 were elevated. Considering that high expression levels of BAF155 were evoked by drastic downregulation of BAF170 and assuming that BAF155 could be silenced by posttranscriptional modification (e.g. methylation) this observation may indicate the destabilization of the entire BAF complex within proliferative astrocytic precursors - AGPs. This destabilization could evict BAF complex from previously regulated places abolishing its activator and repressor functions and therefore allowing for inhibition of neuronal differentiation and activation of astrogliogenesis (in sense of detachment of astrocytic RGCs from AS in form of AGPs), and proliferation. The colour of tested subunits matches the scale shown in (A). Subunits coloured in gray are not covered by the study. AGP, astroglial progenitor; AS, apical surface; CP, cortical plate; Cx, cortex; Me, methylation; MGE, medial ganglionic eminence; as RGCs, astrocytic radial glia; LGE, lateral ganglionic eminence; VZ, ventricular zone.

We found that astrocytic RGCs of all germinal zones assemble BAF complex and that its expression tends to decline as cells detach from the surface of VZ in the form of AGPs. We could also show that previously diminished BAF elements reconstitute within mature, quiescent protoplasmic astrocytes. Thus, these results suggest that the depletion of BAF complex elements may be correlated with the proliferation of astroglial cells. Additionally, we established that BAF complexes expression is generally lowered within astroglial lineage and highly elevated in neurons. This suggests that the downregulation of BAF complex abundance could be crucial for astrogliogenesis and astrocyte proliferation. It thus appears that affecting astrocytic RGCs by BAF complex KO and subsequently conducting further experiments aiming at investigation of astrogliogenesis within impacted forebrain regions was fully justified. The summary of our observations, as well as a hypothetical model of BAF complex reshuffles in neurons, astrocytic RGCs and AGPs of perinatal forebrain are presented in Figure 39.

4.2 Our mouse model with *hGFAP*-Cre driven KO of BAF complex, the lesser evil

Having established that the declining abundance of BAF complex could be crucial for astrogliogenesis and astrocyte proliferation we can turn our attention to the subject of the animal model selected for testing this hypothesis. In the present study we used a transgenic mutant mouse with specific *hGFAP* promoter driven, Cre dependent dcKO of BAF155 and BAF170 (Narayanan et al., 2015; Nguyen et al., 2018; Zhuo et al., 2001). The choice of this model allowed us to effectively eliminate the entire BAF complex from the affected astrocytic RGCs. Despite this clear advantage, this model also suffered from several drawbacks. Both of these will be discussed in the present subchapter.

hGFAP promoter driven recombination, pros and cons

hGFAP-Cre driven tdTOM fluorescence have enabled us to confirm the activity of *hGFAP* promoter within all known dorsal and ventral forebrain astrocytic germinal zones (Bayraktar et al., 2014; Tsai

et al., 2012). This observation was in agreement with previously published work (Anthony and Heintz, 2008). Such activity at first glance appears to be in favour of our designs. Precisely, it allowed us to test the impact of BAF complex depletion on dorsal as well as ventral astrogliogenesis. As described previously (see Chapter 4. Discussion. 4.1), a gradual decline of the majority of investigated BAF subunits could be observed in both cortical and striatal AGPs of perinatal WT forebrain. It is known that astrocytes of cortex and corpus callosum originate from cortical astrocytic RGCs. At the same time astrocytes populating the striatum and ventral pallidum as well as striatum and piriform cortex derive from RGCs of MGE and LGE respectively (see Chapter 3. Results. 3.2. Figure 12D-F) (Tsai et al., 2012). Thus the use of this mouse model allowed us to imitate the decline of BAF complex that we have previously proposed as necessary for the initiation of cortical and striatal AGPs characteristics.

The data obtained from our and other's (Anthony and Heintz, 2008) tracing experiments indicated that the developmental stage during which the activity of *hGFAP* promoter was initiated, differed between astrocytic germinal zones, preceding or succeeding the start of astrogliogenesis.
Accordingly, cortical activity of *hGFAP* promoter started relatively early (around E13.5), affecting neuronal RGCs of medial areas of cortex (Kwan et al., 2012) and further spreading to lateral cortical VZ (active at E15.5). Importantly, this activity persisted over development, allowing the manipulation of cortical astrocytic RGCs (residing in VZ of E17.5 murine cortex). Such gradual recombination starting during the neurogenic period and spreading from medial to lateral areas of cortex has numerous consequences, helpful or otherwise. First of all, it opens the possibility of testing what influence the loss of BAF complex exerts on cortical neurogenesis and astrogliogenesis. Therefore, by use of the same animal model we could verify that BAF complex acts as an activator of neuronal differentiation and repressor of astrogliogenesis and astroglial proliferation (see Chapter 4. Discussion. 4.1. Figure 39). On the other hand, affecting neurons carried a risk of indirect manipulation of astroglial phenotype through a reduction in neuron-derived cytokines and proliferation of reactive astrocytes (detailed description in Chapter 4. Discussion. 4.3) (Anderson et al., 2014; Barnabe-Heider et al., 2005; Freeman, 2010; Miller and Gauthier, 2007). Furthermore, because of gradual spread of *hGFAP* promoter activity, medial and lateral areas of cortex were unequally affected by driven mutation. This forced us into a separate analysis of both cortical regions.

Although we could trace the activity of *hGFAP* promoter within ventral astrocytic germinal zones, our results did not fully match the literature. Our studies indicated that in E15.5 forebrain, only a subpart of MGE was affected by *hGFAP*-Cre driven recombination. This observation is somewhat at

odds with published data indicating that RGCs of E15.5 MGE as well as LGE exhibit the activity of *hGFAP* promoter (Anthony and Heintz, 2008). Moreover, it was shown that this activity starts within few astrocytic RGCs residing in VZ of MGE, as early as at E14.5. Such minimal discrepancy may be explained by the difference in the tracing techniques used to detect the activity of *hGFAP* promoter (the promoter controlled expression of β-galactosidase and X-gal staining used in (Anthony and Heintz, 2008) could be more sensitive than the tdTOM reporter used in our studies). The exact time point of the initiation of astrogliogenic switch within ventral RGCs remains unclear (Minocha et al., 2017). However, it has been reported that astroglia originating from MGE may be produced as early as at E14.5 (Minocha et al., 2015). Thus, considering published data as well as our findings we could assume that the *hGFAP* promoter is active within ventral astrocytic RGCs that produce astrocytes.

Affecting dorsal and ventral astrocytic germinal zones within the same forebrain led to difficulties in the evaluation of the origin of the revealed upregulated astroglial cells. Based on previously published tracing studies, we could follow forebrain astrocyte populations that exhibited *hGFAP*-Cre driven recombination (Tsai et al., 2012). However, our data indicated that BAF complex elimination possibly changes the migratory behaviour of affected cells, likely directing them to the regions of forebrain different than in WT animals (detailed description in Chapter 4. Discussion. 4.3). Thus despite the use of tdTOM tracing we could not fully discern whether the upregulated AGPs and astrocytes originate from dorsal or ventral astrocytic germinal zones. This drawback of the *hGFAP*-Cre dcKO forced us to diversify our approach by using another animal model generated by *in utero* electroporation and *Olig2*-Cre recombination (see Chapter 4. Discussion. 4.3).

BAF complex elimination, whistling past the graveyard

The elimination of all known BAF complex subunits (and thus extinction of the entire BAF complex) can be evoked solely by the dual loss of BAF155 and BAF170 (Narayanan et al., 2015). Indeed, astrocytic RGCs of our *hGFAP*-Cre driven dcKO model were deprived of all tested BAF complex subunits (namely BAF155, BAF170, BRG1 and BAF60a). Similarly, ventral protoplasmic astrocytes of postnatal dcKO mice did not express BAF complex elements (Appendix, Figure 43B). Thus despite the relatively late initiation of *hGFAP*-Cre activity within MGE and LGE, ventral astroglial cells could still be affected by BAF complex KO.

Finally, as we have reported, the *post-partum* mortality of dcKO animals was sorely high, limiting their average lifespan to P3-4. This is due to difficulties with feeding, as these mutants were displaying motor deficits and therefore could not compete for food with their littermates. This was a clear disadvantage of *hGFAP*-Cre dcKO as a model for abnormal astrogliogenesis and astroglial

proliferation. Accordingly, cortical astrogliogenesis has been reported to begin around E17.5 (Kriegstein and Alvarez-Buylla, 2009). However, the whole process of astrogliogenesis (including AGPs migration, local proliferation, terminal differentiation to post mitotic astrocytes and their integration to the neural circuitry) takes place over weeks of postnatal development (Bandeira et al., 2009; Ge and Jia, 2016; Ge et al., 2012; Miller and Gauthier, 2007). Therefore, our animal model limited our study to the early steps of astrogliogenesis influenced by BAF complex depletion. Namely, the high juvenile mortality of dcKO mice prevented the investigation of later stages of astrocytes development.

***hGFAP*-Cre driven KO of BAF complex, the lesser evil**

A better strategy to target specific lineages could help us avoid the drawbacks described above. Literature reports indicate diverse methods that allow to perturb the expression of chosen genes within the astroglial lineage (Anthony and Heintz, 2008; Casper et al., 2007; Jahn et al., 2015; Srinivasan et al., 2016; Xie et al., 2015). Among these, several Cre driver lines have been shown to target astrocytes and their progenitors. However, all described mouse models display shortcomings (e.g. early induction, lack of specificity, etc.) (Casper et al., 2007; Foo and Dougherty, 2013). For instance *GLAST* or *BLBP* promoter driven recombination, albeit reported to be astrocyte specific, have been shown to start in E10.5 cortex, thereby affecting early and late neuronal RGCs as well as astrocytic RGCs (Anthony and Heintz, 2008; Casper et al., 2007). Perhaps viral delivery of Cre to $BAF155^{fl/fl}$_ $BAF170^{fl/fl}$ brain could serve as an alternative method of BAF155 and BAF170 KO within astrocytes of adult animals. While such an approach appears promising at first glance, the damage caused by injection of a viral vector could itself trigger a proliferation of astroglia, evoking reactive astrogliosis at the place of capillary insertion (reaction to the injury, described in (Casper et al., 2007)). Therefore, this method cannot be considered as appropriate for investigation of regulators of astroglia proliferation, as in the case of BAF complex.

In conclusion, our results show that *hGFAP*-Cre driven dcKO affects all forebrain astrocytic germinal zones and allows an effective elimination of the entire BAF complex from the affected astrocytic RGCs. Thus, this animal model, albeit not perfect, still serves our purpose, allowing us to mimic the reduction in BAF subunits expression observed for WT AGPs (see Chapter 4. Discussion. 4.1).

4.3 Phenotype of BAF complex depleted forebrain – favoring astroglia over neurons

Functional competence of mammalian brain depends on cooperation of many distinct cell types (McKenzie et al., 2018; Sloan and Barres, 2014). Among these, the joint action of neurons and

astrocytes has emerged as pivotal in the coordination of neural circuit development and performance (Clarke and Barres, 2013; Khakh and Sofroniew, 2015; Martin et al., 2015; Sloan and Barres, 2014). Importantly, accomplishment of an appropriate astrocyte to neuron ratio has been indicated as crucial for proper brain function (Gallo and Deneen, 2014; Perea et al., 2014; von Bartheld et al., 2016). Tight control of neuronal and astroglial quantities is determined, no doubt, by the molecular events underpinning brain development (Miller and Gauthier, 2007; Sloan and Barres, 2014; Tien et al., 2012).

Our previous studies (see Chapter 4 Discussion. 4.1) led us to propose that the developmental regulation by BAF complex may control the establishment of balanced numbers of neurons and astroglial cells. Accordingly, we hypothesized that the diminished abundance of BAF complex could be crucial for the promotion of astroglia and disruptive for neurogenesis. Thus we generated the *hGFAP*-Cre dcKO mouse model, which enabled us to eliminate the entire BAF complex form the germinal zones of late developing forebrain and thus made it possible to test our hypothesis.

Notably, this *in vivo* deletion of BAF complex led to quantitative alterations in the cellular composition of the forebrain, with visibly increased numbers of astroglia and reduced numbers of neurons. In this subchapter we will discuss the promoted astroglial phenotype found in *hGFAP*-Cre dcKO forebrain, taking all analyzed areas of DP and VP into account (see Chapter 3. Results. 3.3 and 3.4).

Technical considerations

The methods used for revealing the characteristics and the abundance of AGPs in WT and dcKO forebrain may encounter some words of criticism that need to be addressed and hopefully defused before unveiling our final conclusions.

First of all, to the best of our knowledge, so far there are no known universal markers of AGPs. Thus the markers used here for the evaluation of AGPs phenotype (GLAST, BLBP, NFiA and SOX9) are commonly expressed by astrocytic RGCs (Hartfuss et al., 2001; Kang et al., 2012; Molofsky et al., 2012; Nagao et al., 2016; Scott et al., 2010; Shibata et al., 1997). There is therefore a risk of confusing these two cell types. However, it is widely accepted that astrocytic RGCs are differentiated AGPs as soon as they leave astrocytic germinal zones (Minocha et al., 2015; Mission et al., 1991; Pixley and de Vellis, 1984; Schmechel and Rakic, 1979). Thus, our analysis focuses not only on the expression of certain astroglial markers, but also on the spatial distribution of stained cells. In addition, unlike in VP, due to anatomical defects it was not possible for us to reveal VZ of dcKO

cortex. Thus, we chose to evaluate the attachment of given cells to the AS of cortical VZ as a final criterion to distinguish astrocytic RGCs from AGPs. We took this step because it has been well established that differentiated AGPs detach from the VZ and subsequently migrate outside of germinal zones (Cameron and Rakic, 1991; Ge et al., 2012; Guillemot, 2007; Marshall and Goldman, 2002; Minocha et al., 2015; Mission et al., 1991; Molofsky and Deneen, 2015; Rowitch and Kriegstein, 2010). Importantly, we could exclude oRGPs fate of delaminated cells by confirming their expression of typically astroglial NFiA (Deneen et al., 2006; Kang et al., 2012) (see Chapter 3. Results. 3.3). Overall, the simultaneous investigation of astroglial markers expression and the location of stained cells enabled us to specifically study the formation of AGPs in WT and dcKO forebrain.

Secondly, striking anatomical differences between WT and dcKO cortex, especially pronounced in the reduced thickness of its medial areas, may have influenced the interpretation of the AGPs quantifications. Precisely, due to reduced neuronal numbers the amount of DAPI cells revealed for medial area of dcKO was visibly lowered, hence artificially increasing the percentages of dcKO AGPs (quantified per DAPI cells). However this potential confounder could not have been avoided by any other method of investigation. In addition, the absolute numbers of AGPs expressing BLBP revealed for dcKO were higher than these of WT, suggesting that the actual increase in AGPs abundance is directly evoked by the deletion of BAF complex within these cells and is not due to the quantification artifacts.

BAF complex - a guardian of balanced abundance of neurons and astroglia

Overall, the most striking features of dcKO forebrain phenotype were: tremendously increased amount of AGPs, elevated numbers of protoplasmic astrocytes and reduced numbers of late born neurons. Taken together these results inspired the model that we proposed above.

We investigated the numbers of late born neurons in postnatal DP of WT and dcKO mice using a staining against SATB2 (Britanova et al., 2008). Our analysis showed severely reduced SATB2 positive neurons. This held true for medial area of cortex and, to a lesser extent, lateral areas. This indicates that the impairment of late neurogenesis is a cortex wide phenomenon but exhibits a gradient in severity, with medial areas being most affected. This gradient mimics *hGFAP*-Cre activity (see Chapter 3. Results. 3.2. Figure 12) and is likely to be fully explained by it. These results were confirmed by our RNA-seq analysis, which revealed a massive downregulation of transcripts related to neurogenesis, late born neurons and neuronal cellular component. Importantly, the neuronal deficits appeared even more severe at P3 than at E17.5, indicating that there was no postnatal compensation for the impaired embryonic neurogenesis. Therefore, deprivation of BAF complex in

developing cortex results in a pronounced and irreversible loss of upper layer neurons. These results are in good agreement with the model that we have proposed before. Indeed we observed that in WT animals neurons were characterized by high expression levels of BAF subunits. As the KO of BAF155 and BAF170 causes deletion of the entire BAF complex (Narayanan et al., 2015), it was impossible for RGCs to reach the elevated levels of BAF complex that would allow differentiation to neurons (Nguyen et al., 2018). Besides, these results are not surprising given that appropriate BAF complex assembly was shown to be critical for proper neurogenesis (Bachmann et al., 2016; Narayanan et al., 2015; Nguyen et al., 2018; Tang et al., 2013; Tuoc et al., 2013b).

Furthermore, we evaluated the AGPs population in embryonic and postnatal DP of WT and dcKO mice using a range of markers: GLAST, BLBP, NFiA and SOX9 (Hartfuss et al., 2001; Kang et al., 2012; Molofsky et al., 2012; Nagao et al., 2016; Scott et al., 2010; Shibata et al., 1997). Our analysis indicated a greatly increased abundance of cortical AGPs. This was already visible at early stages of cortical astrogliogenesis (at E17.5) as well as at postnatal stages (P3) when astrogliogenesis is known to be in full swing (Freeman, 2010; Gallo and Deneen, 2014; Ge and Jia, 2016; Ge et al., 2012; Gotz and Barde, 2005; Kriegstein and Alvarez-Buylla, 2009; Rowitch and Kriegstein, 2010). Moreover, the AGPs population expanded over developmental time. As in the case of late born neurons, the numbers of AGPs exhibited a medio-lateral cortical gradient. However, this gradient was mirrored when compared to neurons, with higher numbers of AGPs in medial cortical area and lower in lateral area. In addition, our transcriptome analysis at least partly confirmed our immunohistochemistry results, indicating increased gliogenic process within embryonic and postnatal DP of dcKO. These observations were not only pronounced in DP but also in VP indicating again that altered production of AGPs is a common feature of our BAF complex depleted forebrain. Surprisingly, earlier studies yielded conflicting results, indicating that the loss of a single BAF subunit, BRG1, leads to a decrease in numbers of AGPs (Matsumoto et al., 2006). However, the results described there were chiefly focusing on S100β and CD44 expressing AGPs of spinal cord, and thus do not fully reflect our research model. Accordingly, these results seem to confirm the model we previously postulated. Thus, we propose that the downregulated expression of BAF complex subunits in developing WT forebrain and their absence in the dcKO mutants promotes the differentiation of astrocytic RGCs into AGPs.

We also investigated the maturation of protoplasmic astrocyte populations in gray matter (Cahoy et al., 2008; Li et al., 2012; Oberheim et al., 2012). By means of immunostaining against ACSBG1 (Cahoy et al., 2008; Chaboub and Deneen, 2013; Li et al., 2012; Naka-Kaneda et al., 2014) we could reveal an increased abundance of protoplasmic astrocytes in postnatal dcKO VP. This finding is anything but

surprising. Since we found elevated numbers of AGPs in dcKO brains it seems logical to expect higher abundance of maturating astrocytes as well (Tabata, 2015). This is indeed what we found also in LCx, however, we were puzzled that protoplasmic astrocytes numbers were dramatically reduced in medial cortical areas where *hGFAP*-Cre driven BAF KO was most precocious and where we found high numbers of AGPs. Thus, at first glance this observation seemed to contradict our predictions. However, several lines of reasoning lead us to believe that such is not necessarily the case.

First of all, it is possible that AGPs born in MCx die before differentiating to protoplasmic astrocytes. However, our evaluation of cell death contradicted this idea showing that only negligible numbers of DP AGPs were apoptotic. Therefore, there must be another reason for the lack of astrocytes in medial cortical areas.

It is possible that AGPs were first born in MCx, later migrate to healthier areas such as LCx and subsequently differentiate there. This idea seems to be supported by our EGFP tracing performed by means of *in utero* electroporation. Here we could show that dorsal progenitors were highly mobile. Accordingly, a couple of days after electroporation in cortex, labeled cells could be found in more lateral as well as ventral areas of dcKO forebrain. Moreover, our RNA-seq analysis seems to confirm high migratory abilities of BAF complex depleted cells. Indeed, several transcripts upregulated in postnatal dcKO DP are involved in enhancement of cell locomotion and migration. Additional evidence supporting this idea comes from studies on regional allocations of astrocytes (Tsai et al., 2012). It has been shown that the distribution of astroglia is dictated by VZ-patterning. This implies that astroglial cells expressing ventral markers would be restricted into more lateral and ventral areas of forebrain (see Chapter 3. Results. 3.2. Figure 12D-F). Our RNA-seq analysis of postnatal dcKO DP revealed a massive upregulation of markers known to be attributes of ventral areas (e.g. Gli1, data not shown) (Tsai et al., 2012; Yu et al., 2009). Thus it could be that these markers trigger aberrant migration of DP AGPs towards more lateral and ventral regions of dcKO forebrain. Incidentally, this effect would not exclude the contribution of BAF complex depleted astrocytic RGCs of MGE and LGE in the production of the increased numbers of VP protoplasmic astrocytes. We could confirm it by observing increased numbers of ACSBG1 expressing astrocytes in VP of *Olig2*-Cre dcKO mice, as in this model we affected only ventral astrocytic RGCs by BAF complex depletion (Zawadzka et al., 2010).

Additionally, it has been shown that late born neuron derived cytokines are necessary for differentiation of astrocytes (Barnabe-Heider et al., 2005; Freeman, 2010; Miller and Gauthier, 2007). Although the numbers of late born neurons were drastically reduced in dcKO DP, this effect was less pronounced in lateral areas. Thus, it is possible that sufficient amounts of late born neurons survived in lateral cortical areas of dcKO to allow the development of protoplasmic astrocytes, whereas this was not the case in MCx.

However, overall the experimental data explaining the observed lack of protoplasmic astrocytes in MCx of dcKO are parsimonious and further investigations addressing, for instance, the role of cytokines or patterning markers need to be performed in the future.

Rather than contradicting our model, these observations allowed us to refine it. Accordingly, it may be an oversimplification to assume that more AGPs should lead to an increase in numbers of maturating astrocytes. In fact, we propose that BAF complex depletion merely drives the proliferation of AGPs, without causing their maturation towards astrocytes. Thus, one could expect that lowered levels of BAF complex within maturating astrocytes will also lead to their uncontrolled proliferation, what could eventually explain their elevated numbers within VP of dcKO (more details described below).

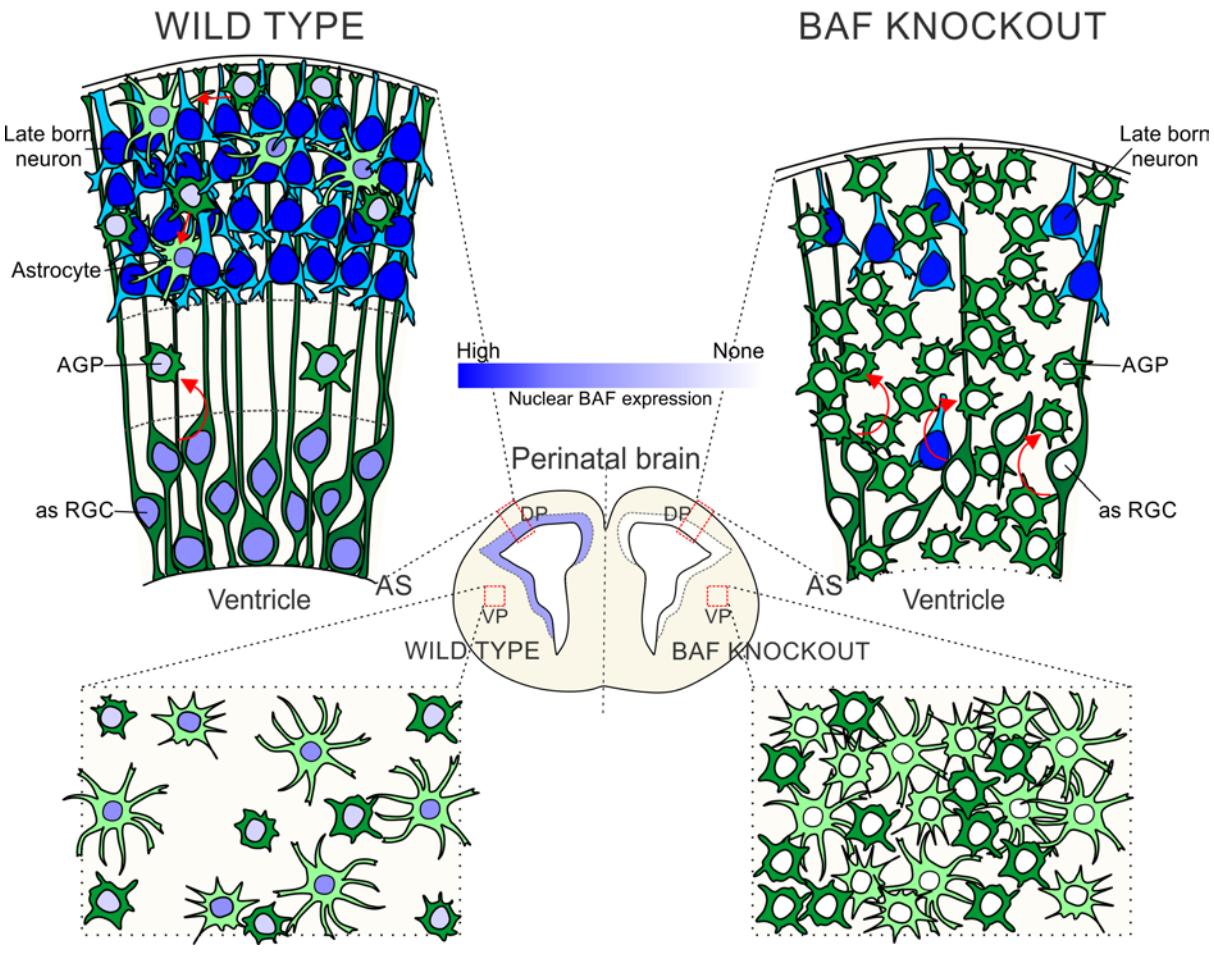

Figure 40 | Increased numbers of astroglia and reduced numbers of neurons in forebrain affected by BAF complex depletion. Scheme depicting our findings. The cartoon shows that in normally developing brain all astrocytic RGCs express BAF complex. In WT animals (shown on the left side) cortical neurogenesis precedes astrogliogenesis and allows for development of neurons that are rich in BAF complex expression. When neurogenesis ceases BAF complex expressing astrocytic RGCs start to delaminate from the AS of VZ (marked by rounded red arrows) and subsequently migrate, proliferate and differentiate to astrocytes (marked by straight red arrows). Notably, the fate of proliferative AGPs

corresponds to downregulated levels of BAF complex within this cell line and the downregulated BAF complex subunits are reconstituted within mature astrocytes Overall, we could reveal the presence of neurons, astrocytic RGCs, AGPs and astrocytes in perinatal (E17.5 and P3, results merged in one cartoon) WT cortex. We could also observe moderate numbers of AGPs and astrocytes in VP of perinatal (P3) WT forebrain indicating active astrogenesis within ventral astroglial germinal zones. BAF complex depletion within dcKO forebrain (showed on the right side) led to decrease in cortical neurogenesis and massive delamination of affected astrocytic RGCs in form of AGPs. In addition the numbers of AGPs found in DP as well as VP of BAF depleted forebrain were tremendously elevated. Strikingly we could reveal increased abundance of protoplasmic astrocytes in several areas of postnatal VP whereas these cells were not present in MCx of dcKO. Centrally placed scale bar refers to the revealed average expression of BAF complex. AGP, astroglial progenitor; AS, apical surface; DP, dorsal pallium; as RGC, astrocytic radial glial cell; VP, ventral pallium.

Overall, all these experimental results can be explained by the model we propose. Thus, it seems plausible that BAF complex plays a crucial role in maintaining a proper ratio of astroglial cells to neurons. Figure 40 summarizes all described findings.

4.4 GLI1 triggered proliferation of astroglia is under tight control of BAF complex

One of the final steps of mammalian brain development that allows the establishment of a proper neuron to astrocyte ratio lies in astroglia proliferation. Indeed it has been shown that during the first postnatal weeks, the abundance of rodent astroglia increases up to 8-fold (Bandeira et al., 2009). Exciting reports of 2-photon imaging and BrdU labelling experiments indicated locally proliferative astroglia as a major source for this expansion (Chaboub and Deneen, 2013; Ge et al., 2012; Tien et al., 2012). However, the little is known about the molecular underpinnings controlling initiation and termination of this process.

Our previous studies (see Chapter 4 Discussion. 4.1) suggested that the developmental regulation by BAF complex may control the establishment of balanced numbers of neurons and astrocytes. Indeed, we could show that the loss of BAF complex from germinal zones of late developing brain causes a dramatic unbalance in populations of neural cells, lowering the abundance of neurons and increasing that of astroglia. Moreover, our model indicates that except for initiation of astrogliogenesis (allowance for detachment of astrocytic RGCs in the form of AGPs), downregulation of BAF complex expression may have a permissive role in astroglial multiplication. In fact several groups have described BAF complex as a proliferation limiting factor that inhibits mitogens e.g. GLI1 (Jagani et al., 2010; Narayanan et al., 2015; Nguyen et al., 2018; Panamarova et al., 2016; Wang et al., 2014; Wu, 2012; Zhan et al., 2011). Thus, we have speculated and further confirmed that the elevated numbers of astroglia deprived of BAF complex are due to their uncontrolled proliferation driven by GLI1. In this subchapter we will discuss the increased proliferation of astroglia found in DP

and VP of *hGFAP*-Cre dcKO forebrain (see Chapter 3. Results. 3.3 and 3.4). At the end, we will focus on the proposed mitogen trigger of astroglia proliferation in the absence of BAF complex – GLI1 (see Chapter 3. Results. 3.5).

Increased proliferation accompanies abundant astroglia

Highly elevated proliferative capacity was a common feature of AGPs and protoplasmic astrocytes of dcKO forebrain and VP, respectively. As we have speculated that downregulated expression of BAF subunits enables astroglia proliferation, this observation confirms our assumptions.

We assessed the proliferation of AGPs and protoplasmic astrocytes by two independent methods: immunostaining of Ki67 (Scholzen and Gerdes, 2000) and IP injection of thymidine analogue - EdU (Chehrehasa et al., 2009; Flomerfelt and Gress, 2016; Vega and Peterson, 2005).
The results of the immunostaining showed that a large fraction of BAF complex depleted AGPs and VP protoplasmic astrocytes expressed Ki67, indicating that these were proliferative. This finding was confirmed for both cell types by EdU incorporation assay.
Furthermore, the results of RNA-seq revealed that a number of transcripts related to proliferation of astrocytes and glioma were significantly upregulated in postnatal DP and VP of dcKO. Moreover, proliferation-related transcripts were already highly elevated in BAF complex depleted DP at E17.5 (showed here and in (Nguyen et al., 2018)).

Importantly, it has been described that neuronal loss triggers inflammation and proliferation of astroglia and astrogliosis (Anderson et al., 2014; Ben Haim et al., 2015; Sofroniew, 2015). Therefore, there is a risk that the elevated numbers of proliferative astrocytes result from reactive astrogliosis, evoked indirectly by BAF complex deletion. In fact, we could find some evidence to that effect: our RNA-seq data showed a notable upregulation of inflammation-related transcripts in cortex. However, immunohistochemistry revealed that BAF complex depleted proliferative astrocytes did not overexpress GFAP, a hallmark of reactive astrogliosis (Liddelow and Barres, 2017; Robel et al., 2011). Therefore reactive astrogliosis is an unlikely explanation of our results.

Taken together, these findings highlight the abnormally high proliferation levels of astroglia in our dcKO mouse model, demonstrating that BAF complex is a powerful regulator of astroglia multiplication. We have found evidence that when BAF complex levels are low, astroglial cells are proliferative. Furthermore, we propose that when BAF complex expression increases, cells exit their proliferative cycles and are eased towards terminal differentiation and quiescence.

BAF complexes regulate proliferation of astroglia via mitogen GLI1

The findings discussed so far clearly show that BAF complex has a powerful influence on astroglia proliferation. In addition, as little is known on the subject (Ge and Jia, 2016; Tien et al., 2012), we sought to investigate which effector that triggers this proliferation could be targeted by BAF complex inhibition. Our RNA-seq data indicated that the mitogenic TF Gli1 and its downstream targets, several of which are known triggers of proliferation (e.g. cyclin D1 (Ccnd1) (Dahmane et al., 1997; Klein and Assoian, 2008; McCubrey et al., 2014; Nilsson et al., 2000), were constitutively upregulated in the brain of E17.5 and P3 dcKO. As the GLI1 is known to be implicated in aberrant proliferation of astroglia (e.g. in glioma) (Clement et al., 2007; Garcia et al., 2010; Pitter et al., 2014), it seems a plausible candidate as a target of inhibition by BAF complex. We could confirm increased levels of Gli1 mRNA by *in situ* hybridization, the results of which showed a massive increase in the number of labeled cells in dorsal and ventral areas of dcKO forebrain. Granted, this chromogenic *in situ* hybridization did not allow us to confirm the identity of the cells in which Gli1 mRNA was upregulated. But given that the dcKO cortex is populated mostly by aberrantly proliferating astroglia, it is very likely that these cells accounted for much, if not most, of the upregulation of Gli1 that emerged from our RNA-seq and *in situ* hybridization data.

Importantly, the upregulation of Gli1 could also be due to its activation by SHH (Dahmane et al., 2001; Palma et al., 2005), indirectly by loss of BAF complex. Two of our findings argue against this possibility. First of all, our RNA-seq data did not show a concomitant increase in Shh, which was downregulated instead. Secondly, *in situ* hybridization for Shh indicated a lower number of positive cells in dcKO cortex. It thus appears that SHH cannot have caused the upregulation of Gli1 in our model, making it all the more plausible that BAF complex deletion was its source. In support of this hypothesis, previous studies have shown that the BAF complex subunit BRG1 binds to the regulatory regions of *Gli1*, directly repressing its transcription (Zhan et al., 2011). In fact, this reciprocity has been proposed to be involved in the regulation of proliferation of cancer cells (Jagani et al., 2010). We have demonstrated the loss of BRG1 in dcKO, providing a convincing mechanism by which GLI1 disinhibition occurs in affected astroglia.

But the most conclusive evidence comes from our experiments with direct inhibition of the GLI1 dependent transcription. Indeed, we could prevent aberrant overproliferation of astrocytes, thereby lowering their numbers in the ventral area of dcKO forebrain, by direct blockade of GLI1 using its antagonist, GANT61 (Lauth et al., 2007). Albeit this experiment warrants further repetitions (the n numbers are low), it identifies GLI1 as a promising candidate trigger of astroglia proliferation.

Therefore, our data does not only indicate that BAF complex deletion causes overproliferation of astroglial cells, but also that this effect is achieved through de-repression of the mitogen, GLI1.

BAF complex controlled GLI1 triggered proliferation of astroglia. Possible scenarios

Proliferation of astroglia may be considered as a good or bad feature for development. On the one hand, it has been shown that it is due to the amplification processes that mammalian astrocyte population expands postnatally (Ge and Jia, 2016; Ge et al., 2012). This expansion enables the brain to achieve appropriate ratios of astroglia to neurons, a prerequisite for proper function (Ge et al., 2012; Herculano-Houzel, 2014; Sloan and Barres, 2014). On the other hand, aberrant overproliferation of astroglia leads to pathological states of brain, such as tumor (e.g. glioma) (Furnari et al., 2007; Irvin et al., 2017).

Despite the fact that several factors have been shown to trigger proliferation of gliomas (Wang et al., 2000; Xu et al., 2013; Yang et al., 2012), little is known about the molecular underpinnings regulating multiplication of astroglia during development (Ge et al., 2012; Tien et al., 2012).

Here we could show that BAF complex inhibits proliferation of astroglia, possibly by repressing transcription of the proliferation-enhancing mitogen, GLI1 (Figure 41). As we could also observe downregulated expression of BAF subunits (including Gli1 repressing BRG1) in premature astroglia (AGPs) of WT mice, we suggest that this could initiate GLI1 transcription within these cells. Overall, this can serve as a causal molecular mechanism for the early postnatal expansion of astrocytic populations (Figure 41A, left panel). In support of this hypothesis, postnatally proliferative astrocytes divide symmetrically, which has been shown to be the primary mode of division upon BAF complex deletion in early RGCs (Ge and Jia, 2016; Nguyen et al., 2018). Besides, overexpression of GLI1 has been also associated with symmetric cellular division (Ferent et al., 2014).

Furthermore, we speculate that the reestablishment of BAF complex within proliferative astroglia could serve as a mechanism that represses Gli1 transcription thereby restraining their proliferative capacities and enforcing terminal differentiation and quiescence (Figure 41A, right panel). However, the present work does not fully confirm such a mechanism, thus additional experiments probing BAF controlled GLI1 activation/repression within WT AGPs/quiescent astrocytes respectively need to be performed in the future.

Additionally, aberrant lack of Gli1 transcription repression caused by BAF complex mutation (or lack of BAF complex expression, as in case of our dcKO) could also be involved in enabling astroglial overproliferation, leading to tumorigenicity and glioma generation (Figure 41B). In support of this hypothesis, reciprocity between GLI1 and BAF complex (BRG1) has been proposed to induce the proliferation of malignant rhabdoid tumors (Jagani et al., 2010). Thus further studies should also

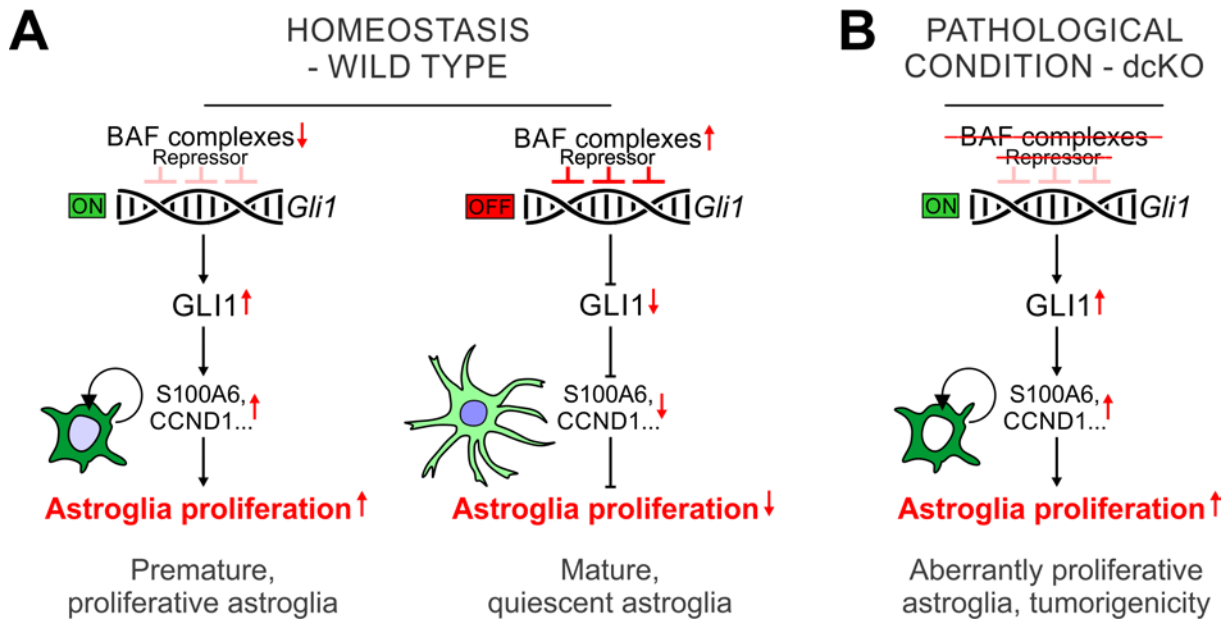

Figure 41 | Proposed model of BAF complexes dependent regulation of astroglia proliferation via mitogen GLI1. (A) In normally developing brain downregulation of BAF complex may lead to derepression of Gli1 transcription increasing amount of mitogenic GLI1, which further induces upregulation of proliferation inducing factors (e.g. known to promote AGPs proliferation – S100A6 (Yamada and Jinno, 2014) or CCND1) thereby enabling perinatal premature astroglia proliferation (left panel). The reestablishment of BAF complex within proliferative astroglia could serve as a mechanism that represses Gli1 transcription thereby restraining their proliferative capacities and enforcing terminal differentiation and quiescence (right panel). (B) Aberrant lack of Gli1 transcription repression caused by elimination of BAF complex (dcKO) enables astroglial overproliferation, leading to pathological states of brain and tumorigenicity. dcKO, double conditional knockout.

investigate the role of the BAF complex and the GLI1 signaling pathway in models of astroglioma.

Overall the model presented in Figure 41 may be erroneous and further investigations are needed to verify it. Still, it serves as a helpful guide for future experimental work.

4.5 Conclusions and perspectives

It is important for proper brain function that appropriate ratios of cell types are achieved (McKenzie et al., 2018; Nedergaard et al., 2003; Robertson, 2013; Sloan and Barres, 2014). Among these, adequate quantitative relation between neurons and astrocytes has been proposed as pivotal for brain performance and large departures from this balance have been involved in neurodevelopmental and psychiatric disorders as well as brain tumors (Clarke and Barres, 2013; Dimou and Gotz, 2014; Gallo and Deneen, 2014; Khakh and Sofroniew, 2015; Martin et al., 2015;

O'Brien et al., 2013; Perea et al., 2014; Sloan and Barres, 2014; von Bartheld et al., 2016). Unquestionably, the basics of the brain cellular composition have the origin in the developmental processes (Bandeira et al., 2009; Kriegstein and Alvarez-Buylla, 2009).

Chromatin regulators, such as BAF complex, exert an influence on cell proliferation and differentiation, making significant contribution to the endeavour of brain development (Narayanan and Tuoc, 2014b; Sokpor et al., 2017; Son and Crabtree, 2014). For instance BAF complex is known to orchestrate neurogenesis and neuronal migration as well as NSCs proliferation and maintenance (Bachmann et al., 2016; Lessard et al., 2007; Matsumoto et al., 2006; Narayanan et al., 2018; Nguyen et al., 2018; Tuoc et al., 2013b; Wiegreffe et al., 2015). Albeit crucial for proper neuronal numbers and functionality, the role of BAF complex in astroglia development has not been extensively investigated to this day. In fact only few sources have addressed this topic, focusing on astrogliogenesis during embryonic developmental stages (Matsumoto et al., 2006) or in adulthood (Ninkovic et al., 2013; Tuoc et al., 2017). However, these studies describe the role of only single BAF complex subunits and therefore are not sufficient to provide information on the dependence of astrogliogenesis on the entire BAF complex assembly. Accordingly, little is known about the general role of BAF complexes in the processes controlling proliferation and differentiation of cells within the astroglial lineage.

We investigated the involvement of BAF complexes in the establishment of balanced neuronal and astroglial numbers by analyzing the phenotype of a mouse model in which two core elements of BAF complex, BAF170 and BAF155 were deleted, leading to the destruction of the entire complex (Narayanan et al., 2015). Applying a combination of genomic and proteomic approaches as well as advanced imaging and cellular quantification methods, we could show that BAF complex deletion resulted in a tremendous depletion of neuronal populations as well as aberrantly increased abundance of proliferative astroglia. As mentioned before, earlier studies have stressed the importance of appropriate BAF complex assemblies for proper neurogenesis, thus our findings consolidate these notions. However our results describing an increased astrogliogenesis driven by massive delamination of AGPs followed by aberrant astroglia proliferation are, to our knowledge, completely novel. On the other hand, a high rate of multiplication upon BAF deletion is not surprising as such, as several groups have indicated the BAF complex as a proliferation limiting factor (Narayanan et al., 2015; Nguyen et al., 2018; Panamarova et al., 2016; Wu, 2012). Furthermore, our RNA-seq experiments, *in situ* hybridization and pharmacological inhibition implicated de-repression of the mitogen GLI1 as a trigger of increased astroglia proliferation upon BAF complex deletion.

We therefore propose a model in which BAF complex regulates the ratio of neurons to astroglia in

normally developing brain. In this model, BAF complex acts upon the balance of neurons and astroglial cells in two ways. First of all, BAF complex promotes neurogenesis. Second, when downregulated, it also acts upon detachment of astrocytic RGCs from the AS of VZ, enabling their differentiation into AGPs. BAF complex also regulates the proliferation of astroglia by repressing the transcription of the proliferation-enhancing mitogen GLI1. Furthermore, the downregulation of BAF complex in premature astroglia can serve as a causal mechanism for the early postnatal expansion of astrocytic populations. This model also indicates a potential mechanism in pathological astroglial overproliferation such as glioma, hinting at a potential role of BAF complex in tumorigenicity. Further studies should investigate the role of the BAF complex and the GLI1 signaling pathway as a potential target for the development of therapeutic drugs, such as the GLI inhibitor GANT61 used in this study.

Summary

In the human central nervous system, astrocytes vastly outnumber neurons and regulate a host of physiological processes critical to its function. Astrocytes form a functional syncytium tiling the brain with minimal overlap between individual cells. This anatomical organization implies that a balanced numbers of neurons and astrocytes must be generated during brain development. In spite of this, very little is known about the molecular events governing proliferation and differentiation in the astroglial lineage that culminate in the establishment of adequate numbers of astrocytes.

In recent years, the chromatin remodeling BAF (Brg1/Brm Associated Factors) complex, a conglomerate of at least 15 protein subunits, has emerged as a key regulator of different steps of neurogenesis, from proliferation of progenitors to differentiation into mature neurons, thus profoundly affecting brain development. However, its functions in astrogliogenesis are largely unknown.

Here, we investigated the involvement of BAF complex in the regulation of cellular proliferation and differentiation in the astroglial lineage of perinatal mouse brain.
We first assessed the expression of several BAF complex subunits in cells of both neuronal and astroglial lineages, and found that the composition of the BAF complex was cell type dependent.
Next, we examined the phenotype of a mouse model in which *hGFAP*-Cre driven conditional knockout of BAF155 and BAF170, two scaffolding subunits, results in the deletion of the entire BAF complex within radial glial progenitors during late neurogenesis and astrogliogenesis. Performing phenotype and gene expression profile analyzes, we found that loss of BAF complex at this developmental stage causes a tremendous depletion of neuronal cells as well as an aberrantly increased abundance of proliferative astroglia in ventral and dorsal telencephalon. Furthermore, we identified an upregulated expression of GLI1 as a causal mechanism of abnormal overproliferation of astroglial cells following BAF complex depletion. This could be demonstrated by inhibition of GLI1 by injection of GANT61, which abolished the aberrant proliferation caused by loss of BAF complex.

We thus propose that cell lineage dependent rearrangements of the composition of the BAF complex play a crucial role in regulating the relative numbers of neurons and astrocytes generated during brain development. This effect is achieved in part by BAF complex dependent repression of the proliferation-enhancing mitogen GLI1 in the astroglial lineage.

References

Abbott, N.J., Rönnbäck, L., and Hansson, E. (2006). Astrocyte–endothelial interactions at the blood–brain barrier. Nature Reviews Neuroscience *7*, 41.

Adams, S., and Pacharinsak, C. (2015). Mouse anesthesia and analgesia. Curr Protoc Mouse Biol *5*, 51-63.

Alcantara Llaguno, S., Chen, J., Kwon, C.H., Jackson, E.L., Li, Y., Burns, D.K., Alvarez-Buylla, A., and Parada, L.F. (2009). Malignant astrocytomas originate from neural stem/progenitor cells in a somatic tumor suppressor mouse model. Cancer Cell *15*, 45-56.

Alfert, A., Moreno, N., and Kerl, K. (2019). The BAF complex in development and disease. Epigenetics Chromatin *12*, 19.

Allahyari, R.V., and Garcia, A.D. (2015). Triggering Reactive Gliosis In Vivo by a Forebrain Stab Injury. J Vis Exp, e52825.

Alqudah, M.A., Agarwal, S., Al-Keilani, M.S., Sibenaller, Z.A., Ryken, T.C., and Assem, M. (2013). NOTCH3 is a prognostic factor that promotes glioma cell proliferation, migration and invasion via activation of CCND1 and EGFR. PLoS One *8*, e77299.

Anderson, M.A., Ao, Y., and Sofroniew, M.V. (2014). Heterogeneity of reactive astrocytes. Neurosci Lett *565*, 23-29.

Andriezen, W.L. (1893). The Neuroglia Elements in the Human Brain. Br Med J *2*, 227-230.

Angevine, J.B., Jr., and Sidman, R.L. (1961). Autoradiographic study of cell migration during histogenesis of cerebral cortex in the mouse. Nature *192*, 766-768.

Anlauf, E., and Derouiche, A. (2013). Glutamine synthetase as an astrocytic marker: its cell type and vesicle localization. Front Endocrinol (Lausanne) *4*, 144.

Annovazzi, L., Mellai, M., Caldera, V., Valente, G., and Schiffer, D. (2011). SOX2 expression and amplification in gliomas and glioma cell lines. Cancer Genomics Proteomics *8*, 139-147.

Anthony, T.E., and Heintz, N. (2008). Genetic lineage tracing defines distinct neurogenic and gliogenic stages of ventral telencephalic radial glial development. Neural Dev *3*, 30.

Arai, Y., and Taverna, E. (2017). Neural Progenitor Cell Polarity and Cortical Development. Front Cell Neurosci *11*, 384.

Arakelyan, A., Zakharyan, R., Hambardzumyan, M., Petrkova, J., Olsson, M.C., Petrek, M., and Boyajyan, A. (2014). Functional genetic polymorphisms of monocyte chemoattractant protein 1 and C-C chemokine receptor type 2 in ischemic stroke. J Interferon Cytokine Res *34*, 100-105.

Araujo, G.L., Araujo, J.A., Schroeder, T., Tort, A.B., and Costa, M.R. (2014). Sonic hedgehog signaling regulates mode of cell division of early cerebral cortex progenitors and increases astrogliogenesis. Front Cell Neurosci *8*, 77.

Arendt, D., Tosches, M.A., and Marlow, H. (2016). From nerve net to nerve ring, nerve cord and brain--evolution of the nervous system. Nat Rev Neurosci *17*, 61-72.

Bachmann, C., Nguyen, H., Rosenbusch, J., Pham, L., Rabe, T., Patwa, M., Sokpor, G., Seong, R.H., Ashery-Padan, R., Mansouri, A.*, et al.* (2016). mSWI/SNF (BAF) Complexes Are Indispensable for the Neurogenesis and Development of Embryonic Olfactory Epithelium. PLoS Genet *12*, e1006274.

Bandeira, F., Lent, R., and Herculano-Houzel, S. (2009). Changing numbers of neuronal and non-neuronal cells underlie postnatal brain growth in the rat. Proc Natl Acad Sci U S A *106*, 14108-14113.

Barca, O., Seoane, M., Senaris, R.M., and Arce, V.M. (2013). Fas/CD95 ligation induces proliferation of primary fetal astrocytes through a mechanism involving caspase 8-mediated ERK activation. Cell Physiol Biochem *32*, 111-120.

Barnabe-Heider, F., Wasylnka, J.A., Fernandes, K.J., Porsche, C., Sendtner, M., Kaplan, D.R., and Miller, F.D. (2005). Evidence that embryonic neurons regulate the onset of cortical gliogenesis via cardiotrophin-1. Neuron *48*, 253-265.

Bayraktar, O.A., Fuentealba, L.C., Alvarez-Buylla, A., and Rowitch, D.H. (2014). Astrocyte development and heterogeneity. Cold Spring Harb Perspect Biol *7*, a020362.

Beaudoin, G.M., 3rd, Lee, S.H., Singh, D., Yuan, Y., Ng, Y.G., Reichardt, L.F., and Arikkath, J. (2012). Culturing pyramidal neurons from the early postnatal mouse hippocampus and cortex. Nat Protoc *7*, 1741-1754.
Bechmann, I., Lossau, S., Steiner, B., Mor, G., Gimsa, U., and Nitsch, R. (2000). Reactive astrocytes upregulate Fas (CD95) and Fas ligand (CD95L) expression but do not undergo programmed cell death during the course of anterograde degeneration. Glia *32*, 25-41.
Ben Haim, L., Carrillo-de Sauvage, M.A., Ceyzeriat, K., and Escartin, C. (2015). Elusive roles for reactive astrocytes in neurodegenerative diseases. Front Cell Neurosci *9*, 278.
Britanova, O., de Juan Romero, C., Cheung, A., Kwan, K.Y., Schwark, M., Gyorgy, A., Vogel, T., Akopov, S., Mitkovski, M., Agoston, D.*, et al.* (2008). Satb2 is a postmitotic determinant for upper-layer neuron specification in the neocortex. Neuron *57*, 378-392.
Brizzee, K.R., and Jacobs, L.A. (1959). The glia/neuron index in the submolecular layers of the motor cortex in the cat. Anat Rec *134*, 97-105.
Brown, A.M., and Ransom, B.R. (2007). Astrocyte glycogen and brain energy metabolism. Glia *55*, 1263-1271.
Brunne, B., Zhao, S., Derouiche, A., Herz, J., May, P., Frotscher, M., and Bock, H.H. (2010). Origin, maturation, and astroglial transformation of secondary radial glial cells in the developing dentate gyrus. Glia *58*, 1553-1569.
Bullock, T.H., and Horridge, G.A. (1965). Structure and function in the nervous systems of invertebrates.
Bunt, J., Osinski, J.M., Lim, J.W., Vidovic, D., Ye, Y., Zalucki, O., O'Connor, T.R., Harris, L., Gronostajski, R.M., Richards, L.J.*, et al.* (2017). Combined allelic dosage of Nfia and Nfib regulates cortical development. Brain and Neuroscience Advances *1*, 2398212817739433.
C. Charles, A., E. Merrill, J., R. Dirksen, E., and J Sanderson, M. (1991). Intercellular signaling in glial cells: Calcium waves and oscillations in response to mechanical stimulation and glutamate, Vol 6.
Cahoy, J.D., Emery, B., Kaushal, A., Foo, L.C., Zamanian, J.L., Christopherson, K.S., Xing, Y., Lubischer, J.L., Krieg, P.A., Krupenko, S.A.*, et al.* (2008). A transcriptome database for astrocytes, neurons, and oligodendrocytes: a new resource for understanding brain development and function. J Neurosci *28*, 264-278.
Caiazzo, M., Giannelli, S., Valente, P., Lignani, G., Carissimo, A., Sessa, A., Colasante, G., Bartolomeo, R., Massimino, L., Ferroni, S.*, et al.* (2015). Direct conversion of fibroblasts into functional astrocytes by defined transcription factors. Stem Cell Reports *4*, 25-36.
Cairns, B.R. (2007). Chromatin remodeling: insights and intrigue from single-molecule studies. Nature Structural &Amp; Molecular Biology *14*, 989.
Cameron, R.S., and Rakic, P. (1991). Glial cell lineage in the cerebral cortex: a review and synthesis. Glia *4*, 124-137.
Cao, Y., Zhang, L., Wei, M., Jiang, X., and Jia, D. (2017). MicroRNA-409-3p Represses Glioma Cell Invasion and Proliferation by Targeting High-Mobility Group Nucleosome-Binding Domain 5. Oncol Res *25*, 1097-1107.
Casper, K.B., Jones, K., and McCarthy, K.D. (2007). Characterization of astrocyte-specific conditional knockouts. Genesis *45*, 292-299.
Chaboub, L.S., and Deneen, B. (2012). Developmental origins of astrocyte heterogeneity: the final frontier of CNS development. Dev Neurosci *34*, 379-388.
Chaboub, L.S., and Deneen, B. (2013). Astrocyte form and function in the developing central nervous system. Semin Pediatr Neurol *20*, 230-235.
Chehrehasa, F., Meedeniya, A.C., Dwyer, P., Abrahamsen, G., and Mackay-Sim, A. (2009). EdU, a new thymidine analogue for labelling proliferating cells in the nervous system. J Neurosci Methods *177*, 122-130.
Chen, J., and Archer, T.K. (2005). Regulating SWI/SNF subunit levels via protein-protein interactions and proteasomal degradation: BAF155 and BAF170 limit expression of BAF57. Mol Cell Biol *25*, 9016-9027.
Chen, J., Bardes, E.E., Aronow, B.J., and Jegga, A.G. (2009). ToppGene Suite for gene list enrichment analysis and candidate gene prioritization. Nucleic Acids Res *37*, W305-311.

Chen, L., Fulcoli, F.G., Ferrentino, R., Martucciello, S., Illingworth, E.A., and Baldini, A. (2012). Transcriptional control in cardiac progenitors: Tbx1 interacts with the BAF chromatin remodeling complex and regulates Wnt5a. PLoS Genet *8*, e1002571.
Choi, J., Ko, M., Jeon, S., Jeon, Y., Park, K., Lee, C., Lee, H., and Seong, R.H. (2012). The SWI/SNF-like BAF complex is essential for early B cell development. J Immunol *188*, 3791-3803.
Chojnacki, A., and Weiss, S. (2008). Production of neurons, astrocytes and oligodendrocytes from mammalian CNS stem cells. Nat Protoc *3*, 935-940.
Clarke, L.E., and Barres, B.A. (2013). Emerging roles of astrocytes in neural circuit development. Nat Rev Neurosci *14*, 311-321.
Clement, V., Sanchez, P., de Tribolet, N., Radovanovic, I., and Ruiz i Altaba, A. (2007). HEDGEHOG-GLI1 signaling regulates human glioma growth, cancer stem cell self-renewal, and tumorigenicity. Curr Biol *17*, 165-172.
Coskun, V., Tsoa, R., and Sun, Y.E. (2012). Epigenetic regulation of stem cells differentiating along the neural lineage. Curr Opin Neurobiol *22*, 762-767.
Costa, M.R., Bucholz, O., Schroeder, T., and Gotz, M. (2009). Late origin of glia-restricted progenitors in the developing mouse cerebral cortex. Cereb Cortex *19 Suppl 1*, i135-143.
Courchet, J., and Polleux, F. (2012). Sonic hedgehog, BOC, and synaptic development: new players for an old game. Neuron *73*, 1055-1058.
Dahmane, N., Lee, J., Robins, P., Heller, P., and Ruiz i Altaba, A. (1997). Activation of the transcription factor Gli1 and the Sonic hedgehog signalling pathway in skin tumours. Nature *389*, 876-881.
Dahmane, N., Sanchez, P., Gitton, Y., Palma, V., Sun, T., Beyna, M., Weiner, H., and Ruiz i Altaba, A. (2001). The Sonic Hedgehog-Gli pathway regulates dorsal brain growth and tumorigenesis. Development *128*, 5201-5212.
De Falco, V., Guarino, V., Avilla, E., Castellone, M.D., Salerno, P., Salvatore, G., Faviana, P., Basolo, F., Santoro, M., and Melillo, R.M. (2007). Biological role and potential therapeutic targeting of the chemokine receptor CXCR4 in undifferentiated thyroid cancer. Cancer Res *67*, 11821-11829.
deAzevedo, L.C., Fallet, C., Moura-Neto, V., Daumas-Duport, C., Hedin-Pereira, C., and Lent, R. (2003). Cortical radial glial cells in human fetuses: depth-correlated transformation into astrocytes. J Neurobiol *55*, 288-298.
Dehay, C., and Kennedy, H. (2007). Cell-cycle control and cortical development. Nat Rev Neurosci *8*, 438-450.
Deneen, B., Ho, R., Lukaszewicz, A., Hochstim, C.J., Gronostajski, R.M., and Anderson, D.J. (2006). The transcription factor NFIA controls the onset of gliogenesis in the developing spinal cord. Neuron *52*, 953-968.
Derouiche, A., and Rauen, T. (1995). Coincidence of L-glutamate/L-aspartate transporter (GLAST) and glutamine synthetase (GS) immunoreactions in retinal glia: evidence for coupling of GLAST and GS in transmitter clearance. J Neurosci Res *42*, 131-143.
Dimou, L., and Gotz, M. (2014). Glial cells as progenitors and stem cells: new roles in the healthy and diseased brain. Physiol Rev *94*, 709-737.
Distler, C., Dreher, Z., and Stone, J. (1991). Contact spacing among astrocytes in the central nervous system: An hypothesis of their structural role. Glia *4*, 484-494.
Djebali, S., Davis, C.A., Merkel, A., Dobin, A., Lassmann, T., Mortazavi, A., Tanzer, A., Lagarde, J., Lin, W., Schlesinger, F*., et al.* (2012). Landscape of transcription in human cells. Nature *489*, 101-108.
Doan, D.N., Veal, T.M., Yan, Z., Wang, W., Jones, S.N., and Imbalzano, A.N. (2004). Loss of the INI1 tumor suppressor does not impair the expression of multiple BRG1-dependent genes or the assembly of SWI/SNF enzymes. Oncogene *23*, 3462.
Dominguez, M.H., Ayoub, A.E., and Rakic, P. (2013). POU-III transcription factors (Brn1, Brn2, and Oct6) influence neurogenesis, molecular identity, and migratory destination of upper-layer cells of the cerebral cortex. Cereb Cortex *23*, 2632-2643.
Doyle, J.P., Dougherty, J.D., Heiman, M., Schmidt, E.F., Stevens, T.R., Ma, G., Bupp, S., Shrestha, P., Shah, R.D., Doughty, M.L*., et al.* (2008). Application of a translational profiling approach for the comparative analysis of CNS cell types. Cell *135*, 749-762.

Elias, M.C., Tozer, K.R., Silber, J.R., Mikheeva, S., Deng, M., Morrison, R.S., Manning, T.C., Silbergeld, D.L., Glackin, C.A., Reh, T.A*., et al.* (2005). TWIST is expressed in human gliomas and promotes invasion. Neoplasia *7*, 824-837.
Erbayraktar, Z., Alural, B., Erbayraktar, R.S., and Erkan, E.P. (2016). Cell division cycle 7-kinase inhibitor PHA-767491 hydrochloride suppresses glioblastoma growth and invasiveness. Cancer Cell Int *16*, 88.
Ferent, J., Cochard, L., Faure, H., Taddei, M., Hahn, H., Ruat, M., and Traiffort, E. (2014). Genetic activation of Hedgehog signaling unbalances the rate of neural stem cell renewal by increasing symmetric divisions. Stem Cell Reports *3*, 312-323.
Fietz, S.A., Kelava, I., Vogt, J., Wilsch-Brauninger, M., Stenzel, D., Fish, J.L., Corbeil, D., Riehn, A., Distler, W., Nitsch, R*., et al.* (2010). OSVZ progenitors of human and ferret neocortex are epithelial-like and expand by integrin signaling. Nat Neurosci *13*, 690-699.
Flomerfelt, F.A., and Gress, R.E. (2016). Analysis of Cell Proliferation and Homeostasis Using EdU Labeling. Methods Mol Biol *1323*, 211-220.
Foo, L.C., and Dougherty, J.D. (2013). Aldh1L1 is expressed by postnatal neural stem cells in vivo. Glia *61*, 1533-1541.
Freeman, M.R. (2010). Specification and morphogenesis of astrocytes. Science *330*, 774-778.
Furnari, F.B., Fenton, T., Bachoo, R.M., Mukasa, A., Stommel, J.M., Stegh, A., Hahn, W.C., Ligon, K.L., Louis, D.N., Brennan, C*., et al.* (2007). Malignant astrocytic glioma: genetics, biology, and paths to treatment. Genes Dev *21*, 2683-2710.
Galizia, C.G., and Lledo, P.-M. (2013). Neurosciences - From Molecule to Behavior: a university textbook (Berlin, Heidelberg: Springer Berlin Heidelberg : Imprint: Springer Spektrum).
Gallo, V., and Deneen, B. (2014). Glial development: the crossroads of regeneration and repair in the CNS. Neuron *83*, 283-308.
Garcia, A.D., Petrova, R., Eng, L., and Joyner, A.L. (2010). Sonic hedgehog regulates discrete populations of astrocytes in the adult mouse forebrain. J Neurosci *30*, 13597-13608.
Ge, W.P., and Jia, J.M. (2016). Local production of astrocytes in the cerebral cortex. Neuroscience *323*, 3-9.
Ge, W.P., Miyawaki, A., Gage, F.H., Jan, Y.N., and Jan, L.Y. (2012). Local generation of glia is a major astrocyte source in postnatal cortex. Nature *484*, 376-380.
Georgala, P.A., Manuel, M., and Price, D.J. (2011). The generation of superficial cortical layers is regulated by levels of the transcription factor Pax6. Cereb Cortex *21*, 81-94.
Ghosh, D., Ulasov, I.V., Chen, L., Harkins, L.E., Wallenborg, K., Hothi, P., Rostad, S., Hood, L., and Cobbs, C.S. (2016). TGFbeta-Responsive HMOX1 Expression Is Associated with Stemness and Invasion in Glioblastoma Multiforme. Stem Cells *34*, 2276-2289.
Gold, S.J., Ni, Y.G., Dohlman, H.G., and Nestler, E.J. (1997). Regulators of G-protein signaling (RGS) proteins: region-specific expression of nine subtypes in rat brain. J Neurosci *17*, 8024-8037.
Goldberg, A.L. (2003). Protein degradation and protection against misfolded or damaged proteins. Nature *426*, 895-899.
Gotz, M., and Barde, Y.A. (2005). Radial glial cells defined and major intermediates between embryonic stem cells and CNS neurons. Neuron *46*, 369-372.
Gotz, M., and Huttner, W.B. (2005). The cell biology of neurogenesis. Nat Rev Mol Cell Biol *6*, 777-788.
Gotz, M., Sirko, S., Beckers, J., and Irmler, M. (2015). Reactive astrocytes as neural stem or progenitor cells: In vivo lineage, In vitro potential, and Genome-wide expression analysis. Glia *63*, 1452-1468.
Gray, G.E., and Sanes, J.R. (1992). Lineage of radial glia in the chicken optic tectum. Development *114*, 271-283.
Guillemot, F. (2007). Cell fate specification in the mammalian telencephalon. Prog Neurobiol *83*, 37-52.
Guy, J., and Staiger, J.F. (2017). The Functioning of a Cortex without Layers. Front Neuroanat *11*, 54.

Halder, R., Hennion, M., Vidal, R.O., Shomroni, O., Rahman, R.U., Rajput, A., Centeno, T.P., van Bebber, F., Capece, V., Garcia Vizcaino, J.C*., et al.* (2016). DNA methylation changes in plasticity genes accompany the formation and maintenance of memory. Nat Neurosci *19*, 102-110.
Hansen, D.V., Lui, J.H., Parker, P.R., and Kriegstein, A.R. (2010). Neurogenic radial glia in the outer subventricular zone of human neocortex. Nature *464*, 554-561.
Hargreaves, D.C., and Crabtree, G.R. (2011). ATP-dependent chromatin remodeling: genetics, genomics and mechanisms. Cell Research *21*, 396.
Hartfuss, E., Galli, R., Heins, N., and Gotz, M. (2001). Characterization of CNS precursor subtypes and radial glia. Dev Biol *229*, 15-30.
Hartline, D.K. (2011). The evolutionary origins of glia. Glia *59*, 1215-1236.
Hayashi, Y., Edwards, N.A., Proescholdt, M.A., Oldfield, E.H., and Merrill, M.J. (2007). Regulation and function of aquaporin-1 in glioma cells. Neoplasia *9*, 777-787.
Heng, X., Guo, Q., Leung, A.W., and Li, J.Y. (2017). Analogous mechanism regulating formation of neocortical basal radial glia and cerebellar Bergmann glia. Elife *6*.
Herculano-Houzel, S. (2014). The glia/neuron ratio: how it varies uniformly across brain structures and species and what that means for brain physiology and evolution. Glia *62*, 1377-1391.
Hermanson, O., Jepsen, K., and Rosenfeld, M.G. (2002). N-CoR controls differentiation of neural stem cells into astrocytes. Nature *419*, 934-939.
Hirabayashi, Y., and Gotoh, Y. (2010). Epigenetic control of neural precursor cell fate during development. Nat Rev Neurosci *11*, 377-388.
Hirabayashi, Y., Suzki, N., Tsuboi, M., Endo, T.A., Toyoda, T., Shinga, J., Koseki, H., Vidal, M., and Gotoh, Y. (2009). Polycomb limits the neurogenic competence of neural precursor cells to promote astrogenic fate transition. Neuron *63*, 600-613.
Ho, L., and Crabtree, G.R. (2010). Chromatin remodelling during development. Nature *463*, 474-484.
Ho, L., Jothi, R., Ronan, J.L., Cui, K., Zhao, K., and Crabtree, G.R. (2009). An embryonic stem cell chromatin remodeling complex, esBAF, is an essential component of the core pluripotency transcriptional network. Proc Natl Acad Sci U S A *106*, 5187-5191.
Hobert, O. (2010). Neurogenesis in the nematode Caenorhabditis elegans. WormBook, 1-24.
Huang, L., Walter, V., Hayes, D.N., and Onaitis, M. (2014). Hedgehog-GLI signaling inhibition suppresses tumor growth in squamous lung cancer. Clin Cancer Res *20*, 1566-1575.
Iadecola, C., and Nedergaard, M. (2007). Glial regulation of the cerebral microvasculature. Nat Neurosci *10*, 1369-1376.
Irvin, D.M., McNeill, R.S., Bash, R.E., and Miller, C.R. (2017). Intrinsic Astrocyte Heterogeneity Influences Tumor Growth in Glioma Mouse Models. Brain Pathol *27*, 36-50.
Jagani, Z., Mora-Blanco, E.L., Sansam, C.G., McKenna, E.S., Wilson, B., Chen, D., Klekota, J., Tamayo, P., Nguyen, P.T., Tolstorukov, M*., et al.* (2010). Loss of the tumor suppressor Snf5 leads to aberrant activation of the Hedgehog-Gli pathway. Nat Med *16*, 1429-1433.
Jahn, H.M., Scheller, A., and Kirchhoff, F. (2015). Genetic control of astrocyte function in neural circuits. Front Cell Neurosci *9*, 310.
Juliandi, B., Abematsu, M., and Nakashima, K. (2010). Chromatin remodeling in neural stem cell differentiation, Vol 20.
Jun, F., Hong, J., Liu, Q., Guo, Y., Liao, Y., Huang, J., Wen, S., and Shen, L. (2017). Epithelial membrane protein 3 regulates TGF-beta signaling activation in CD44-high glioblastoma. Oncotarget *8*, 14343-14358.
Kadoch, C., and Crabtree, G.R. (2015). Mammalian SWI/SNF chromatin remodeling complexes and cancer: Mechanistic insights gained from human genomics. Sci Adv *1*, e1500447.
Kadoch, C., Williams, R.T., Calarco, J.P., Miller, E.L., Weber, C.M., Braun, S.M., Pulice, J.L., Chory, E.J., and Crabtree, G.R. (2017). Dynamics of BAF-Polycomb complex opposition on heterochromatin in normal and oncogenic states. Nat Genet *49*, 213-222.
Kaeser, M.D., Aslanian, A., Dong, M.Q., Yates, J.R., 3rd, and Emerson, B.M. (2008). BRD7, a novel PBAF-specific SWI/SNF subunit, is required for target gene activation and repression in embryonic stem cells. J Biol Chem *283*, 32254-32263.

Kang, H.G., Kim, D.H., Kim, S.J., Cho, Y., Jung, J., Jang, W., and Chun, K.H. (2016). Galectin-3 supports stemness in ovarian cancer stem cells by activation of the Notch1 intracellular domain. Oncotarget *7*, 68229-68241.
Kang, P., Lee, H.K., Glasgow, S.M., Finley, M., Donti, T., Gaber, Z.B., Graham, B.H., Foster, A.E., Novitch, B.G., Gronostajski, R.M.*, et al.* (2012). Sox9 and NFIA coordinate a transcriptional regulatory cascade during the initiation of gliogenesis. Neuron *74*, 79-94.
Kanski, R., van Strien, M.E., van Tijn, P., and Hol, E.M. (2014). A star is born: new insights into the mechanism of astrogenesis. Cell Mol Life Sci *71*, 433-447.
Kasiri, S., Shao, C., Chen, B., Wilson, A.N., Yenerall, P., Timmons, B.C., Girard, L., Tian, H., Behrens, C., Wistuba, II*, et al.* (2017). GLI1 Blockade Potentiates the Antitumor Activity of PI3K Antagonists in Lung Squamous Cell Carcinoma. Cancer Res *77*, 4448-4459.
Khakh, B.S., and Sofroniew, M.V. (2015). Diversity of astrocyte functions and phenotypes in neural circuits. Nat Neurosci *18*, 942-952.
Kidder, B., Palmer, S., and Knott, J. (2009). SWI/SNF-Brg1 Regulates Self-Renewal and Occupies Core Pluripotency-Related Genes in Embryonic Stem Cells, Vol 27.
Klein, E.A., and Assoian, R.K. (2008). Transcriptional regulation of the cyclin D1 gene at a glance. Journal of cell science *121*, 3853-3857.
Kriegstein, A., and Alvarez-Buylla, A. (2009). The glial nature of embryonic and adult neural stem cells. Annu Rev Neurosci *32*, 149-184.
Kriegstein, A., Noctor, S., and Martínez-Cerdeño, V. (2006). Patterns of neural stem and progenitor cell division may underlie evolutionary cortical expansion. Nature Reviews Neuroscience *7*, 883.
Kundu, S., Xiong, A., Spyrou, A., Wicher, G., Marinescu, V.D., Edqvist, P.D., Zhang, L., Essand, M., Dimberg, A., Smits, A.*, et al.* (2016). Heparanase Promotes Glioma Progression and Is Inversely Correlated with Patient Survival. Mol Cancer Res *14*, 1243-1253.
Kwan, K.Y., Sestan, N., and Anton, E.S. (2012). Transcriptional co-regulation of neuronal migration and laminar identity in the neocortex. Development *139*, 1535-1546.
Lachmann, A., Mazloom, A.R., Ma'ayan, A., Xu, H., Krishnan, J., and Berger, S.I. (2010). ChEA: transcription factor regulation inferred from integrating genome-wide ChIP-X experiments. Bioinformatics *26*, 2438-2444.
Lai, Y.J., Tsai, J.C., Tseng, Y.T., Wu, M.S., Liu, W.S., Lam, H.I., Yu, J.H., Nozell, S.E., and Benveniste, E.N. (2017). Small G protein Rac GTPases regulate the maintenance of glioblastoma stem-like cells in vitro and in vivo. Oncotarget *8*, 18031-18049.
Lauth, M., Bergstrom, A., Shimokawa, T., and Toftgard, R. (2007). Inhibition of GLI-mediated transcription and tumor cell growth by small-molecule antagonists. Proc Natl Acad Sci U S A *104*, 8455-8460.
LeComte, M.D., Shimada, I.S., Sherwin, C., and Spees, J.L. (2015). Notch1-STAT3-ETBR signaling axis controls reactive astrocyte proliferation after brain injury. Proc Natl Acad Sci U S A *112*, 8726-8731.
Lee, Y.S., Kang, J.W., Lee, Y.H., and Kim, D.W. (2011). ID4 mediates proliferation of astrocytes after excitotoxic damage in the mouse hippocampus. Anat Cell Biol *44*, 128-134.
Lei, I., West, J., Yan, Z., Gao, X., Fang, P., Dennis, J.H., Gnatovskiy, L., Wang, W., Kingston, R.E., and Wang, Z. (2015). BAF250a Protein Regulates Nucleosome Occupancy and Histone Modifications in Priming Embryonic Stem Cell Differentiation. J Biol Chem *290*, 19343-19352.
Leid, M., Ishmael, J.E., Avram, D., Shepherd, D., Fraulob, V., and Dolle, P. (2004). CTIP1 and CTIP2 are differentially expressed during mouse embryogenesis. Gene Expr Patterns *4*, 733-739.
Lessard, J., Wu, J.I., Ranish, J.A., Wan, M., Winslow, M.M., Staahl, B.T., Wu, H., Aebersold, R., Graef, I.A., and Crabtree, G.R. (2007). An essential switch in subunit composition of a chromatin remodeling complex during neural development. Neuron *55*, 201-215.
Leuba, G., and Garey, L.J. (1989). Comparison of neuronal and glial numerical density in primary and secondary visual cortex of man. Exp Brain Res *77*, 31-38.
Li, Q., Xie, W., Wang, N., Li, C., and Wang, M. (2018a). CDC7-dependent transcriptional regulation of RAD54L is essential for tumorigenicity and radio-resistance of glioblastoma. Transl Oncol *11*, 300-306.

Li, S., Chen, X., Mao, L., Zahid, K.R., Wen, J., Zhang, L., Zhang, M., Duan, J., Duan, J., Yin, X., *et al.* (2018b). Histone deacetylase 1 promotes glioblastoma cell proliferation and invasion via activation of PI3K/AKT and MEK/ERK signaling pathways. Brain Res *1692*, 154-162.
Li, X., Newbern, J.M., Wu, Y., Morgan-Smith, M., Zhong, J., Charron, J., and Snider, W.D. (2012). MEK Is a Key Regulator of Gliogenesis in the Developing Brain. Neuron *75*, 1035-1050.
Li, X.S., Trojer, P., Matsumura, T., Treisman, J.E., and Tanese, N. (2010). Mammalian SWI/SNF-A Subunit BAF250/ARID1 Is an E3 Ubiquitin Ligase That Targets Histone H2B. Molecular and Cellular Biology *30*, 1673-1688.
Liberzon, A., Birger, C., Thorvaldsdottir, H., Ghandi, M., Mesirov, J.P., and Tamayo, P. (2015). The Molecular Signatures Database (MSigDB) hallmark gene set collection. Cell Syst *1*, 417-425.
Liberzon, A., Subramanian, A., Pinchback, R., Thorvaldsdottir, H., Tamayo, P., and Mesirov, J.P. (2011). Molecular signatures database (MSigDB) 3.0. Bioinformatics *27*, 1739-1740.
Liddelow, S.A., and Barres, B.A. (2017). Reactive Astrocytes: Production, Function, and Therapeutic Potential. Immunity *46*, 957-967.
Liu, R.Z., Monckton, E.A., and Godbout, R. (2012). Regulation of the FABP7 gene by PAX6 in malignant glioma cells. Biochem Biophys Res Commun *422*, 482-487.
Lovatt, D., Sonnewald, U., Waagepetersen, H.S., Schousboe, A., He, W., Lin, J.H., Han, X., Takano, T., Wang, S., Sim, F.J., *et al.* (2007). The transcriptome and metabolic gene signature of protoplasmic astrocytes in the adult murine cortex. J Neurosci *27*, 12255-12266.
Love, M.I., Huber, W., and Anders, S. (2014). Moderated estimation of fold change and dispersion for RNA-seq data with DESeq2. Genome Biol *15*, 550.
Lui, J.H., Hansen, D.V., and Kriegstein, A.R. (2011). Development and evolution of the human neocortex. Cell *146*, 18-36.
Ma, S., Pang, C., Song, L., Guo, F., and Sun, H. (2015). Activating transcription factor 3 is overexpressed in human glioma and its knockdown in glioblastoma cells causes growth inhibition both in vitro and in vivo. Int J Mol Med *35*, 1561-1573.
Madisen, L., Zwingman, T.A., Sunkin, S.M., Oh, S.W., Zariwala, H.A., Gu, H., Ng, L.L., Palmiter, R.D., Hawrylycz, M.J., Jones, A.R., *et al.* (2010). A robust and high-throughput Cre reporting and characterization system for the whole mouse brain. Nat Neurosci *13*, 133-140.
Maher, F., Vannucci, S., and Simpson, I. (1994). Glucose transporter proteins in brain, Vol 8.
Malatesta, P., Hartfuss, E., and Gotz, M. (2000). Isolation of radial glial cells by fluorescent-activated cell sorting reveals a neuronal lineage. Development *127*, 5253-5263.
Manfredsson, F.P. (2016). Gene therapy for neurological disorders methods and protocols (New York: Humana Press).
Mao, X.G., Hutt-Cabezas, M., Orr, B.A., Weingart, M., Taylor, I., Rajan, A.K., Odia, Y., Kahlert, U., Maciaczyk, J., Nikkhah, G., *et al.* (2013). LIN28A facilitates the transformation of human neural stem cells and promotes glioblastoma tumorigenesis through a pro-invasive genetic program. Oncotarget *4*, 1050-1064.
Marin-Padilla, M. (1978). Dual origin of the mammalian neocortex and evolution of the cortical plate. . Anat Embryol (Berl), 109-126.
Marshall, C.A., and Goldman, J.E. (2002). Subpallial dlx2-expressing cells give rise to astrocytes and oligodendrocytes in the cerebral cortex and white matter. J Neurosci *22*, 9821-9830.
Martin, R., Bajo-Graneras, R., Moratalla, R., Perea, G., and Araque, A. (2015). Circuit-specific signaling in astrocyte-neuron networks in basal ganglia pathways. Science *349*, 730-734.
Martynoga, B., Drechsel, D., and Guillemot, F. (2012). Molecular control of neurogenesis: a view from the mammalian cerebral cortex. Cold Spring Harb Perspect Biol *4*.
Mashtalir, N., D'Avino, A.R., Michel, B.C., Luo, J., Pan, J., Otto, J.E., Zullow, H.J., McKenzie, Z.M., Kubiak, R.L., St Pierre, R., *et al.* (2018). Modular Organization and Assembly of SWI/SNF Family Chromatin Remodeling Complexes. Cell *175*, 1272-1288 e1220.
Mathew, E., Collins, M.A., Fernandez-Barrena, M.G., Holtz, A.M., Yan, W., Hogan, J.O., Tata, Z., Allen, B.L., Fernandez-Zapico, M.E., and di Magliano, M.P. (2014). The transcription factor GLI1 modulates the inflammatory response during pancreatic tissue remodeling. J Biol Chem *289*, 27727-27743.

Matsumoto, S., Banine, F., Struve, J., Xing, R., Adams, C., Liu, Y., Metzger, D., Chambon, P., Rao, M.S., and Sherman, L.S. (2006). Brg1 is required for murine neural stem cell maintenance and gliogenesis. Dev Biol *289*, 372-383.
Mayer, S.I., Rossler, O.G., Endo, T., Charnay, P., and Thiel, G. (2009). Epidermal-growth-factor-induced proliferation of astrocytes requires Egr transcription factors. J Cell Sci *122*, 3340-3350.
McCubrey, J.A., Steelman, L.S., Bertrand, F.E., Davis, N.M., Sokolosky, M., Abrams, S.L., Montalto, G., D'Assoro, A.B., Libra, M., Nicoletti, F.*, et al.* (2014). GSK-3 as potential target for therapeutic intervention in cancer. Oncotarget *5*, 2881-2911.
McKenzie, A.T., Wang, M., Hauberg, M.E., Fullard, J.F., Kozlenkov, A., Keenan, A., Hurd, Y.L., Dracheva, S., Casaccia, P., Roussos, P.*, et al.* (2018). Brain Cell Type Specific Gene Expression and Co-expression Network Architectures. Sci Rep *8*, 8868.
Meng, Z.X., Tao, W., Sun, J., Wang, Q., Mi, L., and Lin, J.D. (2018). Uncoupling Exercise Bioenergetics From Systemic Metabolic Homeostasis by Conditional Inactivation of Baf60 in Skeletal Muscle. Diabetes *67*, 85-97.
Metaxakis, A., Petratou, D., and Tavernarakis, N. (2018). Multimodal sensory processing in Caenorhabditis elegans. Open Biol *8*.
Meyer, K., and Kaspar, B.K. (2017). Glia-neuron interactions in neurological diseases: Testing non-cell autonomy in a dish. Brain Res *1656*, 27-39.
Michelucci, A., Bithell, A., Burney, M.J., Johnston, C.E., Wong, K.Y., Teng, S.W., Desai, J., Gumbleton, N., Anderson, G., Stanton, L.W.*, et al.* (2016). The Neurogenic Potential of Astrocytes Is Regulated by Inflammatory Signals. Mol Neurobiol *53*, 3724-3739.
Miller, F.D., and Gauthier, A.S. (2007). Timing is everything: making neurons versus glia in the developing cortex. Neuron *54*, 357-369.
Minocha, S., Valloton, D., Arsenijevic, Y., Cardinaux, J.R., Guidi, R., Hornung, J.P., and Lebrand, C. (2017). Nkx2.1 regulates the generation of telencephalic astrocytes during embryonic development. Sci Rep *7*, 43093.
Minocha, S., Valloton, D., Ypsilanti, A.R., Fiumelli, H., Allen, E.A., Yanagawa, Y., Marin, O., Chedotal, A., Hornung, J.P., and Lebrand, C. (2015). Nkx2.1-derived astrocytes and neurons together with Slit2 are indispensable for anterior commissure formation. Nat Commun *6*, 6887.
Mission, J.P., Takahashi, T., and Caviness, V.S., Jr. (1991). Ontogeny of radial and other astroglial cells in murine cerebral cortex. Glia *4*, 138-148.
Miyata, T., Kawaguchi, A., Okano, H., and Ogawa, M. (2001). Asymmetric inheritance of radial glial fibers by cortical neurons. Neuron *31*, 727-741.
Molofsky, A.V., and Deneen, B. (2015). Astrocyte development: A Guide for the Perplexed. Glia *63*, 1320-1329.
Molofsky, A.V., Kelley, K.W., Tsai, H.H., Redmond, S.A., Chang, S.M., Madireddy, L., Chan, J.R., Baranzini, S.E., Ullian, E.M., and Rowitch, D.H. (2014). Astrocyte-encoded positional cues maintain sensorimotor circuit integrity. Nature *509*, 189-194.
Molofsky, A.V., Krencik, R., Ullian, E.M., Tsai, H.H., Deneen, B., Richardson, W.D., Barres, B.A., and Rowitch, D.H. (2012). Astrocytes and disease: a neurodevelopmental perspective. Genes Dev *26*, 891-907.
Molyneaux, B.J., Arlotta, P., Menezes, J.R., and Macklis, J.D. (2007). Neuronal subtype specification in the cerebral cortex. Nat Rev Neurosci *8*, 427-437.
Moncayo, G., Grzmil, M., Smirnova, T., Zmarz, P., Huber, R.M., Hynx, D., Kohler, H., Wang, Y., Hotz, H.R., Hynes, N.E.*, et al.* (2018). SYK inhibition blocks proliferation and migration of glioma cells and modifies the tumor microenvironment. Neuro Oncol *20*, 621-631.
Nagao, M., Ogata, T., Sawada, Y., and Gotoh, Y. (2016). Zbtb20 promotes astrocytogenesis during neocortical development. Nat Commun *7*, 11102.
Naka-Kaneda, H., Nakamura, S., Igarashi, M., Aoi, H., Kanki, H., Tsuyama, J., Tsutsumi, S., Aburatani, H., Shimazaki, T., and Okano, H. (2014). The miR-17/106-p38 axis is a key regulator of the neurogenic-to-gliogenic transition in developing neural stem/progenitor cells. Proc Natl Acad Sci U S A *111*, 1604-1609.

Nakashima, K., Takizawa, T., Ochiai, W., Yanagisawa, M., Hisatsune, T., Nakafuku, M., Miyazono, K., Kishimoto, T., Kageyama, R., and Taga, T. (2001). BMP2-mediated alteration in the developmental pathway of fetal mouse brain cells from neurogenesis to astrocytogenesis. Proc Natl Acad Sci U S A *98*, 5868-5873.
Namihira, M., and Nakashima, K. (2013). Mechanisms of astrocytogenesis in the mammalian brain. Curr Opin Neurobiol *23*, 921-927.
Narayanan, R. (2017). BAF155 regulates the genesis of basal progenitors through both Pax6-dependent and independent mechanisms during cerebral cortex development.
Narayanan, R., Pham, L., Kerimoglu, C., Watanabe, T., Castro Hernandez, R., Sokpor, G., Ulmke, P.A., Kiszka, K.A., Tonchev, A.B., Rosenbusch, J.*, et al.* (2018). Chromatin Remodeling BAF155 Subunit Regulates the Genesis of Basal Progenitors in Developing Cortex. iScience *4*, 109-126.
Narayanan, R., Pirouz, M., Kerimoglu, C., Pham, L., Wagener, R.J., Kiszka, K.A., Rosenbusch, J., Seong, R.H., Kessel, M., Fischer, A.*, et al.* (2015). Loss of BAF (mSWI/SNF) Complexes Causes Global Transcriptional and Chromatin State Changes in Forebrain Development. Cell Rep *13*, 1842-1854.
Narayanan, R., and Tuoc, T. (2014a). Roles of chromatin remodeling BAF complex in neural differentiation and reprogramming, Vol 356.
Narayanan, R., and Tuoc, T.C. (2014b). Roles of chromatin remodeling BAF complex in neural differentiation and reprogramming. Cell Tissue Res *356*, 575-584.
Nedergaard, M., Ransom, B., and Goldman, S.A. (2003). New roles for astrocytes: redefining the functional architecture of the brain. Trends Neurosci *26*, 523-530.
Nguyen, H., Kerimoglu, C., Pirouz, M., Pham, L., Kiszka, K.A., Sokpor, G., Sakib, M.S., Rosenbusch, J., Teichmann, U., Seong, R.H.*, et al.* (2018). Epigenetic Regulation by BAF Complexes Limits Neural Stem Cell Proliferation by Suppressing Wnt Signaling in Late Embryonic Development. Stem Cell Reports *10*, 1734-1750.
Nguyen, H., Sokpor, G., Pham, L., Rosenbusch, J., Stoykova, A., Staiger, J.F., and Tuoc, T. (2016). Epigenetic regulation by BAF (mSWI/SNF) chromatin remodeling complexes is indispensable for embryonic development. Cell Cycle *15*, 1317-1324.
Nilsson, M., Unden, A.B., Krause, D., Malmqwist, U., Raza, K., Zaphiropoulos, P.G., and Toftgard, R. (2000). Induction of basal cell carcinomas and trichoepitheliomas in mice overexpressing GLI-1. Proc Natl Acad Sci U S A *97*, 3438-3443.
Ninkovic, J., Steiner-Mezzadri, A., Jawerka, M., Akinci, U., Masserdotti, G., Petricca, S., Fischer, J., von Holst, A., Beckers, J., Lie, C.D.*, et al.* (2013). The BAF complex interacts with Pax6 in adult neural progenitors to establish a neurogenic cross-regulatory transcriptional network. Cell Stem Cell *13*, 403-418.
Noctor, S.C., Martinez-Cerdeno, V., Ivic, L., and Kriegstein, A.R. (2004). Cortical neurons arise in symmetric and asymmetric division zones and migrate through specific phases. Nat Neurosci *7*, 136-144.
Noctor, S.C., Martinez-Cerdeno, V., and Kriegstein, A.R. (2008). Distinct behaviors of neural stem and progenitor cells underlie cortical neurogenesis. J Comp Neurol *508*, 28-44.
O'Brien, E.R., Howarth, C., and Sibson, N.R. (2013). The role of astrocytes in CNS tumors: pre-clinical models and novel imaging approaches. Front Cell Neurosci *7*, 40.
Obara, M., Szeliga, M., and Albrecht, J. (2008). Regulation of pH in the mammalian central nervous system under normal and pathological conditions: facts and hypotheses. Neurochem Int *52*, 905-919.
Oberheim, N.A., Goldman, S.A., and Nedergaard, M. (2012). Heterogeneity of astrocytic form and function. Methods Mol Biol *814*, 23-45.
Oberheim, N.A., Takano, T., Han, X., He, W., Lin, J.H., Wang, F., Xu, Q., Wyatt, J.D., Pilcher, W., Ojemann, J.G.*, et al.* (2009). Uniquely hominid features of adult human astrocytes. J Neurosci *29*, 3276-3287.
Oberheim, N.A., Wang, X., Goldman, S., and Nedergaard, M. (2006). Astrocytic complexity distinguishes the human brain. Trends Neurosci *29*, 547-553.
Oh, J., Sohn, D.H., Ko, M., Chung, H., Jeon, S.H., and Seong, R.H. (2008). BAF60a interacts with p53 to recruit the SWI/SNF complex. J Biol Chem *283*, 11924-11934.

Olave, I., Wang, W., Xue, Y., Kuo, A., and Crabtree, G.R. (2002). Identification of a polymorphic, neuron-specific chromatin remodeling complex. Genes Dev *16*, 2509-2517.
Oliver, T.G., Grasfeder, L.L., Carroll, A.L., Kaiser, C., Gillingham, C.L., Lin, S.M., Wickramasinghe, R., Scott, M.P., and Wechsler-Reya, R.J. (2003). Transcriptional profiling of the Sonic hedgehog response: a critical role for N-myc in proliferation of neuronal precursors. Proc Natl Acad Sci U S A *100*, 7331-7336.
Palma, V., Lim, D.A., Dahmane, N., Sanchez, P., Brionne, T.C., Herzberg, C.D., Gitton, Y., Carleton, A., Alvarez-Buylla, A., and Ruiz i Altaba, A. (2005). Sonic hedgehog controls stem cell behavior in the postnatal and adult brain. Development *132*, 335-344.
Panamarova, M., Cox, A., Wicher, K.B., Butler, R., Bulgakova, N., Jeon, S., Rosen, B., Seong, R.H., Skarnes, W., Crabtree, G.*, et al.* (2016). The BAF chromatin remodelling complex is an epigenetic regulator of lineage specification in the early mouse embryo. Development *143*, 1271-1283.
Park, J.W., Wollmann, G., Urbiola, C., Fogli, B., Florio, T., Geley, S., and Klimaschewski, L. (2018). Sprouty2 enhances the tumorigenic potential of glioblastoma cells. Neuro Oncol *20*, 1044-1054.
Paxinos, G., and Franklin, K.B.J. (2001). The mouse brain in stereotaxic coordinates, 2nd edn (San Diego: Academic Press).
Paxinos, G., Halliday, G., Watson, C., Koutcherov, Y., and Wang, H. (2006). Atlas of the Developing Mouse Brain: E17.5, P0 and P6
Pelczar, P., Zibat, A., van Dop, W.A., Heijmans, J., Bleckmann, A., Gruber, W., Nitzki, F., Uhmann, A., Guijarro, M.V., Hernando, E.*, et al.* (2013). Inactivation of Patched1 in mice leads to development of gastrointestinal stromal-like tumors that express Pdgfralpha but not kit. Gastroenterology *144*, 134-144 e136.
Pellerin, L., and Magistretti, P.J. (1994). Glutamate uptake into astrocytes stimulates aerobic glycolysis: a mechanism coupling neuronal activity to glucose utilization. Proc Natl Acad Sci U S A *91*, 10625-10629.
Pellerin, L., and Magistretti, P.J. (2012). Sweet sixteen for ANLS. J Cereb Blood Flow Metab *32*, 1152-1166.
Perea, G., Navarrete, M., and Araque, A. (2009). Tripartite synapses: astrocytes process and control synaptic information. Trends Neurosci *32*, 421-431.
Perea, G., Sur, M., and Araque, A. (2014). Neuron-glia networks: integral gear of brain function. Front Cell Neurosci *8*, 378.
Peres, E.A., Valable, S., Guillamo, J.S., Marteau, L., Bernaudin, J.F., Roussel, S., Lechapt-Zalcman, E., Bernaudin, M., and Petit, E. (2011). Targeting the erythropoietin receptor on glioma cells reduces tumour growth. Exp Cell Res *317*, 2321-2332.
Petrik, D., Latchney, S.E., Masiulis, I., Yun, S., Zhang, Z., Wu, J.I., and Eisch, A.J. (2015). Chromatin Remodeling Factor Brg1 Supports the Early Maintenance and Late Responsiveness of Nestin-Lineage Adult Neural Stem and Progenitor Cells. Stem Cells *33*, 3655-3665.
Phelan, M.L., Sif, S., Narlikar, G.J., and Kingston, R.E. (1999). Reconstitution of a core chromatin remodeling complex from SWI/SNF subunits. Mol Cell *3*, 247-253.
Pierfelice, T.J., Schreck, K.C., Dang, L., Asnaghi, L., Gaiano, N., and Eberhart, C.G. (2011). Notch3 activation promotes invasive glioma formation in a tissue site-specific manner. Cancer Res *71*, 1115-1125.
Pinto, L., Mader, M.T., Irmler, M., Gentilini, M., Santoni, F., Drechsel, D., Blum, R., Stahl, R., Bulfone, A., Malatesta, P.*, et al.* (2008). Prospective isolation of functionally distinct radial glial subtypes--lineage and transcriptome analysis. Mol Cell Neurosci *38*, 15-42.
Pitter, K.L., Tamagno, I., Feng, X., Ghosal, K., Amankulor, N., Holland, E.C., and Hambardzumyan, D. (2014). The SHH/Gli pathway is reactivated in reactive glia and drives proliferation in response to neurodegeneration-induced lesions. Glia *62*, 1595-1607.
Pixley, S.K., and de Vellis, J. (1984). Transition between immature radial glia and mature astrocytes studied with a monoclonal antibody to vimentin. Brain Res *317*, 201-209.
Pollen, A.A., Nowakowski, T.J., Chen, J., Retallack, H., Sandoval-Espinosa, C., Nicholas, C.R., Shuga, J., Liu, S.J., Oldham, M.C., Diaz, A.*, et al.* (2015). Molecular identity of human outer radial glia during cortical development. Cell *163*, 55-67.

Pontious, A., Kowalczyk, T., Englund, C., and Hevner, R.F. (2008). Role of intermediate progenitor cells in cerebral cortex development. Dev Neurosci *30*, 24-32.
Popovitchenko, T., and Rasin, M.R. (2017). Transcriptional and Post-Transcriptional Mechanisms of the Development of Neocortical Lamination. Front Neuroanat *11*, 102.
Porter, A.G., and Janicke, R.U. (1999). Emerging roles of caspase-3 in apoptosis. Cell Death Differ *6*, 99-104.
Poston, R.G., Dunn, C.J., Sarkar, P., and Saha, R.N. (2018). Persistent 6-OH-BDE-47 exposure impairs functional neuronal maturation and alters expression of neurodevelopmentally-relevant chromatin remodelers. Environ Epigenet *4*, dvx020.
Pun, P., Kan, E.M., Salim, A., Li, Z.H., Ng, K.C., Moochhala, S., Ling, E.-A., Tan, M.H., and Lu, J. (2011). Low Level Primary Blast Injury in Rodent Brain. Frontiers in Neurology *2*.
Qiu, X., Jiao, J., Li, Y., and Tian, T. (2016). Overexpression of FZD7 promotes glioma cell proliferation by upregulating TAZ. Oncotarget *7*, 85987-85999.
Rakic, P. (1974). Neurons in Rhesus Monkey Visual Cortex: Systematic Relation between Time of Origin and Eventual Disposition. Science *183*, 425-427.
Rakic, P. (1982). Early developmental events: Cell lineages, acquisition of neuronal positions, and areal and laminar development, Vol 20.
Robel, S., Berninger, B., and Gotz, M. (2011). The stem cell potential of glia: lessons from reactive gliosis. Nat Rev Neurosci *12*, 88-104.
Robertson, J.M. (2013). Astrocyte domains and the three-dimensional and seamless expression of consciousness and explicit memories. Med Hypotheses *81*, 1017-1024.
Robertson, J.M. (2014). Astrocytes and the evolution of the human brain. Med Hypotheses *82*, 236-239.
Ronan, J.L., Wu, W., and Crabtree, G.R. (2013). From neural development to cognition: unexpected roles for chromatin. Nat Rev Genet *14*, 347-359.
Rose, C.R., Felix, L., Zeug, A., Dietrich, D., Reiner, A., and Henneberger, C. (2017). Astroglial Glutamate Signaling and Uptake in the Hippocampus. Front Mol Neurosci *10*, 451.
Rowitch, D.H., and Kriegstein, A.R. (2010). Developmental genetics of vertebrate glial-cell specification. Nature *468*, 214-222.
Runic, R., Lockwood, C.J., Ma, Y., Dipasquale, B., and Guller, S. (1996). Expression of Fas ligand by human cytotrophoblasts: implications in placentation and fetal survival. J Clin Endocrinol Metab *81*, 3119-3122.
Rush, S.Z., Abel, T.W., Valadez, J.G., Pearson, M., and Cooper, M.K. (2010). Activation of the Hedgehog pathway in pilocytic astrocytomas. Neuro Oncol *12*, 790-798.
Sahara, S., and O'Leary, D.D. (2009). Fgf10 regulates transition period of cortical stem cell differentiation to radial glia controlling generation of neurons and basal progenitors. Neuron *63*, 48-62.
Saito, T. (2006). In vivo electroporation in the embryonic mouse central nervous system. Nat Protoc *1*, 1552-1558.
Saito, T., and Nakatsuji, N. (2001). Efficient gene transfer into the embryonic mouse brain using in vivo electroporation. Dev Biol *240*, 237-246.
Samanta, J., Grund, E.M., Silva, H.M., Lafaille, J.J., Fishell, G., and Salzer, J.L. (2015). Inhibition of Gli1 mobilizes endogenous neural stem cells for remyelination. Nature *526*, 448-452.
Sanvoranart, T., Supokawej, A., Kheolamai, P., Y, U.P., Poungvarin, N., Sathornsumetee, S., and Issaragrisil, S. (2016). Targeting Netrin-1 in glioblastoma stem-like cells inhibits growth, invasion, and angiogenesis. Tumour Biol *37*, 14949-14960.
Satheesha, S., Manzella, G., Bovay, A., Casanova, E.A., Bode, P.K., Belle, R., Feuchtgruber, S., Jaaks, P., Dogan, N., Koscielniak, E.*, et al.* (2016). Targeting hedgehog signaling reduces self-renewal in embryonal rhabdomyosarcoma. Oncogene *35*, 2020-2030.
Sauer, B. (1998). Inducible gene targeting in mice using the Cre/lox system. Methods *14*, 381-392.
Scemes, E., and Spray, D.C. (2004). The Astrocytic Syncytium. In, pp. 165-179.
Schaeren-Wiemers, N., Andre, E., Kapfhammer, J.P., and Becker-Andre, M. (1997). The expression pattern of the orphan nuclear receptor RORbeta in the developing and adult rat nervous system

suggests a role in the processing of sensory information and in circadian rhythm. Eur J Neurosci *9*, 2687-2701.
Schildge, S., Bohrer, C., Beck, K., and Schachtrup, C. (2013). Isolation and culture of mouse cortical astrocytes. J Vis Exp.
Schitine, C., Nogaroli, L., Costa, M.R., and Hedin-Pereira, C. (2015). Astrocyte heterogeneity in the brain: from development to disease. Front Cell Neurosci *9*, 76.
Schiweck, J., Eickholt, B.J., and Murk, K. (2018). Important Shapeshifter: Mechanisms Allowing Astrocytes to Respond to the Changing Nervous System During Development, Injury and Disease. Front Cell Neurosci *12*, 261.
Schmechel, D.E., and Rakic, P. (1979). A Golgi study of radial glial cells in developing monkey telencephalon: morphogenesis and transformation into astrocytes. Anat Embryol (Berl) *156*, 115-152.
Schnitzer, J., Franke, W.W., and Schachner, M. (1981). Immunocytochemical demonstration of vimentin in astrocytes and ependymal cells of developing and adult mouse nervous system. J Cell Biol *90*, 435-447.
Scholzen, T., and Gerdes, J. (2000). The Ki-67 protein: from the known and the unknown. J Cell Physiol *182*, 311-322.
Scott, C.E., Wynn, S.L., Sesay, A., Cruz, C., Cheung, M., Gomez Gaviro, M.V., Booth, S., Gao, B., Cheah, K.S., Lovell-Badge, R*., et al.* (2010). SOX9 induces and maintains neural stem cells. Nat Neurosci *13*, 1181-1189.
Seyfried, N.T., Huysentruyt, L.C., Atwood, J.A., 3rd, Xia, Q., Seyfried, T.N., and Orlando, R. (2008). Up-regulation of NG2 proteoglycan and interferon-induced transmembrane proteins 1 and 3 in mouse astrocytoma: a membrane proteomics approach. Cancer Lett *263*, 243-252.
Shibata, T., Yamada, K., Watanabe, M., Ikenaka, K., Wada, K., Tanaka, K., and Inoue, Y. (1997). Glutamate transporter GLAST is expressed in the radial glia-astrocyte lineage of developing mouse spinal cord. J Neurosci *17*, 9212-9219.
Simard, M., and Nedergaard, M. (2004). The neurobiology of glia in the context of water and ion homeostasis. Neuroscience *129*, 877-896.
Sloan, S.A., and Barres, B.A. (2014). Mechanisms of astrocyte development and their contributions to neurodevelopmental disorders. Curr Opin Neurobiol *27*, 75-81.
Sofroniew, M.V. (2009). Molecular dissection of reactive astrogliosis and glial scar formation. Trends Neurosci *32*, 638-647.
Sofroniew, M.V. (2015). Astrocyte barriers to neurotoxic inflammation. Nat Rev Neurosci *16*, 249-263.
Sofroniew, M.V., and Vinters, H.V. (2010). Astrocytes: biology and pathology. Acta Neuropathol *119*, 7-35.
Sohn, D.H., Lee, K.Y., Lee, C., Oh, J., Chung, H., Jeon, S.H., and Seong, R.H. (2007). SRG3 interacts directly with the major components of the SWI/SNF chromatin remodeling complex and protects them from proteasomal degradation. J Biol Chem *282*, 10614-10624.
Sokpor, G., Xie, Y., Rosenbusch, J., and Tuoc, T. (2017). Chromatin Remodeling BAF (SWI/SNF) Complexes in Neural Development and Disorders. Front Mol Neurosci *10*, 243.
Son, E.Y., and Crabtree, G.R. (2014). The role of BAF (mSWI/SNF) complexes in mammalian neural development. Am J Med Genet C Semin Med Genet *166C*, 333-349.
Srinivasan, R., Lu, T.Y., Chai, H., Xu, J., Huang, B.S., Golshani, P., Coppola, G., and Khakh, B.S. (2016). New Transgenic Mouse Lines for Selectively Targeting Astrocytes and Studying Calcium Signals in Astrocyte Processes In Situ and In Vivo. Neuron *92*, 1181-1195.
Staahl, B.T., Tang, J., Wu, W., Sun, A., Gitler, A.D., Yoo, A.S., and Crabtree, G.R. (2013). Kinetic analysis of npBAF to nBAF switching reveals exchange of SS18 with CREST and integration with neural developmental pathways. J Neurosci *33*, 10348-10361.
Stiles, C.D., and Rowitch, D.H. (2008). Glioma stem cells: a midterm exam. Neuron *58*, 832-846.
Su, X., Liu, X., Ni, L., Shi, W., Zhu, H., Shi, J., Chen, J., Gu, Z., Gao, Y., Lan, Q*., et al.* (2016). GFAP expression is regulated by Pax3 in brain glioma stem cells. Oncol Rep *36*, 1277-1284.

Subramanian, A., Tamayo, P., Mootha, V.K., Mukherjee, S., Ebert, B.L., Gillette, M.A., Paulovich, A., Pomeroy, S.L., Golub, T.R., Lander, E.S*., et al.* (2005). Gene set enrichment analysis: a knowledge-based approach for interpreting genome-wide expression profiles. Proc Natl Acad Sci U S A *102*, 15545-15550.
Sun, W., Cornwell, A., Li, J., Peng, S., Osorio, M.J., Aalling, N., Wang, S., Benraiss, A., Lou, N., Goldman, S.A*., et al.* (2017). SOX9 Is an Astrocyte-Specific Nuclear Marker in the Adult Brain Outside the Neurogenic Regions. J Neurosci *37*, 4493-4507.
Szabo-Rogers, H.L., Smithers, L.E., Yakob, W., and Liu, K.J. (2010). New directions in craniofacial morphogenesis. Dev Biol *341*, 84-94.
Tabata, H. (2015). Diverse subtypes of astrocytes and their development during corticogenesis. Front Neurosci *9*, 114.
Tang, G., Liu, D., Xiao, G., Liu, Q., and Yuan, J. (2016). Transcriptional repression of FOXO1 by KLF4 contributes to glioma progression. Oncotarget *7*, 81757-81767.
Tang, J., Yoo, A.S., and Crabtree, G.R. (2013). Reprogramming human fibroblasts to neurons by recapitulating an essential microRNA-chromatin switch. Curr Opin Genet Dev *23*, 591-598.
Tansey, F.A., Farooq, M., and Cammer, W. (1991). Glutamine synthetase in oligodendrocytes and astrocytes: new biochemical and immunocytochemical evidence. J Neurochem *56*, 266-272.
Tiberi, L., van den Ameele, J., Dimidschstein, J., Piccirilli, J., Gall, D., Herpoel, A., Bilheu, A., Bonnefont, J., Iacovino, M., Kyba, M*., et al.* (2012). BCL6 controls neurogenesis through Sirt1-dependent epigenetic repression of selective Notch targets. Nat Neurosci *15*, 1627-1635.
Tien, A.-C., Tsai, H.-H., Molofsky, A.V., McMahon, M., Foo, L.C., Kaul, A., Dougherty, J.D., Heintz, N., Gutmann, D.H., Barres, B.A*., et al.* (2012). Regulated temporal-spatial astrocyte precursor cell proliferation involves BRAF signalling in mammalian spinal cord. Development *139*, 2477-2487.
Tramontin, A.D., Garcia-Verdugo, J.M., Lim, D.A., and Alvarez-Buylla, A. (2003). Postnatal development of radial glia and the ventricular zone (VZ): a continuum of the neural stem cell compartment. Cereb Cortex *13*, 580-587.
Trotter, K.W., and Archer, T.K. (2008). The BRG1 transcriptional coregulator. Nucl Recept Signal *6*, e004.
Tsai, H.H., Li, H., Fuentealba, L.C., Molofsky, A.V., Taveira-Marques, R., Zhuang, H., Tenney, A., Murnen, A.T., Fancy, S.P., Merkle, F*., et al.* (2012). Regional astrocyte allocation regulates CNS synaptogenesis and repair. Science *337*, 358-362.
Tuoc, T., Dere, E., Radyushkin, K., Pham, L., Nguyen, H., Tonchev, A.B., Sun, G., Ronnenberg, A., Shi, Y., Staiger, J.F*., et al.* (2017). Ablation of BAF170 in Developing and Postnatal Dentate Gyrus Affects Neural Stem Cell Proliferation, Differentiation, and Learning. Mol Neurobiol *54*, 4618-4635.
Tuoc, T., Narayanan, R., and Stoykova, A. (2013a). BAF chromatin remodeling complex: Cortical size regulation and beyond, Vol 12.
Tuoc, T.C., Boretius, S., Sansom, S.N., Pitulescu, M.E., Frahm, J., Livesey, F.J., and Stoykova, A. (2013b). Chromatin regulation by BAF170 controls cerebral cortical size and thickness. Dev Cell *25*, 256-269.
Ugbode, C.I., Smith, I., Whalley, B.J., Hirst, W.D., and Rattray, M. (2017). Sonic hedgehog signalling mediates astrocyte crosstalk with neurons to confer neuroprotection. J Neurochem *142*, 429-443.
Underhill, C., Qutob, M.S., Yee, S.P., and Torchia, J. (2000). A novel nuclear receptor corepressor complex, N-CoR, contains components of the mammalian SWI/SNF complex and the corepressor KAP-1. J Biol Chem *275*, 40463-40470.
Vasile, F., Dossi, E., and Rouach, N. (2017). Human astrocytes: structure and functions in the healthy brain. Brain Struct Funct *222*, 2017-2029.
Vega, C.J., and Peterson, D.A. (2005). Stem cell proliferative history in tissue revealed by temporal halogenated thymidine analog discrimination. Nat Methods *2*, 167-169.
Verkhratsky, A., Zorec, R., and Parpura, V. (2017). Stratification of astrocytes in healthy and diseased brain. Brain Pathol *27*, 629-644.
Vogel-Ciernia, A., and Wood, M.A. (2014). Neuron-specific chromatin remodeling: a missing link in epigenetic mechanisms underlying synaptic plasticity, memory, and intellectual disability disorders. Neuropharmacology *80*, 18-27.

Voigt, T. (1989). Development of glial cells in the cerebral wall of ferrets: direct tracing of their transformation from radial glia into astrocytes. J Comp Neurol *289*, 74-88.
von Bartheld, C.S., Bahney, J., and Herculano-Houzel, S. (2016). The search for true numbers of neurons and glial cells in the human brain: A review of 150 years of cell counting. J Comp Neurol *524*, 3865-3895.
Wagener, R.J., David, C., Zhao, S., Haas, C.A., and Staiger, J.F. (2010). The somatosensory cortex of reeler mutant mice shows absent layering but intact formation and behavioral activation of columnar somatotopic maps. J Neurosci *30*, 15700-15709.
Wallace, V.A., and Raff, M.C. (1999). A role for Sonic hedgehog in axon-to-astrocyte signalling in the rodent optic nerve. Development *126*, 2901-2909.
Walsh, A.M., Kapoor, G.S., Buonato, J.M., Mathew, L.K., Bi, Y., Davuluri, R.V., Martinez-Lage, M., Simon, M.C., O'Rourke, D.M., and Lazzara, M.J. (2015). Sprouty2 Drives Drug Resistance and Proliferation in Glioblastoma. Mol Cancer Res *13*, 1227-1237.
Wang, D., Grammer, J.R., Cobbs, C.S., Stewart, J.E., Jr., Liu, Z., Rhoden, R., Hecker, T.P., Ding, Q., and Gladson, C.L. (2000). p125 focal adhesion kinase promotes malignant astrocytoma cell proliferation in vivo. J Cell Sci *113 Pt 23*, 4221-4230.
Wang, L., Hou, S., and Han, Y.G. (2016a). Hedgehog signaling promotes basal progenitor expansion and the growth and folding of the neocortex. Nat Neurosci *19*, 888-896.
Wang, W., Xue, Y., Zhou, S., Kuo, A., Cairns, B.R., and Crabtree, G.R. (1996). Diversity and specialization of mammalian SWI/SNF complexes. Genes Dev *10*, 2117-2130.
Wang, X., Haswell, J.R., and Roberts, C.W. (2014). Molecular pathways: SWI/SNF (BAF) complexes are frequently mutated in cancer--mechanisms and potential therapeutic insights. Clin Cancer Res *20*, 21-27.
Wang, Y., Hsu, J.M., Kang, Y., Wei, Y., Lee, P.C., Chang, S.J., Hsu, Y.H., Hsu, J.L., Wang, H.L., Chang, W.C.*, et al.* (2016b). Oncogenic Functions of Gli1 in Pancreatic Adenocarcinoma Are Supported by Its PRMT1-Mediated Methylation. Cancer Res *76*, 7049-7058.
Wasilewski, D., Priego, N., Fustero-Torre, C., and Valiente, M. (2017). Reactive Astrocytes in Brain Metastasis. Front Oncol *7*, 298.
Watson, L.A., and Tsai, L.H. (2017). In the loop: how chromatin topology links genome structure to function in mechanisms underlying learning and memory. Curr Opin Neurobiol *43*, 48-55.
Werry, E.L., Barron, M.L., and Kassiou, M. (2015). TSPO as a target for glioblastoma therapeutics. Biochem Soc Trans *43*, 531-536.
Wiegreffe, C., Simon, R., Peschkes, K., Kling, C., Strehle, M., Cheng, J., Srivatsa, S., Liu, P., Jenkins, N.A., Copeland, N.G.*, et al.* (2015). Bcl11a (Ctip1) Controls Migration of Cortical Projection Neurons through Regulation of Sema3c. Neuron *87*, 311-325.
Woodworth, M.B., Greig, L.C., Liu, K.X., Ippolito, G.C., Tucker, H.O., and Macklis, J.D. (2016). Ctip1 Regulates the Balance between Specification of Distinct Projection Neuron Subtypes in Deep Cortical Layers. Cell Rep *15*, 999-1012.
Wu, J.I. (2012). Diverse functions of ATP-dependent chromatin remodeling complexes in development and cancer. Acta Biochim Biophys Sin (Shanghai) *44*, 54-69.
Wu, J.I., Lessard, J., Olave, I.A., Qiu, Z., Ghosh, A., Graef, I.A., and Crabtree, G.R. (2007). Regulation of dendritic development by neuron-specific chromatin remodeling complexes. Neuron *56*, 94-108.
Xia, L., Huang, Q., Nie, D., Shi, J., Gong, M., Wu, B., Gong, P., Zhao, L., Zuo, H., Ju, S.*, et al.* (2013). PAX3 is overexpressed in human glioblastomas and critically regulates the tumorigenicity of glioma cells. Brain Res *1521*, 68-78.
Xie, A.X., Petravicz, J., and McCarthy, K.D. (2015). Molecular approaches for manipulating astrocytic signaling in vivo. Front Cell Neurosci *9*, 144.
Xu, P., Zhang, A., Jiang, R., Qiu, M., Kang, C., Jia, Z., Wang, G., Han, L., Fan, X., and Pu, P. (2013). The different role of Notch1 and Notch2 in astrocytic gliomas. PLoS One *8*, e53654.
Yamada, J., and Jinno, S. (2012). Upregulation of calcium binding protein, S100A6, in activated astrocytes is linked to glutamate toxicity. Neuroscience *226*, 119-129.

Yamada, J., and Jinno, S. (2014). S100A6 (calcyclin) is a novel marker of neural stem cells and astrocyte precursors in the subgranular zone of the adult mouse hippocampus. Hippocampus *24*, 89-101.
Yang, C., Iyer, R.R., Yu, A.C., Yong, R.L., Park, D.M., Weil, R.J., Ikejiri, B., Brady, R.O., Lonser, R.R., and Zhuang, Z. (2012). beta-Catenin signaling initiates the activation of astrocytes and its dysregulation contributes to the pathogenesis of astrocytomas. Proc Natl Acad Sci U S A *109*, 6963-6968.
Yang, Y., Higashimori, H., and Morel, L. (2013). Developmental maturation of astrocytes and pathogenesis of neurodevelopmental disorders. J Neurodev Disord *5*, 22.
Yoo, A.S., and Crabtree, G.R. (2009). ATP-dependent chromatin remodeling in neural development. Curr Opin Neurobiol *19*, 120-126.
Yoo, A.S., Staahl, B.T., Chen, L., and Crabtree, G.R. (2009). MicroRNA-mediated switching of chromatin-remodelling complexes in neural development. Nature *460*, 642-646.
Yu, F., Ng, S.S., Chow, B.K., Sze, J., Lu, G., Poon, W.S., Kung, H.F., and Lin, M.C. (2011). Knockdown of interferon-induced transmembrane protein 1 (IFITM1) inhibits proliferation, migration, and invasion of glioma cells. J Neurooncol *103*, 187-195.
Yu, M., Yu, S., Xue, Y., Yu, H., Chen, D., Wei, X., and Liu, Y. (2018). Over-Expressed FEZF1 Predicts a Poor Prognosis in Glioma and Promotes Glioma Cell Malignant Biological Properties by Regulating Akt-ERK Pathway. J Mol Neurosci *65*, 411-419.
Yu, W., Wang, Y., McDonnell, K., Stephen, D., and Bai, C.B. (2009). Patterning of ventral telencephalon requires positive function of Gli transcription factors. Dev Biol *334*, 264-275.
Yue, C., Niu, M., Shan, Q.Q., Zhou, T., Tu, Y., Xie, P., Hua, L., Yu, R., and Liu, X. (2017). High expression of Bruton's tyrosine kinase (BTK) is required for EGFR-induced NF-kappaB activation and predicts poor prognosis in human glioma. J Exp Clin Cancer Res *36*, 132.
Yun, A., Kang, B., Kim, C.Y., Jeong, D., Bae, D., Kim, E., Jung, H., Han, H., Jeon, H.-N., Kim, H.*, et al.* (2017). TRRUST v2: an expanded reference database of human and mouse transcriptional regulatory interactions. Nucleic Acids Research *46*, D380-D386.
Zahreddine, H.A., Culjkovic-Kraljacic, B., Assouline, S., Gendron, P., Romeo, A.A., Morris, S.J., Cormack, G., Jaquith, J.B., Cerchietti, L., Cocolakis, E.*, et al.* (2014). The sonic hedgehog factor GLI1 imparts drug resistance through inducible glucuronidation. Nature *511*, 90.
Zawadzka, M., Rivers, L.E., Fancy, S.P., Zhao, C., Tripathi, R., Jamen, F., Young, K., Goncharevich, A., Pohl, H., Rizzi, M.*, et al.* (2010). CNS-resident glial progenitor/stem cells produce Schwann cells as well as oligodendrocytes during repair of CNS demyelination. Cell Stem Cell *6*, 578-590.
Zhan, X., Shi, X., Zhang, Z., Chen, Y., and Wu, J.I. (2011). Dual role of Brg chromatin remodeling factor in Sonic hedgehog signaling during neural development. Proc Natl Acad Sci U S A *108*, 12758-12763.
Zhang, S.C. (2001). Defining glial cells during CNS development. Nat Rev Neurosci *2*, 840-843.
Zhang, Y., Chen, K., Sloan, S.A., Bennett, M.L., Scholze, A.R., O'Keeffe, S., Phatnani, H.P., Guarnieri, P., Caneda, C., Ruderisch, N.*, et al.* (2014). An RNA-sequencing transcriptome and splicing database of glia, neurons, and vascular cells of the cerebral cortex. J Neurosci *34*, 11929-11947.
Zhang, Y., Sloan, S.A., Clarke, L.E., Caneda, C., Plaza, C.A., Blumenthal, P.D., Vogel, H., Steinberg, G.K., Edwards, M.S., Li, G.*, et al.* (2016). Purification and Characterization of Progenitor and Mature Human Astrocytes Reveals Transcriptional and Functional Differences with Mouse. Neuron *89*, 37-53.
Zhang, Z., Wlodarczyk, B.J., Niederreither, K., Venugopalan, S., Florez, S., Finnell, R.H., and Amendt, B.A. (2011). Fuz regulates craniofacial development through tissue specific responses to signaling factors. PLoS One *6*, e24608.
Zhao, X., Chen, Y., Zhu, Q., Huang, H., Teng, P., Zheng, K., Hu, X., Xie, B., Zhang, Z., Sander, M.*, et al.* (2014). Control of astrocyte progenitor specification, migration and maturation by Nkx6.1 homeodomain transcription factor. PLoS One *9*, e109171.
Zhao, Y., Kwan, K.M., Mailloux, C.M., Lee, W.K., Grinberg, A., Wurst, W., Behringer, R.R., and Westphal, H. (2007). LIM-homeodomain proteins Lhx1 and Lhx5, and their cofactor Ldb1, control Purkinje cell differentiation in the developing cerebellum. Proc Natl Acad Sci U S A *104*, 13182-13186.

Zhuo, L., Theis, M., Alvarez-Maya, I., Brenner, M., Willecke, K., and Messing, A. (2001). hGFAP-cre transgenic mice for manipulation of glial and neuronal function in vivo. Genesis *31*, 85-94.

Appendix

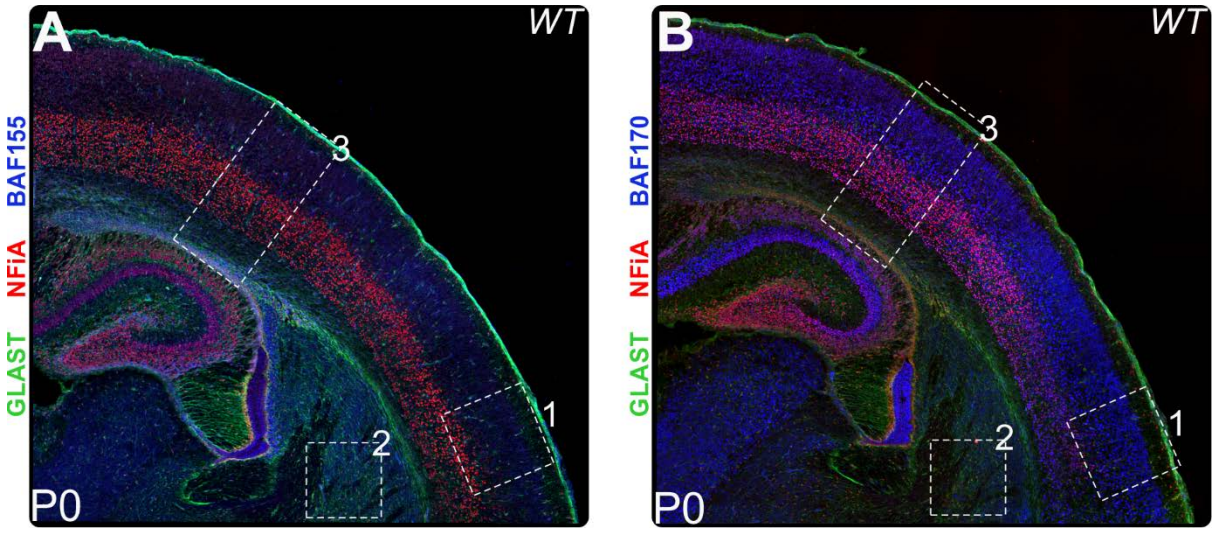

Figure 42 | Expression of BAF complex subunits in AGPs of perinatal murine brain. (A-B) Immunofluorescence analysis of P0 mouse WT coronal brain sections stained with antibodies to astroglial progenitor markers; GLAST (in green) and NFiA (in red) together with antibodies detecting BAF complex subunits (in blue, pseudo coloured): BAF155 (A) and BAF170 (B). Magnified picture taken in the delineated areas no 1 are shown in Figure 7 and 9. Pictures of areas no 2 are presented in Figure 8 and 10. Figure 11 focuses on analysis of area no 3. WT, wild type.

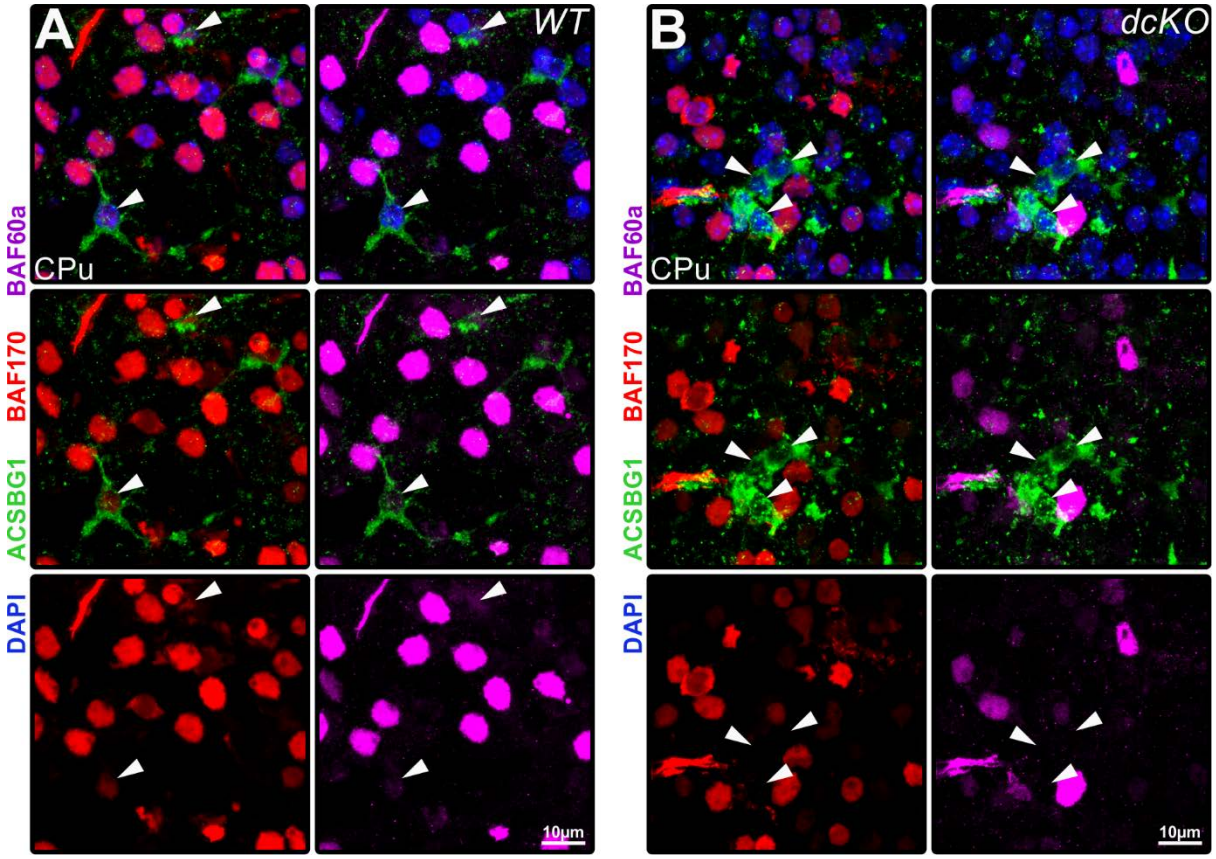

Figure 43 | Loss of BAF complex subunits in ventral astrocytes affected by BAF155/BAF170 dcKO. (A-B) Immunofluorescence analysis of P3 mouse WT (A) and dcKO (B) coronal brain sections of CPu stained with antibodies to protoplasmic astrocyte marker ACSBG1 (in green) together with antibodies detecting BAF complex subunits: BAF170 (in red) and BAF60a (in magenta). ACSBG1 positive astrocytes expressing (in WT, A) or lacking the expression (in dcKO, B) of investigated BAF subunits pointed by arrowheads. dcKO, double conditional knockout; WT, wild type.

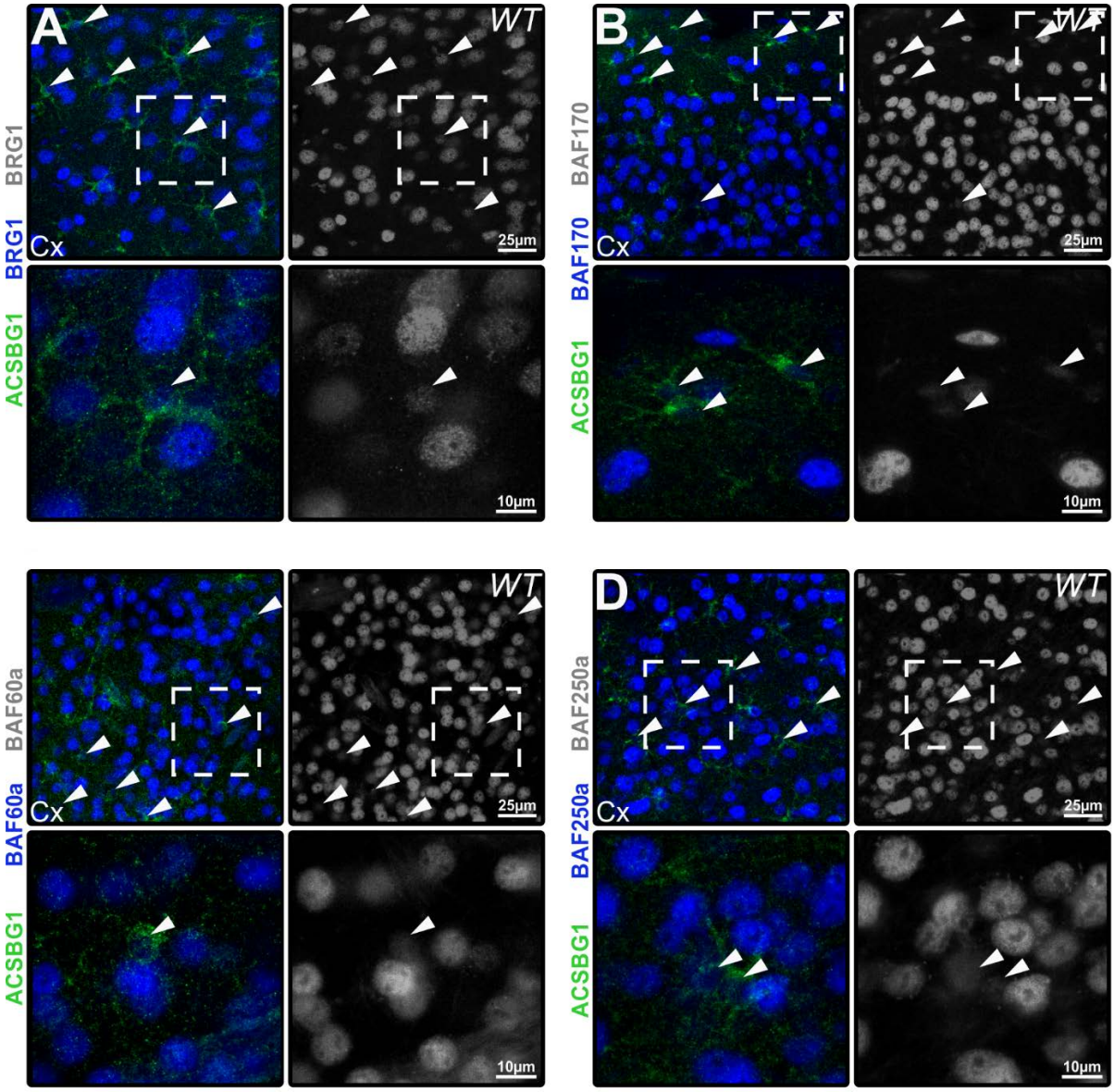

Figure 44 | Expression of BAF complex subunits in cortical protoplasmic astrocytes of adult mice. (A-D) Immunofluorescence analysis of P60 mouse WT coronal cortical sections stained with antibodies to protoplasmic astrocyte marker ACSBG1 (in green) together with antibodies detecting BAF complex subunits (in blue, pseudo-coloured): BRG1 (A), BAF170 (B), BAF60a (C) and BAF250a (D). For each right panels are single channel grey scale images of corresponding BAF subunit staining. Bottom panels of each are magnified insets of delineated areas. ACSBG1 positive astrocytes expressing given BAF subunit pointed by arrowheads. Cx, cortex; WT, wild type.

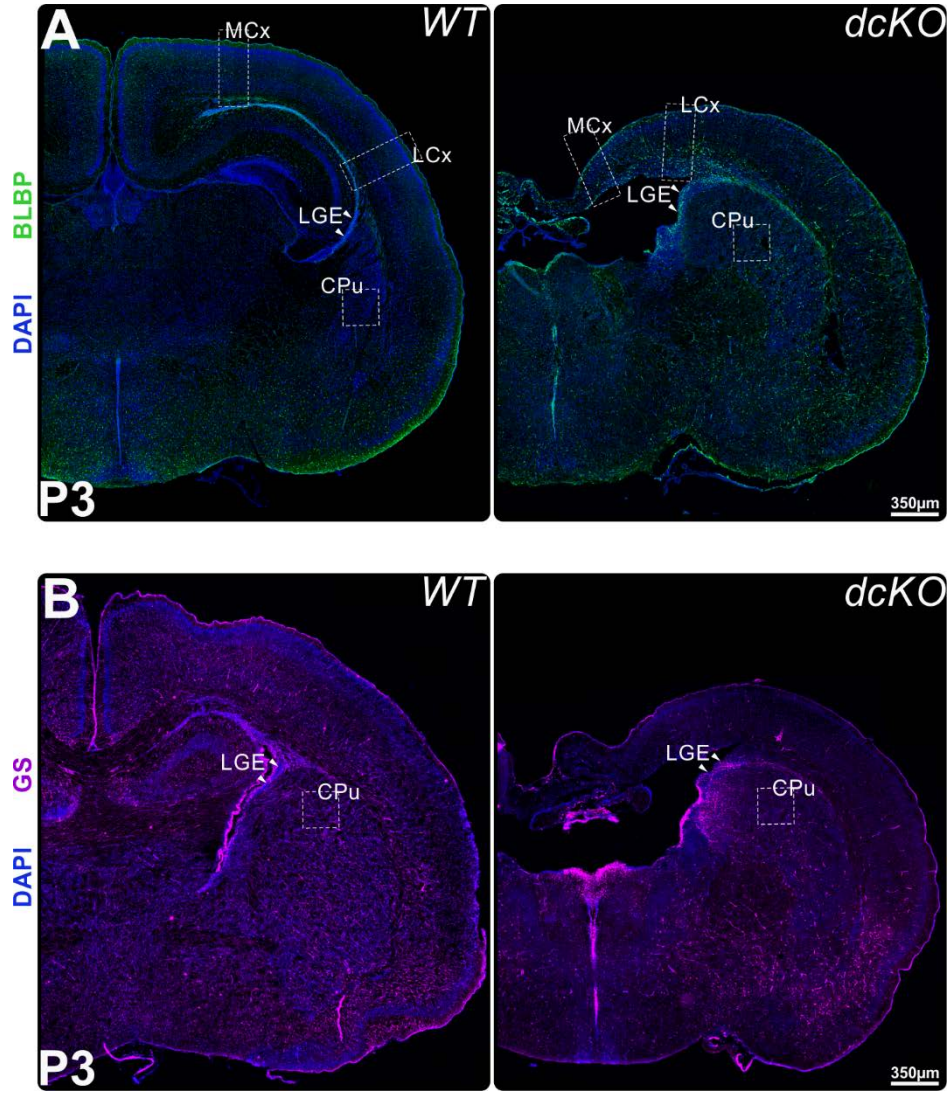

Figure 45 | Expression of astroglial markers in P3 WT and dcKO brains. Pictures are overviews supplementing Figure 17 (A) and Figure 29. CPu, caudate putamen; dcKO, double conditional knockout; MCx, medial cortex (refers to the M1 area); LCx, lateral cortex (refers to the S1 area), LGE, lateral ganglionic eminence, WT, wild type.

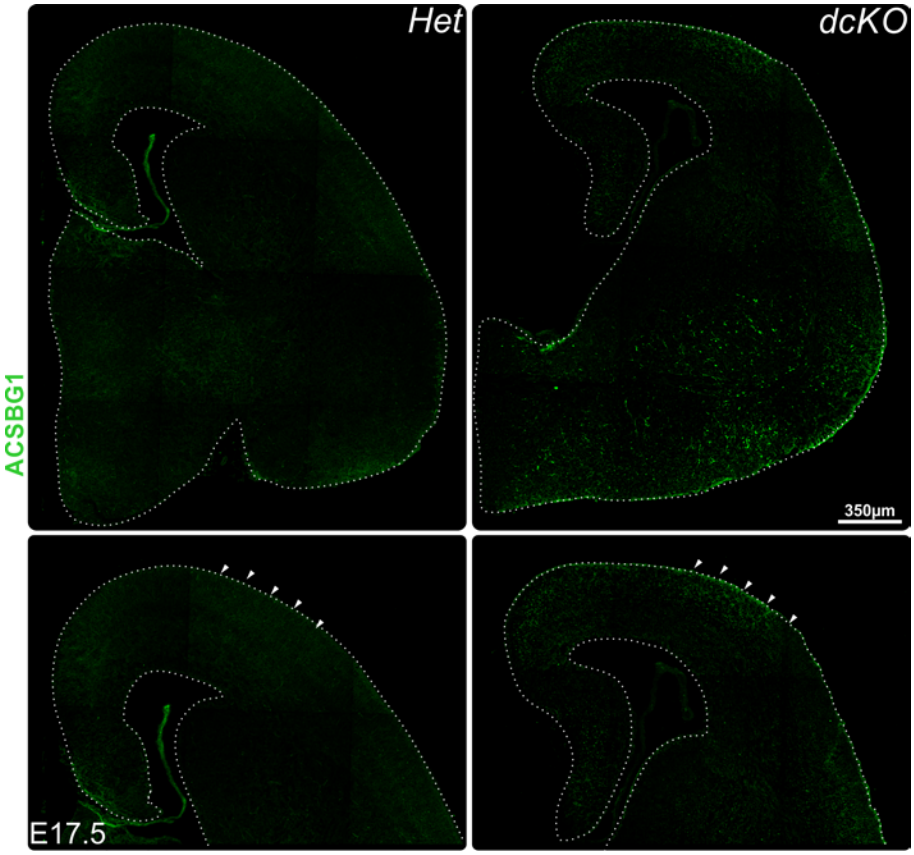

Figure 46 | Expression of ACSBG1 positive protoplasmic astrocytes in E17.5 WT and dcKO brains. Pictures are overviews supplementing Figure 23 and Figure 32A. Arrowheads indicate cortical regions. None of genotypes exhibited ACSBG1 positive astrocyte staining in DP. Note the prominent ACSBG1 staining in ventral areas of dcKO brain. dcKO, double conditional knockout; WT, wild type.

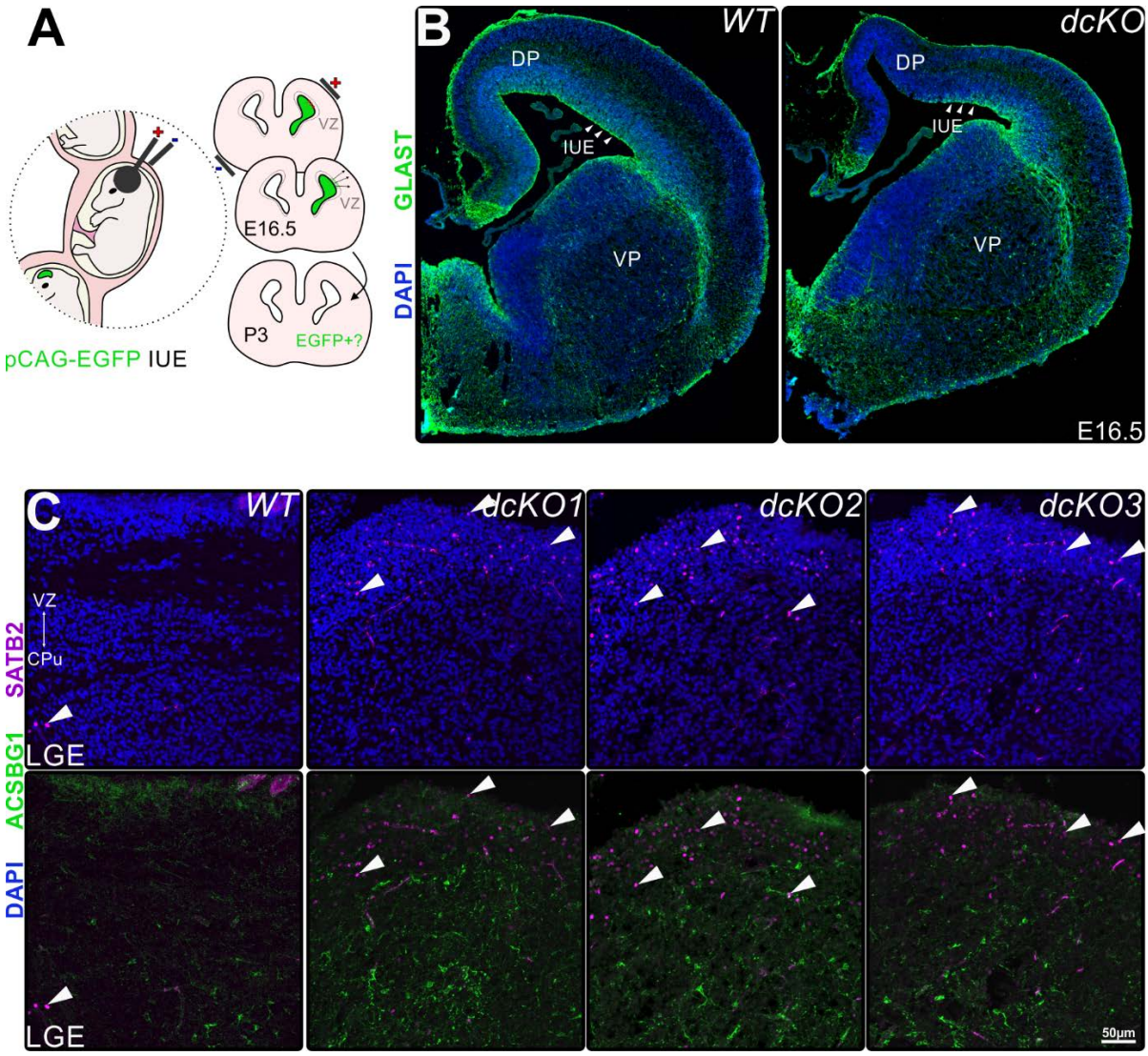

Figure 47 | The distribution of perinatal RGCs progenies differs between WT and dcKO brains (supplementary to Figure 26). (A) Scheme explaining the principle of distribution studies conducted by means of EGFP plasmid i*n utero* injection and electroporation (IUE). (B) Anatomy and GLAST expression in E16.5 WT and dcKO brains. Arrowheads point the place aimed for electroporation (note: GLAST expression was preserved in LCx of dcKO brains). (C) LGE and striatum areas of WT and 3 independent dcKO mice exhibiting staining for SATB2 and ACSBG1. Arrowheads indicate cells positive for SATB2. The directions towards VZ and CPu are indicated by two headed arrow. CPu, caudate putamen; dcKO, double knockout; DP, dorsal pallium; IUE, *in utero* electroporation; LGE, lateral ganglionic eminence; VP, ventral pallium; VZ, ventricular zone; WT, wild type.

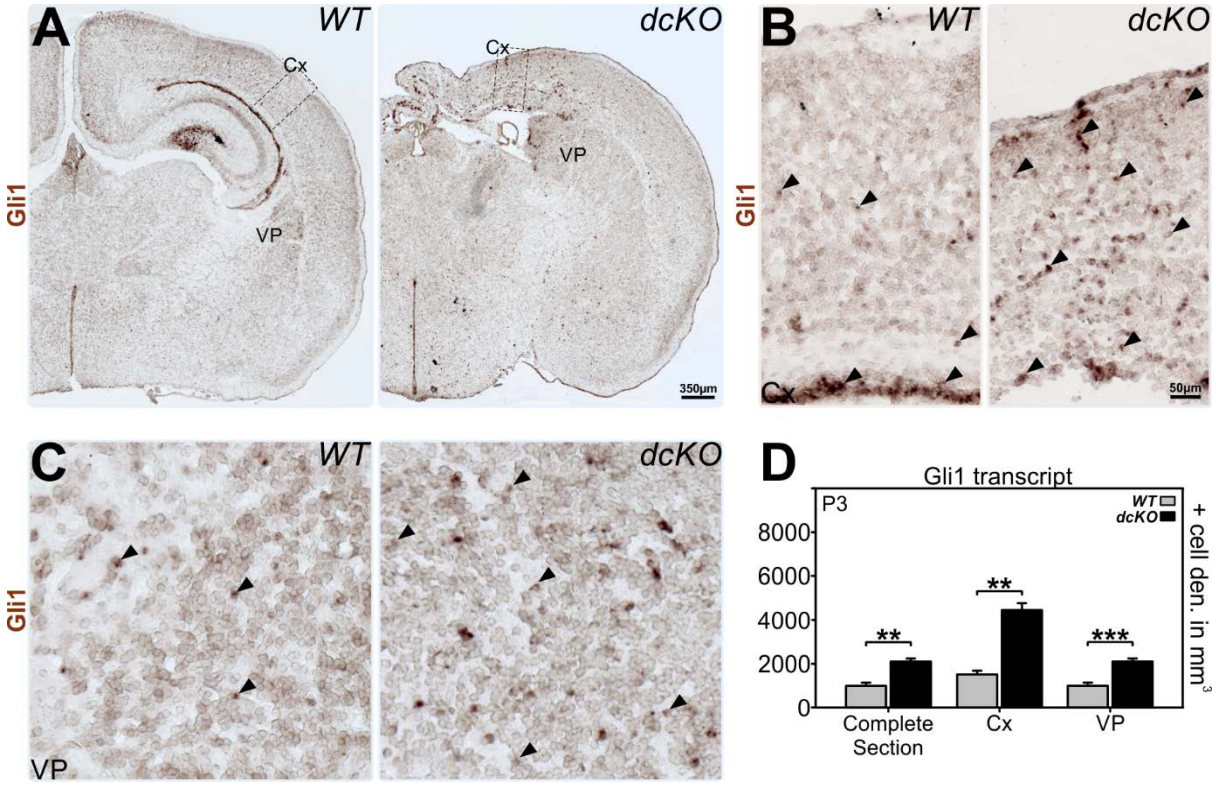

Figure 48 | Upregulation of Gli1 transcript in P3 dcKO brain (supplementary to Figure 37). (A, C) *In situ* hybridization of coronal brain sections through WT and dcKO P3 murine Cx (developing M1 area) staining Gli1 mRNA. (A) Overview pictures of WT and dcKO stained brain sections (B-C) Magnified insets of (B) developing M1 area and (C) CPu - indicated in (A). Full arrowheads indicate Gli1 mRNA positive cells. (D) Densities of cells expressing Gli1 mRNA found in cubic mm of complete brain slice, cortex and VP. Data are averages ± σ of n=3 experimental replicates; ***p≤0.001, **p≤0.01 in t student test. Cx, cortex; dcKO, double knockout; VP, ventral pallium; WT, wild type.

Acknowledgments

A scientific project is a journey that nobody can manage to go through alone. This work would not have been possible without the contribution of many others who encouraged me, taught me and helped me. I am sincerely grateful for all this support.

First and foremost I would like to express my deep gratitude to Prof. Jochen F. Staiger and Dr. Tran Tuoc for giving me the opportunity to work at the Institute for Neuroanatomy of the University Medical Center of Göttingen. I am forever grateful to them for providing me with a fantastic scientific environment, where I had the privilege to contribute to an exciting area of research. Their continuous support and wealth of knowledge were a constant source of inspiration for which I cannot thank them enough.

I sincerely thank Prof. Thomas Dresbach and Prof. André Fischer, members of my thesis committee, for the critical input and encouragement that helped me to refine my work. I would like to repeat my gratitude to Prof. André Fischer and his group members, Dr. Cemil Kerimoglu and Susanne Burkhardt for collaboration on RNA sequencing experiments.

I wish to acknowledge the Facility for Innovative Light Microscopy at the Max Planck Institute for Biophysical Chemistry in Göttingen for granting me access to their infrastructure. I am especially thankful to Dr. Dirk Kamin who taught me much about the confocal microscopy.

I consider myself lucky to have been a member of the great team of the department of Neuroanatomy. Having this opportunity was definitely one of the highlights of my PhD.
I am eternally grateful to Linh Pham, Sandra Heinzl and Particia Sprysch for providing excellent technical support. Linh not only took care of genotyping the animals and helped with immunohistochemistry, but also taught me tissue isolation and *in utero* electroporation. I am deeply thankful for her invaluable help. Sandra provided outstanding support for *in situ* hybridization experiments, preparing solutions and patiently teaching me the whole method. I am grateful to Patricia who helped me with slice preparations and stainings and always found time to offer expert assistance. Many thanks to Pavel Truschow, Alvar Prönneke and Julien Guy for their support with data analysis, graphics design and custom written scripts. The efforts of Pavel are greatly appreciated. Many of the analysis presented in this thesis were made possible only by his masterful contributions. His willingness to help was a constant reassurance for me. Thank you Pavel! Alvar

taught me a lot about microscopy and together with Pavel provided support with R scripts for which I am deeply grateful. I am thankful to Julien who introduced me to MatLab and CorelDRAW, enabling me to produce most of the illustrations presented in this thesis. Julien also taught me stereotaxic surgery and animal care for which I wish to extend my gratitude. I could not have been luckier with my lovely office mates, Nieves Mingo Moreno and Ramanathan Narayanan. Thank you for the support, happiness and camaraderie you brought into my daily life. I am especially grateful to Nieves. Her friendship gave me the courage I needed and without which this thesis would not be in the reader's hands. All these years, you have been a great colleague and more. Thank you! I would like to express my gratitude to the rest of the colleagues from the Institute for Neuroanatomy for creating a wonderful atmosphere and for their help and support whenever needed. I am especially grateful to Mirko for his help with IT and Martin for his shrewd advice. Furthermore, it has been a blessing to work with Eman, Martin, Michael, Alvar, Georg and Pavel who have been wonderful colleagues for all these years.

My life in Göttingen blessed me with a chance to meet two outstanding polish scientists that became my best friends, Joanna and Asia. Joanna provided me with a lot of support during the first part of my PhD, both personally and professionally, for which I am forever grateful. The fantastic time we had in and outside of the lab made my life in Göttingen much more pleasant and will never be forgotten. Meeting Asia was as impactful as meeting someone can be. I cannot overstate how happy I am to have made her acquaintance. Her constant support has been very dear to me this last few years. Nothing can be said here that does Joanna and Asia justice, apart from reaffirming my friendship. Dzięki dziewczyny!

I want to thank my parents for giving me the best possible preparation for this PhD by teaching me the value of hard work. The loving care that they and my sister provided me with has been my greatest source of courage. Thank you very much.

Finally, thank you Julien, for the source of constant support, unconditional love and infinitive inspiration that you have been to me for all these years. Sharing my life and love with you is a blessing that no words can describe.

Thank you!

Kamila Kiszka

Curriculum vitae

Kamila Anna Kiszka

Planckstrasse 15, 37073 Göttingen
kamila.kiszka@mpibpc.mpg.de

Personal information

Born on the 19.07.1989 in Myślenice, Poland
Polish citizenship, marital status: single

Education

2015 – 2019	**Doctorate in Neuroscience** GGNB, Molecular Physiology of the Brain Georg-August University, Göttingen, Germany Project title: "The role of BAF chromatin remodeling complex in neural cell differentiation and neuronal reprogramming" (supervised by Prof. Jochen F. Staiger and Dr. Tran Tuoc)
2011 – 2013	**Master in Biochemistry (with honors)** Department of Cellular Biochemistry Jagiellonian University, Kraków, Poland Thesis title: "Identification and characterization of novel meiosis-specific genes and transdifferentiation of somatic cells into germ stem cells" (supervised by Prof. Wolfgang Engel and Dr. Aneta Kasza) Master's thesis conducted at the Institute of Human Genetics, University of Göttingen
2008 – 2011	**Bachelor in Biology (with honors)** Department of Glycoconjugate Biochemistry Jagiellonian University, Kraków, Poland Thesis title: "Estrogen receptors; structure, localization, significance in melanoma" (supervised by Prof. Anna Lityńska and Dr. Małgorzata Przybyło)
2005 – 2008	**High School education** Science profile (extended biology, chemistry and physics program) Jan III Sobieski High School, Kraków, Poland

Professional experience

2018 – present **Research assistant**
Max Planck Institute for Biophysical Chemistry, Göttingen, Germany
Department of NanoBiophotonics
(head: Prof. Stefan W. Hell)

Main duties: perform rodent hippocampal slices isolation and culture; perform animal surgeries (cranial window implantation, anesthetic infusion and tracheotomy); *in vivo* STED microscopy

2014 – 2018 **Research assistant**
University Medical Center (UMG), Göttingen, Germany
Institute of Neuroanatomy
(head: Prof. Jochen F. Staiger)

Main duties: conduct and perform experimental research centered on *in vivo* and *in vitro* brain imaging in mice using epifluorescent, confocal and two-photon microscopy; manage transgenic animal colonies; perform animal surgeries, conduct post-operational care; perfuse intracardially, prepare and establish retroviral production protocol; perform *in vivo* and *in vitro* viral transduction; prepare RNA sample and analyze RNA sequencing data, implement fluorescence activated cell sorting, isolate and preserve animal tissue samples; isolate and culture mouse neural stem cells

2012 –2014 **Research assistant**
University Medical Center (UMG), Göttingen, Germany
Institute of Human Genetics
(head: Prof. Wolfgang Engel)

Main duties: generate plasmid constructs; produce and purify recombinant proteins; conduct protein-protein interaction studies (GST pull-down, mass spectrometry); maintain bacterial strains; perform molecular biology analyses (Western blot, qRT PCR, luciferase assay); handle various cell lines (e.g. mouse ES and iPS cells, parthenogenetic stem cells, fibroblasts, neurons); prepare genetically modified cell lines (by transfection, retroviral transduction and electroporation); conduct reprogramming of somatic cells to pluripotent/germ cells; prepare tissue and cells for imaging (fixation, cryo/paraffin preservation and sectioning, immuno-, alkaline phosphatase, Giemsa and)

2011–2012 **Student fellow**
Jagiellonian University, Kraków, Poland
Department of Cellular Biochemistry
(head: Prof. Joanna Bereta)

Main duties: extract DNA and RNA from cells; conduct cloning implementing mutagenesis techniques

2010 **Student fellow**
Collegium Medicum, Jagiellonian University (CMUJ), Kraków, Poland
Department of Clinical Biochemistry
(head: Prof. Bogdan Solnica)

Main duties: conduct analytical biochemistry experiments (human blood sample investigation)

Publications

2019 BAF chromatin remodeling complexes regulate astrogliogenesis and astrocytes proliferation via GLI1 signaling pathway during embryonic brain development and postnatally

Kiszka K. A., Kerimoglu C., Fischer A., Staiger J. F., Tuoc T.
(in preparation)

2018 Chromatin remodeling BAF155 subunit regulates the genesis of basal progenitors in developing cortex

Narayanan R., Pham L., Kerimoglu C., Watanabe T., Hernandez R. C., Sokpor G., Ulmke P. A., **Kiszka K. A.**, Tonchev A. B., Rosenbusch J., Seong R. H., Teichmann U., Frahm J., Fischer A., Bonn S., Stoykova A., Staiger J. F., Tuoc T.
iScience **4**, 109–126 (2018)

2018 Epigenetic regulation by BAF (mSWI/SNF) complexes limits neural stem cell proliferation by suppressing Wnt signaling in late embryonic development

Nguyen H., Kerimoglu C., Pirouz M., Pham L., **Kiszka K. A.**, Sokpor G., Sakib M. S., Rosenbusch J., Teichmann U., Seong R. H., Stoykova A., Fischer A., Staiger J. F., Tuoc T.
Stem Cell Rep. **10 (6)**, 1734–1750 (2018)

2015 Loss of BAF (mSWI/SNF) complexes causes global transcriptional and chromatin state changes in forebrain development

Narayanan R., Pirouz M., Kerimoglu C., Pham L., Wagener R. J., **Kiszka K. A.**, Rosenbusch J., Kessel M., Fischer A., Stoykova A., Staiger J. F., and Tuoc T.
Cell Rep. **13**, 1842–1854 (2015)

Conference posters

2018 BAF complexes regulate differentiation of neural progenitors in late brain development

Kiszka K. A., Kerimoglu C., Fischer A., Staiger J. F., Tuoc T.
(22nd Biennial Meeting of the International Society for Developmental Neuroscience, Nara, Japan)

2017 BAF complexes regulate astrocytogenesis during brain development

Kiszka K. A., Kerimoglu C., Pirouz M., Fischer A., Staiger J. F., Tuoc T.
(4th Biennial Neuroscience Symposium "ENCEPHALON", Göttingen, Germany)

Teaching experience

2015	Method course for students of the first year of International Max Planck Research School (IMPRS) MSc/PhD Neuroscience Program Georg-August University, Göttingen, Germany Preparation of immunohistological brain sample and imaging
2015	Supervision of the lab rotation of Killian Vasco Hinze, student of Developmental, Neural and Behavioral Biology Program Georg-August University, Göttingen, Germany Project: "Investigation of apoptotic processes in BAF complex depleted mouse brain"
2015	Supervision of the lab rotation of Tizibt Ashine Bogale, student of IMPRS MSc/PhD Neuroscience Program Georg-August University, Göttingen, Germany Project: "The role of BAF complex in reactive astrogliosis and glial scar formation"
2011	Method course for students of the first year of Biochemistry MSc Program Jagiellonian University, Kraków, Poland Transformation and maintenance of bacterial strains. Plasmid DNA extraction by minipreparation

Activities

2017	Main organizer of the 4th biennial Neuroscience Symposium "ENCEPHALON" Göttingen, Germany
2015	Participation in workshop "Manipulation and visualization of physiological and pathophysiological functions of glia" Bilbao, Spain
2013	*Inter alia* co-founder of Biochemistry Students Society "NZYME" Kraków, Poland
2011 – 2012	Tutoring volunteer for primary school, gymnasium and high school students
2011 – 2012	Many scientific and didactic biochemical shows

Additional informations

Certificates	FELASA certificate, function ABD (accreditation to perform animal experiments, since April 2015; accreditation to design procedures and projects, since February 2019)
	Diploma of pedagogical training (accreditation to teach biology and chemistry in primary school, gymnasium and high school, since June 2012)
Computer skills	Microsoft Office, CorelDRAW Graphics Suite, Adobe Illustrator and Photoshop, ImageJ, Zeiss Zen, Neurolucida, LasX, SigmaPlot, basic knowledge of R and MatLab
Languages	Native speaker of Polish; fluent in English; intermediate in German (B1); intermediate in French (B1); knowledge of Latin